Overcrowded alkene-based molecular motors: from single molecule to multimotor systems

Arjen Cnossen

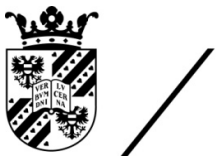

university of groningen

The research described in this thesis was carried out within the Stratingh Institute for Chemistry, University of Groningen, The Netherlands.

This research project was financially supported by Nanoned and an ERC grant (No. 227897).

Printed by Ipskamp drukkers B.V., Enschede, The Netherlands.

Cover: “Dutch Sunrise” by Sander van der Werf
Noordermolen, Noorddijk, Groningen

RIJKSUNIVERSITEIT GRONINGEN

Overcrowded alkene-based molecular motors: from single molecule to multimotor systems

Proefschrift

ter verkrijging van het doctoraat in de
Wiskunde en Natuurwetenschappen
aan de Rijksuniversiteit Groningen
op gezag van de
Rector Magnificus, dr. E. Sterken,
in het openbaar te verdedigen op
vrijdag 1 maart 2013
om 12:45 uur

door

Arjen Cnossen

geboren op 9 april 1984

te Wymbritseradiel

Promotor:	Prof. dr. B.L. Feringa
Copromotor:	Dr. W.R. Browne
Beoordelingscommissie:	Prof. dr. A.M. Brouwer Prof. dr. A. Herrmann Prof. dr. S.R. Meech

ISBN: 978-90-367-6001-0 (print)
978-90-367-6000-3 (digital)

Contents

Chapter 1: Unidirectional light-driven molecular motors based on overcrowded alkenes

Over the last two decades, interest in nanotechnology has led to the design and synthesis of a toolbox of nanoscale versions of macroscopic devices and components.[1,2,3] In molecular nanotechnology, linear motors based on rotaxanes and rotary motors based on overcrowded alkenes are particularly promising for performing work at the nanoscale. In this chapter the progress on light-driven molecular motors based on overcrowded alkenes is reviewed. Both the so-called first and second generation molecular motors are discussed, as well as their potential applications.

Alkene isomerization

Unsymmetrically substituted alkenes (*i.e.* $R^1R^2C{=}CR^3R^4$ with $R^1 \neq R^2$ and $R^3 \neq R^4$) have two isomers: an *E* and a *Z* form. The thermal barrier to rotation around the carbon-carbon double bond means that these two forms can usually not interconvert easily. This has been used as the basis for molecular switches such as stilbene.[4] The two forms can be distinguished spectroscopically and could thus potentially be used as bits in an optical data storage system as $E \rightarrow Z$ or $Z \rightarrow E$ isomerization can be induced with light.[5] A major problem with stilbenes is that they tend to undergo side reactions upon irradiation: oxidative cyclization of *Z*-stilbene yields phenanthrene, which cannot revert to its original form.[6]

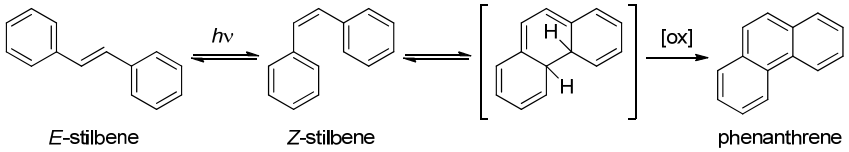

Scheme 1 Isomerization and oxidative cyclization of stilbene.

Oxidative cyclization can be prevented by *ortho*-substitution. The introduction of substituents can lead to steric overcrowding around the double bond; the area where the substituents come into proximity is often referred to as the *fjord* region. If the substituents are large enough, the planarity of the double bond is disrupted and a variety of twisted or folded conformations can be adopted; these include helically shaped conformations. These types of compounds still undergo photoisomerization and can be applied as chiroptical molecular switches.[7,8] The introduction of stereogenic centers on these switches led to the development of rotary molecular motors.[9,10]

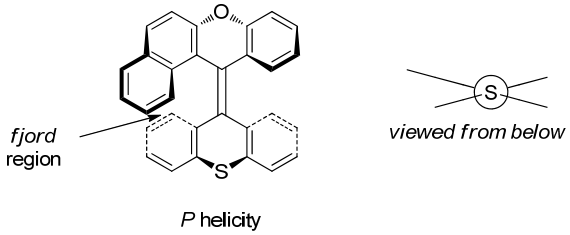

Scheme 2 Example of an overcrowded alkene which shows helicity.

First generation molecular motors

The so-called first generation molecular motors comprise two identical halves connected by a central double bond, which is the axis of rotation. Both halves feature a stereocenter,

which is a key element in controlling the rotation process. In principle there are four diastereoisomers, but typically only the *R*,*R* and *S*,*S* are obtained synthetically. The stereocenters play an important role in determining the conformation of the two parts; the methyl groups at the stereocenters in **1** adopt an axial conformation because of steric interactions with the opposite half of the molecule. Minimization of the steric interactions between both the aromatic groups and the substituents at the stereocenter results in a *syn*-folded conformation being the most favorable one when the overcrowded alkene has the *E* configuration. In the *Z* configuration, an *anti*-folded conformation is the lowest in energy.

When *E*-**1** is irradiated with UV light, a photochemical *E*-*Z* isomerization takes place (Scheme 3). When the molecule is in the excited state, the central double bond gains more single bond character and rotation around this bond becomes possible. The rotation is still limited by the steric interactions between the two halves, so full 360° rotation is not possible. Instead, a nearly one-half rotation takes place and *Z*-unstable **1** is formed. This photoisomerization is a reversible reaction and under continuous irradiation a photostationary state (PSS) between *E*-stable **1** and *Z*-unstable **1** is established. The ratio of the stable and unstable forms at the PSS is dependent on the absorbance of the two forms and the quantum yields for isomerization. These properties depend on the irradiation wavelength and the structure of the molecular motor involved.

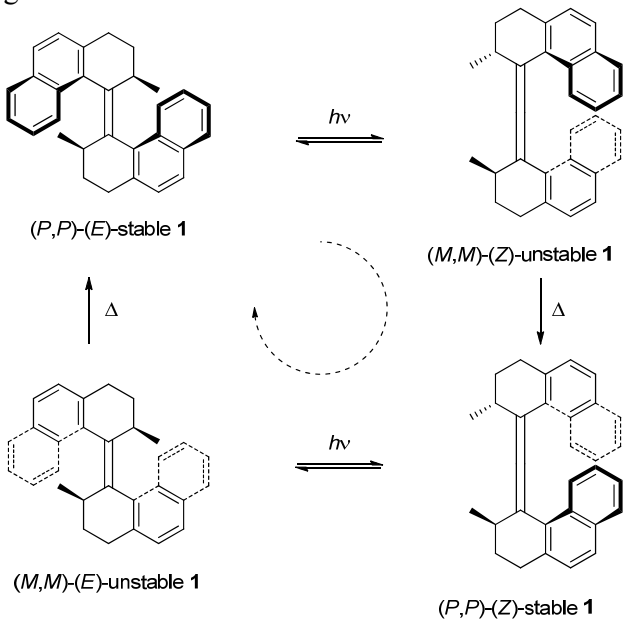

Scheme 3 Isomerization processes leading to unidirectional rotation in first generation molecular motor **1**.[11]

The photochemical *E*-*Z* isomerization leaves the substituents at the stereogenic centers in an equatorial conformation, which is unfavorable due to steric interactions. The steric strain is released by a thermally activated step in which the helical conformation of the molecule is inverted. For this to occur, the aromatic parts of both halves need to slip past each other. Two ring flips allow the substituents at the stereogenic centers to adopt a more favorable axial conformation. The rate of this step is strongly dependent on the steric interactions in the *fjord* region. For the first system (Scheme 3), the half-life is in the range of hours, but by variation of the structure and reducing the size of the aromatic groups in the *fjord* region this has been reduced significantly.[12] Nevertheless, even in the fastest of rotary motors the thermal helix inversion is by far slower than the photoisomerization step, which takes place on the picosecond timescale.[13]

A second photoisomerization from *Z*-stable **1** leads to the formation of *E*-unstable **1**. Again, this is a photoequilibrium, and a photostationary state is established. The newly formed *E*-unstable **1** is thermodynamically unstable and relaxes to *E*-stable **1** through a helix inversion, completing one full 360° rotation. It was shown that this helix inversion is in fact a two-step process and proceeds via an intermediate in which the two halves of the motor have opposite helicity.[14] However, this intermediate can not be observed in the majority of cases because the second step has a much lower activation barrier. The thermal helix inversion steps are the rate determining step in the rotation process. The thermal relaxation from *E*-unstable to *E*-stable is faster than that from *Z*-stable to *Z*-unstable as there are less steric interactions. The thermodynamic parameters for the thermal helix inversion are typically determined using Eyring analysis to evaluate the speed of rotation. From the $\Delta^{\ddagger}G°$ of the thermal helix inversion the half-life at room temperature can be calculated. The $\Delta^{\ddagger}G°$ for the molecular motors which have been synthesized to date cover a wide range,[12] with the lowest under 40 kJ/mol and the highest well over 100 kJ/mol, resulting in half-lives of under a microsecond and over one year, respectively (Table 1).

Table 1 Reaction rates and half-life for processes with various $\Delta^{\ddagger}G°$.

$\Delta^{\ddagger}G°$ (kJ/mol)	k (s^{-1})	half-life at rt
126.0	2.20×10^{-10}	1 century
114.7	2.20×10^{-8}	1 year
108.6	2.67×10^{-7}	1 month
105.1	1.15×10^{-6}	1 week
100.4	8.02×10^{-6}	1 day
92.6	1.93×10^{-4}	1 hour
82.6	1.16×10^{-2}	1 minute
72.7	6.93×10^{-1}	1 second
55.8	6.93×10^{2}	1 millisecond
39.0	6.93×10^{5}	1 microsecond
22.1	6.93×10^{8}	1 nanosecond

A number of different structures have been synthesized in order to optimize the rotation process (by improving the PSS and tuning the rate of thermal helix inversion) and to explore the limits of the system (Scheme 4, Table 2). The influence of the size of the group at the stereogenic center was investigated in **2**-**4** and **5**-**7**. Exchanging the methyl group in **2** for an ethyl group (**3**) causes a slight increase in the amount of the unstable form in the obtained photostationary states. There is no influence on the rate of thermal helix inversion. However, introducing an isopropyl group has a dramatic effect on the rates of thermal helix inversion.[14] The *Z*-unstable form could not be observed due to rapid conversion to the *Z*-stable form, even at -60 °C. Conversion of *E*-unstable **4** to *E*-stable **4** on the other hand was extremely slow, and an intermediate form with mixed helicity was observed. Contraction of the six-membered ring to a five-membered ring as in **5** was thought to increase rate of thermal relaxation due to a decrease of steric hindrance in the *fjord* region.[15] However, due to the reduced flexibility steric hindrance can no longer be relieved by folding. The red shift of the UV/vis absorption indicates that the central double bond is more strained in **5** than in **1**. Still, the expected reduction in the barrier to thermal isomerization was observed, presumably due to ground state destabilization. The observed photostationary states for **5** are slightly less favorable. Compound **6** with long alkyl chains at the stereogenic center is similar in behavior to **5**,[16] however, when

sterically demanding *tert*-butyl groups are introduced (**7**), anomalous behavior is observed.[17] Irradiation of either *E*-stable or *Z*-stable **7** yields *Z*-unstable **7** quantitatively. Subsequent heating leads to the formation of *E*-stable **7**. Formation of the *E*-unstable form could not be detected, and thus it could not be proven that **7** is a unidirectional molecular motor. Recently, compound **8** was reported, in which the naphthalene moieties are replaced by xylyl moieties.[18] This changes the steric hindrance in the *fjord* region, increasing the half-life of the *Z*-unstable form while decreasing that of the *E*-unstable form. While the photostationary state ratios obtained after irradiation are poor in the desired unstable form, it still acts as a unidirectional molecular motor. A major advantage is its synthetic accessibility: it can be prepared in only two steps from commercially available starting materials.

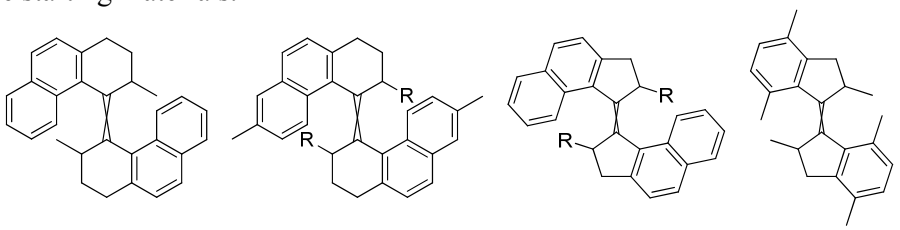

1 **2**: R = Me, **3**: R = Et, **4**: R = *i*Pr **5**: R = Me, **6**: R = $C_{16}H_{33}$, **7**: R = *t*Bu **8**

Scheme 4 First generation molecular motors **1**-**8**.

Table 2 Properties of first generation molecular motors **1**-**8**.

Motor	λ_{max} *E* (nm)	PSS (*E*:*Z*-unstable)	$\Delta^{\ddagger}G°$ *Z*-unstable to *Z* (kJ/mol)	λ_{max} *Z* (nm)	PSS (*Z*:*E*-unstable)	$\Delta^{\ddagger}G°$ *E*-unstable to *E* (kJ/mol)
1[11]	330	5:95[a]	-	330	10:90[a]	-
2[14]	333	15:85[a]	91	333	8:92[a]	107
3[14]	335	3:97[a]	91	335	5:95[a]	107
4[14]	338	0:100[a,b]	-	-	-	124, 131
5[15,19]	368	21:79[a]	93	369	22:78[a]	80
6[16]	373	16:84[a]	91	373	12:88[a]	79
7[17]	367	-	-	380	-	-
8[18]	309	52:48[c]	101	306	89:11[b]	71

[a] hexane, λ >280 nm [b] conversion to *E*-unstable [c] $CDCl_3$, λ_{max} = 313 nm

Because of the steric overcrowding around the central double bond, synthesis of the first generation molecular motors can be challenging. Generally a McMurry reaction is used for the homocoupling of two suitably substituted ketones. From this reaction, only the *S*,*S* and *R*,*R* diastereoisomers are obtained; the *S*,*R* and *R*,*S* are not formed.[14] It would be desirable to directly obtain a single enantiomer, because while each individual molecule undergoes unidirectional rotation, in the racemic mixture this averages out. Moreover, enantiomerically pure material enables the use of CD spectroscopy to follow the photochemical and thermal isomerization processes. Motor **1** could be obtained as a single enantiomer by McMurry coupling of its enantiopure ketone precursor.[20] However, an approach to obtain an enantiopure first generation molecular motor **5** by McMurry coupling of enantiopure ketone failed due to rapid racemization of the ketone under the reaction conditions.[15] An improved synthesis was reported later in which racemization was suppressed, yielding an enantiopure motor in eight steps.[21]

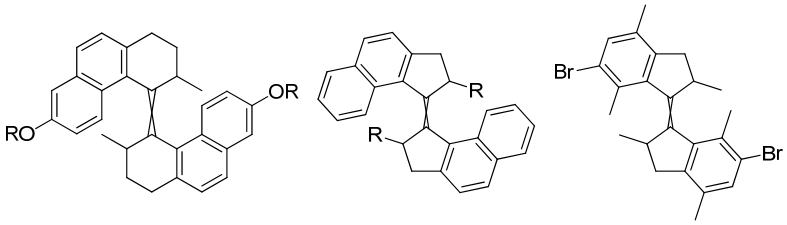

Scheme 5 Functionalization of first generation molecular motors.

Functionalization of molecular motors is a crucial step towards utilizing their unique properties. To use them as molecular switches or rotary motors, they need to act on something to perform a specific function. This could be achieved by doping into, for example, polymer matrices, but a more direct approach is simply linking them covalently to an object. In this regard, synthetic accessibility is of course a limiting factor. Furthermore, the influence functionalization has on the operation of the motor should also be considered. This has led to three general ways of functionalizing first generation molecular motors (Scheme 5). The first approach is the introduction of an ether functionality on the naphthalene moieties in **1**.[22] The second approach is the replacement of the methyl group at the stereogenic center of **5** by a different group. Motors with various aromatic groups, substituted phenyl and benzyl moieties and even biphenyls have been synthesized.[23] These modifications only have a significant effect on the thermal helix inversion from unstable *Z* to stable *Z*; the other isomerization steps are practically unaffected. This method is rather laborious, however, as the substituents have to be introduced in an early stage of the synthesis. The third and most versatile method is the introduction of a bromide on the xylyl moieties in motor **8**.[24] This allows for further functionalization, for example via palladium catalyzed cross-couplings, and has been used successfully to construct systems in which photocontrol over different processes and interactions could be obtained (*vide infra*).

Second generation molecular motors

In second generation molecular motors, the two halves connected by the central double bond are not the same. One half is replaced by a tricyclic aromatic group and there is only one stereogenic center present.[25] The rotation operates according to the same principles as for the first generation motors (Scheme 6). First, an *E*-*Z* isomerization takes place under influence of UV light. This isomerization is accompanied by a change in the overall helicity of the molecule and leaves it in a thermodynamically disfavored conformation. In this conformation the substituent at the stereogenic center is in a (pseudo)equatorial orientation, which pushes it towards the lower half. To relieve this steric hindrance, the molecule undergoes a thermally activated helix inversion after which the substituent at the stereogenic center again adopts a more favorable axial orientation. This completes a 180° rotation of the upper half relative to the lower half. In the case of a symmetrical lower half this regenerates the original conformation. A second photoisomerization and thermal helix inversion completes the full rotation.

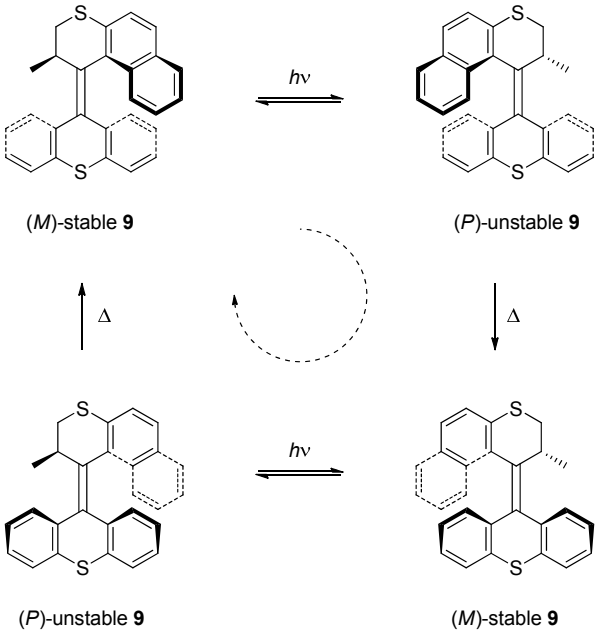

Scheme 6 Isomerization processes leading to unidirectional rotation in second generation molecular motor **9**.

As with first generation motors, many different structural motifs of second generation molecular motors were explored to gain insight into the isomerization processes. Motors with six-membered (hetero)cycles at both sides of the central double bond were found to be relatively slow (Scheme 7, Table 3). Due to the presence of six-membered rings, these molecules are relatively flexible and have a number of conformations that are close in energy.[26] Values for the $\Delta^{\ddagger}G°$ of the rate-determining thermal helix inversion are around 100 kJ/mol, resulting in a half-life in the order of days. Changing a single atom in the upper or lower half (**9-14**) can change the $\Delta^{\ddagger}G°$ by up to 12 kJ/mol.[25,27,28] This was previously analyzed in the context of different bond lengths, but this proved to be complicated by accompanying effects such as folding.[12] The conformational dynamics during isomerization of motors **9-11** is further studied in Chapter 2 to explore in which way the bridging atoms influence isomerization.

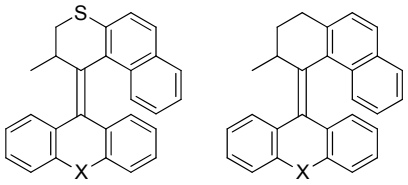

9: X = S
10: X = O
11: X = $C(CH_3)_2$
12: X = NBoc
13: X = $C(CH_3)_2$
14: X = S
15: X = CH=CH

Scheme 7 Second generation molecular motors **9-15**.

Table 3 Properties of second generation molecular motors **9-15**.

Motor	λ_{max} (nm)	PSS (stable:unstable)	$\Delta^{\ddagger}G°$ (kJ/mol)
9[25]	324	8:92[a,d]	106
10[25]	326	23:77[b,e]	100
11[27]	320	8:92[a,d]	106
12[28]	361	23:77[c,d]	110
13[27]	-	1:99[a,d]	94
14[27]	-	1:99[a,d]	92
15[27]	-	25:75[a,d]	103

[a] $\lambda > 280$ [b] $\lambda_{max} = 365$ nm [c] $\lambda = 355$ nm [d] toluene d_8 [e] benzene d_6

While exploring structural variations that are tolerated without compromising the unidirectional rotation, several systems were encountered in which the limits were

reached (Scheme 8, Table 4). When the stereogenic center is moved away from the *fjord* region as in **16**, the unidirectionality of the rotation is compromised.[29] As the difference between the stable and unstable form becomes smaller, the thermal helix inversion becomes an equilibrium. However, there still is an overall preferred direction of rotation. In motor **17**, the direction of rotation can be completely inverted.[30] Base-catalyzed epimerization converts the unstable form to the stable form of the other enantiomer, which rotates in the opposite direction.

Motor **18** is substituted with a nitrogen atom in the upper half and a ketone in the lower half in an attempt to control the rate of thermal helix inversion by changing the electronic rather than the steric environment.[31] Having an electron donating and an electron withdrawing group in direct conjugation across the central double bond results in more single bond character, which facilitates thermal helix inversion. While the $\Delta^{\ddagger}G°$ for thermal helix inversion of **18** was indeed found to be significantly lower than for **9**-**15**, evidently the barrier for thermal *E*-*Z* isomerization was also lowered, and part of the unstable form relaxed via this pathway rather than helix inversion, reducing the overall unidirectionality.

Because the rate limiting step in the rotation is the thermal helix inversion, attempts were made to reduce the steric hindrance around the double bond. This would make it easier for the upper half to slip past the lower half in the thermal helix inversion. However, when the upper half of motors **13**-**15** was simply truncated, photocyclization occurs similar to stilbenes. Only when a seven-membered ring was used in the lower half (**19**) did these overcrowded alkenes still behave as a molecular motor.[32] Also, the desired reduction in the $\Delta^{\ddagger}G°$ of the thermal helix inversion was not achieved.

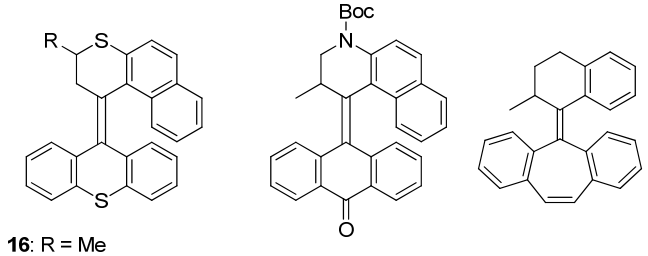

16: R = Me
17: R = $(CH_3)_2NC(O)$ **18** **19**

Scheme 8 Second generation molecular motors **16**-**19**.

Table 4 Properties of second generation molecular motors **16**-**19**.

Motor	λ_{max} (nm)	PSS (stable:unstable)	$\Delta^{\ddagger}G°$ (kJ/mol)
16[29]	333	31:69[a,d]	107
17[30]	326	38:62[b,d]	108
18[31]	365	35:65[c,e]	82
19[32]	277	32:68[a,f]	107

[a] $\lambda > 280$ [b] $\lambda > 312$ [c] $\lambda_{max} = 365$ nm [d] $CDCl_3$ [e] toluene d_8 [f] benzene d_6

A more successful approach was to contract the six-membered rings on the central olefinic bond to five-membered rings (Scheme 9, Table 5). This resulted in a reduction in the $\Delta^{\ddagger}G°$ for thermal helix inversion of about 20 kJ/mol compared to the motors with six-membered rings, increasing the overall rate of rotation significantly.[33] In general, the photostationary states in these systems are lower with respect to the unstable form. A series of motors with groups of various sizes at the stereogenic center showed an interesting trend in the rate of thermal helix inversion: sterically more demanding groups give higher rates (**20**-**23**).[34] The rationalization for this is that while larger groups increase steric hindrance, this effect is more pronounced in the unstable form than in the transition

state, thus resulting in a lower barrier. The photostationary states are not affected by the size of R^1. The presence of electron withdrawing groups at R^2 on the other hand significantly increases the amount of unstable form at the photostationary state (**24**, **25**) while an electron donating group (**26**) decreases the amount.[35] However, electron withdrawing or donating groups have no effect on the rate of thermal helix inversion. These motors are further studied in Chapter 3.

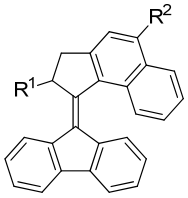

20: R^1 = Me, R^2 = H
21: R^1 = *i*Pr, R^2 = H
22: R^1 = Ph, R^2 = H
23: R^1 = *t*Bu, R^2 = H
24: R^1 = Me, R^2 = Cl
25: R^1 = Me, R^2 = CN
26: R^1 = Me, R^2 = OMe

Scheme 9 Second generation molecular motors **20**-**26**.

Table 5 Properties of second generation molecular motors **20**-**26**.

Motor	λ_{max} (nm)	PSS (stable:unstable)	$\Delta^{\ddagger}G°$ (kJ/mol)
20[33,34]	390	25:75[a]	85
21[34]	390	11:89[a]	84
22[34]	390	14:86[a]	88
23[34]	390	12:88[a]	60
24[35]	400	30:70[a]	86
25[35]	410	18:82[a]	86
26[35]	400	43:57[a]	86

[a] λ_{max} = 365 nm, toluene d_8

In motors **27**-**29** the steric hindrance in the *fjord* region is reduced by decreasing the size of the aromatic group in the upper half (Scheme 10, Table 6). Replacement of the naphthyl unit by a benzothiophene in **27** lowers the barrier for thermal helix inversion, leading to faster overall rotation.[36] While simple truncation of the upper half proved unsuccessful in six-membered ring motors due to photocyclization, blocking the position next to the double bond in the upper half with a methyl group proved to be practical. The reduced steric hindrance in **28** results in faster rotation compared to naphthalene-containing motor **20**.[18] Replacing the methyl group with a methoxy group lowers the barrier to thermal helix inversion even further to 51 kJ/mol for motor **29**, making it the fastest fluorene-based motor to date.[37]

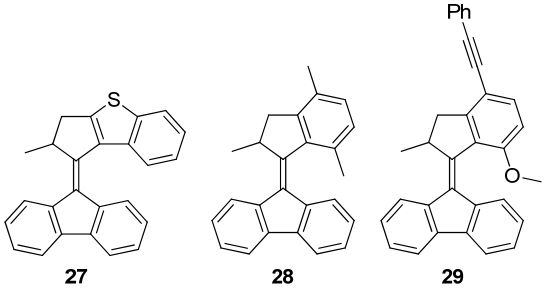

Scheme 10 Second generation molecular motors **27**-**29**.

Table 6 Properties of second generation molecular motors **27**-**29**.

Motor	λ_{max} (nm)	PSS (stable:unstable)	$\Delta^{\ddagger}G°$ (kJ/mol)
27[36]	355	33:67[a,b]	66
28[18]	360	25:75[a,c]	79
29[37]	361	30:70[a,d]	51

[a] λ_{max} = 365 nm [b] THF d_8 [c] toluene d_8 [d] *i*-pentane

In motors **30** and **31** a six-membered ring is used in the upper half, while a five-membered ring is used in the lower half (Scheme 11, Table 7). The barriers for thermal helix inversion were found to be very high,[38] and recent results suggest that the barrier for thermal *E*-*Z* isomerization is lower, which limits their use as a molecular motor.[39] However, due their high photostationary state they are good candidates for use as a chiral, bistable molecular switch with a large change in geometry. Also, their absorption is shifted towards the visible region, which could allow for application in a wide range of systems (see also Chapter 4).

The combination of a five-membered ring in the upper half and a six-membered ring in the lower half resulted in the fastest motors known to date, with theoretical rotation rates

up to the MHz regime (**32**-**36**).[28,40] Because the isomerization process takes place on the microsecond timescale, analysis is challenging and the synthesis of these motors was reported several years earlier than proof of their functioning as a molecular motor.[41,42] Eventually, time-resolved techniques such as transient-absorption spectroscopy proved to be key in the characterization of the short-lived intermediates. Faster rotation could be crucial to overcome Brownian motion.[43] Furthermore, if a certain amount of work could be performed in one rotation, faster rotation means more work can be performed in the same timeframe. Motor **35** was especially promising as it has a nitrogen atom in the lower half which could be exploited for further functionalization, however, this presented more challenges than initially expected.[44] Motor **36** is thought to have the lowest barrier to thermal helix inversion of all the motors synthesized to date. However, the low half-life of the unstable form precluded accurate determination of the thermodynamic parameters.[42]

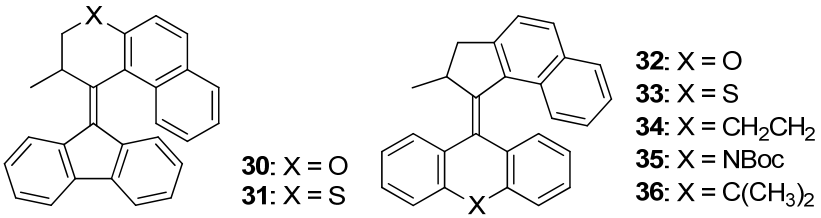

Scheme 11 Second generation molecular motors **30**-**35**.

Table 7 Properties of second generation molecular motors **30**-**35**.

Motor	λ_{max} (nm)	PSS (stable:unstable)	$\Delta^{\ddagger}G°$ (kJ/mol)
30[38]	410	<5:>95[a]	117
31[38]	410	<5:>95[a]	109
32[40]	-	-	42
33[40]	-	-	34
34[40]	-	-	57
35[28]	358	-	38
36[42]	-	-	~27

[a] λ_{max} = 365 nm, $CDCl_3$

The synthesis of second generation molecular motors generally involves more steps than that of first generation molecular motors. However, a convergent route can be followed, in which the upper and lower part are synthesized separately and only connected in the final step. For this final coupling, a Barton-Kellogg reaction between a thioketone and a diazo compound has proven to be most successful.[45,46] Using this reaction, the steric hindrance is increased stepwise and the final products can be obtained in moderate to good yields. As for the first generation motors, the synthesis of enantiomerically pure second generation motors is desirable because it removes the need for costly and time-consuming HPLC separations. To date, the successful synthesis of enantiomerically pure motors has been limited. During the key step in the synthesis, the Barton-Kellogg coupling, rapid racemization of enantiomerically pure starting materials is observed. Only when a TBDMS-protected hydrazone was converted *in situ* to the corresponding diazo compound, did coupling with thioketones proceed with retention of enantiomeric excess (ee).[47] Recently a number of potential new synthetic routes towards overcrowded alkenes were reported.[48,49] These route are based on carbopalladation cascades and have been shown to retain the ee of their starting materials throughout the reaction, which is highly promising. However, the lengthy synthesis of the starting materials and the limited scope may preclude their application in the near future.

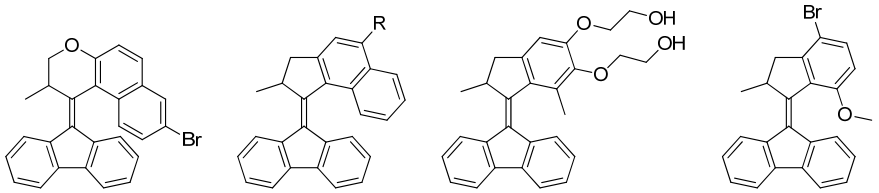

Scheme 12 Examples of second generation molecular motors with different rotation speeds and different moieties that allow for further functionalization in the upper half.

The functionalization of second generation motors has been demonstrated with several approaches, both in the upper half (Scheme 12) and in the lower half (Scheme 13). Aryl bromides can conveniently be introduced in overcrowded alkenes **20**, **29** and **31** to allow for further functionalization via, for example, palladium-catalyzed cross-coupling reactions.[37,50,51] Ether moieties such as in **26** can also be used for the covalent linking to other molecules, as is also demonstrated in Chapters 4 and 6 of this thesis. Several motors for surface modification based on **28** have been reported. Two ether moieties allow for double anchoring to a surface, which may improve the stability and reduce free rotation of the molecule relative to the surface.[52]

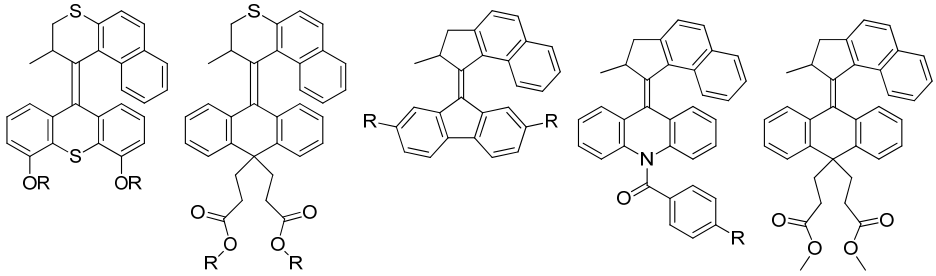

Scheme 13 Examples of second generation molecular motors with different rotation speeds and different moieties that allow for further functionalization in the lower half.

Modification of the lower half can conveniently be performed as well. In the slower motors such as **9** and **11**, functionalization can be achieved via ether or ester moieties. Motor **20** can be functionalized on the 2-position of the lower half with bromide or ether functionalities. Functionalization in other positions of the fluorene is also an option, as is demonstrated in Chapter 3. The nitrogen atom in fast motor **35** can also be exploited for further functionalization, however, recent results using an ester modified version of **36** are very promising, and this is synthetically more accessible. Overall, there are many different methods for functionalization of second generation molecular motors. This gives the freedom to focus on selecting the desired properties of the motor, in terms of rate of thermal relaxation, UV/vis absorption and PSS. A suitable way to introduce further functionality can then be found.

Applications

Overcrowded alkene-based molecular motors have several distinctive properties that may be exploited in a variety of applications.[53] They are different from simple rotors[54] in that they require an energy input. However, this also means they may be suitable for converting energy input into work. Using light and heat as energy inputs means that their operation is non-invasive and there is no build-up of used 'fuel' reagents.[55] Furthermore, molecular motors are chiral, and their rotation proceeds in only one direction, which separates them from many systems based on molecular switches. Finally, they are capable of continuous rotation if irradiation and heat are supplied simultaneously,[56] making them suitable for repetitive or continuous work. In many cases, functionalization is necessary to

exploit the unique properties of molecular motors. The introduction of substituents can affect the photochemical or thermal isomerization processes;[57,58] nevertheless, to date there are several successful examples.

From relative to absolute rotation

Controlled rotation in solution can be overwhelmed by Brownian motion, which makes it impossible to harness useful work from these systems.[59,60] Immobilization on a surface is a potential solution by converting the relative rotation of one part of the molecule with respect to the other to absolute rotation relative to the surface.[61] To this end, molecular motors equipped with thiol 'legs' were synthesized which self-assemble onto gold surfaces (**37**, Scheme 14).[62,63] Proximity to the gold surface can quench the photochemistry, however, by increasing the distance between the motor and the surface the quenching is reduced sufficiently to allow the photoisomerization to take place.[64] Other types of surface immobilization were also explored: amide formation (**38**)[65] and the azide-alkyne Huisgen cycloaddition (**39**, **40**)[66,67] with functionalized monolayers on quartz and self-assembly of alkyl silane-modified motors on mica (**41**).[52] Two types of surface-bound rotary motors can be distinguished: with the rotation parallel to the surface (azimuthal) or perpendicular to the surface (altitudinal). The latter might be used to either control surface properties or to present a certain functional group or retract it into the monolayer, making it unavailable for interaction with other molecules.

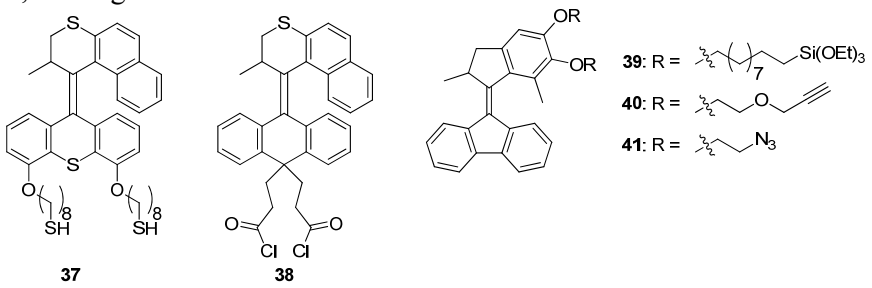

Scheme 14 Several second generation molecular motors for surface attachment.

Coupled rotation

Transmission of molecular rotation from one (part of a) molecule to another is a fundamentally interesting concept.[54] In most cases, molecular rotors are used to study coupled rotation.[68] However, if a unidirectional molecular motor is used instead, it may be possible to induce directionality in a geared system. In compound **42** a xylyl unit was attached to the lower half of an overcrowded alkene-based switch (Scheme 15). By switching between the *E* and *Z* forms, the rotation of the xylyl group could be controlled.[69] This was also attempted with motor **43**, however, anomalous photochemistry was observed.[57] Still, in all four different states of the motor the rate of rotation of the xylyl group is different. In the first generation motor **44** control over rotation around a single bond was also achieved.[70] In the *Z* form, the anisole units rotate freely. In the *E* form on the other hand the rotation is slowed down, as was shown with ^{1}H NMR and EXSY measurements. In molecular motor **45**, rotation of the biphenyl is geared with thermal helix inversion of the motor. It was shown that during the thermal helix inversion of the unstable form to the stable form a half-rotation of the biphenyl takes place.[71] The lower anisole moiety performs a 180° rotation relative to the fluorene, and the helicity of the biphenyl is inverted. The direction of this rotation is coupled to the rotation of the motor. However, free rotation of the biphenyl can still take place in the unstable and stable form.

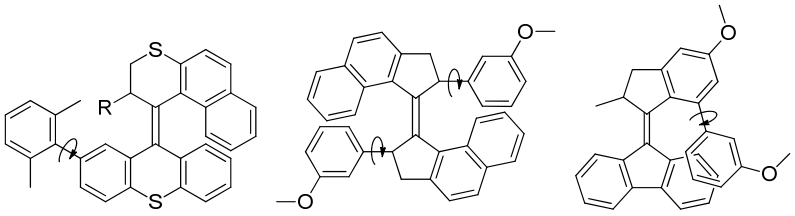

42: R = H
43: R = Me

44 **45**

Scheme 15 Molecular switch and motors for the control of rotation.

Chirality switching

The fact that molecular motors can be switched between two states of opposite helicity has been exploited in a number of ways. Molecular motors have been used to control the chirality of polymeric systems. By attaching a single motor to a polyisocyanate chain, which is normally in a dynamic equilibrium between two helical conformations,[72] the polymer conformation could selectively be switched between *P* helicity, *M* helicity or a racemic state.[73] Further studies in this field are described in Chapter 5.

In polyisocyanates that form a lyotropic liquid crystalline (LC) phase a similar switching was achieved, which allows for control of the magnitude and sign of the supramolecular helical pitch of the LC phase.[50] Intermolecular transfer of chirality is exploited in the use of molecular motors as chiral dopants in liquid crystals.[74,75] By introducing enantiomerically pure motor **20**, the nematic phase is converted to a cholesteric phase. Moreover, the photochemical and thermal isomerization can still be performed, which is accompanied by a change in the helicity of the dopant. In this way switching of the chirality of the cholesteric phase can be achieved.[76] It was found that microscale particles placed on top the LC phase rotated along with the LC phase during switching, demonstrating an impressive transfer from a conformational change at the molecular scale to reorganization at the mesoscale leading to motion on the microscale.[77,78] It should be noted, however, that the rotation of the microparticles is caused by the switching of the helicity of the motor, and not directly by the rotation. This means that rotation of the particles is not indefinite but stops as the photostationary state is reached.

Precise positioning of functionality

First generation molecular motors based on **8** have been used for the precise positioning of functional groups. Motor **8** is especially suitable for this because it has a large geometrical change upon isomerization and it can be synthesized and functionalized in a relatively straightforward manner. By attaching perylene fluorophores in **46**, the effect of positioning on their aggregation was studied using fluorescence spectroscopy.[24] In the *E* form, the perylenes show fluorescence comparable to that of non-aggregated perylene in solution. After photoisomerization to the *Z* form, the fluorescence intensity at shorter wavelength increases, demonstrating the formation of H-aggregates caused by increased proximity of the perylene units. In a similar way control over magnetic interactions was obtained by attaching two TEMPO groups to the motor in **47**.[79] In the *E* form, EPR showed no interaction between the radicals, but in the *Z* form a strong coupling was observed. In a final example, a photoswitchable organocatalyst, the chirality of the motor also plays a key role. In compound **48** two different groups are attached to the molecular motor core: a thiourea, which can activate enones by hydrogen bonding, and a DMAP, which can act as a nucleophilic catalyst or as a base.[80] In the *Z* form, these two groups are brought into close proximity and they catalyze the 1,4-addition of thiophenols to cyclohexenones. Depending on the helicity of the system, whether it is in the stable or unstable form, either enantiomer of the product can be obtained. Using UV light, the

catalyst can be switched on (*Z*) or off (*E*), and by controlling the thermal relaxation the chirality of the product can be chosen.

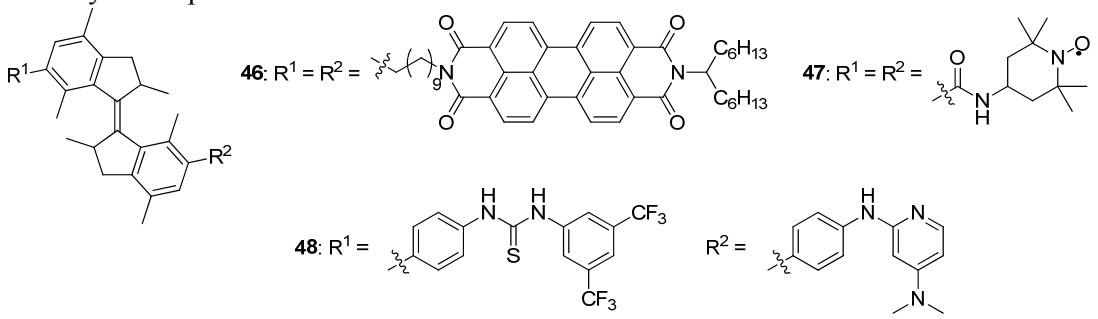

Scheme 16 Functionalized first generation motors **46**-**48**.

Directed motion

Perhaps the most appealing and intuitive application for a molecular motor is as an engine in a nanocar, inspiring a number of designs in recent literature.[81] Recently, a molecule capable of directed motion across a surface by repetitive isomerization was reported.[82] Nanocar **49**, containing four molecular motors, could be visualized on a copper surface using low temperature ultra-high vacuum STM. *E*-*Z* isomerization of the motor units was induced electrochemically with the STM tip, after which thermal helix inversion is thought to take place, resulting in a small displacement of the molecule. Because thermal helix inversion is essentially a one-way process, multiple consecutive isomerizations lead to movement across the surface with a preferred directionality, depending on the stereochemistry of the multimotor system **49**. This is the first example in which the unidirectional character of the rotation of a molecular motor is truly applied. STM studies of molecular motors under ambient conditions are described in Chapter 6.

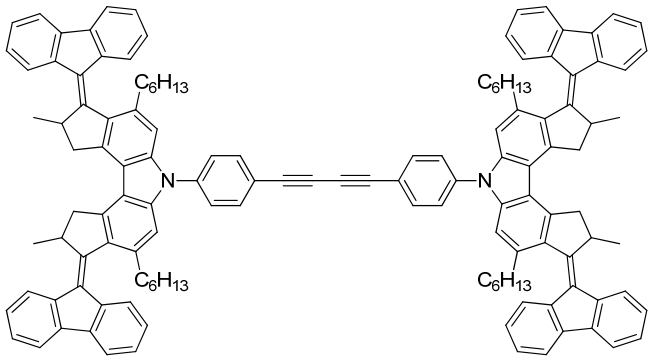

49

Scheme 17 Nanocar **49** comprising four molecular motors fused to a scaffold.

Conclusion

We have come a long way since the development of the first molecular motors. A wide variety of first and second generation molecular motors have been synthesized with a range of properties. For first generation molecular motors, the half-lives of the unstable form are between seconds and days. Most of these motors have very favorable photostationary states, making them relatively efficient. Motor **8** is the best candidate for future applications: its synthesis is short and it is easy to functionalize. With the second generation motors, an even wider range of properties can be covered. Some could achieve rotation rates of more than one million per second, while others are better viewed as

bistable switches. We now have a good understanding of their functioning and the factors that influence this, which can help us in developing applications for these molecules. Compounds **30** and **31** are most suitable in case bistable switching is needed. Motors based on **20** and **28** are convenient for other applications, in which unidirectional rotation is required. The synthesis and functionalization of these compounds is well-known. Moreover, the thermal relaxation of the unstable form is slow enough that it can comfortably be characterized without the need for cryogenic temperatures, while it still fast enough to proceed in a reasonable timeframe at room temperature or under mild heating. The application of the ultrafast motors such as **35** and **36** is still challenging due to the difficulties in characterizing the rotation. The use of ultrafast spectroscopy techniques can help to overcome this challenge in the near future. The application of molecular motors should focus on exploiting their unique properties: large geometrical changes during isomerization, control over chirality and repetitive, unidirectional rotation. Two excellent examples in the recent literature are the control of the stereochemical outcome of an asymmetric reaction by dynamic control of the chiral environment and directional movement of a nanocar across a surface powered by four molecular motors.

Aim of this thesis and contents of upcoming chapters

In this thesis the goal is to explore how the rotation of second generation molecular motors might be applied as a tool in chemical nanotechnology. Unidirectional rotation could be envisioned in powering nanocars or transporting molecules. However, successful application of these molecules requires a comprehensive understanding of how they function. In the first chapters the rotary function of the motors is studied. The characterization of structural changes during the isomerization processes of the motors is crucial for applying their molecular motion. In the later chapters, molecular motors are incorporated into various multicomponent systems and their function is evaluated under different conditions.

In Chapter 2 the conformational dynamics of molecular motors is studied using a combination of computational chemistry and spectroscopy. Density functional theory calculations allow for insight in the structure of various intermediates and the calculation results are supported by (time-resolved) UV/vis and CD spectroscopy to gain a deeper understanding of the conformational changes and motions during thermal relaxation of the unstable form.

Chapter 3 focuses on the photochemical *E*-*Z* isomerization of molecular motors. Both vibrational spectroscopy and ultrafast time-resolved fluorescence up-conversion spectroscopy are employed to characterize the structural changes during photoisomerization.

In Chapter 4 the photoisomerization is performed using visible light by energy transfer from palladium tetraphenylporphyrin. Efficient energy transfer from the porphyrin triplet state results in unidirectional rotation in the motor. This process was characterized using a range of spectroscopic techniques.

Chapter 5 describes multimotor systems and their self-assembly at the liquid/solid interface. The formation of ordered monolayers may be important in extracting work from molecular motors by taking advantage of their cooperative motion.

Chapter 6 deals with the incorporation of molecular motors in polymers. Two approaches are described to obtain photocontrol over the properties of these polymers. The synthesis of a polyisocyanate was unsuccessful due to the instability of the monomer. In a second approach, ring-opening polymerization yielded a highly functionalized polymer of which the conformation can be influenced with light.

References

[1] E. R. Kay, D. A. Leigh, F. Zerbetto, *Angew. Chem. Int. Ed.* **2007**, *46*, 72-191.
[2] W. R. Browne, B. L. Feringa, *Nature Nanotechnol.* **2006**, *1*, 25-35.
[3] V. Balzani, A. Credi, M. Venturi, *Chem. Soc. Rev.* **2009**, *38*, 1542-1550.
[4] H. Meier, *Angew. Chem. Int. Ed.* **1992**, *31*, 1399-1420.
[5] For a basic explanation of the photoisomerization of carbon-carbon double bonds see: N. J. Turro, V. Ramamurthy, J. C. Scaiano, *Principles of Molecular Photochemistry: An Introduction*, University Science Books, Sausolito, **2009**, pp.348-351.
[6] K. B. Jørgensen, *Molecules* **2010**, *15*,4334-4358.
[7] B. L. Feringa, R. A. van Delden, N. Koumura, E. M. Geertsema, *Chem. Rev.* **2000**, *100*, 1789-1816.
[8] W. R. Browne, B. L. Feringa in *Molecular Switches* (Eds.: B. L. Feringa, W. R. Browne), Wiley-VCH, Weinheim, **2011**, pp. 121-179.
[9] B. L. Feringa, *Acc. Chem. Res.* **2001**, *34*, 504-513.
[10] B. L. Feringa, *J. Org. Chem.* **2007**, *72*, 6635-6652.
[11] N. Koumura, R. W. J. Zijlstra, R. A. van Delden, N. Harada, B. L. Feringa, *Nature* **1999**, *401*, 152-155.
[12] M. M. Pollard, M. Klok, D. Pijper, B. L. Feringa, *Adv. Funct. Mater.* **2007**, *17*, 718-729.
[13] R. Augulis, M. Klok, B. L. Feringa, P. H. M. van Loosdrecht, *Phys. Stat. Sol. C* **2009**, *6*, 181-184.
[14] M. K. J. ter Wiel, R. A. van Delden, A. Meetsma, B. L. Feringa, *J. Am. Chem. Soc.* **2005**, *127*, 14208-14222.
[15] M. K. J. ter Wiel, R. A. van Delden, A. Meetsma, B. L. Feringa, *J. Am. Chem. Soc.* **2003**, *125*, 15076-15086.
[16] G. Caroli. M. G. Kwit, B. L. Feringa, *Tetrahedron* **2008**, *64*, 5956-5962.
[17] M. K. J. ter Wiel, M. G. Kwit, A. Meetsma, B. L. Feringa, *Org. Biomol. Chem.* **2007**, *5*, 87-96.
[18] M. M. Pollard, A. Meetsma, B. L. Feringa, *Org. Biomol. Chem.* **2008**, *6*, 507-512.
[19] S. Kuwahara, T. Fujita, N. Harada, *Eur. J. Org. Chem.* **2005**, 4544-4556.
[20] N. Harada, N. Koumura, B. L. Feringa, *J. Am. Chem. Soc.* **1997**, *119*, 7256-7264.
[21] T. Fujita, S. Kuwahara, N. Harada, *Eur. J. Org. Chem.* **2005**, 4533-4543.
[22] M. K. J. ter Wiel, B. L. Feringa, *Synthesis* **2005**, *11*, 1789-1796.
[23] G. Caroli, *Ph. D. Thesis*, University of Groningen, **2012**.
[24] J. Wang, A. Kulago, W. R. Browne, B. L. Feringa, *J. Am. Chem. Soc.* **2010**, *132*, 4191-4196.
[25] N. Koumura, E. M. Geertsema, A. Meetsma, B. L. Feringa, *J. Am. Chem. Soc.* **2000**, *122*, 12005-12006.
[26] For compound **9**, this was demonstrated in an extensive theoretical study, see: G. Pérez-Hernández, L. González, *Phys. Chem. Chem. Phys.* **2010**, *12*, 12279-12289.
[27] N. Koumura, E. M. Geertsema, M. B. van Gelder, A. Meetsma, B. L. Feringa, *J. Am. Chem. Soc.* **2002**, *124*, 5037-5051.
[28] A. A. Kulago, E. M. Mes, M. Klok, A. Meetsma, A. M. Brouwer, B. L. Feringa, *J. Org. Chem.* **2010**, *75*, 666-679.
[29] R. A. van Delden, M. K. J. ter Wiel, H. de Jong, A. Meetsma, B. L. Feringa, *Org. Biomol. Chem.* **2004**, *2*, 1531-1541.
[30] N. Ruangsupapichat, M. M. Pollard, S. R. Harutyunyan, B. L. Feringa, *Nature Chem.* **2011**, *3*, 53-60.
[31] D. Pijper, R. A. van Delden, A. Meetsma, B. L. Feringa, *J. Am. Chem. Soc.* **2005**, *127*, 17612-17613.
[32] E. M. Geertsema, N. Koumura, M. K. J. ter Wiel, A. Meetsma, B. L. Feringa, *Chem. Commun.* **2002**, 2962-2963.
[33] J. Vicario, A. Meetsma, B. L. Feringa, *Chem. Commun*. **2005**, 5910-5912.
[34] J. Vicario, M. Walko, A. Meetsma, B. L. Feringa, *J. Am. Chem. Soc.* **2006**, *128*, 5127-5135.
[35] M. M. Pollard, P. V. Wesenhagen, D. Pijper, B. L. Feringa, *Org. Biomol. Chem.* **2008**, *6*, 1605-1612.
[36] T. Fernández Landaluce, G. London, M. M. Pollard, P. Rudolf, B. L. Feringa, *J. Org. Chem.* **2010**, *75*, 5323-5325.
[37] A. Cnossen, D. Pijper, T. Kudernac, M. M. Pollard, N. Katsonis, B. L. Feringa, *Chem. Eur. J.* **2009**, *15*, 2768-2772.
[38] M. Klok, M. Walko, E. M. Geertsema, N. Ruangsupapichat, J. C. M. Kistemaker, A. Meetsma, Ben. L. Feringa, *Chem. Eur. J.* **2008**, *14*, 11183-11193.
[39] L.-J. Ugen, *Master's research*, University of Groningen, **2012-2013**.
[40] M. Klok, N. Boyle, M. T. Pryce, A. Meetsma, W. R. Browne, B. L. Feringa, *J. Am. Chem. Soc.* **2008**, *130*, 10484-10485.
[41] M. K. J. ter Wiel, J. Vicario, S. G. Davey, A. Meetsma, B. L. Feringa, *Org. Biomol. Chem.* **2005**, *3*, 28-30.
[42] M. Klok, *Ph. D. Thesis*, University of Groningen, **2009**.
[43] M. Klok, W. R. Browne, B. L. Feringa, *Phys. Chem. Chem. Phys.* **2009**, *11*, 9124-9131.
[44] A. Kulago, *Ph. D. Thesis*, University of Groningen, **2011**.

[45] D. H. R. Barton, B. J. Willis, *J. Chem. Soc., Perkin Trans. 1* **1972**, 305-310.
[46] J. Buter, S. Wassenaar, R. M. Kellogg, *J. Org. Chem.* **1972**, *37*, 4045-4060.
[47] T. C. Pijper, D. Pijper, M. M. Pollard, F. Dumur, S. G. Davey, A. Meetsma, B. L .Feringa, *J. Org. Chem.* **2010**, *75*, 825-838.
[48] L. F. Tietze, A. Düfert, F. Lotz, L. Sölter, K. Oum, T. Lenzer, T. Beck, R. Herbst-Irmer, *J. Am. Chem. Soc.* **2009**, *131*, 17879-17884.
[49] H. Liu, M. El-Salfiti, M. Lautens, *Angew. Chem. Int. Ed.* **2012**, *51*, DOI: 10.1002/anie.201204226.
[50] N. Ruangsupapichat, *Ph. D. Thesis*, University of Groningen, **2012**.
[51] D. Pijper, M. G. M. Jongejan, A. Meetsma, B. L. Feringa, *J. Am. Chem. Soc.* **2008**, *130*, 4541-4552.
[52] G. London, *Ph. D. Thesis*, University of Groningen, **2011**.
[53] A. Coskun, M. Banaszak, R. D. Astumian, J. F. Stoddart, B. A. Grzybowski, *Chem. Soc. Rev.* **2012**, *41*, 19-30.
[54] G. S. Kottas, L. I. Clarke, D. Horinek, J. Michl, *Chem. Rev.* **2005**, *105*, 1281-1376.
[55] G. Haberbauer, *Angew. Chem. Int. Ed.* **2011**, *50*, 6415-6418.
[56] E. M. Geertsema, S. J. van der Molen, M. Martens, B. L. Feringa, *Proc. Natl. Acad. Sci. U. S. A.* **2009**, *106*, 16919-16924.
[57] M. K. J. ter Wiel, R. A. van Delden, A. Meetsma, B. L. Feringa, *Org. Biomol. Chem.* **2005**, *3*, 4071-4076.
[58] J.-F. Morin, Y. Shirai, J. M. Tour, *Org. Lett.* **2006**, *8*, 1713-1716.
[59] D. A. Leigh, E. M. Pérez, *Top. Curr. Chem.* **2006**, *265*, 185-208.
[60] R. D. Astumian, *Phys. Chem. Chem. Phys.* **2007**, *9*, 5067-5083.
[61] N. Katsonis, M. Lubomska, M. M. Pollard, B. L. Feringa, P. Rudolf, *Prog. Surf. Sci.* **2007**, *82*, 407-434.
[62] R. A. van Delden, M. K. J. ter Wiel, M. M. Pollard, J. Vicario, N. Koumura, B. L. Feringa, *Nature* **2005**, *437*, 1337-1340.
[63] M. M. Pollard, M. K. J. ter Wiel, R. A. van Delden, J. Vicario, N. Koumura, C. R. van den Brom, A. Meetsma, B. L. Feringa, *Chem. Eur. J.* **2008**, *14*, 11610-11622.
[64] G. T. Carroll, M. M. Pollard, R. A. van Delden, B. L. Feringa, *Chem. Sci.* **2010**, *1*, 97-101.
[65] M. M. Pollard, M. Lubomska, P. Rudolf, B. L. Feringa, *Angew. Chem. Int. Ed.* **2007**, *46*, 1278-1280.
[66] G. London, G. T. Carroll, T. Fernández Landaluce, M. M. Pollard, P. Rudolf, B. L. Feringa, *Chem. Commun.* **2009**, 1712-1714.
[67] G. T. Carroll, G. London, T. Fernández Landaluce, P. Rudolf, B. L. Feringa, *ACS Nano* **2011**, *5*, 622-630.
[68] D. K. Frantz, A. Linden, K. K. Baldridge, Jay. S. Siegel, *J. Am. Chem. Soc.* **2012**, *134*, 1528-1535.
[69] M. K. J. ter Wiel, B. L. Feringa, *Tetrahedron* **2009**, *65*, 4332-4339.
[70] A. S. Lubbe, N. Ruangsupapichat, G. Caroli, B. L. Feringa, *J. Org. Chem.* **2011**, *76*, 8599-8610.
[71] J. Kistemaker, *Master's Thesis*, University of Groningen, **2010**.
[72] M. M. Green, N. C. Peterson, T. Sato, A. Teramoto, R. Cook, S. Lifson, *Science* **1995**, *268*, 1860-1866.
[73] D. Pijper, B. L. Feringa, *Angew. Chem. Int. Ed.* **2007**, *46*, 3693-3696.
[74] R. Eelkema, *Ph. D. Thesis*, University of Groningen, **2006**.
[75] M. G. M. Jongejan, *Ph. D. Thesis*, University of Groningen, **2010**.
[76] For details on the nature of the interaction between the dopant and the LC host, see: A. Bosco, M. G. M. Jongejan, R. Eelkema, N. Katsonis, E. Lacaze, A. Ferrarini, B. L. Feringa, *J. Am. Chem. Soc.* **2008**, *130*, 14615-14624.
[77] R. Eelkema, M. M. Pollard, J. Vicario, N. Katsonis, B. Serrano Ramon, C. W. M. Bastiaansen, D. J. Broer, B. L. Feringa, *Nature* **2006**, *440*, 163.
[78] R. Eelkema, M. M. Pollard, N. Katsonis, J. Vicario, D. J. Broer, B. L. Feringa, *J. Am. Chem. Soc.* **2006**, *128*, 14397-14407.
[79] J. Wang, L. Hou, W. R. Browne, B. L. Feringa, *J. Am. Chem. Soc.* **2011**, *133*, 8162-8164.
[80] J. Wang, B. L. Feringa, *Science* **2011**, *331*, 1429-1432.
[81] G. Vives, J. M. Tour, *Acc. Chem. Res.* **2009**, *42*, 473-487.
[82] T. Kudernac, N. Ruangsupapichat, M. Parschau, B. Maciá, N. Katsonis, S. R. Harutyunyan, K.-H. Ernst, B. L. Feringa, *Nature* **2011**, *479*, 208-211.

Chapter 2: Structural dynamics of overcrowded alkene-based molecular motors during thermal isomerization[I]

In this chapter a series of molecular motors with different bridging groups in the lower half is studied, with a focus on the structural dynamics during thermal isomerization. A combination of DFT calculations and various spectroscopic techniques is employed to study the effect of the bridging group on the conformational dynamics. It was found that the extent to which the bridging group can accommodate the increased folding in the transition state is the main factor in rationalizing the differences in barrier height.

Introduction

Molecular machines such as rotary motors have the potential to play a central role in nanotechnology.[1,2] Understanding the mechanism of their rotation is crucial for optimization of their function and application. The molecular motors developed in our group are based on sterically overcrowded alkenes.[3] Our 'second generation' molecular motors typically consist of a tricyclic lower half or stator connected via a double bond to a chiral, naphthalene substituted (hetero)cyclic upper half that acts as a rotor (e.g. **1**-**4**, Scheme 1).[4,5] These compounds undergo repetitive unidirectional rotation of the upper half relative to the lower half under the influence of UV irradiation and heat. The UV light powers an *E*-*Z* isomerization, which leaves the compound in a thermodynamically unfavorable conformation. A thermally activated helix inversion relieves steric hindrance and brings the molecule back to its initial, most stable conformation (Scheme 2).

Sterically overcrowded alkenes (e.g. **5**, **6**, Scheme 1) can interconvert between a broad spectrum of conformations as has been studied thoroughly by Agranat and coworkers.[6] A combination of experimental and computational chemistry has been used to study this type of compounds and their properties.[7,8,9,10,11] Second generation molecular motors show similar conformations, where folding of the upper and lower half and twisting around the double bond relieves steric strain in the molecule. During the rotation process, there are many intermediates with different degrees of folding and twisting, resulting in a complex, dynamic conformational behavior.

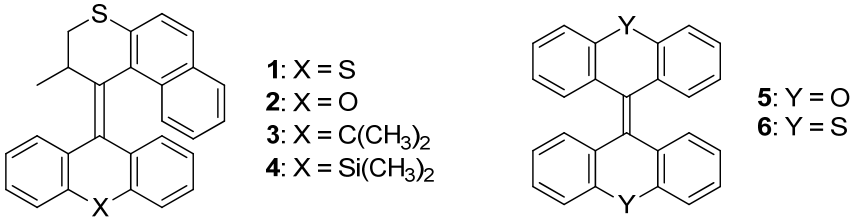

Scheme 1 Molecular motors **1**-**4** and bistricyclic enes **5** and **6**.

Structural modifications can have a large impact on the rotary processes of these types of molecular motor, as was observed upon replacing the methyl group at the stereogenic center,[12] or when the naphthalene part of the upper half was truncated.[13] Similarly, the conformational dynamics of bistricyclic (aromatic) enes are sensitive to the nature of the bridging group.[6] However, it was observed experimentally that the bridging atom X in the

[I] The work presented in this chapter will be published: A. Cnossen, J. C. M. Kistemaker, T. Kojima, B. L. Feringa, *manuscript in preparation*

lower half of motors **1-3** has a relatively small effect on the rate of thermal helix inversion.[4] The reason for this is not entirely clear. Different bridging groups have different bond lengths and angles; therefore a change in conformational stability is expected. Evidently, this does not strongly affect the rate determining step of the thermal helix inversion.

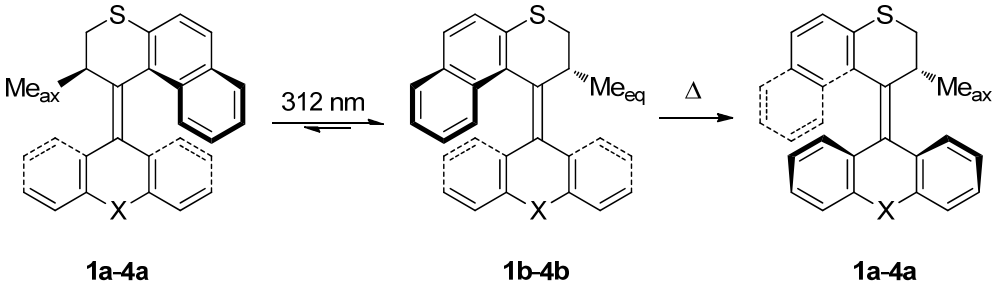

1a-4a **1b-4b** **1a-4a**

Scheme 2 Isomerization processes of **1-4** upon UV irradiation at 312 nm and subsequent heating.

Here we present an experimental study of both the thermal isomerization and the photochemistry of a series of second generation molecular motors in combination with density functional theory (DFT) calculations. Molecular motor **1** has been studied extensively and its rotary processes have been examined in detail both in solution[4,5,14] and on gold nanoparticles.[15,16] Furthermore, it has been used in more complex systems, albeit with varying degrees of success.[17,18,19] The results obtained for **1** can be used as a benchmark to validate the results of the DFT calculations, and the methodology can be extended to the other compounds in the series. Compounds **2** and **3** were reported to act as molecular motors previously, but have not been studied extensively.[4] The introduction of a silicon bridging group in compound **4** further extends this series of motors. The replacement of sulfur by a dimethyl silyl bridging group in thioxanthene derivatives is known to yield similar structures, but increased folding is observed.[20] This could have an effect on the rate of thermal helix inversion; during the thermal helix inversion, the naphthalene part slips over the lower half. The more the lower half is folded, the more facile this slipping is, thereby allowing for faster rotation. Also, a ring flip takes place in the lower half, which may be affected by the variations in the bridging group. The effect on photochemical isomerization has to date received little attention in this regard. This study is expected to provide greater insight into the structure of the intermediates involved in the rotary action of the molecular motor, and how the structural and dynamic properties are affected by the nature of the bridging group. A better understanding of the rotation will help in the design of molecular motors and their incorporation into more sophisticated multicomponent systems.

Results and discussion

Synthesis

The synthesis of compounds **1-3** was reported previously.[4] The synthesis of compound **4** is summarized in Scheme 3. The key step in the synthesis of second generation molecular motors is the introduction of the sterically overcrowded olefinic bond, which is generally achieved using a Barton-Kellogg coupling reaction. Precursors **7** and **9** are known compounds and were synthesized according to literature procedures in 3[4] and 7[20,21] steps, respectively. Hydrazone **7** was oxidized to the corresponding diazo compound **8** with phenyliodine diacetate at 0 °C. In parallel, the ketone functionality in **9** was converted to the thioketone using Lawesson's reagent. Both **8** and **10** are highly reactive compounds

which should not be stored, but were found to react together at room temperature to form episulfide **11** in 40% yield. Desulfurization occurs upon treatment with copper bronze in refluxing *p*-xylene to yield molecular motor **4**.

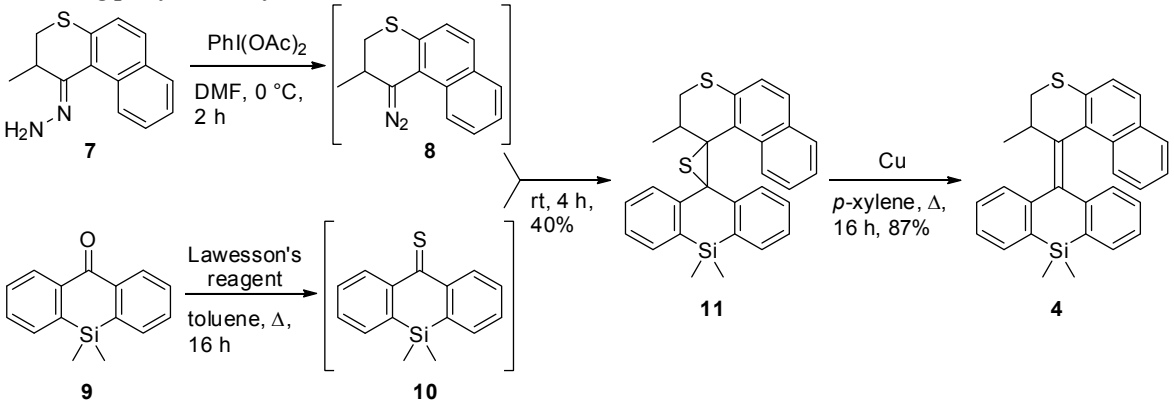

Scheme 3 Synthesis of molecular motor **4**.

Compound **4** was characterized by ^{1}H and ^{13}C NMR as well as HRMS. In the ^{1}H NMR spectrum, the typical coupling patterns for the hydrogen atoms of the substituted thiopyran ring were observed. The two methyl groups on silicon are not equivalent, as one adopts a (pseudo)axial conformation towards the naphthalene unit, whereas the other is in an equatorial position, pointing away from the rest of the molecule. This results in absorptions in the ^{13}C NMR spectrum at -4.4 and -1.1 ppm.

Conformational analysis

Geometry optimizations of motors **1**-**4** were performed on the B3LYP/6-31G(d,p) level of theory. Compound **1** is known to exist in an *anti*-folded conformation as its global energy minimum (Scheme 4a), from earlier DFT calculations[26,27] and X-ray analysis.[4] In this *anti*-folded structure steric hindrance is relieved by folding away the upper and lower half in opposite direction with respect to the central double bond. Similar folded structures were found for **2**-**4**: the tricyclic lower half is folded to the back and the naphthalene part points forward, with the methyl group in an axial orientation to minimize steric interactions. Some key structural parameters are collected in Table 1.

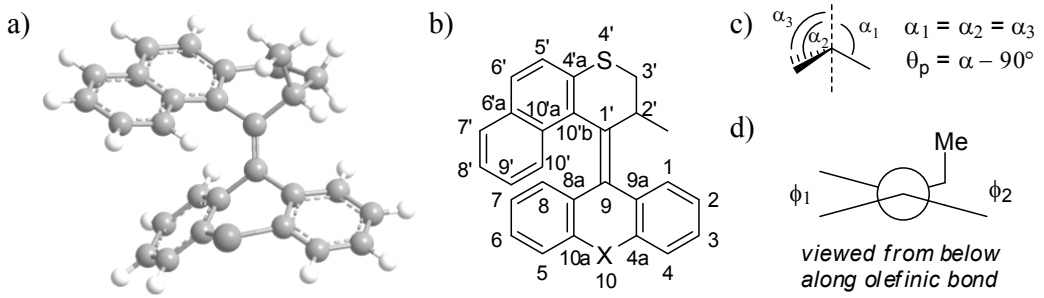

Scheme 4 a) Geometry optimized structure of **1**. b) Numbering scheme for **1**-**4**. c) Definition of pyramidalization angle θ_p. d) Schematic representation of dihedral angles ϕ_1 and ϕ_2 of the C9-C1' bond.

The conformation of the upper half of these molecules is practically identical in all cases, and does not seem to be influenced by the lower half. The central carbon-carbon double bond has a bond length of 136 pm, which is only slightly elongated compared to 134 pm for a normal carbon-carbon double bond. Although the compound appears strained, there is little pyramidalization (Scheme 4c) at the carbon atoms of the double bond; the strain is

mostly relieved by folding of upper and lower parts. In the upper half this is reflected by the axial position of the methyl group. In the lower half the angle between the two phenyl rings deviates significantly from 180° (folding angle 129-144°). Differences are introduced here because of different bond lengths to the bridging groups and differences in preferred bond angles. Incidentally, compound **2** which shows the least folding, also shows the largest pyramidalization at C9. It is noteworthy that for the dihedral angles at the double bond (Scheme 4d) in **1** and **2** a very low torsion angle is observed at the naphthalene side. For compounds **3** and **4**, one of the methyl substituents on the bridging group experiences steric hindrance from the naphthalene, and the dihedral angle on that side is the largest.

Table 1 Calculated bond lengths and angles for motors **1**-**4**.

Motor	θ_p C1' (°)	C1'-C9 bond length (Å)	ϕ_1 C10'b-C1'-C9-C8a (°)	ϕ_2 C2'-C1'-C9-C9a (°)	θ_p C9 (°)	Folding lower half (°)
1	0.68	1.36	1.2	6.3	0.68	132
2	1.0	1.36	0.25	9.9	1.5	144
3	0.88	1.36	6.7	2.6	0.21	132
4	0.80	1.36	4.2	1.5	0.076	129

Photoisomerization

Irradiation of compounds **1a**-**4a** in *n*-hexane at 312 nm results in a photochemical *E*-*Z*-isomerization. As a consequence nearly one-half rotation of the upper half relative to the lower half takes place and the thermally unstable isomers **1b**-**4b** are generated, with the methyl group in an unfavorable equatorial position (Scheme 2). This process can be followed by UV/vis absorption, CD and ^{1}H NMR spectroscopy.

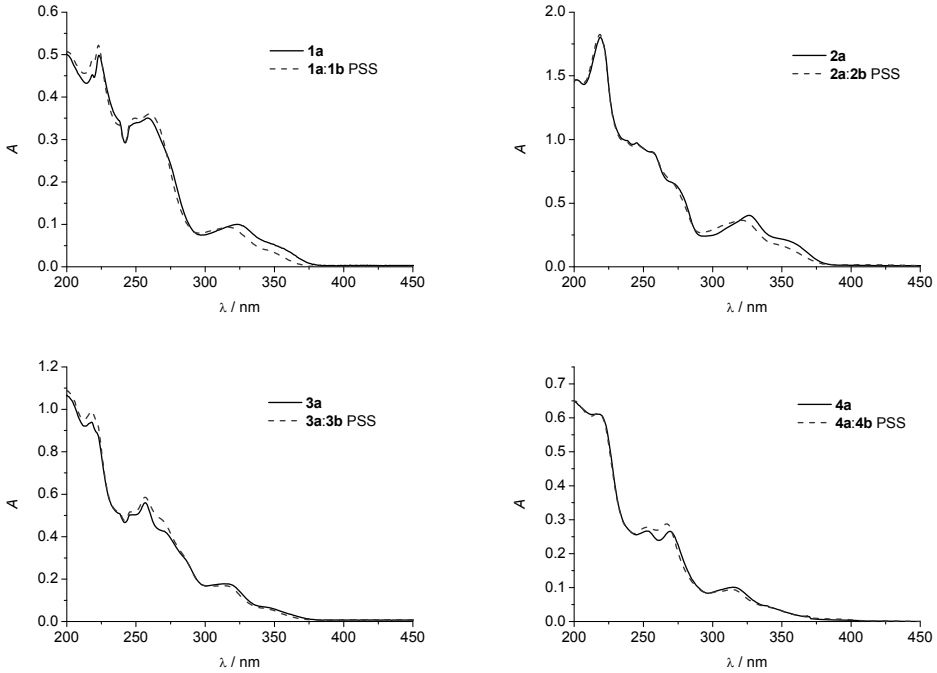

Figure 1 UV/vis absorption spectra in *n*-hexane of **1a**-**4a** (black lines) and the PSS mixture of **1a**-**4a** and **1b**-**4b** obtained after irradiation at 312 nm (red dashed lines).

In the UV/vis absorption spectra of **1-4** in *n*-hexane a decrease in the absorption around 350 nm is observed upon irradiation at 312 nm (Figure 1). For **1**, **3** and **4** this is accompanied by an increase in absorption in the 250-275 nm range, for **2** an increase around 300 nm is observed. Clear isosbestic points are observed, which indicates a unimolecular process takes place. At room temperature, thermal relaxation is not observed within one hour. Heating the solution to 70 °C overnight results in the full reversal of the spectral changes.

The quantum yield for the photoisomerization of **1-4** was determined by irradiation (312±1 nm) of a concentrated solution in toluene. The conversion to unstable **1b-4b** was followed by UV/vis absorption spectroscopy at 375 nm. The rate of conversion was then compared to the rate of decomposition of ferrioxalate under the same conditions of irradiation according to standard procedures[22] to give the quantum yield for photoisomerization (Table 2).

The photochemical *E-Z* isomerization is an equilibrium. In a photoequilibrium between species A and B, the reaction rate *r* is dependent on the quantum yield Φ and the absorbance:

$$r_{A\rightarrow B} \propto \Phi_{A\rightarrow B}\, \varepsilon_A\, [A] \qquad (1)$$

In which ε_A is the molar absorptivity of A. When equilibrium is reached, the rate of the forward reaction A→B is equal to the rate of the reverse reaction B→A:

$$r_{A\rightarrow B} = r_{B\rightarrow A} \qquad (2)$$

From (1) and (2), the quantum yield for the reverse reaction can be calculated:

$$\Phi_{B\rightarrow A} = \frac{\Phi_{A\rightarrow B}\, \varepsilon_A\, [A]}{\varepsilon_A\, [B]} \qquad (3)$$

Using equation (3), the quantum yield for the reverse photoisomerization for motors **1-4** was calculated using the PSS ratio determined by ^{1}H NMR spectroscopy and the measured quantum yield for the forward reaction (Table 2). The quantum yields for photoisomerization are all low, between 0.55% and 1.6%, presumably because there is a favorable pathway for internal conversion available from the excited state. Furthermore, **1-4** all show fluorescence, which competes with photoisomerization. For motor **2** the quantum yield for the reverse reaction is even higher than for the forward reaction. In the end, this would mean that the efficiency for the rotation is low, but as long as the thermal helix inversion takes place, the rotation remains unidirectional.[23,24]

Table 2: Photochemical conversion **1a-4a** to **1b-4b** (toluene solution, λ = 312 nm).

Motor	PSS ratio[a]	$\Phi_{\mathbf{a\rightarrow b}}$[b]	$\Phi_{\mathbf{b\rightarrow a}}$[c]
1	8:92[d]	1.6%	0.91%
2	38:62	0.55%	0.75%
3	8:92[d]	1.5%	0.17%
4	19:81	0.83%	0.12%

[a]Determined by ^{1}H NMR spectroscopy. [b]Determined by ferrioxalate actinometry. [c]Calculated from PSS ratio and quantum yield forward. [d]From reference 4.

Enantiomerically pure material for CD spectroscopy was obtained by chiral stationary phase HPLC. Due to the steric overcrowding around the central double bond, molecules **1a-4a** cannot be flat, but adopt a helical shape. This is expressed in the CD spectrum by a strong band between 250 and 300 nm and a weaker band of opposite sign at ca. 350 nm (Figure 2). Upon irradiation, the unstable forms **1b-4b** are formed, which have opposite

helicity. For **1**, **3** and **4** this is seen as an inversion of the major bands in the CD spectrum. For **2**, a complete inversion is not observed because the PSS is relatively rich in **2a**; instead a reduction in intensity of the signal due to the formation of **2b** is observed. Assignment of the absolute stereochemistry from the CD spectra of the stable and unstable form was achieved using time-dependent DFT with the B3LYP functional and the 6-31G++(d,p) basis set. The calculated spectra are overlaid with the experimental spectra (Figure 2). Since it is known that this method has a systematic deviation in the excitation energies,[25] the calculated spectra were shifted by 15 nm, to better show the agreement with the experimental data. Furthermore, the spectra were normalized to the strongest absorption band in the spectrum of compound **4**.

The overall shapes of the calculated CD spectra fit reasonably to the experimental data. Two main factors should be considered to explain the deviations. In the first place, the calculations simulate the compound in the gas phase, whereas the measurements are conducted in solution. Second, it is likely that there are multiple conformations that contribute to the experimental CD spectrum. The predicted spectrum is the spectrum of the molecule in its lowest energy conformation, but it is possible that there are several conformations which are close in energy, and thus are present under experimental conditions, that have a significantly different contribution to the overall CD spectrum. The results of the calculations are, however, sufficient to discriminate between the two possible helicities and can be used to assign the absolute stereochemistry.

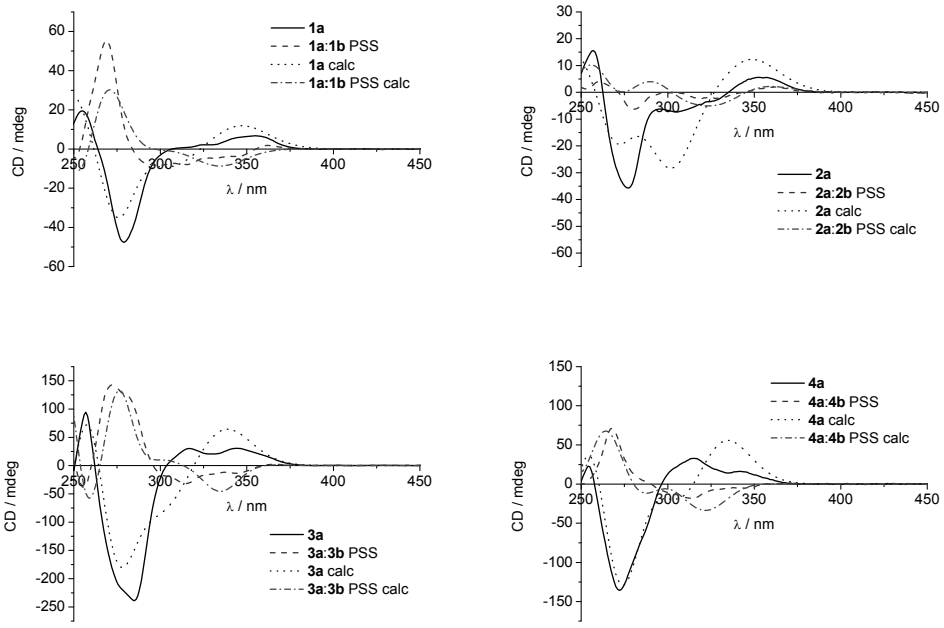

Figure 2 CD spectra in *n*-hexane of **1a**-**4a** (full lines) and the PSS mixture of **1a**-**4a** and **1b**-**4b** obtained after irradiation at 312 nm (dashed lines) compared to the calculated CD spectra of **1a**-**4a** (dotted lines) and the PSS mixture (dot-dash lines).

Thermal helix inversion

After photoisomerization, the motor is present in a thermodynamically unfavorable conformation. A thermal helix inversion relieves steric strain and allows the molecule to reach its structure of minimum energy again (**1a**-**4a**). Computational studies of this process have been reported for compound **1**.[26,27] Our calculations confirmed these results

for the most part, revealing the same intermediates and transition states, however, their order is different as well as their relative energies.
Two possible pathways were established for the thermal helix inversion, A and B. In both pathways the same steps occur, but in a different order (Figure 3). In both pathways, an initial ring flip in the thiopyran of the upper half brings the methyl group on the stereogenic centre from an equatorial to an axial position, reaching the *anti*-folded, twisted intermediate I1. This intermediate is common to both pathways. For pathway A, the upper half subsequently slips over the lower half to give twisted *syn*-folded I2, and finally a ring flip in the lower half leads to the global energy minimum, *anti*-folded **1a**. In pathway B, the order of these two steps is inverted: first a ring flip in the lower half occurs to reach *syn*-folded twisted I3, and then the upper half slips past the lower half. In both cases the rate determining step was found to be when the naphthalene moiety of the upper half slips over the lower half, going through transition state TS2 or TS6 in pathway A and B, respectively.

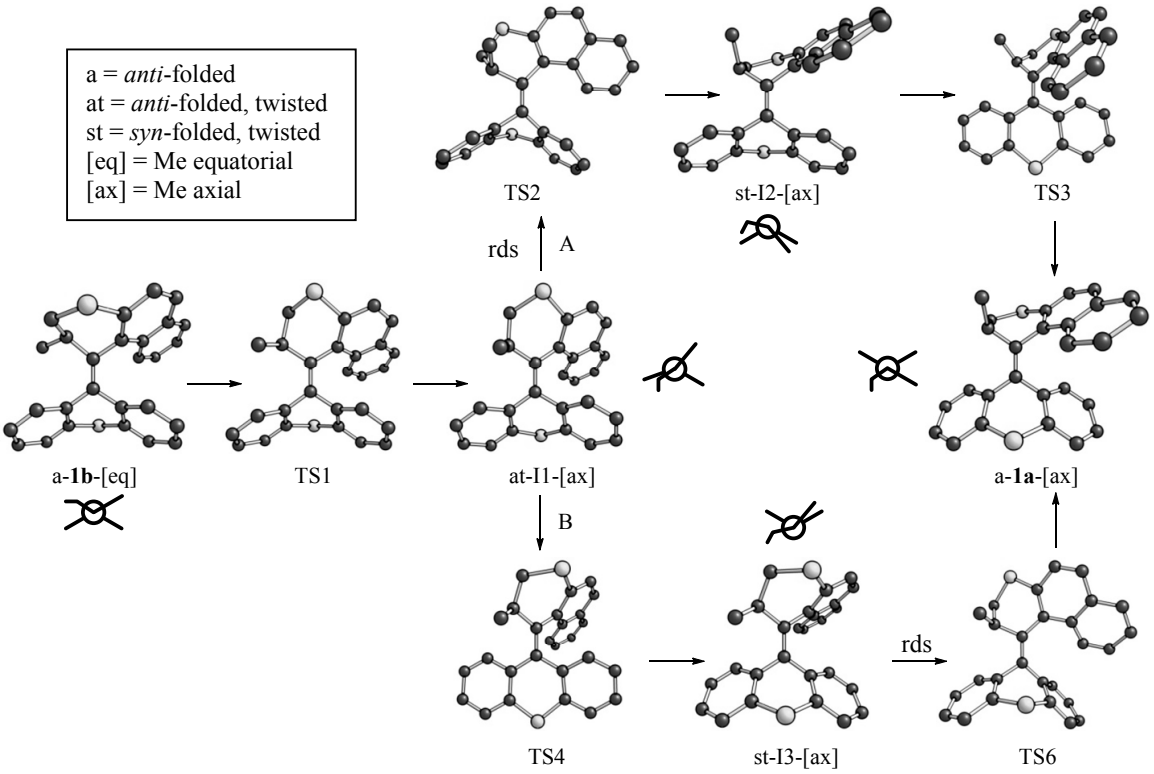

Figure 3 Thermal conversion from unstable **1b** to stable **1a** via pathways A (top) and B (bottom). With all intermediates a schematic top view of the molecule along the olefinic double bond is drawn. The rate-determining ring flip in the upper half is indicated with rds.

Another intermediate I4 (Figure 4a) was found, which was reported previously to be an intermediate in the thermal helix inversion of **1**.[27] This intermediate can indeed be reached from I3: a ring flip in the upper half brings the methyl group from an axial position back to an equatorial position. However, when calculating the intrinsic reaction coordinate (IRC) for the rate-determining transition state TS6, it turned out that I4 is not on the minimum energy pathway for motor **1**. Rather, I4 represents a conformational cul-de-sac, and to reach the global energy minimum **1a**, it needs to go back through I3 (Figure 4b).

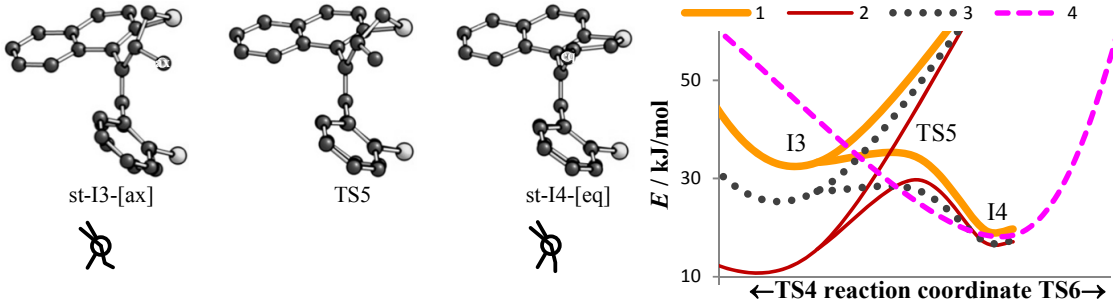

Figure 4 a) Conversion of *syn*-folded I3 with the methyl group in an axial orientation through TS5 to *syn*-folded I4 with the methyl group in an equatorial orientation. b) Energy profile along the reaction coordinate for the conversion of I3 to I4 via TS5.

Intermediates and transition states of similar geometry were found for motors **2** and **3**, although there are differences in relative energies. Whereas the pathways for thermal helix inversion for motors **1-3** are similar, motor **4** deviates somewhat. In pathway A, the same intermediates were found, but TS2 does not connect I2 and I1. When the intrinsic reaction coordinate was calculated for TS2, it was found that TS2 does not connect to I1, but rather goes directly to **4b**. Intermediate I1 does still exist, but it is not on the minimum energy pathway. From I2 a ring flip in the lower half takes place and **4a** is reached via TS3, as for motors **1-3**. In pathway B, an intermediate with a geometry similar to I3, in which the methyl group at the stereogenic center is in an axial orientation, could not be found. In this pathway, I1 is directly connected to I4 (Figure 4b). Intermediate I4 is not a conformational cul-de-sac for motor **4** as it is for **1-3**, but leads to the global energy minimum **4a** via TS6.

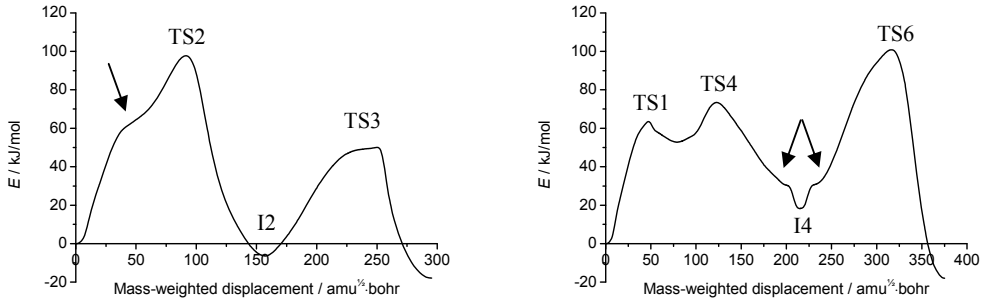

Figure 5 Minimum energy pathway A (left) and B (right) for the thermal helix inversion of **4b** to **4a** calculated with stride 0.5 amu^{½} Bohr. The arrows indicate geometries that are minima for **1-3**.

Since different intermediates for motor **4** were found than for **1-3**, calculation of the complete reaction pathway for the thermal helix inversion was carried out (Figure 5). In the IRC of pathway A, a leveling off can be seen close to the geometry of I1, as indicated by the arrow, but this intermediate is not on the minimum energy pathway. Similarly, in pathway B the curve levels off close to I3, indicated by the arrows, but this is not a true minimum. With a ring flip in the upper half the methyl group is brought to an equatorial conformation, reaching a minimum in I4. From intermediate I4, a similar geometry is again adopted on the path to TS6.

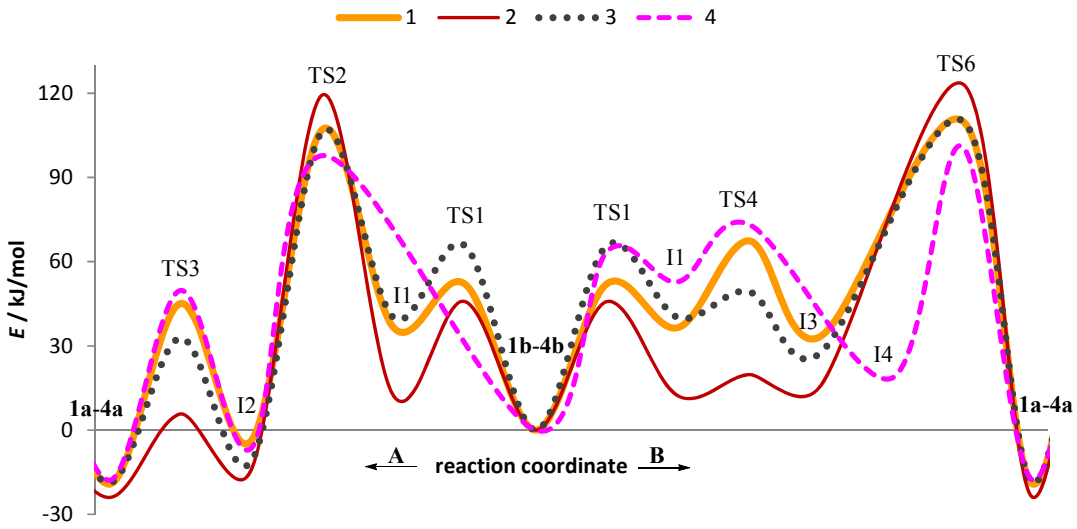

Figure 6 Energy profile along the reaction coordinate for thermal helix inversion of motors **1**-**4**.

The energy of all the transition states and intermediates was calculated, and plotted to compare motors **1-4** with each other (Figure 6). The unstable forms **1b-4b** were normalized at 0 kJ/mol, which allows for ready comparison of the energy barriers. In all cases, pathway A was found to have a slightly lower energy than pathway B, contrary to what was reported previously for motor **1**.[27] However, the difference is only *ca*. 4 kJ/mol. Compared to compound **1** the transition states in which either the upper or the lower half undergoes a ring flip are significantly lower in energy for compound **2**. However, the rate-determining transition states TS2 and TS6, in which then naphthalene upper half moves over the lower half, are higher in energy. This can be rationalized by the small folding angle of the oxygen-bridged lower half: it inverts readily but it does not fold away enough to let the upper half slip past. For compound **3** the rate-determining transition states have the same energy as for **1**. The transition state TS1 for the initial ring flip in the upper half was found to be higher in energy, despite the fact that hardly any structural change takes place in the lower half during this step. The ring flip in the lower half on the other hand has a lower barrier. In the series **1-4**, silicon-bridged motor **4** has the lowest barrier for the rate-determining step. Due to the larger folding angle in the lower half the naphthalene upper half can easily slip past.

The energy barriers calculated with DFT can be compared to the experimentally obtained Gibbs free energy of activation ($\Delta^{\ddagger}G°$) for the thermal relaxation of **1b-4b**. For motors **1-3**, $\Delta^{\ddagger}G°$ for the thermal isomerization was reported previously and for compound **4** it was determined here. A solution of **4** was irradiated (312 nm) to the PSS, and then the relaxation was followed over time using CD spectroscopy (Figure 7a). This was performed at four temperatures; Eyring analysis (Figure 7b) then provided a $\Delta^{\ddagger}G°$ of 93.3 kJ/mol for compound **4**.

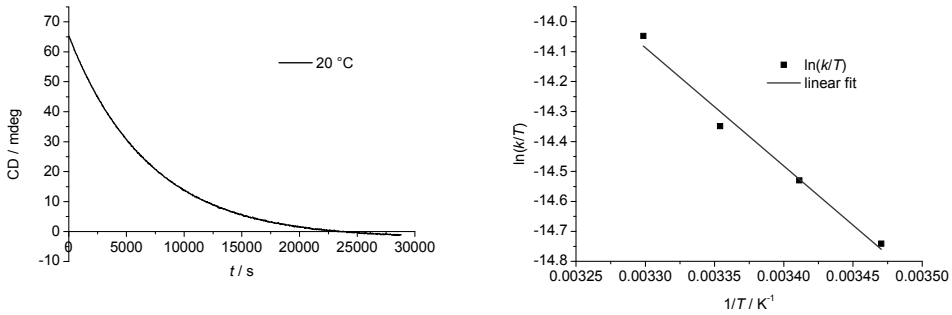

Figure 7 a) Decrease in CD signal (270 nm) of **4b** at 20 °C followed over time. b) Eyring plot for the thermal isomerization of **4**.

The self-consistent field (SCF) energies are in good agreement with experimentally determined data, with the exception of **2**, for which the calculated value is 19 kJ/mol higher than the measured barrier (Table 3). The calculated barrier could be invalid, but this is unlikely as the calculations show a good correspondence with the measured data for the other compounds. A more probable explanation is that there is an additional process with a lower barrier, such as thermal *E-Z* isomerization. The barrier for thermal *E-Z* isomerization of dixanthylene **5** is around 75 kJ/mol,[28] which is considerably lower than for dithioxanthylene **6** (115 kJ/mol[7]). In that case, the main factor for a low barrier to thermal *E-Z* isomerization was proposed to be ground state destabilization.[6] If in the present case the barrier for thermal *E-Z* isomerization is also relatively low, this would explain the results obtained. That would also imply that **2** does not in fact act as a molecular motor, but rather switches back and forth between two states. To confirm this, the barrier for thermal *E-Z* isomerization should be calculated. Furthermore, from an experimental point of view, the molecule should be substituted in a way that allows discrimination of the thermal helix inversion and the thermal *E-Z* isomerization pathways. A detailed study of thermal *E-Z* isomerization in compound **2** is currently underway.

Table 3: Barrier for thermal helix inversion of **1b**-**4b** to **1a**-**4a**.

Motor	$\Delta^{\ddagger}G°$ (kJ/mol) (measured)	SCF energy (kJ/mol) (calculated)
1	106[a]	106
2	100[a]	119
3	106[a]	106
4	93.3	97.2

[a]From ref 4.

The barrier for thermal helix inversion of the unstable form of **4** is lower than for the other motors in the series. Compound **4** shows the most folding in the lower half, which facilitates the slipping of the upper half over the lower half in the rate determining step in the thermal helix inversion. This trend seems to hold for the other motors in the series, however, this pertains to the geometry in the ground state. Considering the folding of the lower half for the different motors in the unstable form going to the transition state, the folding increases by 20° in all cases (Table 4). A more appropriate explanation for the differences in thermal isomerization is that the differences in the barriers are dependent on how well the bridging group can accommodate the extra folding that is needed to reach the transition state.

Table 4 Folding of the lower half in the **1b**-**4b** and TS2.

Motor	Folding TS2 (°)	Folding unstable (°)
1	110	128
2	118	139
3	110	128
4	106	125

To further support this, an NBO analysis was performed. Natural bond orbitals (NBOs) are a way to describe the electron density on a molecule in a way that relates well to classical Lewis structures, and was pioneered by Weinhold and coworkers.[29] It gives a combination of atomic orbitals that depicts localized bonds and lone pairs, which can make it easier to pinpoint differences in bonding when different molecules are compared. NBO analysis is typically used to study partial bonds in systems involving hydrogen bonding, donor-acceptor interactions and delocalization,[30,31] and also bonding in strained molecules.[32,33] An NBO analysis was performed on the unstable form and TS2 of motors **1**-**4**; the energies of all electrons in the orbitals on the bridging group were summed (Table 5). The methyl groups on carbon and silicon in **3** and **4** were also taken into account, because weakening of the sp^2 C-X bonds (*i.e.* 10a-X and 4a-X) may be partially compensated by strengthening of the bonds to the methyl groups.[34]
The difference between the transition state and the unstable form reflects the energy loss on the bridging group X that needs to be overcome upon isomerization. The energy differences on X between the transition state and the unstable form follow the same trend as the barrier heights, with the lowest value found for silicon and the highest for oxygen. This shows that indeed the barrier of thermal helix inversion can be correlated to the energy cost of reaching the transition state geometry in the bridging group. Using the NBO analysis, it is shown that the main contributing factor to the difference in barrier heights is located on the bridging group. The better the bridging group can accommodate the increased folding upon going to the transition state, the lower the overall barrier of the rate-determining step.

Table 5 NBO analysis of the bridging group in motors **1**-**4**.

Motor	ΔE TS2-unstable (kJ/mol)	SCF energy barrier (kJ/mol)
1	35.6	107
2	44.2	119
3	39.0	106
4	16.6	93.3

Conclusions

The photochemical and thermal isomerization processes of a series of second generation molecular motors were characterized and studied with UV/vis absorption, CD and NMR spectroscopy. Various bridging groups in the lower half influence the process of rotation because of small differences in conformation. Motors **1**-**4** undergo photochemical *E*-*Z* isomerization upon UV irradiation (312 nm). This process can be followed using UV/vis absorption and CD spectroscopy, which shows the formation of the corresponding unstable forms with opposite helicity. This was supported by TD-DFT calculations, which also allow us to assign the absolute stereochemistry of the enantiomers. The

quantum yields of photoisomerization were determined to be in the range of 0.5-1.6%. For compound **2** the quantum yield for the 'reverse' reaction was found to be higher than the 'forward' direction. Still, a favorable PSS can be obtained because of the difference in absorption between the stable and the unstable form at the wavelength of irradiation.
The thermal relaxation of the unstable form of motors **1**-**4** was modeled using DFT calculations. Two pathways for thermal helix inversion were established for these motors. In both pathways compound **2** has the highest barrier and the silicon-bridged motor **4** the lowest. This latter motor behaves somewhat differently compared to the other compounds, in that its thermal helix inversion proceeds via different intermediates. However, the transition state of the rate determining step still has similar geometry to that of motors **1**-**3**.
There is a good agreement between the calculated energy barrier and the Gibbs free energy of activation for the thermal relaxation for motors **1**, **3** and **4**. For compound **2**, the barrier calculated for the thermal helix inversion is significantly higher than the empirical value of $\Delta^{\ddagger}G°$ for thermal relaxation that was measured. Most probable, thermal relaxation of the unstable form of **2** does not proceed via helix inversion. A possible alternative is thermal *E*-*Z* isomerization, which would compromise the rotation process. However, further investigation is necessary to confirm this.
A clear correlation between the ground state geometries and the $\Delta^{\ddagger}G°$ for thermal helix inversion could not be found. The folding angle in the lower half gives an indication, however, that the main factor is the energy cost to increase the degree of folding to the level needed in the transition state. This energy cost is lowest for the silicon bridged motor **4**, which also shows the most folding in the lower half in the ground state.
Overall, our understanding of the rotation process of these second generation molecular motors has greatly increased by combining experimental work with computational data. The DFT calculations allow for visualization of the conformational behavior and can predict geometries of intermediates and transition states and their energy. This work will help in identifying new motor topologies to explore and to understand how to incorporate them into more advanced systems to take advantage of their unique dynamics.

Acknowledgements
The synthesis of compound **4** was performed by Tatsuo Kojima. Computational chemistry on the thermal helix inversion was performed by Jos Kistemaker. Both are gratefully acknowledged for their contributions.

Experimental section

Synthesis

General
Unless stated otherwise all reagents were obtained from commercial sources and used as received without further purification. Solvents for reactions were reagent grade and distilled and dried according to standard procedures. Column chromatography was performed on silica gel (Aldrich 60, 230-400 mesh) using positive pressure. Solvents for spectroscopic studies were spectrophotometric grade (UVASOL Merck). NMR spectra were recorded on a Varian Gemini-200 (^{1}H: 200 MHz, ^{13}C: 50 MHz), Varian VXR-300 (^{1}H: 300 MHz), Varian AMX400 (^{1}H: 400 MHz, ^{13}C: 100 MHz) or Varian Unity Plus (^{1}H: 500 MHz, ^{13}C: 125 MHz) spectrometer. Chemical shifts are denoted in δ-units (ppm)

relative to the residual solvent peak ($CDCl_3$: ^1H δ = 7.26, ^{13}C δ = 77.0; DMSO: ^1H δ = 2.49, ^{13}C δ = 39.5). The splitting parameters are designated as follows: s = singlet, d = doublet, t = triplet, q = quartet, m = multiplet, dd = doublet of doublets, br = broad. (HR)MS spectra were obtained with an AEI MS-902. HPLC was performed on a Shimadzu semi-prep system consisting of a LC-20T pump, a DGU-20A degasser, a CBM-20A control module, a SIL-20AC autosampler, a SPD-M20A diode array detector and a FRC-10A fraction collector.

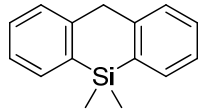

5,5-dimethyl-5,10-dihydrodibenzo[*b*,*e*]siline

This compound was prepared via a modified literature procedure:[21] to a solution of bis(2-bromophenyl)methane (12 g, 37 mmol) in Et_2O (150 mL) was added a solution of *n*-BuLi (1.6 M in hexane, 50 mL, 77 mmol) at 0 °C. The resulting yellow mixture was stirred for 1 h at 0 °C followed by the dropwise addition of dichlorodimethylsilane (5.3 mL, 44 mmol) at -78 °C. The cooling bath was removed and the mixture was stirred overnight. The resulting colorless precipitation was removed by filtration and washed with Et_2O. The organic layer was washed with water and dried on Na_2SO_4. The removal of the organic solvent gave 9.4 g of the title compound with high enough purity for the next reaction. ^1H NMR (300 MHz, $CDCl_3$) δ 0.54 (s, 6H), 3.98 (s, 2H), 7.12-7.31 (m, 4H), 7.35 (d, *J* = 7.0 Hz, 2H), 7.56 (dd, *J* = 6.7, 1.6 Hz, 2H).

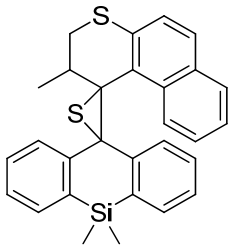

Episulfide 11

A mixture of ketone **9** (0.30 g, 1.3 mmol) and Lawesson's reagent (0.61 g, 1.5 mmol) in toluene (8 mL) was heated at reflux for 15 h. After filtration of the precipitate the solvent was removed under reduced pressure. The residue was dissolved in a minimum amount of dichloromethane and absorbed immediately onto silica (1 g) under reduced pressure. This was loaded onto a small silica column (3 g) and a blue band was rapidly eluted with pentane to yield 0.15 g of impure thioketone **10** as a blue solid. Compound **8** is unstable under ambient conditions and was used immediately without any further purification. In parallel, to a solution of hydrazone **7** (0.15 g, 0.63 mmol) in DMF (10 mL) at 0 °C was added $PhI(OAc)_2$ (0.20 g 0.63 mmol). The resulting mixture was stirred for 2 h at 0 °C and then transferred into the flask containing thioketone **10**. The resulting solution was stirred for 7 h at rt and poured into water followed by extraction with ethyl acetate. The organic layer was washed with water three times and dried on Na_2SO_4. The solvents were removed under reduced pressure followed by column chromatography (SiO_2, pentane) yielding episulfide **11** (0.12 g, 40% based on hydrazone **7**) as a colorless solid. ^1H NMR (400 MHz, $CDCl_3$) δ 0.18 (s, 3H), 0.87 (s, 3H), 1.06 (d, *J* = 6.9 Hz, 3H), 2.19 (dd, *J* = 12.0, 5.8 Hz, 1H), 2.28 (dd, *J* = 12.0, 9.2 Hz, 1H), 2.80 (ddd, *J* = 9.2, 6.9, 5.8 Hz, 1H), 6.28 (ddd, *J* = 8.2, 7.4, 1.6 Hz, 1H), 6.80 (td, *J* = 7.2, 1.1 Hz, 1H), 6.83 (d, *J* = 8.3 Hz,

1H), 7.02 (d, J = 8.2 Hz, 1H), 7.24 (dd, J = 7.2, 1.5 Hz, 1H), 7.28 (d, J = 8.4 Hz, 1H), 7.35-7.43 (m, 3H), 7.53 (ddd, J = 8.6, 6.7, 1.4 Hz, 1H), 7.62-7.67 (m, 2H), 8.27 (dd, J = 7.4, 1.6 Hz, 1H), 8.80 (d, J = 8.7 Hz, 1H); ^{13}C NMR (100 MHz, $CDCl_3$) δ 0.5 (q), 3.4 (q), 21.5 (q), 35.3 (t), 40.9 (d), 64.1 (s), 66.4 (s), 122.9 (d), 124.4 (d), 125.4 (d), 125.5 (d), 126.0 (d), 126.6 (d), 126.9 (d), 127.2 (d), 128.1 (d), 128.3 (d), 129.2 (d), 131.2 (d), 131.3 (s), 132.3 (s), 132.4 (d), 134.3 (d), 134.7 (s), 135.9 (s), 138.1 (s), 138.9 (s), 143.1 (s), 144.7 (s); HRMS (ESI+): calcd for $C_{29}H_{27}S_2Si^+$ $[M+H]^+$ 467.1318, found 467.1312.

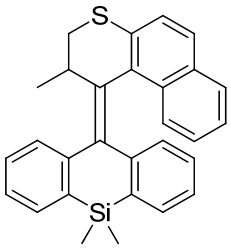

5,5-dimethyl-10-(2-methyl-2,3-dihydro-1*H*-benzo[*f*]thiochromen-1-ylidene)-5,10-dihydrodibenzo[*b*,*e*]siline 4

A mixture of episulfide **11** (0.10 g, 0.21 mmol) and copper bronze (0.14 g, 2.1 mmol) in *p*-xylene (3 mL) was heated at reflux for 14 h. The resulting mixture was passed through a short plug of silica using dichloromethane as eluent. Removal of the organic solvents followed by column chromatography (SiO_2), pentane:EtOAc = 100:1) afforded alkene **4** (81 mg, 87%) as a colorless solid. ^{1}H NMR (400 MHz, $CDCl_3$) δ 0.64 (s, 3H), 0.75 (s, 3H), 0.77 (d, J = 7.0 Hz, 3H), 2.92 (dd, J = 11.7, 4.0 Hz, 1H), 3.62 (dd, J = 11.7, 8.6 Hz, 1H), 4.15-4.20 (m, 1H), 6.28 (d, J = 8.1 Hz, 1H), 6.42 (t, J = 7.6 Hz, 1H), 6.75 (t, J = 7.3 Hz, 1H), 6.95 (dd, J = 8.4, 6.9 Hz, 1H), 7.12 (dd, J = 8.1, 6.9 Hz, 1H), 7.33 (t, J = 7.3 Hz, 1H), 7.37 (d, J = 7.1 Hz, 1H), 7.43 (t, J = 7.6 Hz, 1H), 7.44-7.49 (m, 2H), 7.58 (d, J = 8.1 Hz, 1H), 7.63 (d, J = 8.5 Hz, 1H), 7.67-7.71 (m, 2H); ^{13}C NMR (100 MHz, $CDCl_3$) δ -4.4 (q), -1.1 (q), 20.5 (q), 34.9 (d), 37.5 (t), 124.3 (d), 124.9 (d), 125.1 (d), 125.4 (d), 126.1 (d), 126.5 (d), 127.2 (d), 127.4 (d), 127.4 (d), 128.1 (d), 128.3 (d), 128.4 (d), 130.9 (s), 131.6 (s), 132.3 (d), 133.0 (d), 134.5 (s), 135.4 (s), 135.5 (s), 137.3 (s), 137.5 (s), 138.0 (s), 146.5 (s), 147.8 (s); HRMS (ESI+): calcd for $C_{29}H_{27}SSi^+$ $[M+H]^+$ 435.1597, found 435.1594.

HPLC resolution

Compound **1**: Chiralcel ODH column, 99.8:0.2 *n*-heptane:2-propanol, T = 40 °C, flow rate 0.5 mL/min, retention times 9 min, 11 min.

Compound **2**: Chiralpak ADH column, 99:1 *n*-heptane:2-propanol, T = 40 °C, flow rate 0.5 mL/min, retention times 11 min, 13 min.

Compound **3**: Chiralcel ODH column, 99.8:0.2 *n*-heptane:2-propanol, T = 40 °C, flow rate 0.5 mL/min, retention times 18 min, 21 min.

Compound **4**: Chiralcel ODH column, 99.9:0.1 *n*-heptane:2-propanol, T = 40 °C, flow rate 0.5 mL/min, retention times 18 min, 23 min.

Computational chemistry

The Gaussian 09 program was used for geometry optimizations and the calculation of energies.[35] Initial geometries were optimized using semi-empirical PM3. Geometry optimizations were performed on B3LYP/6-31G(d,p) using tight convergence criteria. To ensure minima and transition states were reached, frequency analyses of the obtained structures were evaluated; all minima had no imaginary frequencies while all transition

states were first-order. Energies reported are SCF energies. CD spectra were calculated using B3LYP/6-31++G(d,p). IRC calculations were performed using the Firefly QC package,[36] which is partially based on the GAMESS (US)[37] source code, using the Gonzalez-Schlegel second order method. For natural bond order analysis, the NBO 3.1 program embedded in Gaussian 09 was used.[38]

UV/vis absorption and CD spectroscopy

UV/Vis absorption spectra were measured on a Jasco V-630 or a Hewlett-Packard 8453 spectrometer. CD spectra were measured on a Jasco J-815 CD spectrometer. All spectra were recorded at rt using spectroscopic grade *n*-hexane as a solvent. Irradiation was performed using a spectroline ENB-280C/FE lamp (λ_{max} = 312 nm). To ensure photostationary state was reached, several spectra were recorded at set intervals.

References

[1] D. A. Leigh, F. Zerbetto, E. R. Kay, *Angew. Chem. Int. Ed.* **2007**, *46*, 72-191.
[2] W. R. Browne, B. L. Feringa, *Nature Nanotechnol.* **2006**, *1*, 25-35.
[3] N. Koumura, R. W. J. Zijlstra, R. A. van Delden, N. Harada, B. L. Feringa, *Nature* **1999**, *401*, 152-155.
[4] N. Koumura, E. M. Geertsema, M. B. van Gelder, A. Meetsma, B. L. Feringa, *J. Am. Chem. Soc.* **2002**, *124*, 5037-5051.
[5] N. Koumura, E. M. Geertsema, A. Meetsma, B. L. Feringa, *J. Am. Chem. Soc.* **2000**, *122*, 12005-12006.
[6] P. U. Biedermann, J. J. Stezowski, I. Agranat, *Eur. J. Org. Chem.* **2001**, 15-34, and references therein.
[7] B. L. Feringa, W. F. Jager, B. de Lange, *Tetrahedron Lett.* **1992**, *33*, 2887-2890.
[8] P. U. Biedermann, J. J. Stezowski, I. Agranat, *Chem. Eur. J.* **2006**, *12*, 3345-3354.
[9] N. Assadi, S. Pogodin, S. Cohen, A. Levy, I. Agranat, *Struct. Chem.* **2009**, *20*, 541-556.
[10] M. Black, C. Woodford, N. S. Mills, *J. Org. Chem.* **2011**, *76*, 2286-2290.
[11] A. M. Piekarski, N. S. Mills, A. Yousef, *J. Am. Chem. Soc.* **2008**, *130*, 14883-14890.
[12] J. Vicario, M. Walko, A. Meetsma, B. L. Feringa, *J. Am. Chem. Soc.* **2006**, *128*, 5127-5135.
[13] E. M. Geertsema, N. Koumura, M. K. J. ter Wiel, A. Meetsma, B. L. Feringa, *Chem. Commun.* **2002**, 2962-2963.
[14] E. M. Geertsema, S. J. van der Molen, M. Martens, B. L. Feringa, *P. Natl. Acad. Sci. USA* **2009**, *106*, 16919-16924.
[15] R. A. van Delden, M. K. J. ter Wiel, M. M. Pollard, J. Vicario, N. Koumura, B. L. Feringa, *Nature* **2005**, *437*, 1337-1340.
[16] M. M. Pollard, M. K. J. ter Wiel, R. A. van Delden, J. Vicario, N. Koumura, C. R. van den Brom, A. Meetsma, B. L. Feringa, *Chem. Eur. J.* **2008**, *14*, 11610-11622.
[17] R. A. van Delden, N. Koumura, A. Schoevaars, A. Meetsma, B. L. Feringa, *Org. Biomol. Chem.* **2003**, *1*, 33-35.
[18] M. K. J. ter Wiel, R. A. van Delden, A. Meetsma, B. L. Feringa, *Org. Biomol. Chem.* **2005**, *3*, 4071-4076.
[19] J.-F. Morin, Y. Shirai, J. M. Tour, *Org. Lett.* **2006**, *8*, 1713-1716.
[20] J. Y. Corey, M. J. Dye, R. L. Farrell, M. V. Mitchell, *J. Organomet. Chem.* **1978**, *153*, 127-135.
[21] F. Bickelhaupt, C. Jongsma, P. de Koe, R. Lourens, N. R. Mast, G. L. van Mourik, H. Vermeer, R. J. M. Weustink, *Tetrahedron* **1976**, *32*, 1921-1930.
[22] *Handbook of Photochemistry* (Eds.: M. Montalti, A. Credi, L. Prodi, M. T. Gandolfi), CRC Press, Boca Raton, **2006**, pp. 602-604.
[23] M. Klok, W. R. Browne, B. L. Feringa, *Phys. Chem. Chem. Phys.* **2009**, *11*, 9124-9131.
[24] E. M. Geertsema, S. J. van der Molen, M. Martens, B. L. Feringa, *Proc. Natl. Acad. Sci. U. S. A.* **2009**, *106*, 16919-16924.
[25] S. Grimme, F. Neese, *J. Chem. Phys.* **2007**, *127*, 154116.
[26] M. Klok, M. Walko, E. M. Geertsema, N. Ruangsupapichat, J. C. M. Kistemaker, A. Meetsma, B. L. Feringa, *Chem. Eur. J.* **2008**, *14*, 11183-11193.
[27] G. Pérez-Hernández, L. González, *Phys. Chem. Chem. Phys.* **2010**, *12*, 12279-12289.
[28] I. Agranat, Y. Tapuho, *J. Am. Chem. Soc*. **1979**, *101*, 665-671.
[29] J. P. Foster, F. Weinhold, *J. Am. Chem. Soc.* **1980**, *102*, 7211-7218.
[30] A. E. Reed, L. A. Curtiss, F. Weinhold, *Chem. Rev.* **1988**, *88*, 899-926.
[31] N. Kobayashi, T. Ishizaki, K. Ishii, H. Konami, *J. Am. Chem. Soc.* **1999**, *121*, 9096-9110.
[32] R. R. Sauers, J. S. Harris, *J. Org. Chem.* **2001**, *66,* 7951-7954.

[33] A. Ebrahimi, F. Deyhimi, H. Roohi, *J. Mol. Struct. (Theochem)* **2003**, *626*, 223-229.
[34] M.-C. Ou, S.-Y. Chu, *J. Mol. Struct. (Theochem)* **1995**, *357*, 141-146.3
[35] Gaussian 09, Revision B.01, M. J. Frisch, G. W. Trucks, H. B. Schlegel, G. E. Scuseria, M. A. Robb, J. R. Cheeseman, G. Scalmani, V. Barone, B. Mennucci, G. A. Petersson, H. Nakatsuji, M. Caricato, X. Li, H. P. Hratchian, A. F. Izmaylov, J. Bloino, G. Zheng, J. L. Sonnenberg, M. Hada, M. Ehara, K. Toyota, R. Fukuda, J. Hasegawa, M. Ishida, T. Nakajima, Y. Honda, O. Kitao, H. Nakai, T. Vreven, J. A. Montgomery, Jr., J. E. Peralta, F. Ogliaro, M. Bearpark, J. J. Heyd, E. Brothers, K. N. Kudin, V. N. Staroverov, R. Kobayashi, J. Normand, K. Raghavachari, A. Rendell, J. C. Burant, S. S. Iyengar, J. Tomasi, M. Cossi, N. Rega, J. M. Millam, M. Klene, J. E. Knox, J. B. Cross, V. Bakken, C. Adamo, J. Jaramillo, R. Gomperts, R. E. Stratmann, O. Yazyev, A. J. Austin, R. Cammi, C. Pomelli, J. W. Ochterski, R. L. Martin, K. Morokuma, V. G. Zakrzewski, G. A. Voth, P. Salvador, J. J. Dannenberg, S. Dapprich, A. D. Daniels, Ö. Farkas, J. B. Foresman, J. V. Ortiz, J. Cioslowski, and D. J. Fox, Gaussian, Inc., Wallingford CT, **2009**.
[36] Alex A. Granovsky, Firefly version 7.1.G, www http://classic.chem.msu.su/gran/firefly/index.html
[37] M. W. Schmidt, K. K. Baldridge, J. A. Boatz, S. T. Elbert, M. S. Gordon, J. H. Jensen, S. Koseki, N. Matsunaga, K. A. Nguyen, S. Su, T. L. Windus, M. Dupuis, J. A. Montgomery, *J. Comput. Chem.* **1993**, *14*, 1347-1363.
[38] NBO Version 3.1, E. D. Glendening, A. E. Reed, J. E. Carpenter, and F. Weinhold.

Chapter 3: Spectroscopic studies of structural dynamics during photoisomerization of second generation molecular motors[I]

In this chapter a series of molecular motors with different electron donating and electron withdrawing substituents is studied, with a focus on the structural dynamics during photoisomerization. In time-resolved fluorescence up-conversion measurements two coherently excited vibrational modes were identified which likely represent twisting or pyramidalization around the double central bond. Ground state vibrational spectroscopy studies were performed which form the groundwork for future time-resolved vibrational spectroscopy to unambiguously assign these vibrational modes.

Introduction

Since the first development of light-driven rotary molecular motors based on overcrowded alkenes in 1999,[1] considerable effort has focused on improving the original system. This has led to the design of many structural variants of the original molecular motor.[2] In this way, a good understanding of the effects that influence the speed and unidirectionality of the rotation has been obtained (see also Chapter 1). As discussed in earlier chapters, these motors operate by photochemical isomerizations followed by thermal helix inversions. Since the photoisomerization takes place on short timescales, efforts to increase the rate of rotation of these molecular motors have focused on the thermal helix inversion. Several examples where the rate of thermal helix inversion has been controlled by changing the steric crowding around the central double bond were discussed in the previous chapters. In an attempt to control the rate of thermal helix inversion by changing electronic properties rather than the steric environment, a series of molecular motors was synthesized with electron donating and electron withdrawing groups in conjugation across the central double bond to a fluorenyl lower half. It was anticipated that a donating group at the 5' position increases single bond character in the C9-C1' bond (Scheme 1).[3] Increased single bond character would result in a longer C-C bond and greater flexibility. This in turn could facilitate the thermal helix inversion, the rate of which is dependent on the steric hindrance between the upper and lower part of the molecule.

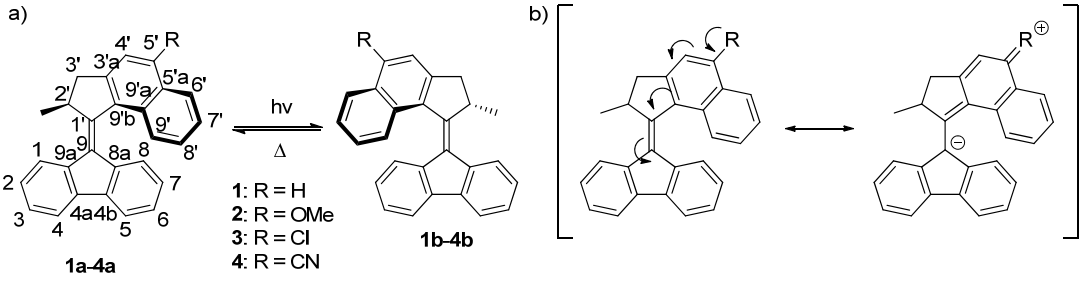

Scheme 1 a) Motors **1**-**4** with electron donating and electron withdrawing substitutents. b) In the case of an electron donating substituent, the central double bond is expected to have more single bond character which could facilitate thermal helix inversion.

[I] Part of the work presented in this chapter has been published: J. Conyard, K. Addison, I. A. Heisler, A. Cnossen, W. R. Browne, B. L. Feringa, S. R Meech, *Nature Chem.* **2012**, *4*, 547-551.

Unfortunately, no effect of the substituents on the thermal helix inversion was observed outside of experimental uncertainty, however, there was a distinct effect on the photoisomerization.[3] The photostationary states obtained after UV irradiation were more favorable with electron withdrawing substituents (e.g. **3**, **4**), and this could not be rationalized by differences in the UV/vis absorption spectra. These findings prompted us to study the photoisomerization of these motors and the effects of substituents on the photochemistry in more detail.

Information regarding the structure of the product of the photoisomerization has been obtained from UV/vis absorption, circular dichroism and NMR spectroscopy. Studies into the events *during* the photoisomerization of motors have been limited so far. Transient-absorption experiments allow for a qualitative description of the potential energy surfaces of the ground and excited states to be constructed.[4]

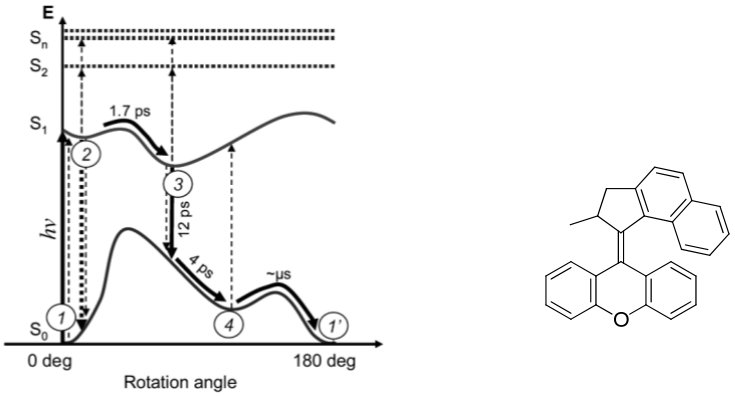

Figure 1 Schematic potential energy surface for a second generation molecular motor. After photoexcitation of the initial state (1→2), the molecule relaxes over a small barrier to a minimum in the excited state (2→3). From this minimum, the molecule relaxes to the ground state and reaches the unstable form (3→4). Thermal helix inversion from the unstable form takes place on much longer timescale. Figure reproduced from ref 4.

Furthermore, computational studies on two different first generation molecular motors supported the empirical observation that there is a preferred direction of rotation upon photoexcitation.[5,6] This was explained by a steeply sloped potential energy surface (PES) in the excited state that leads to a conical intersection where a nonadiabatic transition from the excited state to the ground state takes place. In other words, the stable *trans* isomer isomerizes preferentially towards the unstable *cis* after excitation and not to unstable *trans*, and the stable *cis* photoisomerizes to the unstable *trans* and not to unstable *cis*. Two examples of calculations on second generation molecular motors show similar results, and predict relaxation of the excited state after photoexcitation towards a conical intersection on the picosecond timescale.[7,8] During relaxation, both a twisting motion around the axis of rotation and a pronounced pyramidalization at C9 is predicted. The geometry in the conical intersection shows a twist angle of 120° between the upper half and the fluorene moiety (C9'b-C9-C1'-C9a). The pyramidalization in the excited state seems counter-intuitive, because pyramidalization in the ground state mostly takes place on C1', leaving the conjugated fluorene system intact. Presumably, steric interactions are minimized in this geometry.

In this chapter experimental evidence to support these findings using various spectroscopic techniques is presented. In the first part of the chapter, the isomerization processes of a series of motors are characterized. In the second part of the chapter, the use of vibrational spectroscopy as a tool to study the isomerization of molecular motors is

explored. Motor **1** is examined more in-depth to gain insight into the structural dynamics during photoisomerization.

Results and discussion

Synthesis

The synthesis of compounds **1-4** was performed following previously reported procedures (Scheme 2). Starting from a suitably substituted naphthalene, a one pot Friedel-Crafts acylation/Nazarov cyclization yields **6**. Conversion of the ketone moiety to a thioketone was performed with Lawesson's reagent. Reaction of the appropriate thioketone with 9-diazofluorene followed by desulfurization yields motors **1-3** in relatively good yields.

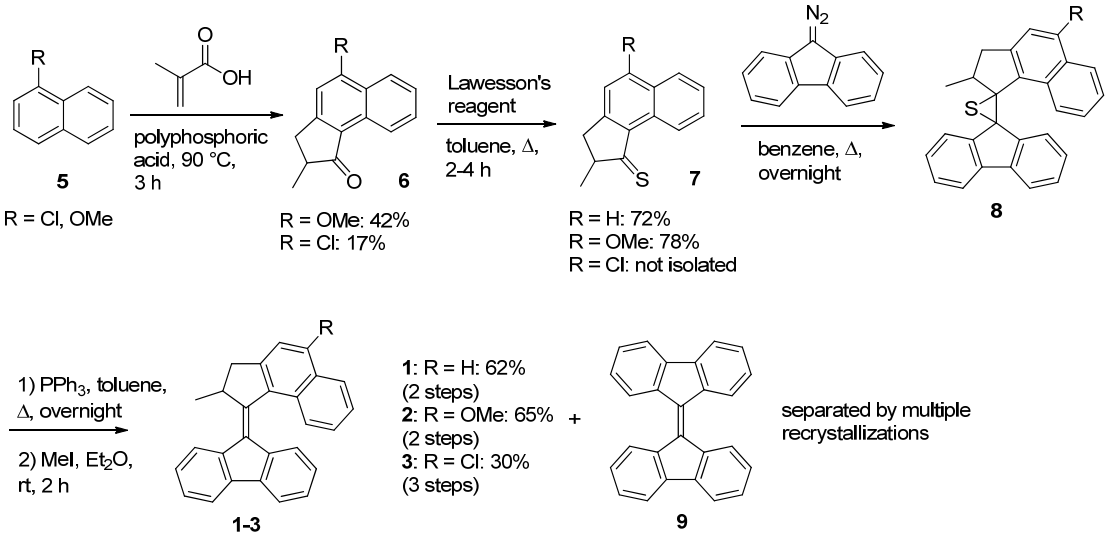

Scheme 2 Synthesis of substituted motors **1-3**.

A common by-product in this reaction is bifluorenylidene **9**, which can be difficult to separate from apolar motors **1** and **3** by column chromatography. Crystallization from hot heptane yields **1** and **3** as yellow to orange blocks whereas **9** crystallizes as orange-red needles. Repeated crystallization and manual separation of the crystals afforded samples with a purity of >99% by HPLC. Motor **4** was obtained via palladium-catalyzed cyanation of chloro-substituted motor **3** (Scheme 3).

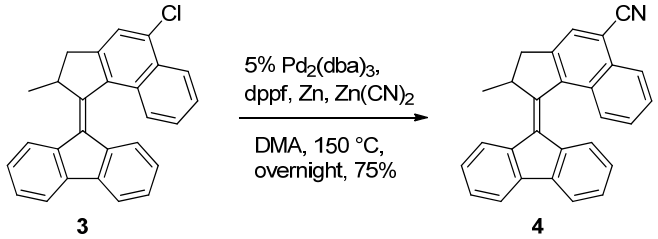

Scheme 3 Synthesis of substituted motor **4**.

During the photoisomerization step, the upper part of the molecule performs a nearly one-half rotation relative to the lower half. A fifth molecular motor (**19**) was designed in which both the upper and lower half are functionalized to study whether or not this has an effect on the rate of photoisomerization. These substituents may act as paddles, hindering the rotation by increasing interactions with the solvent, in which case the photoisomerization may be retarded. Phenylacetylene was chosen as a substituent because

it is relatively rigid, has a minor electronic effect and can be introduced conveniently in both the upper and the lower half via palladium-catalyzed cross-coupling reactions. The 3 and 6 position of the fluorene were chosen for functionalization because the substituents point away from the *fjord* region and a minimum of steric interactions with the upper half is expected. In this way, the conformation of the motor is expected to be comparable to that of **1**-**4**, as well as the rate of thermal isomerization.

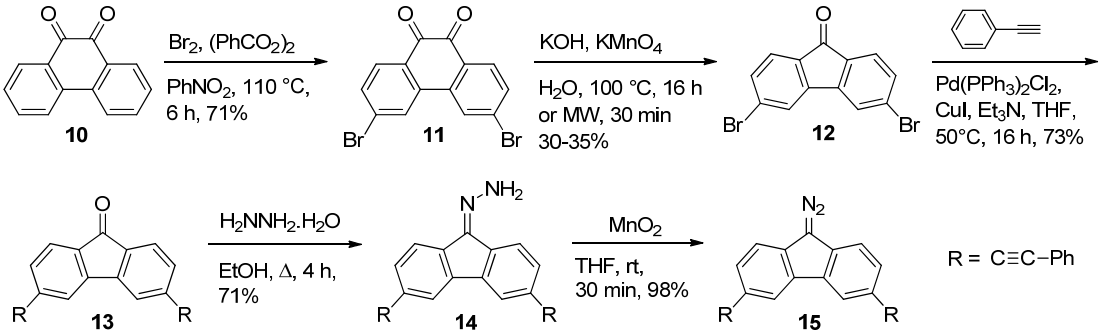

Scheme 4 Synthesis of phenylacetylene-functionalized diazofluorene **15**.

For the synthesis of the lower half, bromination of 9,10-phenanthrenequinone yields compound **11** in the first step (Scheme 4). This could be converted to **12** by heating with KOH and $KMnO_4$ resulting in a benzilic acid rearrangement followed by oxidative decarboxylation. Instead of classical conditions, the reaction could also be performed under microwave irradiation; this did not improve the yield however, and scaled up poorly at more than 1 g. Sonogashira coupling of phenylacetylene to **12** proceeded smoothly to give phenylacetylene-substituted fluorenone **13**. Hydrazone formation was effected by heating of **13** with hydrazine hydrate in ethanol. Hydrazone **14** was oxidized to **15** in nearly quantitative yield with MnO_2. Although degradation of **15** was not observed, it was not stored but used immediately in the next step.

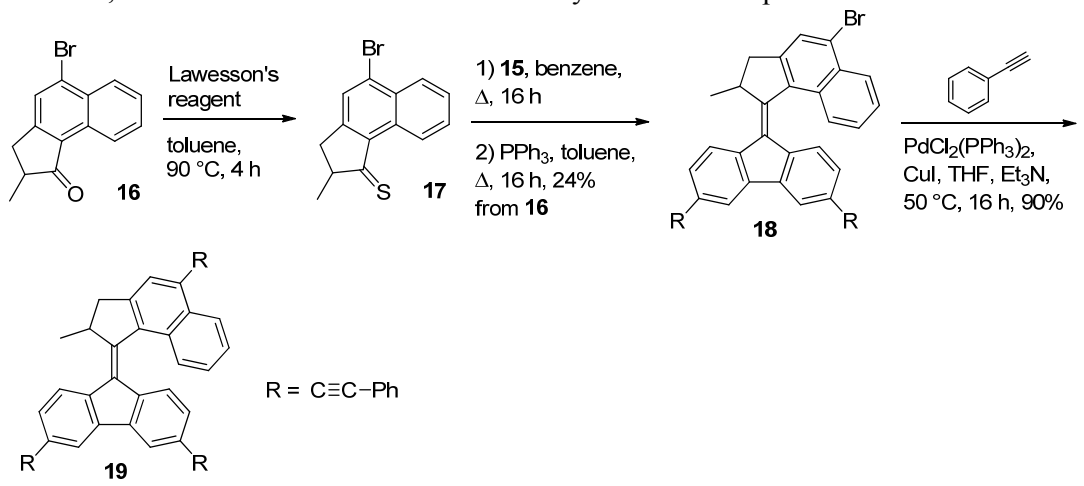

Scheme 5 Synthesis of phenylacetylene-substituted motor **19**.

For the coupling to the lower half, bromide-substituted ketone **16** was converted to thioketone **17** with Lawesson's reagent (Scheme 5). Thioketone **17** was reacted with diazo compound **15** in a Barton-Kellogg reaction, followed by desulfurization, yielding bromide-functionalized motor **18** in 24% over three steps. Finally, Sonogashira coupling of phenylacetylene to **18** provided motor **19** in good yield.

Conformational analysis

The optimized geometry of compounds **1**-**4** and **19** was calculated in both the stable and unstable form on the B3LYP/6-31G(d,p) level of theory. The length of the central double bond (C9-C1'), the twist angle between the upper and lower half (the dihedral angle C9'b-C1'-C9-C8a) and the pyramidalization of C1' give an indication of the distortion of the double bond due to the steric overcrowding (Table 1). The pyramidalization on an atom is defined as the angle between one of its bonds and the basal plane of the pyramid made up of the atom and its substituents; for a 'perfect' sp^2-hybridized carbon atom this is 0°, for a 'perfect' sp^3 carbon atom it is 19.5 (see also Chapter 2).

Table 1 Selected calculated bond lengths and distortion angles for motors **1**-**4** and **19**.

		Stable form			Unstable form		
Motor	R	Bond length C9-C1' (pm)	Twist angle C9'b-C1'-C9-C8a (°)	Pyramid-alization (°)	Bond length C9-C1' (pm)	Twist angle C9'b-C1'-C9-C8a (°)	Pyramid-alization (°)
1	H	136.94	14.15	2.74	137.74	153.29	1.27
2	OMe	137.08	14.44	2.61	137.92	153.32	1.27
3	Cl	136.92	13.97	2.83	137.73	153.44	1.29
4	CN	136.91	14.03	2.78	137.73	153.25	1.31
19	CCPh	137.35	14.82	2.68	135.25	154.87	1.19

The central double bond C9-C1' is in all cases only slightly elongated compared to a normal double bond (137 vs 134 pm). There is no significant difference in the C9-C1' bond length between **1**-**4** and **19**, and there is no clear effect of electron donating or electron withdrawing groups. The twist angle reflects the fact that the molecule can not be flat due to steric interactions, and as a consequence adopts a helical shape. In the stable form, it is around 14° for **1**-**4** and **19**, in the unstable form around 153°, with a slightly larger value for **19**. The pyramidalization at C1' is less in the unstable form than in the stable form, presumably because it is in a twisted conformation. The twist angle across the double bond is larger, which allows for less pyramidalization.

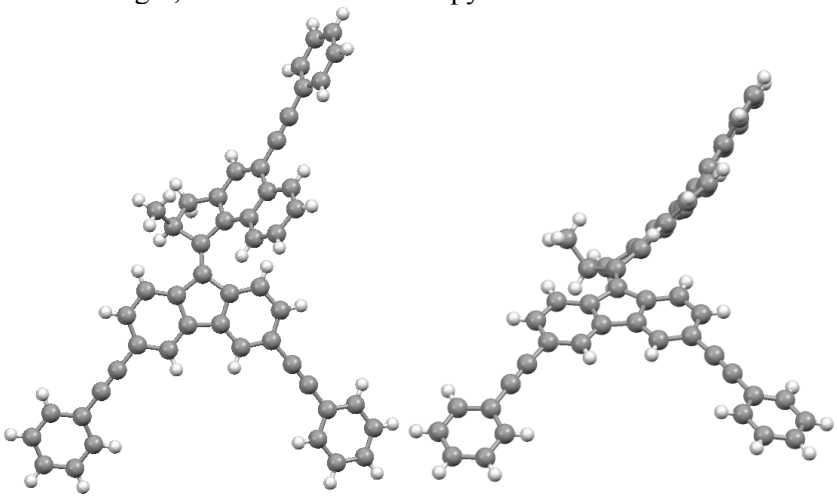

Figure 2 X-ray structure of motor **19**.

The optimized geometry of **19** was compared to the crystal structure. Single crystals of **19** suitable for X-ray analysis were obtained by crystallization from hot heptane; the analysis was performed by Dr. Martin Lutz at Utrecht University. As expected, the fluorene part of the molecule is flat, while the five-membered ring in the upper half shows considerable distortion. The twist angle, which is the angle between the fluorene lower half and the naphthalene upper half, is 16.6(2)°. The bond length for the central olefinic bond is 136.69(16) pm. The sp^2 carbon that is part of the central double bond shows considerable sp^3 character. The pyramidalization is calculated from the bond angles and is 2.64°. Overall, the structure of **19** is as expected for an overcrowded alkene and is similar to the structure of **1** and related motors.[9,10] The distortions also show a reasonably good correlation to the calculated structure.
From the results of the conformational analysis we can rationalize the observation that there is no difference in the rate of thermal helix inversion for motors **1**-**4** (*vide supra*). From the lack of variation in the length of the central double bond, we can conclude that the expected resonance contribution of the electron donating and withdrawing groups is negligible in both the stable and unstable form, at least in the ground state. There is also no significant difference in conformation, reflected from the twist angle and pyramidalization; therefore, there is no difference in rate of thermal helix inversion.

Quantum yield of photoisomerization

Photoisomerization of the thermally stable form of motors **1**-**4** and **19** generates the thermally unstable form **1b**-**4b**, **19b** (Scheme 6). This reaction can also take place in the reverse direction, which yields the same product as the thermal relaxation. When the temperature is low enough such that thermal relaxation is negligible, irradiation leads to a photostationary state (PSS). The ratio of products in the PSS is dependent on the photochemical quantum yield of photoisomerization. This also has an impact on the overall rotation rate as was shown in an extensive theoretical study.[11]

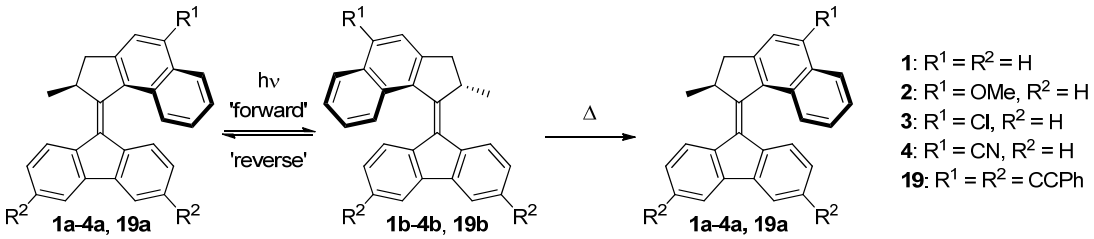

Scheme 6 Photoisomerization and thermal relaxation in motors **1**-**4** and **19**.

The quantum yield for photoisomerization of compounds **1**-**4** and **19** was determined by irradiation at 365 nm of a toluene solution of the compound (OD >> 1) at 5 °C. The conversion to the respective unstable isomer was followed at 475 nm. Short irradiation times were used to ensure the conversion was low and can be approximated as being linear with respect to time. The rate was then compared to the rate of decomposition of ferrioxalate according to standard procedures[12] to give the quantum yield for photoisomerization (Table 2). From this quantum yield and the photostationary state obtained after prolonged irradiation, the quantum yield for the reverse photoisomerization from the unstable to the stable form can also be calculated (see also Chapter 2).
The quantum yields for **1**-**4** and **19** are in the order of 0.2-0.05. The quantum yield for the reverse photoisomerization is higher than for the forward reaction; the fact that favorable PSSs are obtained is mainly due to the choice of irradiation wavelength. The quantum yields are significantly higher than those obtained for the second generation motors presented in Chapter 2, which were in the range of 0.005-0.015.

Table 2 Photostationary state and quantum yield for the photoisomerization of motors **1-4** and **19**.

Motor	R	PSS (stable:unstable)[a]	$\Phi_{forward}$	$\Phi_{reverse}$
1	H	25:75	0.14	0.50
2	OMe	43:57	0.048	0.17
3	Cl	30:70	0.15	0.69
4	CN	18:82	0.20	0.39
19	CCPh	45:55	0.057	0.046

[a] λ_{max} = 365 nm, toluene d_8

Fluorescence up-conversion

The processes in the excited state occur on a short timescale, and hence spectroscopic techniques with high time resolution are needed to obtain experimental data which test the conclusions drawn from the computational studies. Fluorescence up-conversion spectroscopy is a pump-probe technique, which allows for the study of molecular processes with ultrashort lifetimes.[13] The basic setup is shown in Scheme 7.[14] A femtosecond laser pulse is passed through an up-conversion crystal, which generates the second harmonic. This is separated from the fundamental output by a dichroic mirror and focused on the sample. The resulting fluorescence of the sample is focused on a second up-conversion crystal. The main beam in the meantime is delayed on an optical delay line, and set to arrive at the second up-conversion crystal at the desired time delay. An up-converted signal is then generated by sum frequency mixing, which is linearly proportional to the fluorescence of the sample. The up-converted signal is selected with a monochromator and passed on to the detector. The time resolution of the measurement is limited by the width of the laser pulses; it can be determined by measuring the Raman scattering of the solvent. Typically a resolution of 50-100 fs can be obtained.

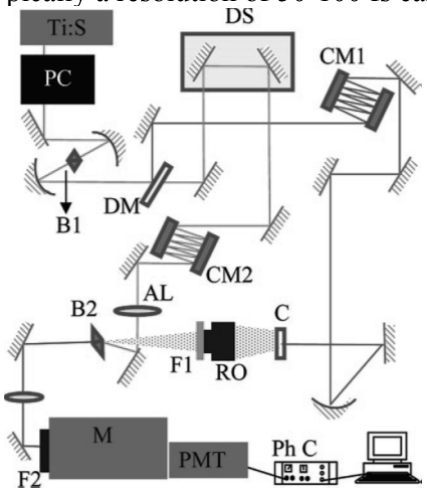

Scheme 7 Femtosecond fluorescence up-conversion experimental setup: PC = prism compressor; B1 = 50 μm BBO crystal; B2 = 100 μm BBO crystal; DM = dichroic mirror; DS = delay stage; CM1 = GSM012 chirped mirrors; CM2 = GSM216 chirped mirrors; RO = reflective objective; F1 = GG455 Schott filter; F2 = UG11 Schott filter; AL = achromatic lens; C = 1 mm cell; M = monochromator; PMT = photomultiplier tube; Ph C = photon counter. Image reproduced from ref 14.

Fluorescence up-conversion spectroscopy was used to learn more about the processes in the excited state of motors **1-4**. The fluorescence of these compounds is weak; the quantum yield is estimated to be $<10^{-4}$, however, since the up-converted signal is shifted from the fundamental output of the laser, a good signal to noise ratio can still be obtained. Compounds **1-4** all show ultrafast fluorescence decay in DCM solution (Figure 3), with **4**

being the fastest and **2** the slowest. The timescales of the fluorescence decay correlate well with the excited state lifetimes of 1-2 ps that were observed previously.4 Interestingly, compound **2** has the lowest photochemical quantum yield and shows the slowest decay in the up-conversion spectroscopy studies. Compound **4**, with the highest quantum yield, also has the fastest decay. To determine whether a real correlation exists here, further studies are required. The time-resolved fluorescence of **19** is currently under investigation in the group of prof. dr. S. R. Meech in Norwich.

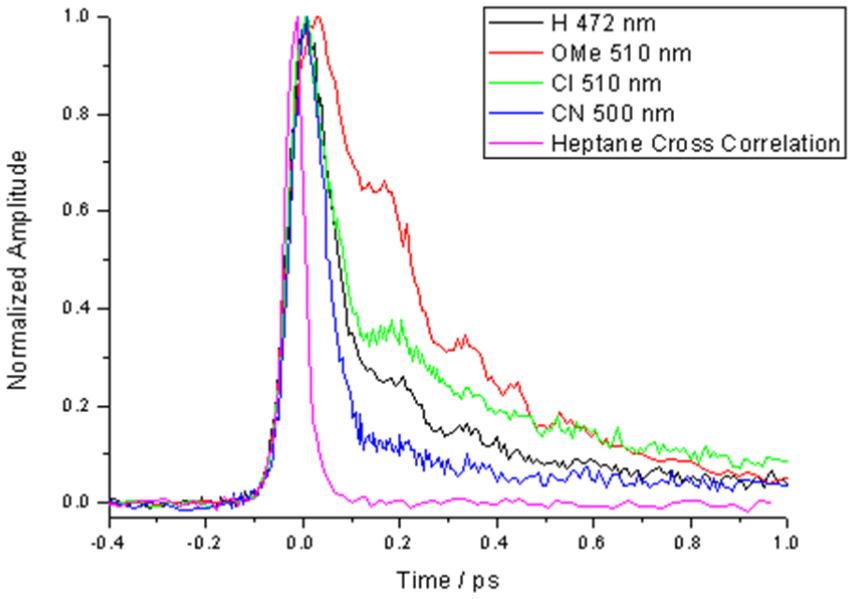

Figure 3 Normalized time-resolved fluorescence of motors **1**-**4** in CH_2Cl_2 at their respective fluorescence maxima.

In all the decay traces, an oscillation is superimposed on the decay. The fluorescence decay data for compound **1** was studied in more detail, to investigate whether or not these oscillations are an artifact or represent real processes.[15] To accurately fit the data, two exponential decays and two damped oscillators are necessary. It is proposed that the fluorescence is quenched by structural relaxation on the excited state surface. From the initial Franck-Condon excited state, the molecule relaxes to a non-emissive state, from where it can slowly decay to the ground state. The two damped oscillators could be coherently excited vibrational modes; the frequencies are 3.4±0.2 THz (113±7 cm^{-1}) and 5.4±0.4 THz (180±12 cm^{-1}), respectively. Skeletal vibrations of organic molecules typically have energies in this range, and it is proposed that the oscillations represent vibrational motion of the molecule in the excited state. The question remains whether the modes are involved in the process of rotation, or if they are simply spectator modes.[16,17,18] It has been shown that during the rotation two key structural changes take place in the molecule, namely rotation around C1'-C9 and pyramidalization at C9. If these processes can be correlated to one or both of the oscillations, it would be a major step towards understanding the excited state processes of these molecular motors. Learning enough about the system may allow for optimization of the photoisomerization step via coherent laser control: by making use of specifically shaped laser pulses, the formation of one product can be favored over another.[19]

In order to gain more insight in the vibrational processes going on in the excited state, vibrational spectroscopy was performed. Both IR spectroscopy and Raman spectroscopy may be suitable techniques to attempt to assign coherently excited vibrational modes. Eventually, time-resolved spectroscopy should be used; however, first steady-state spectroscopy will be used to see whether differences between the stable and the unstable form of the motor can be observed.

Raman spectroscopy

If a structural change is caused by a vibration that is accompanied by a change in polarizability, it can be studied using Raman spectroscopy.[20] In this way, information about vibrational modes in the ground state can be obtained. Raman signals are typically weak, but when a molecule is excited at a wavelength close to an electronic transition resonance enhancement of modes associated with that electronic transition are enhanced by up to 10^6 times.[21]

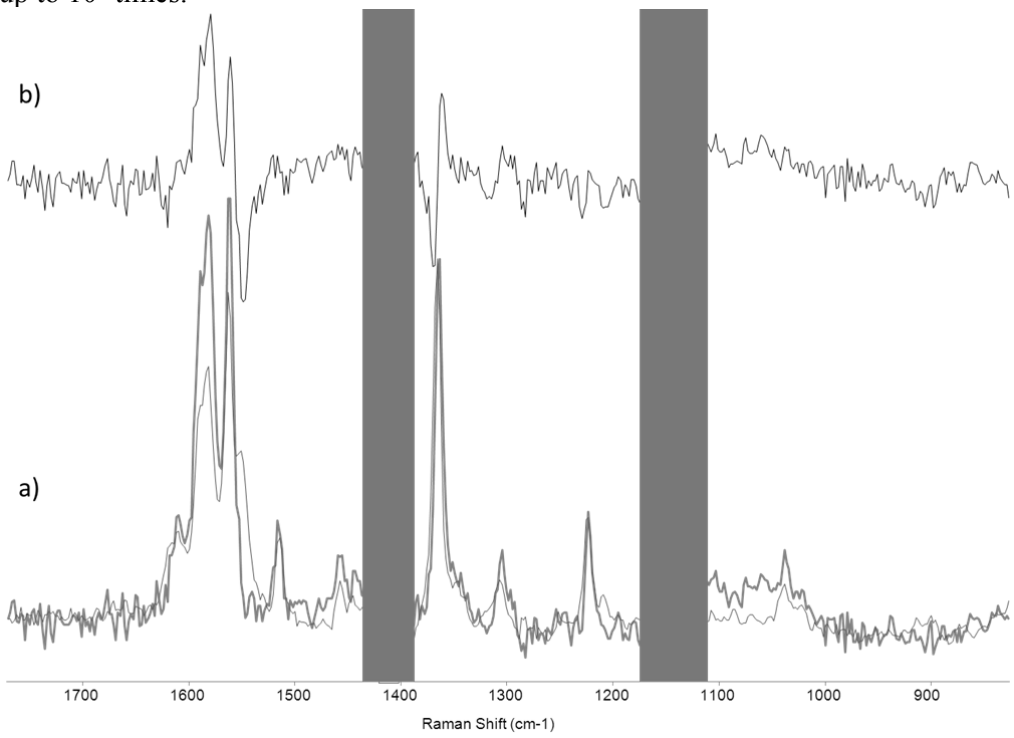

Figure 4 a) Resonance Raman spectrum at 355 nm of **1a** in DCM recorded in a flow cell (thin grey line) and the PSS mixture of **1a** and **1b** obtained after irradiation at 355 nm (thick black line). b) Difference spectrum. The shaded boxes are regions in which solvent bands obscure the features of compound **1**.

The resonance Raman spectrum of **1** was recorded in DCM at 355 nm (Figure 4a). Irradiation at this wavelength initiates photoisomerization, which means that during the measurement unstable **1b** will be formed. To obtain the Raman spectrum of **1a**, a flow cell was used to avoid build-up of **1b**. The Raman spectrum of **1b** was obtained by first irradiating the sample to the PSS at 355 nm. Upon photoisomerization there are clear changes in the band around 1580 cm^{-1}, which is assigned to the central double bond of the motor. A smaller shift in the band at 1370 cm^{-1} is evident in the difference spectrum (Figure 4b).

By making use of resonance Raman and comparison of the spectra with the non-resonant Raman spectrum, vibrational modes that are coupled to electronic excitation can be identified. In this way the coherently excited vibrational modes seen in the up-conversion

fluorescence spectroscopy may be identified. The non-resonant Raman spectrum of crystalline **1** was obtained at 785 nm (Figure 5). This was compared to the resonance Raman spectrum in solution. Since DCM shows Raman scattering at low wavenumbers, it was not suitable for these measurements. Cyclohexane shows two strong solvent bands around 400 cm^{-1} but is otherwise satisfactory.

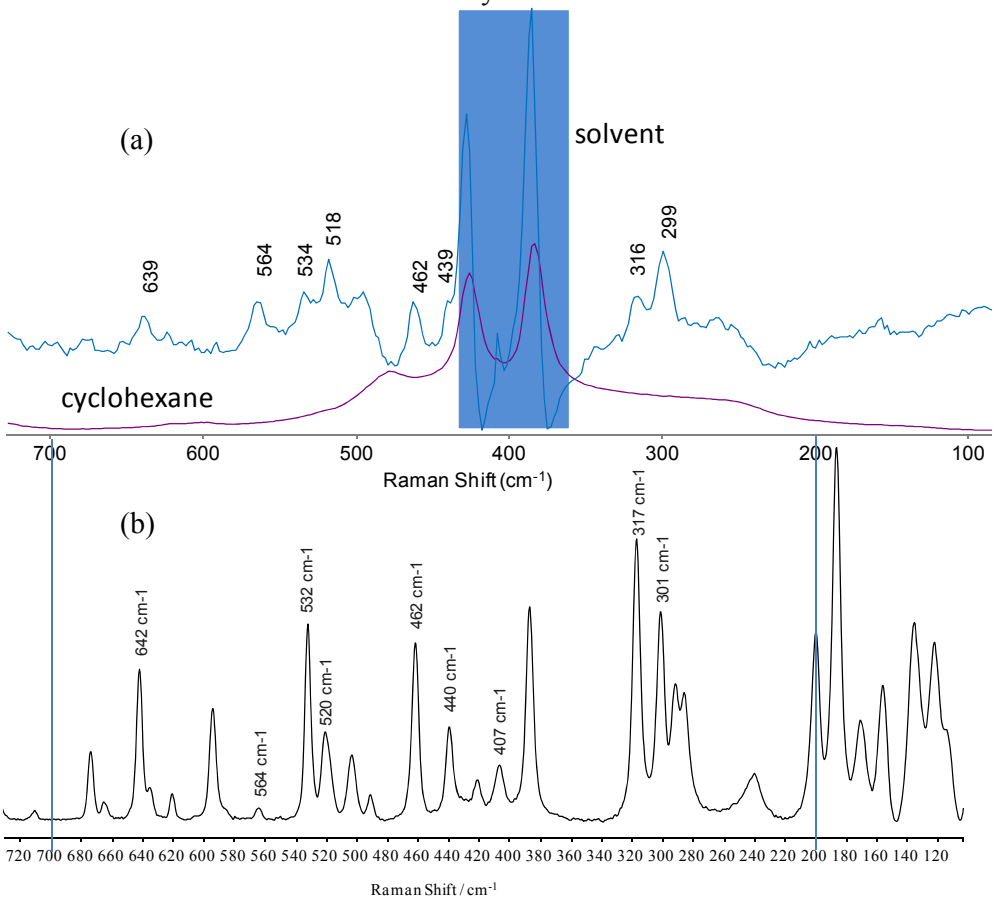

Figure 5 a) Ground state resonance Raman spectrum of **1** in cyclohexane and Raman spectrum of cyclohexane. b) Non-resonant Raman spectrum of **1** in the solid state.

From comparison of the two spectra, the bands in the resonance Raman spectrum correspond well with modes in the non-resonant Raman spectrum. There is a band in the non-resonant Raman spectrum matching the minor higher frequency excited state mode seen in the time-resolved fluorescence up-conversion spectrum at 180 cm^{-1}, but it is not observed as resonantly enhanced. The two resonantly-enhanced modes at the lowest wavenumbers were observed at 301 cm^{-1} and 317 cm^{-1}.

To identify these enhanced modes, the spectrum was calculated using DFT on the B3LYP/cc-pVTZ level of theory using Gaussian 09.[22] The calculated spectrum shows excellent agreement with the experimental spectrum (Figure 6). The y-axis of the calculated spectrum was scaled by a factor of 0.965, to correct for known deviations between results obtained using this basis set and empirical data.[23] The intensity of the bands below 1000 cm^{-1} is severely underestimated relative to the bands above 1000 cm^{-1}. However, if the bands in this region are expanded, their position and their relative intensity are in good agreement with the experimental spectrum. There are some bands present in the experimental spectrum which are absent in the calculated spectrum; these

are assumed to be lattice modes.[24] Lattice modes will not be present in the calculated spectrum, as the molecule is simulated in an isolated environment.

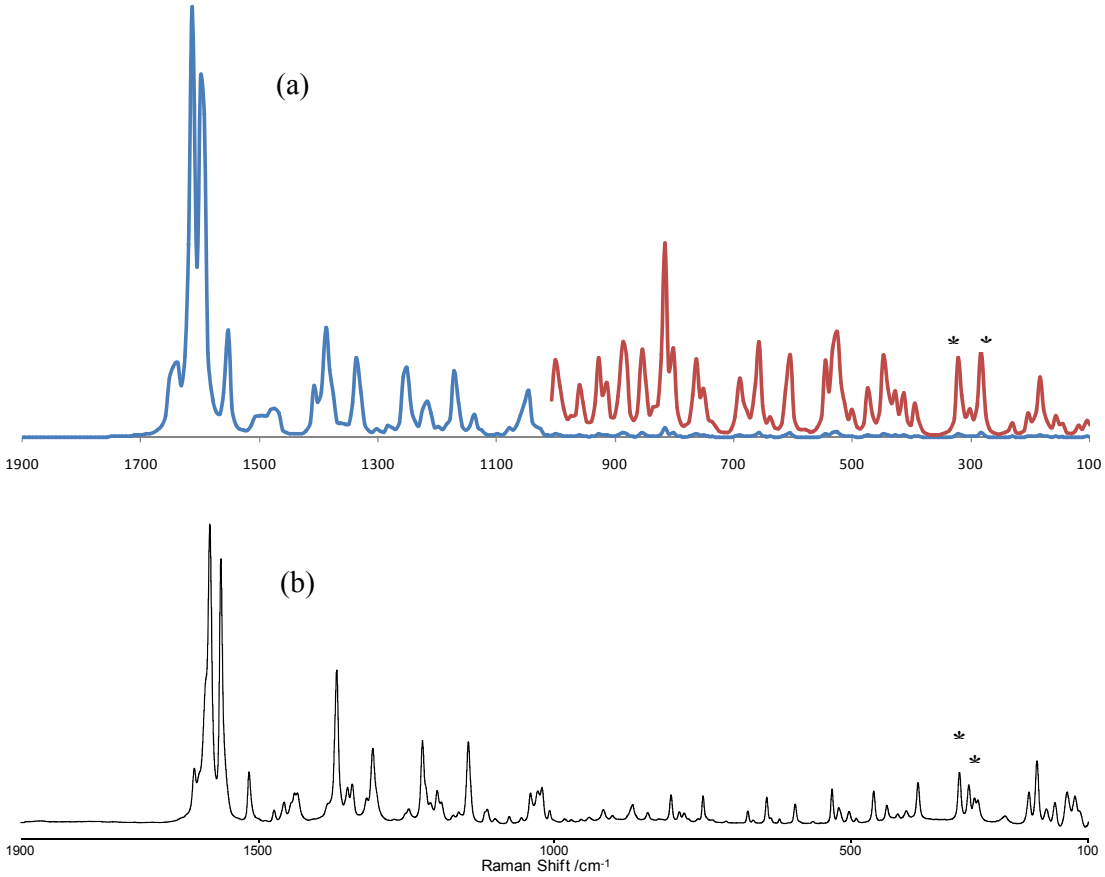

Figure 6 a) Calculated Raman spectrum of **1** with the region <1000 cm^{-1} expanded. b) Experimental Raman spectrum of **1**. The low-frequency modes matching the frequencies enhanced in the resonance Raman spectrum are marked with an asterisk.

From the calculations, the atomic displacements involved in the modes that showed resonance enhancement can be visualized. The mode at 301 cm^{-1} shows a small out-of-plane movement of C9, where pyramidalization is expected to take place. However, many more displacements are involved, such as twisting and rocking of the aromatic groups. In the mode at 317 cm^{-1} no out-of-plane movement or twisting around the central double bond is observed. A clear pyramidalization mode was found at 392 cm^{-1}; unfortunately, this region is obscured in the experimental spectrum by overlap with strong solvent bands.

Both in the experimental and in the computational work, modes that match the coherently excited modes seen by time-resolved fluorescence up-conversion were not observed. However, the Raman spectra and the calculations yield ground-state frequencies, which can not be directly assigned to excited state modes. The fact that a resonance enhancement of low-wavenumber modes is observed in the Raman spectrum at 355 nm does mean that these modes are coupled to the excitation. Calculation of the vibrational modes in the excited state would be a valuable addition to the experimental results. These calculations are not trivial however, and fall outside the scope of the current study.[25]

With respect to following thermal isomerization in fast motors, the spectral differences between the stable and unstable state are sufficiently large for nanosecond time-resolved Raman, which will be explored in the future.

IR spectroscopy

Whereas Raman spectroscopy shows vibrational modes that cause a change in polarizability, IR spectroscopy shows vibrations that are accompanied by a change in dipole moment and could thus provide additional information. However, IR spectroscopy below 500 cm^{-1} is challenging as special, delicate optics are needed which are still transparent at those wavenumbers. Obtaining information specifically about the potential twisting and pyramidalization modes may be difficult, but we were first interested to see whether we can follow the photoisomerization of compound **1**. The steady-state IR spectrum of a DCM solution of **1** shows a strong band at 1450 cm^{-1} and several medium bands in the 1300-1600 cm^{-1} region which correspond to C-C double bond stretching vibrations (Figure 7). Upon UV irradiation (365±20 nm), a new band appears 1540 cm^{-1} and the shoulder at 1430 cm^{-1} increases noticeably, similar to that observed using Raman spectroscopy. These changes were found to be reversible when the sample was left at rt for 30 min in the dark. Because there is a strong solvent band from 1200-1300 cm^{-1}, no accurate information could be obtained in this region, even after subtraction of the solvent bands; therefore the solid state spectrum of **1** was recorded.

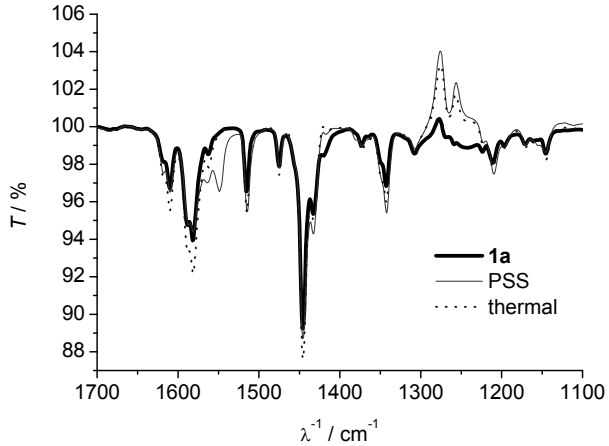

Figure 7 FT-IR spectrum of compound **1** in DCM solution before irradiation (thick line), after irradiation to PSS (thin line) and after thermal relaxation (dotted line). The feature between 1200 and 1300 cm^{-1} are caused by an imperfect subtraction of strong solvent bands in that region.

A solution of **1** in DCM was dropcast on an ATR crystal and the solvent was allowed to evaporate before the spectrum was recorded. Irradiation (365 nm) of the film for 2 min did not result in any changes in the spectrum; *i.e.* photoisomerization of **1** does not take place in the solid state, or isomerization only takes place in the upper layer of the film, which is too far from the surface of the ATR crystal. The solution of **1** was irradiated until the UV/vis absorption spectrum showed that PSS was reached; then the solid state spectrum was recorded before significant thermal reversion of **1b** to **1a** took place. Clear differences between the two spectra can be observed, which were similar to those observed by resonance Raman spectroscopy (Figure 5, Figure 8).

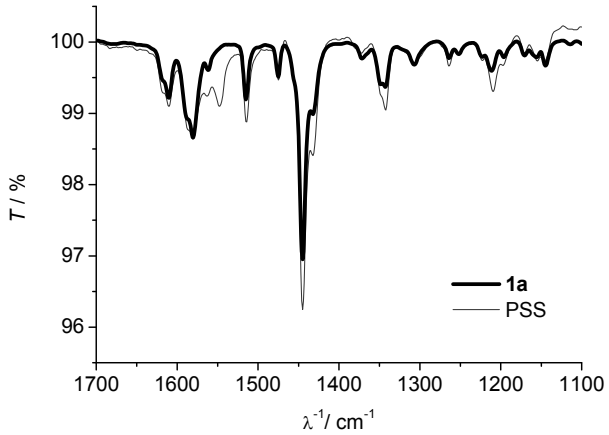

Figure 8 FT-IR spectrum of a film of compound **1** before (thick line) and after (thin line) irradiation to PSS.

To see whether thermal recovery of **1a** takes places, spectra of a film of the PSS mixture were taken with 10 min intervals. Thermal reversion in the solid state was significantly slower than in solution, but nevertheless it takes place. Over 30 min the new band at 1550 cm^{-1} only decreased by about 15%; in the same time the solution of the PSS mixture had recovered fully. This is in agreement with the literature data9 on the thermal recovery of **1** in solution; a half-life of 190 s is reported which means >99% recovery in 30 min. The decrease in half-life is attributed to steric crowding. A decrease in the rate of thermal relaxation was reported previously in mono- and multilayers of molecular motors attached to surfaces, where steric crowding is also thought to play an important role.[26]

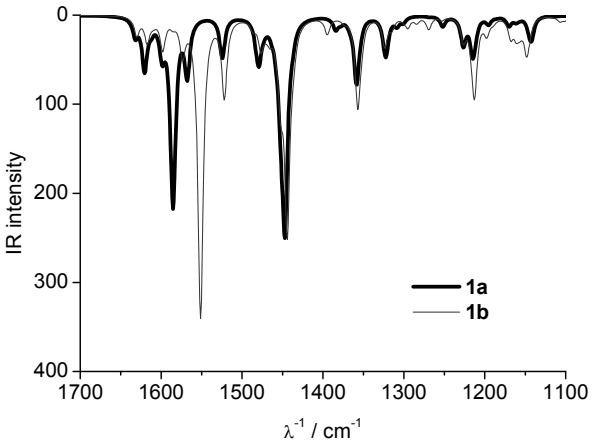

Figure 9 Calculated IR spectra of **1a** (full line) and **1b** (dashed line). The x-axis was scaled by a factor of 0.965. [23]

To be able to assign the bands to specific vibrational modes, the IR spectra of both the stable and the unstable form were calculated using DFT on the B3LYP/cc-pVTZ level of theory (Figure 9). The calculated spectrum shows good agreement with the experimental spectrum regarding the position of peaks, but the intensities vary. The main change in the spectrum that is expected based the calculation is indeed seen in the experimental spectrum, but much less pronounced. This can be partially explained by the fact that a PSS mixture of **1a** and **1b** is obtained. From the calculation, the motions involved in each

vibration can be determined. The band at 1590 cm^{-1}, which undergoes the largest change upon irradiation and shifts to 1550 cm^{-1}, includes a stretching vibration of the central double bond as a major component.
From these results it is clear that IR spectroscopy can be used to follow the photoisomerization step in molecular motors. This opens up the possibility to use time-resolved IR spectroscopy to study the excited-state processes. Following vibrational modes in real time provides direct insight into the structural dynamics, as is evidenced in studies on for example isomerization in retinal proteins and in photochromic switches.[27] Vibrational circular dichroism (VCD) might also prove to be a useful tool to further study the photoisomerization. VCD is an established spectroscopic technique for the determination of absolute chirality.[28] Since the helicity of the motor changes upon photoisomerization, it should be possible to follow this process; this might even be possible on ultra-short timescales.[29]

Conclusion

The isomerization processes of a series of second generation molecular motors **1**-**4** with electron donating and withdrawing groups were studied using various spectroscopic techniques. It was previously reported3 that there is no effect of the substituents on the rate of thermal helix inversion. This was reflected in the conformational analysis of these motors, where no variation was found in the bond length of the central double bond, and all adopt the same conformation. In the time-resolved fluorescence up-conversion spectra we observed that a decay takes place in the excited state on a timescale of picoseconds, in accordance with earlier computational studies. Furthermore, two coherently excited vibrational modes were identified. Vibrational spectroscopy was employed to attempt to assign these modes. Using Raman spectroscopy, two vibrational modes were identified at 317 and 301 cm^{-1}, respectively, which showed a resonance enhancement using 355 nm excitation. From DFT calculations we conclude that neither of these is the expected twisting or pyramidalization mode. A clear pyramidalization mode was found; however, this was calculated to be at higher wavenumber than the modes from the time-resolved experiments and could not be observed experimentally.
The photoisomerization of motor **1** could also be followed using steady-state IR spectroscopy. A shift from 1580 to 1540 cm^{-1} was observed upon generation of the unstable form, accompanied by a number of smaller shifts. This band was assigned to vibrational mode that has a stretching of the central double bond as its major component using DFT calculations. This work paves the way for time-resolved vibrational spectroscopy, which will be performed in collaboration with the group of prof. W. J. Buma in Amsterdam to provide further insight in the structural dynamics during photoisomerization. Detailed information about the excited state enables the possibility to use coherent control to optimize the photoisomerization. Using specifically shaped laser pulses, the outcome of photochemical reaction can be influenced, which could be applied to improve the quantum yield of molecular motors.[30]

Acknowledgements

The fluorescence up-conversion spectroscopy described in this chapter was performed by Jamie Conyard, prof. dr. Steve Meech and coworkers, who are gratefully acknowledged for their contributions.

Experimental section

Synthesis

For general considerations, see Chapter 2. Column chromatography was performed on a Grace Reveleris system. IR spectroscopy was performed on a PerkinElmer Spectrum 400 FT-IR. 3,6-dibromophenanthrene-9,10-dione **11**, 3,6-dibromo-9*H*-fluoren-9-one **12**[31] and 5-bromo-2-methyl-2,3-dihydro-1*H*-cyclopenta[*a*]naphthalen-1-one **16**[32] were synthesized according to previously reported procedures.

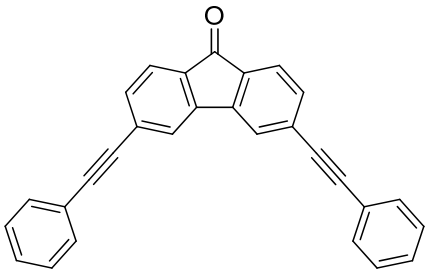

3,6-bis(phenylethynyl)-9*H*-fluoren-9-one 13

In a dried Schlenk tube was placed 3,6-dibromofluorenone **12** (275 mg, 0.81 mmol), $Pd(PPh_3)_2Cl_2$ (29 mg, 0.041 mmol) and CuI (4.6 mg, 0.025 mmol). The vessel was evacuated and backfilled with argon three times. Phenylacetylene (0.22 mL, 2.0 mmol), triethylamine (1 mL) and THF (5 mL) were added. The reaction mixture was heated to 50 °C for 16 h, and then the volatiles were removed *in vacuo*. The residue was purified by column chromatography (gradient 0 to 100% CH_2Cl_2 in pentane) and the product was recrystallized from EtOH yielding **13** (228 mg, 74%) as yellow crystals. mp >200 °C; ^{1}H NMR (400 MHz, $CDCl_3$) δ 7.72-7.64 (m, 4H), 7.62-7.54 (m, 4H), 7.48 (d, J = 7.6 Hz, 2H), 7.43-7.35 (m, 6H); ^{13}C NMR (75 MHz, $CDCl_3$) δ 191.9 (C), 143.7 (2C), 133.6 (2C), 132.6 (2CH), 131.8 (4CH), 129.8 (2C),128.9 (2CH), 128.5 (4CH), 124.2 (2CH), 123.3 (2CH), 122.5 (2C), 93.2 (2C), 89.0 (2C); HRMS (ESI^+) calcd for $C_{29}H_{17}O$ [M+H] 381.1274, found 381.1262.

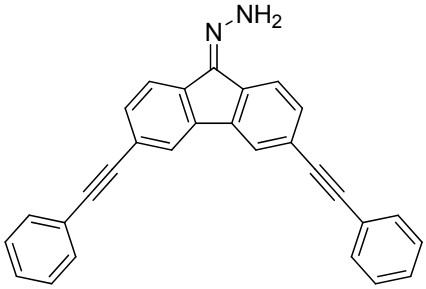

(3,6-bis(phenylethynyl)-9*H*-fluoren-9-ylidene)hydrazine 14

To a suspension of **13** (250 mg, 0.66 mmol) in EtOH (20 mL) was added hydrazine hydrate (2 mL). The reaction mixture was heated to reflux for 4 h, during which all the starting material slowly dissolved. The flask was slowly cooled to 0 °C and a precipitate formed, which was isolated by filtration. The crude product was washed with cold EtOH (2 x 5 mL) to yield **14** (186 mg, 71%) as a yellow solid. ^{1}H NMR (400 MHz, $CDCl_3$) δ 7.93 (s, 1H), 7.90-7.81 (m, 2H), 7.72 (d, J = 7.9 Hz, 1H), 7.63-7.46 (m, 6H), 7.43-7.31 (m, 6H), 6.52 (bs, 2H); ^{13}C NMR (75 MHz, $CDCl_3$) δ 144.3 (C), 140.7 (C), 138.0 (2C), 132.0 (2CH), 131.9 (3CH), 131.5 (CH), 123.0 (C), 128.8 (CH), 128.7 (2CH), 128.6

(2CH), 128.5 (CH), 125.3 (CH), 124.8 (C), 123.9 (CH), 123.4 (2C), 123.1 (CH), 121.4 (C), 120.9 (CH), 91.6 (C), 90.4 (C), 90.1 (C), 89.5 (C); HRMS (ESI^+) calcd for $C_{29}H_{19}N_2$ [M+H] 395.1543, found 381.1531.

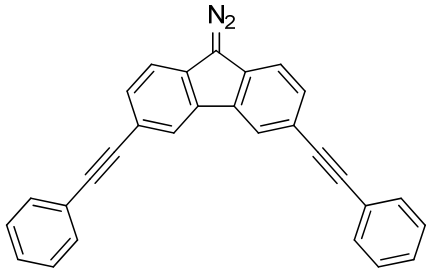

9-diazo-3,6-bis(phenylethynyl)-9*H*-fluorene 15

Compound **14** (185 mg, 0.47 mmol) was dissolved in THF (5 mL) and MnO_2 (204 mg, 2.35 mmol) was added. The reaction mixture was stirred at rt for 30 min then filtered through Celite. The solvent was removed *in vacuo* yielding **15** (181 mg, 98%) as a red solid. Compound **15** was not stored but used immediately in the next step. ^{1}H NMR (300 MHz, $CDCl_3$) δ 8.14 (s, 2H), 7.62-7.54 (m, 6H), 7.49 (d, *J* = 8.1 Hz, 2H), 7.44-7.30 (m, 6H).

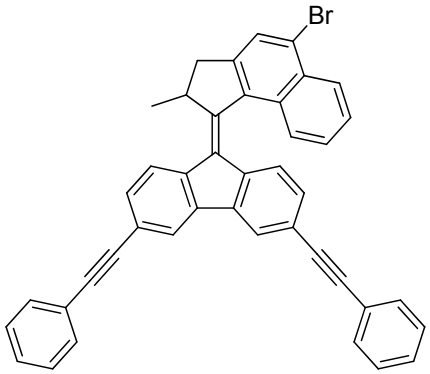

9-(5-bromo-2-methyl-2,3-dihydro-1*H*-cyclopenta[*a*]naphthalen-1-ylidene)-3,6-bis(phenylethynyl)-9*H*-fluorene 18

To a solution of **16** (500 mg, 1.8 mmol) in toluene (8 mL) was added Lawesson's reagent (1.5 g, 3.6 mmol). The suspension was heated to reflux for 3 h, and then the solvent was removed *in vacuo*. The residue was passed through a short silica column (toluene); the first colored band was collected yielding about 175 mg (0.6 mmol) of crude thioketone **17**. This was redissolved in benzene (15 mL) and **15** (250 mg, 0.63 mmol) was added and the solution was heated to reflux for 16 h. Triphenylphosphine (200 mg, 0.76 mmol) was added and heating was continued for another 16 h. The volatiles were removed *in vacuo* and the residue was purified by column chromatography (gradient 0 to 100% CH_2Cl_2 in pentane) yielding **18** (283 mg, 25%) as an orange solid. ^{1}H NMR (400 MHz, $CDCl_3$) δ 8.39 (d, *J* = 8.5 Hz, 1H), 8.04 (s, 1H), 8.00-7.89 (m, 3H), 7.76 (d, *J* = 7.1 Hz, 1H), 7.66-7.50 (m, 7H), 7.44-7.30 (m, 8H), 7.00 (d, *J* = 8 Hz, 1H), 6.62 (d, *J* = 8 Hz, 1H), 4.38-4.25 (m, 1H), 3.60 (dd, *J* = 15.1, 5.5 Hz, 1H), 2.77 (d, *J* = 15.3 Hz, 1H), 1.40 (d, *J* = 6.7 Hz, 3H); ^{13}C NMR (75 MHz, $CDCl_3$) δ 152.1 (C), 148.2 (C), 139.8 (C), 139.6 (C), 139.2 (C), 137.2 (C), 136.5 (C), 131.9 (2CH), 131.8 (2CH), 131.1 (C), 130.9 (CH), 130.8 (C), 130.6 (C), 129.9 (CH), 128.7 (CH), 128.6 (2CH), 128.5 (4CH), 128.3 (CH), 128.0 (CH), 127.9 (CH), 127.2 (CH), 126.3 (C), 125.8 (CH), 124.2 (CH), 123.6 (2C), 123.3 (CH), 122.7

(CH), 122.1 (C), 121.9 (C), 90.6 (C), 90.4 (3C), 45.7 (CH), 41.9(CH_2), 19.6 (CH_3); HRMS (ESI^+) calcd for $C_{43}H_{28}Br$ [M+H] 623.1369, found 623.1358.

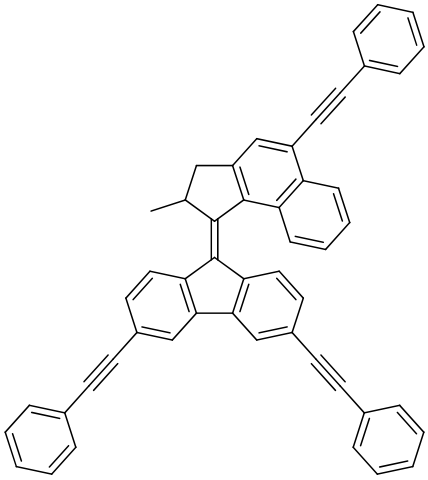

9-(2-methyl-5-(phenylethynyl)-2,3-dihydro-1*H*-cyclopenta[*a*]naphthalen-1-ylidene)-3,6-bis(phenylethynyl)-9*H*-fluorene 19

In a dried Schlenk tube was placed **18** (102 mg, 0.16 mmol), $Pd(PPh_3)_2Cl_2$ (11 mg, 0.016 mmol) and CuI (3 mg, 0.02 mmol). The vessel was evacuated and backfilled with argon three times. Phenylacetylene (0.2 mL), Et_3N (1 mL) and THF (5 mL) were added and the solution was heated to 50 °C for 16 h. The volatiles were removed *in vacuo* and the residue was purified by column chromatography (gradient 0 to 50% CH_2Cl_2 in pentane) yielding **19** as an orange solid. ^1H NMR (400 MHz, $CDCl_3$) δ 8.60 (d, J = 8.3 Hz, 1H), 8.05 (s, 1H), 7.96 (d, J = 8.0 Hz, 2H), 7.89 (s, 1H), 7.80 (d, J = 8.4 Hz, 1H), 7.71 (d, J = 7.6 Hz, 2H), 7.68-7.57 (m, 4H), 7.54 (d, J = 7.6 Hz 2H), 7.49-7.29 (m, 10H), 7.02 (d, J = 8.2 Hz, 1H), 6.68 (d, J = 8.2 Hz, 1H), 4.33 (m, 1H), 3.61 (dd, J = 15.1, 5.5 Hz, 1H), 2.80 (d, J = 15.2 Hz, 1H), 1.42 (d, J = 6.7 Hz, 3H); HRMS (ESI^+) calcd for $C_{51}H_{33}$ [M+H] 645.2577, found 645.2555.

Computational chemistry

The Gaussian 09 program was used for geometry optimizations and the calculation of energies. Initial geometries were optimized using semi-empirical PM3. Geometry optimizations were then performed using B3LYP/cc-pVTZ using tight convergence criteria. UltraFine grid was used for numerical integrations. To ensure minima and transition states were reached, frequency analyses of the obtained structures were evaluated; all reported minima had no imaginary frequencies.

References

[1] N. Koumura, R. W. J. Zijlstra, R. A. van Delden, N. Harada, B. L. Feringa, *Nature* **1999**, *401*, 152-155.
[2] M. M. Pollard, M. Klok, D. Pijper, B. L. Feringa, *Adv. Funct. Mater.* **2007**, *17*, 718-729.
[3] M. M. Pollard, P. V. Wesenhagen, D. Pijper, B. L. Feringa, *Org. Biomol. Chem.* **2008**, *6*, 1605-1612.
[4] R. Augulis, M. Klok, B. L. Feringa, P. H. M. van Loosdrecht, *Phys. Stat. Sol. C* **2009**, *6*, 181-184.
[5] A. Kazaryan, M. Filatov, *J. Phys. Chem. A* **2009**, *113*, 11630-11634.
[6] F. Liu, K. Morokuma, *J. Am. Chem. Soc.* **2012**, *134*, 4864-4876.
[7] Y. Amatatsu, *J. Phys. Chem. A* **2011**, *115*, 13611-13618.
[8] A. Kazaryan, J. C. M. Kistemaker, L. V. Schäfer, W. R. Browne, B. L. Feringa, M. Filatov, *J. Phys. Chem. A* **2010**, *114*, 5058-5067.

[9] J. Vicario, A. Meetsma, B. L. Feringa, *Chem. Commun.* **2005**, 5910-5912.
[10] J. Vicario, M. Walko, A. Meetsma, B. L. Feringa, *J. Am. Chem. Soc.* **2006**, *128*, 5127-5135.
[11] M. Klok, W. R. Browne, B. L. Feringa, *Phys. Chem. Chem. Phys.* **2009**, *11*, 9124-9131.
[12] *Handbook of Photochemistry* (Eds.: M. Montalti, A. Credi, L. Prodi, M. T. Gandolfi), CRC Press, Boca Raton, **2006**, pp. 602-604.
[13] *Principles of Fluorescence Spectroscopy* (Ed.: J. R. Lakowicz), Springer, New York, **2006**, pp. 128-129.
[14] I. A. Heisler, M. Kondo, S. R. Meech, *J. Phys. Chem. B* **2009**, *113*, 1623-1631.
[15] J. Conyard, K. Addison, I. A. Heisler, A. Cnossen, W. R. Browne, B. L. Feringa, S. R Meech, *Nature Chem.* **2012**, *4*, 547-551.
[16] C. Hennig, S. Schmatz, *Chem. Phys. Lett.* **2007**, *445*, 250-255.
[17] S. T. Banks, C. S. Tautermann, S. M. Remmert, D. C. Clary, *J. Chem. Phys.* **2009**, *131*, 044111.
[18] G. Käb, C. Schröder, D. Schwarzer, *Phys. Chem. Chem. Phys.* **2002**, *4*, 271-278.
[19] M. Dantus, V. V. Lozovoy, *Chem. Rev.* **2004**, *104*, 1813-1859.
[20] *Modern Raman Spectroscopy* (Eds.: E Smith, G. Dent), John Wiley & Sons, Chichester, **2005**.
[21] D. P. Strommen, K. Nakamoto, *J. Chem. Educ.* **197**, *54*, 474-478.
[22] Gaussian 09, Revision **B.1**, M. J. Frisch, G. W. Trucks, H. B. Schlegel, G. E. Scuseria, M. A. Robb, J. R. Cheeseman, G. Scalmani, V. Barone, B. Mennucci, G. A. Petersson, H. Nakatsuji, M. Caricato, X. Li, H. P. Hratchian, A. F. Izmaylov, J. Bloino, G. Zheng, J. L. Sonnenberg, M. Hada, M. Ehara, K. Toyota, R. Fukuda, J. Hasegawa, M. Ishida, T. Nakajima, Y. Honda, O. Kitao, H. Nakai, T. Vreven, J. A. Montgomery, Jr., J. E. Peralta, F. Ogliaro, M. Bearpark, J. J. Heyd, E. Brothers, K. N. Kudin, V. N. Staroverov, R. Kobayashi, J. Normand, K. Raghavachari, A. Rendell, J. C. Burant, S. S. Iyengar, J. Tomasi, M. Cossi, N. Rega, J. M. Millam, M. Klene, J. E. Knox, J. B. Cross, V. Bakken, C. Adamo, J. Jaramillo, R. Gomperts, R. E. Stratmann, O. Yazyev, A. J. Austin, R. Cammi, C. Pomelli, J. W. Ochterski, R. L. Martin, K. Morokuma, V. G. Zakrzewski, G. A. Voth, P. Salvador, J. J. Dannenberg, S. Dapprich, A. D. Daniels, Ö. Farkas, J. B. Foresman, J. V. Ortiz, J. Cioslowski, and D. J. Fox, Gaussian, Inc., Wallingford CT, 2009.
[23] In accordance with the vibrational frequency scaling factors from the Computational Chemistry Comparison and Benchmark Database, release 15b, August 2011, which can be found under http://cccbdb.nist.gov.
[24] J. P. Pinan, R. Ouillon, P. Ranson, *J. Phys. Chem.* **1998**, *109*, 5469-5480.
[25] M. Chiba, T. Tsuneda, K. Hirao, *J. Chem. Phys.* **2006**, *124*, 144106.
[26] G. T. Carroll, G. London, T. Fernández Landaluce, P. Rudolf, B. L. Feringa, *ACS Nano*, **2011**, *5*, 622-630.
[27] E. T. J. Nibbering, H. Fidder, E. Pines, *Annu. Rev. Phys. Chem.* **2005**, *56*, 337-367.
[28] Y. He, B. Wang, R. K. Dukor, L. A. Nafie, *Appl. Spectrosc.* **2011***, 61*, 699-723.
[29] H. Rhee, J.-H. Choi, M. Cho, *Acc. Chem. Res.* **2010**, *43*, 1527-1536.
[30] G. Pérez-Hernández, A. Pelzer, L. González, T. Seideman, *New J. Phys.* **2010**, *12*, 075007.
[31] K. Brunner, A. van Dijken, H. Börner, J. J. A. M. Bastiaansen, N. M. M. Kiggen, B. M. W. Langeveld, *J. Am. Chem. Soc.* **2004**, *126*, 6035-6042.
[32] N. Ruangsupapichat, *Ph. D. Thesis*, University of Groningen, **2012**.

Chapter 4: Driving unidirectional molecular rotary motors with visible light by intra- and intermolecular energy transfer from palladium porphyrin[I]

In this chapter the development of a visible light-driven molecular motor is described. By using palladium tetraphenylporphyrin as a triplet sensitizer, the photoisomerization step of the motor could be performed using green light. Triplet energy transfer from the porphyrin to the motor can take place both in intra- and intermolecular fashion and is shown to be very efficient. Importantly, the unidirectional character of the rotation is preserved.

Introduction

Light driven molecular switches and more recently linear and rotary motors show promise in future nanosystems and devices based on integrated molecular components.[1,2,3,4,5] Near and mid UV light is typically required to operate most photoactive molecular systems, such as azobenzene[6,7] and diarylethene[8,9] switches and overcrowded alkene-based motors.[10,11] Red and near IR light-driven molecular components are, however, highly desirable, in expanding for instance their application to biological systems, where UV light can trigger undesirable responses, including cellular apoptosis. Shifting to longer wavelength also reduces irradiation-induced damage to soft material devices based on organic molecules. In certain cases this has been achieved by shifting the absorption spectrum to the visible region through the use of substituents.[12] However, to provide sufficient energy to drive photochemical reactions with red light typically it is expected that two-photon absorption would be required.[13] One solution is sensitization of switches through energy transfer from appended chromophores to induce isomerization. An example in nature is found in the exogenous chromophore used to trigger rhodopsin with long wavelength light, used by deep-sea fish for vision.[14,15] Some examples in the recent literature illustrate the use of sensitized photochemistry in diarylethene switching[16] and in a catenane-based molecular rotor.[17] Stoddart, Balzani and Credi and coworkers used an energy transfer relay to drive a rotaxane-based linear molecular motor with visible light.[18] The incorporation of molecular motors into more complex systems is desirable as it allows for advanced functions to be driven with external stimuli. However, the dynamic properties in systems combining molecular switches or motors with other chromophores can be affected by crosstalk. For example when four azobenzenes were attached to the *meso*-positions of a porphyrin, it was found that *E-Z* photoisomerization no longer took place.[19] A recent study by Tour showed that the incorporation of a second generation molecular motor into a molecular car equipped with wheels derived from fullerenes lead to complete quenching of the photochemistry of the motor by the fullerenes.[20]

Motivated by the rich literature on the photoisomerization of stilbene and related olefin chromophores,[2122,23] we considered using an exogenous chromophore to drive the molecular motor function. In this way, visible light that is not (directly) absorbed by the molecular motor can be used to drive the rotary cycle by employing for example a porphyrin chromophore to harvest and relay photochemical energy (Scheme 1).[24,25] A

[I] The work presented in this chapter has been published: A. Cnossen, L. Hou, M. M. Pollard, P. V. Wesenhagen, W. R. Browne, B. L. Feringa, *J. Am. Chem. Soc.* **2012**, *134*, 17613-17619.

number of examples of metalloporphyrins that can sensitize the isomerization of stilbene and its derivatives by irradiating at wavelengths longer than the lowest absorption of stilbene have been reported.[26,27,28] In the present study both inter- and intramolecular energy transfer as a means of driving a rotary motor was examined.

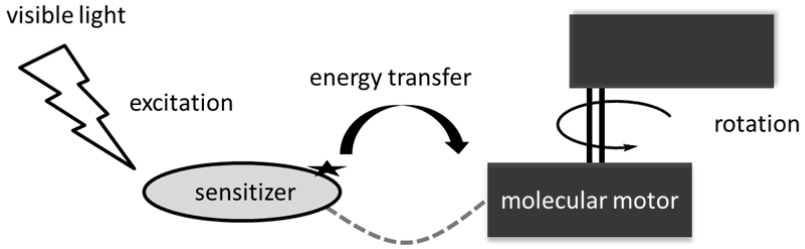

Scheme 1 Rotation of a molecular motor driven by energy transfer from a sensitizer which absorbs visible light.

In our previous studies, motors such as **1** operated by the direct absorption of a photon to excite the molecules to a singlet excited state, followed by relaxation to a twisted state ($^1p^*$) that may either decay forward to give the thermally unstable isomer **1b** or backward to give the starting alkene **1a** (Scheme 2a).[29,30] By using a triplet sensitizer, a lower lying triplet excited state of the molecular motor can be accessed. Following this excitation pathway the molecule can adopt a twisted state ($^3p^*$). Taking this approach is nontrivial, however, since in addition to competing electron-transfer processes, achieving equally favorable photostationary states is challenging.[31] This twisted state does not necessarily have the same geometry as that reached on the singlet excited state surface, and in principle could have a different preference for relaxation towards the unstable or the stable form (Scheme 2b).[32]

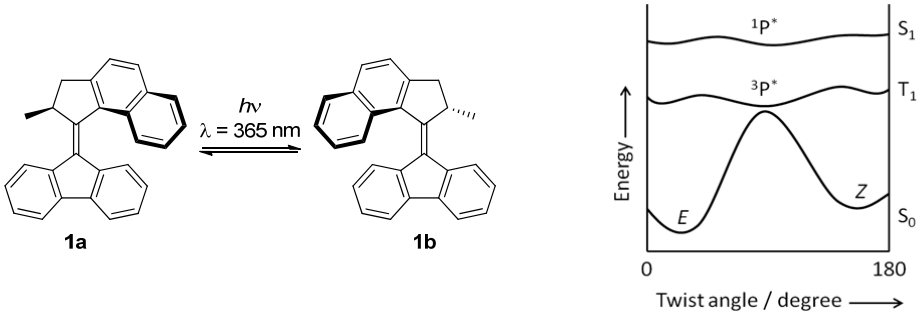

Scheme 2 a) Photoisomerization of **1a** to **1b** driven by UV light. b) Schematic energy profile along the rotation reaction coordinate of an asymmetrically substituted alkene.[33]

Since the photoisomerization goes via a triplet state, it is likely that the photostationary states will change with respect to those obtained from direct excitation. The photostationary state depends on the efficiency of the excitation and the decay ratio. If there is a large energy difference between the triplet excited state of the stable and the unstable forms, the energy transfer efficiency to both forms will be different. Also, if the excited state has a preference for decay to either the stable or the unstable form, this will have an influence on the photostationary state obtained.

The overall rate of the rotation of the molecular motor depends on the rate of the thermal helix inversion step, because it is much slower than the photoisomerization step, although at high rates the irradiation intensity and concentration also start to play a role.[34] If the photoisomerization proceeds via a triplet mechanism, the photochemistry might occur on

a longer timescale, but since the thermal helix inversion of **1** has a half-life of several minutes,[29] this will still be rate limiting.

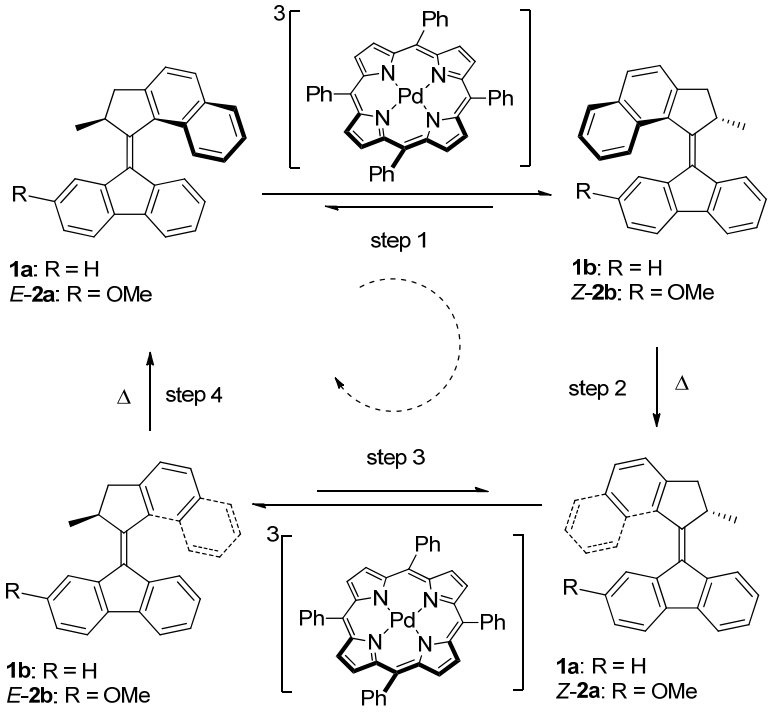

Scheme 3 Excitation of palladium tetraphenylporphyrin with visible light followed by efficient intersystem crossing generates the triplet porphyrin excited state. Intermolecular energy transfer to the molecular motor drives photoisomerization of the central olefinic bond. Thermal helix inversion of the unstable form completes one half rotation.

An important aspect in this approach is whether the rotation of the motor remains unidirectional. If the photoisomerization via the triplet state proceeds analogously to that of the singlet process, it is expected that overall the rotation will still be unidirectional. Indeed, even though the photoisomerization is reversible, the subsequent thermal helix inversion is essentially one-way, which ensures that the rotation can only operate in one overall direction (Scheme 3). However, one can envision that in the triplet excited state other processes can take place, which could allow ill-defined interconversion of the stable or unstable forms.

Results and discussion

Molecular design

We selected palladium tetraphenylporphyrin (PdTPP) as a sensitizer to investigate the possibility of harnessing longer wavelength light to drive the rotary cycle of **1** through intermolecular energy transfer. This chromophore is well suited for the purpose because it has a relatively long-lived triplet state lifetime (up to 2 ms)[35] and has a strong absorption at wavelengths longer than those of the motor, allowing for selective excitation of PdTPP in the presence of **1**. With a triplet energy of 178 kJ/mol,[35] the excited state energy of ^{3}[PdTPP] is significantly lower than that of the singlet excited state of motor **1** (~300 kJ/mol). The triplet excited state energy of motor **1** is unknown, however, it can be estimated using time-dependent density functional theory (TD-DFT) calculations. TD-

DFT calculations on the B3LYP/6-31G(d,p)[36,37,38] level of theory gives a value of 182 kJ/mol, which is comparable with that of PdTPP. [39]
In addition to intermolecular energy transfer[40] from the sensitizer and the molecular motor, a covalent system was designed to allow for intramolecular energy transfer, to increase the effective molarity and thus the efficiency of energy transfer. In energy transfer processes, the distance and orientation between the donor and acceptor is important.[41] In the covalent system employed a flexible, non-conjugated linker is used (*vide infra*), which precludes through-bond interactions, with an ester formation as the final coupling step. Substitution at this position of the motor has no effect on the thermal helix inversion, although the photostationary state is affected by electron donating or withdrawing substituents.[42] In a different molecular motor the effect of substitution with large alkyl groups was also reported to be minimal,[43] so we expect no significant difference in behavior between the motor unit in **13** and compound **1.**

Synthesis

The synthesis of target motor **9** with an ethylene glycol spacer for attachment of the porphyrin is shown in Scheme 4. Starting from 1-methoxynaphthalene **3**, ketone **4** was synthesized in a one pot Friedel-Crafts acylation/Nazarov cyclization in moderate yield. Deprotection of the phenol could be carried out conveniently by heating with pyridine hydrochloride. Purification of the resulting naphthol **5** was somewhat hampered by poor solubility, however, the crude product could be used directly in the next step. Alkylation of **5** with *tert*-butyl chloroacetate gave **6** in good yield. Conversion of the ketone moiety to a thioketone was effected by Lawesson's reagent. Thioketone **7** was found to be stable towards column chromatography and could be stored for several days at ambient conditions without noticeable degradation. The sterically overcrowded olefinic bond was introduced by a Barton-Kellogg coupling between **7** and 9-diazofluorene. A mixture of olefin **8** and the corresponding episulfide was obtained, which was not separated but instead treated with triphenylphosphine yielding functionalized motor **8** in 65% yield. Attempts to hydrolyze the ester functionality in **8** for subsequent coupling to an alcohol substituted porphyrin failed under both acidic and basic conditions. However, reduction of the ester to an alcohol using $LiAlH_4$ proceeded in good yield. In ^1H NMR, compound **9** shows the typical splitting pattern of the protons on the cyclopentene ring. Further characterization was performed with ^{13}C NMR and high-resolution mass spectrometry (HR-MS).

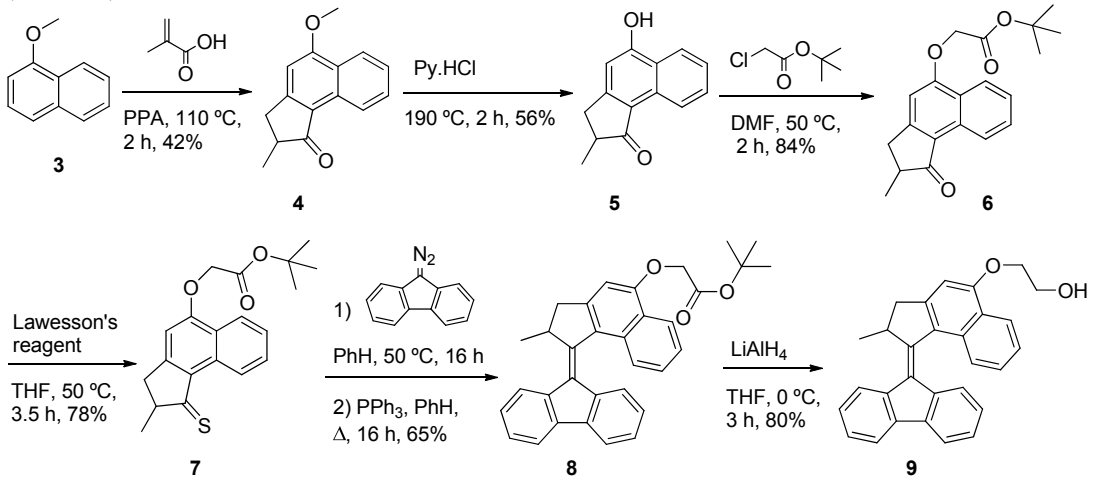

Scheme 4 Synthesis of (2-hydroxyethoxy)-functionalized motor **9**.

An acid functionalized porphyrin was synthesized in three steps to allow coupling to **9**. First, pyrrole was reacted with a 3:1 mixture of benzaldehyde and methyl 4-formylbenzoate to provide a statistical mixture of ester functionalized porphyrins. This mixture was separated by silica column chromatography to give **10** in 12% yield. Next, the ester moiety was hydrolyzed with potassium hydroxide following a procedure by Tomé *et al*.[44] Finally, the porphyrin was palladated under mild conditions[45] to provide carboxylic acid functionalized porphyrin **12** in quantitative yield. Palladation can conveniently be monitored by the disappearance of the NH absorption in the ^{1}H NMR spectrum at -2.8 ppm, and in the collapse of the four Q-bands in the UV/vis spectrum to two due to higher symmetry.[46]

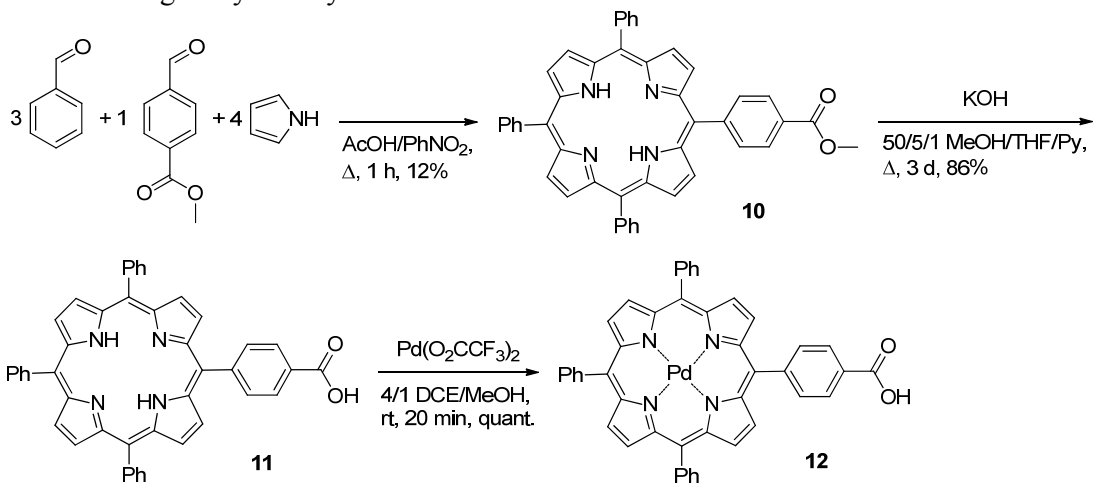

Scheme 5 Synthesis of PdTPP-COOH.

The alcohol moiety in **9** was reacted with **12** in a carbodiimide-mediated esterification to give **13** in 88% yield. Compound **13** was characterized by ^{1}H and ^{13}C NMR and HR-MS. For control experiments, free-base analogue **14** was also synthesized by coupling motor **9** to **11**.

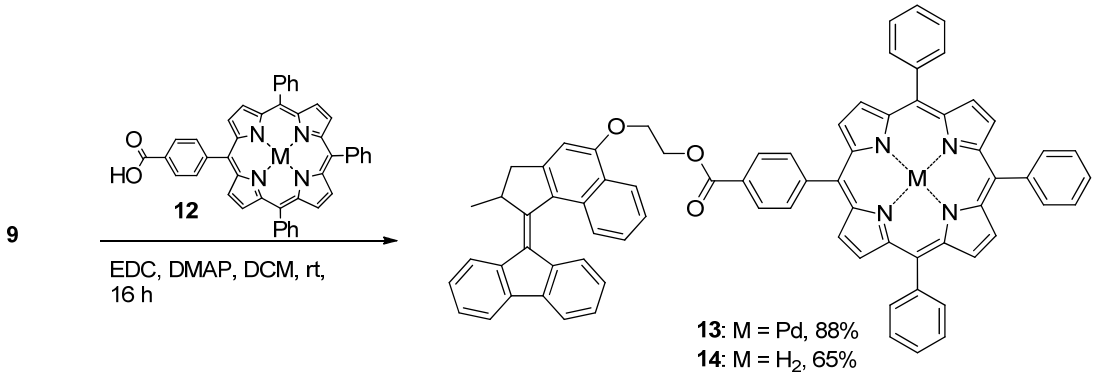

Scheme 6 Synthesis of TPP-motor conjugates **13** and **14**.

Photoisomerization by intermolecular energy transfer

Sensitization of the photoisomerization of **1** by collisional energy transfer from PdTPP was studied in 1,2-dichloroethane at 293 K. The UV/vis absorption spectra of **1a** and the PSS mixture of **1a** and **1b** obtained after irradiation at 365 nm is shown in Figure 1. The absorption spectra of **1** overlap partially with the absorption spectrum of PdTPP, with the Soret band of the porphyrin dominating the absorption spectrum.

Irradiation of the porphyrin at 420 nm would also lead to direct excitation and isomerization of **1**. Hence irradiation was carried out at a wavelength resonant with one of the Q-bands (indicated by the arrow in Figure 1) of the porphyrin, at longer wavelength than the absorption of both the stable and the unstable forms of **1**. Excitation at 530-550 nm was achieved by the use of a visible light source with an appropriate band pass filter or a 532 nm pulsed laser.

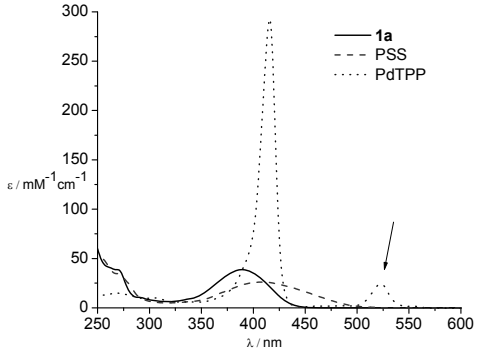

Figure 1 UV/vis absorption spectra of **1a** (black line), the PSS mixture of **1a** and **1b** obtained after irradiation with 365 nm (red dashed line) and PdTPP (blue dotted line).

An argon purged solution of **1** alone and a 1:1 mixture of PdTPP and **1** (5 μM) was irradiated at 532 nm (pulsed laser, 6 ns, 10 Hz). A red shift in the absorption was observed, corresponding to the photoisomerization of motor **1** (Figure 2), as observed before upon direct irradiation of **1** with UV light. The change in absorption is minor and partially obscured by the overlap with the porphyrin absorption, but is nevertheless reproducible. In contrast, when a solution of **1** only was irradiated under the same conditions no changes were observed in the UV/vis absorption spectrum, confirming that the photochemistry of **1** cannot be driven directly at 532 nm.

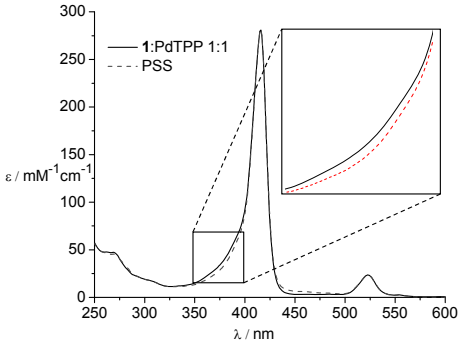

Figure 2 UV/vis absorption spectra of a mixture of **1** and PdTPP (full line) and the same mixture after irradiation at 532 nm (dashed line). Inset: expansion of the 350-400 nm region.

CD spectroscopy was employed to further characterize the photoisomerization of **1**. Enantiomerically pure *(S)*-**1** was obtained by preparative chiral stationary phase HPLC. The absolute configuration was assigned based on comparison of the CD spectrum to the spectrum predicted by TD-DFT calculations on the B3LYP/6-31G(d,p) level of theory (Figure 3a). Upon irradiation at 532 nm of a 1:1 mixture of *(S)*-**1** and PdTPP in chloroform, the major bands in the CD spectrum start to decrease in intensity, which implies the formation of the unstable form with opposite helicity (Figure 3b). The bands do not invert fully, even upon prolonged irradiation, which can be rationalized by a relatively low PSS; from the decrease in signal intensity a ratio **1a**:**1b** of about 75:25 can be estimated. Upon heating to 40 °C for 20 min, the spectral changes in both the UV/vis absorption and the CD spectra are reversed.

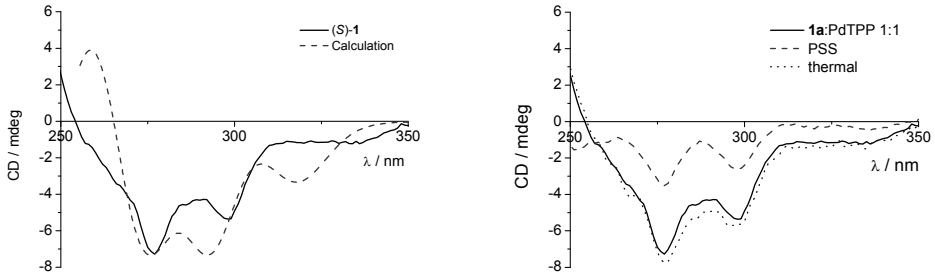

Figure 3 a) CD spectrum measured for **1** (black line) and normalized calculated CD spectrum for (*S*)-**1** (red dashed line). b) CD spectra of a mixture of **1** and PdTPP (full line) and the same mixture after irradiation at 532 nm (dashed line) and subsequent heating to 40 °C for 20 min (dotted line). The spectrum after heating has a slightly higher intensity due to a small change in concentration during heating.

Unidirectionality of the sensitized rotation process

A central question in driving photoisomerization by triplet sensitization rather than direct excitation is whether or not the unidirectionality of the rotary motor function is retained. Previously, the unidirectionality of the rotary motor function of **1** under direct excitation (365 nm) was established by CD and ^{1}H NMR spectroscopy.[29] To be able to distinguish the four distinct steps in the rotary cycle of the motor, a methoxy substituent was introduced in the lower half. Compound **2** was synthesized according to literature procedures,[29] analogous to **1**, and the *E* and *Z* isomers were separated by column chromatography.

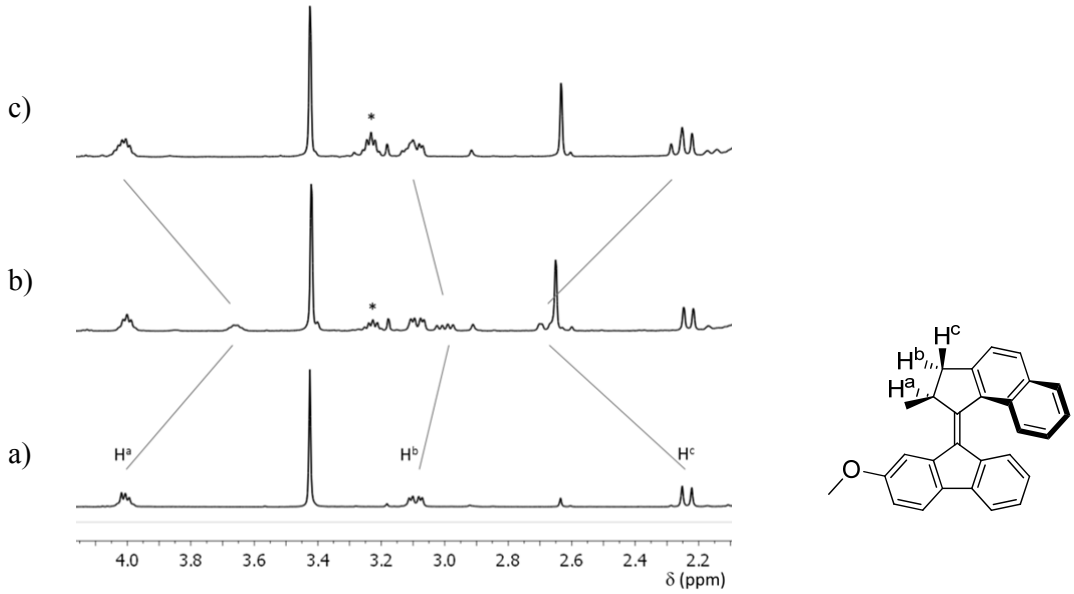

Figure 4 Partial ^{1}H NMR spectrum (-40 °C, toluene-d_8) of a) a mixture of PdTPP and *E*-**2a** before irradiation; b) mixture of *E*-**2a** and *Z*-**2b** obtained upon irradiation at 546 nm at -40 °C and c) mixture of *E*-**2a** and *Z*-**2a** obtained upon warming to 40 °C for 20 min. * = ethanol

A 1:1 mixture of PdTPP and **2** (18 mM) was irradiated at -40 °C in toluene-d_8 at 546 nm (+/-5 nm). The initial isomer *E*-**2a** of the molecular motor was converted to the thermally unstable *Z*-**2b** (Scheme 3, step 1). Characteristic changes in the ^{1}H NMR spectrum are the shift of the alkyl signals and the appearance of a signal of the methoxy group at 2.6 ppm (Figure 4). At the PSS, the ratio of *E*-**2a** to *Z*-**2b** was 64:36. Warming the mixture at 40 °C for 20 min resulted in the conversion of *Z*-**2b** to *Z*-**2a** (Scheme 3, step 2). The alkyl signals recover at their original positions, while the intensity of the new methoxy signal remains unchanged, indicating the formation of the *Z*-**2a** isomer.

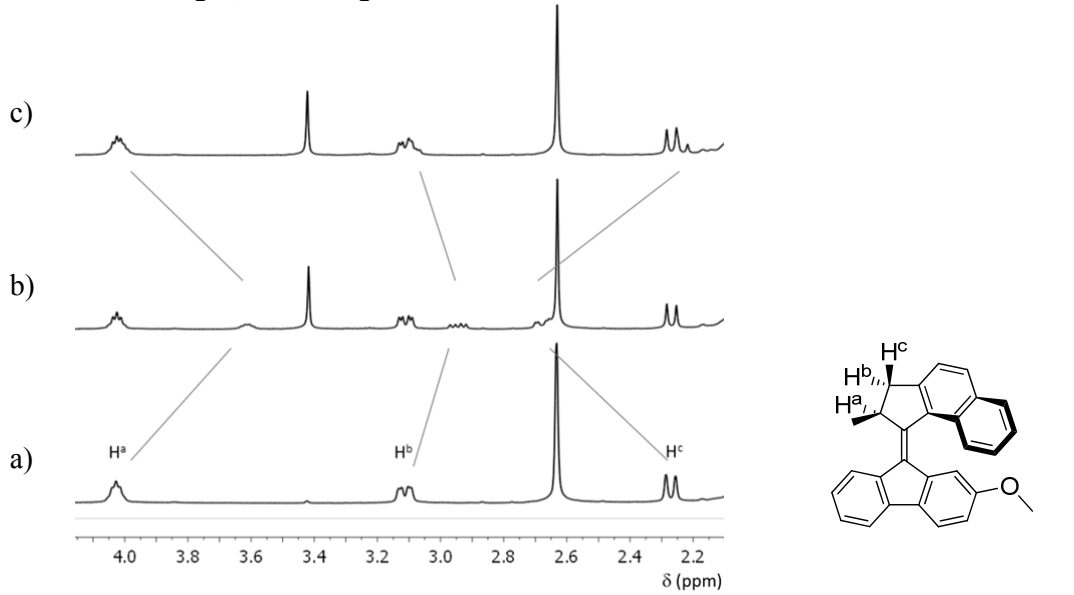

Figure 5 Partial ^{1}H NMR spectrum (-40 °, toluene-d_8) of a) a mixture of PdTPP and *Z*-**2a** before irradiation; b) mixture of *Z*-**2a** and *E*-**2b** obtained upon irradiation at 546 nm at -40 °C and c) mixture of *Z*-**2a** and *E*-**2a** obtained upon warming to 40 °C for 20 min.

A similar series of experiments was performed with *Z*-**2a** (Figure 5). When a mixture of *Z*-**2a** and PdTPP was irradiated at 546 nm, the signal of the alkyl protons shifted, indicating the formation of thermally unstable *E*-**2b** (Scheme 3, step 3). Likewise the signal of the methoxy group at 2.6 ppm decreases with an increase in the intensity of the methoxy signal (3.4 ppm) of *E*-**2b** (Figure 5). At the PSS, the ratio of *Z*-**2a** to *E*-**2b** was 65:35. Upon warming, the alkyl signals shift back to their original position, while the intensity of the methoxy signal remains the same (Scheme 3, step 4). This shows that all of the thermally unstable form generated by photoisomerization in steps 1 and 3 is converted to the expected thermally stable form and that the rotation is unidirectional.

Photoisomerization by intramolecular energy transfer

In motor-porphyrin hybrid **13**, the energy transfer is expected to take place in an intramolecular fashion to drive the photoisomerization of the motor (Scheme 7). Because the motor is covalently linked to the sensitizer, the effective molarity will be high and energy transfer should proceed more efficiently than in the intermolecular case.

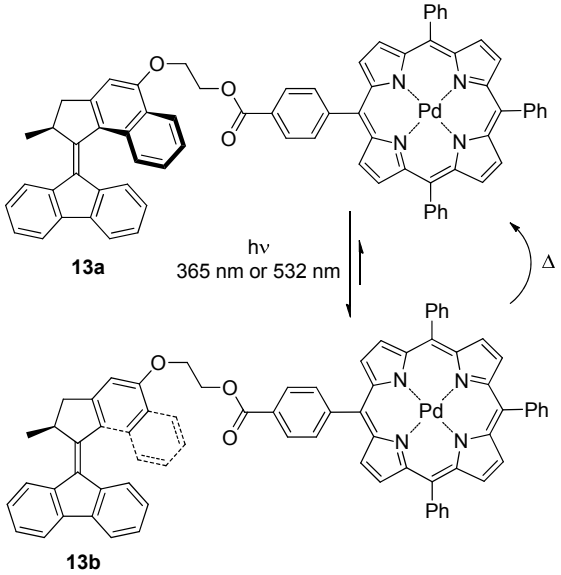

Scheme 7 Expected isomerization behavior of **13.**

When irradiated with visible light (532 nm, 6 ns, 10 Hz) for 10 s, the photostationary state of an argon purged solution of **13** was reached, and this resulted in an increase of the absorbance between 450 nm and 500 nm with a concomitant small red-shift of the shoulder around 375 nm (Figure 6a), similar to what was observed for **1**. The isomerization was performed repetitively: the same sample was irradiated at 532 nm for 10 s and left in the dark for 20 min for four cycles and the change in the absorbance was monitored at 460 nm (Figure 6b). The excellent repeatability of the UV/vis absorption spectral changes of **13** indicates that the photoisomerization of the motor part is reversible and degradation does not occur.

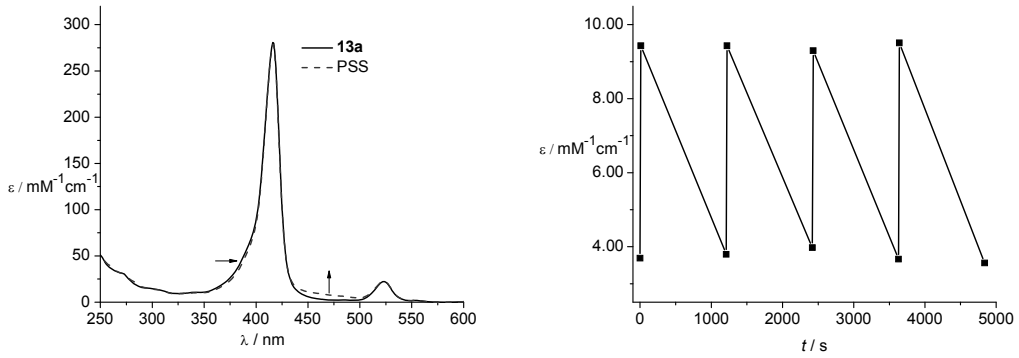

Figure 6 a) UV/vis absorption spectrum of **13a** (black line) and the mixture of **13a** and **13b** obtained after irradiation at 532 nm (red dashed line); b) Molar absorptivity at 460 nm of a solution of **13** alternately irradiated at 532 nm for 10 s and left in the dark at rt for 20 min.

The changes in the UV/vis absorption spectrum upon irradiation are somewhat obscured by overlap of the strong Soret band of the porphyrin. However, with CD spectroscopy clear spectral changes are also expected in the 250-350 nm region, where the porphyrin has negligible absorption. Indeed, when a solution of (*R*)-**13a** is irradiated at 532 nm, a distinct decrease in signal is observed (Figure 7). As was the case for **1**, complete inversion is not observed, presumably due to a relatively poor PSS (*vide infra*). The observed spectral changes are fully reversible when thermal helix inversion is allowed to take place. If the palladium-free porphyrin **14** is used instead of **13**, no changes are observed in either the UV/vis absorption or the CD spectrum. Prolonged irradiation led to irreversible changes in the CD spectrum, which are attributed to degradation.

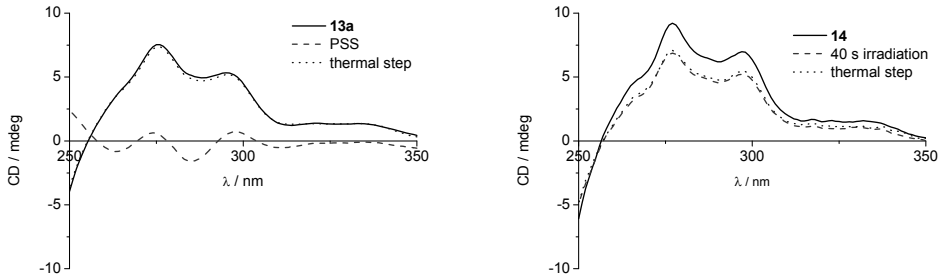

Figure 7 a) CD spectra of **13a** (black line) and the mixture of **13a** and **13b** obtained after 10 s irradiation at 532 nm (red dashed line) and the mixture after the thermal step (blue dotted line). b) CD spectra of **14** before (black line) and after 40 s irradiation at 532 nm (red dashed line) and after the thermal step (blue dotted line).

At 138 kJ/mol, the triplet excited state energy of free-base tetraphenylporphyrin (H_2TPP) is considerably lower than that of both PdTPP and motor **1**, so triplet energy transfer is not expected in this case.[47] Energy transfer from the porphyrin in the singlet excited state cannot take place because it is too low in energy relative to the singlet excited state of **1**. These results indicate that the energy transfer in the case of the palladated porphyrin goes via triplet energy transfer.

The photostationary state for the sensitized isomerization between **12a** and thermally unstable **12b** was determined by ^{1}H NMR spectroscopy. A solution of **12a** in toluene-d_8 was irradiated (532 nm) at -40 °C until further changes were not observed. By comparing

the integrals of the absorptions of **12a** and **12b** in the alkyl region the photostationary state ratio **12a**:**12b** was determined to be 67:33. This is similar to the 57:43 ratio obtained under direct irradiation (365 nm) for a methoxy-substituted analogue of **1**.[42]
The photochemical quantum yield of the visible light-driven photoisomerization was determined to be 0.11±2 using potassium reineckate as a standard.[48,49] This quantum yield is almost as high as the one obtained for direct excitation, which is 0.14, showing that similar efficiency can be reached using visible light.[50]

Luminescence lifetime and quenching

The results of the irradiation experiments using non-metallated motor-porphyrin hybrid **14** implied that the rotation in case of visible light irradiation proceeds via triplet energy transfer. To demonstrate this conclusively, the luminescence lifetimes of the porphyrins were measured. Steady-state emission spectra of PdTPP, a mixture of PdTPP and **1** with a ratio of 1:2.5 and motor-PdTPP hybrid **13** in 1,2-dichloroethane under argon atmosphere were recorded (Figure 8a). PdTPP irradiated with visible light (532 nm) gives fluorescence at 610 nm and phosphorescence at 710 nm.[51] The phosphorescence intensity and quantum yield of PdTPP are significantly reduced by the molecular motor, both in an inter- and intramolecular fashion, which is attributed to the energy transfer from PdTPP to the motor. The quenching of phosphorescence in **13** was stronger than in the mixture of **1** and PdTPP under the same conditions. In contrast, the fluorescence intensity and quantum yield of PdTPP were not influenced by the presence of the molecular motor. This confirms the energy transfer is not via singlet energy transfer but via triplet energy transfer. As a control, the steady-state fluorescence of H_2TPP was compared to that of **14** (Figure 8b); singlet energy transfer was not observed and there was no change in the fluorescence quantum yield.

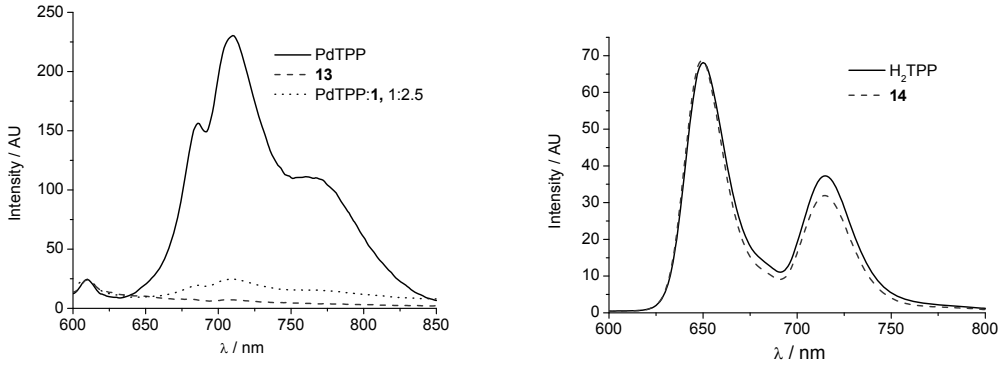

Figure 8 a) Emission spectra of PdTPP (2×10^{-5} M, black line), a 1:2.5 mixture of PdTPP and **1** (PdTPP 2×10^{-5} M, **1** 5×10^{-5} M, red dashed line), and **13** (2×10^{-5} M, blue dotted line) in degassed 1,2-dichloroethane, excited at λ = 532 nm at room temperature; b) Emission spectra of H_2TPP (black line) and **14** (red dashed line) excited at 418 nm (chloroform solution, 1×10^{-5} M).

The intra- and intermolecular energy transfer were further studied by means of time resolved emission spectroscopy. The phosphorescence decay curves of PdTPP, a 1:2.5 mixture of PdTPP and **1**, and **13** were recorded at 710 nm (Figure 9a). The lifetimes were fitted using first order exponential decay kinetics. The phosphorescence lifetime was reduced from 34 µs for PdTPP to 9 µs for the mixture, and to 0.41 µs for **13**, which confirms that quenching of PdTPP triplet excited state occurs. As expected, the covalent system **13** shows more efficient energy transfer than the mixture of PdTPP and **1**. The phosphorescence lifetime of PdTPP in the presence of the motor at concentrations between 0.0 and 0.5 mM in 1,2-dichloroethane in an argon-saturated environment was

determined and the data is shown in the form of a Stern-Volmer plot (τ_0/τ vs. motor concentration, Figure 9b). A linear fit yielded a bimolecular quenching rate constant k_q of 1.8×10^9 M^{-1} s^{-1} for the quenching of ^{3}PdTPP* by **1**. The diffusion-controlled rate constant 1,2-dichloroethane is known to be 8.9×10^9 M^{-1} s^{-1} at 25 °C.[52] This indicates that energy transfer is diffusion rate controlled.

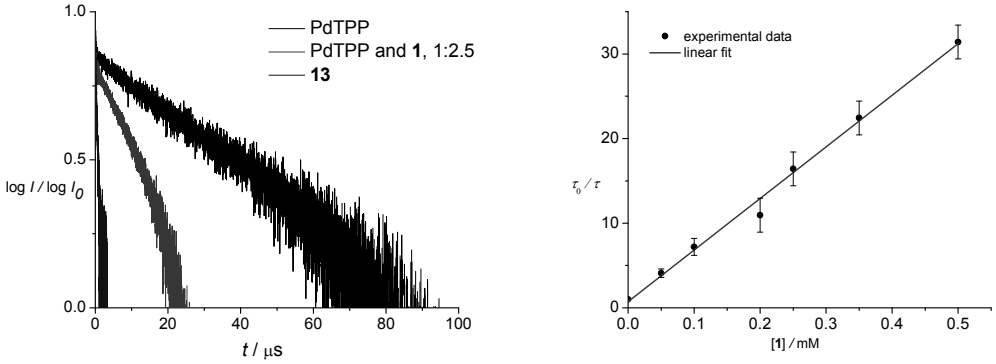

Figure 9 a) Room temperature phosphorescence lifetime measurement of PdTPP (black line), a 1:2.5 mixture of PdTPP and **1** (red dash), and **13** (blue dot) in 1,2-dichloroethane with degassing by at least three freeze-pump-thaw cycles. The traces were measured at 710 nm after excitation (532 nm, 6 ns, 10 Hz); b) Stern-Volmer plot for quenching of PdTPP by **1** (black points) and linear fit (red line).

Conclusion

In conclusion, the photoisomerization in second generation molecular motors can be driven by visible light when a suitable triplet sensitizer is employed. Energy transfer from the triplet excited state of PdTPP to the motor leads to the formation of the unstable form, which subsequently undergoes thermal helix inversion resulting in unidirectional rotation of the upper half relative to the lower half. The photoisomerization was characterized by UV/vis, CD and ^{1}H NMR spectroscopy and it was found that the sensitized photoisomerization proceeds similar to photoisomerization by direct irradiation; the main difference is that the PSS is decreased to a minor extent with respect to the unstable form. Energy transfer from the porphyrin to the motor takes place conveniently in an intermolecular fashion to drive the photoisomerization. However, covalent linking of the motor to the porphyrin increases the efficiency substantially.

Using excitation at longer wavelengths than 546 nm is in principle possible. However, energy transfer to motor **1** requires that the triplet excited state energy of the sensitizer is higher than that of **1**. Considering the triplet excited state energies of PdTPP (178 kJ/mol) and H_2TPP (138 kJ/mol), the current limit is between 672-872 nm. An alternative approach is to use motor structures with lower triplet excited state energies. Ultimately, driving the photoisomerization of overcrowded alkene-based motors with IR light would expand their use to biological systems

Acknowledgements

Phosphorescence lifetime measurements and Stern-Volmer quenching kinetics were performed by Lili Hou, who is gratefully acknowledged for her contributions.

Experimental section

Synthesis

General

For more general remarks, see Chapter 2. Palladium tetraphenylporphyrin,[45] motors **1** and **2**,[29] 9-diazofluorenone and ketone **4**[42] were synthesized according to literature procedures.

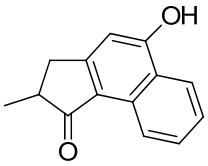

5-hydroxy-2-methyl-2,3-dihydro-1*H*-cyclopenta[*a*]naphthalen-1-one 5

To pyridine hydrochloride (6.0 g, 52 mmol) at 150 °C was added **4** (550 mg, 2.43 mmol). The mixture was heated to 190 °C for 2 h, after which it was allowed to cool to rt. The solid mass was partitioned between H_2O (200 mL) and ethyl acetate (200 mL). The organic layer was washed with 0.5 M aqueous HCl (100 mL), H_2O (100 mL) and brine (100 mL) and dried on Na_2SO_4. The solvent was removed *in vacuo* and the crude product was purified by column chromatography (SiO_2, 2:1 pentane:ethyl acetate, R_f = 0.3) yielding **5** (286 mg, 56 %) as an orange solid. mp >200 °C; ^{1}H NMR (300 MHz, DMSO) δ 11.35 (br s, 1H), 8.93 (d, *J* = 8.1 Hz, 1H), 8.17 (d, *J* = 8.4 Hz, 1H), 7.63 (t, *J* = 7.3 Hz, 1H), 7.49 (t, *J* = 7.3 Hz, 1H), 6.88 (s, 1H), 3.32 (overlaps with H_2O, dd, *J* = 17.9 Hz, 7.3 Hz, 1H), 2.65 (d, *J* = 17.2 Hz, 2H), 1.17 (d, *J* = 6.6 Hz, 3H); ^{13}C NMR (75 MHz, DMSO) δ 207.6 (C), 161.0 (C), 160.4 (C), 131.2 (C), 129.8 (CH), 126.0 (CH), 124.7 (C), 123.6 (CH), 123.5 (CH), 121.8 (C), 106.3 (CH), 42.1 (CH), 35.6 (CH_2), 17.2 (CH_3); HRMS (ESI^+) calcd. for $C_{14}H_{13}O_2$ [M+H] 213.0910, found 213.0910.

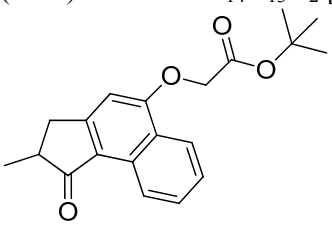

***tert*-butyl 2-((2-methyl-1-oxo-2,3-dihydro-1*H*-cyclopenta[*a*]naphthalen-5-yl)oxy)acetate 6**

To a suspension of **5** (235 mg, 1.11 mmol) and K_2CO_3 (209 mg, 1.5 mmol) in DMF (12 mL) at 50 °C was added *t*-butyl chloroacetate (0.5 mL, 3.5 mmol) and the mixture was stirred at 50 °C for 2 h. The reaction mixture was diluted with ethyl acetate (100 mL) and washed with H_2O (3 x 100 mL) and brine (100 mL) and dried on Na_2SO_4. The volatiles were removed *in vacuo* and the crude product was purified by column chromatography (SiO_2, 5:2 pentane:ethyl acetate, R_f = 0.5) yielding **6** (305 mg, 84%) as a yellow solid. mp 129.6-131.5 °C; ^{1}H NMR (300 MHz, $CDCl_3$) δ 9.13 (d, *J* = 8.7 Hz, 1H), 8.38 (d, *J* = 8.1 Hz, 1H), 7.69 (t, *J* = 7.5 Hz, 1H), 7.56 (t, *J* = 7.5 Hz, 1H), 6.66 (s, 1H), 4.79 (s, 2H), 3.42 (dd, *J* = 18.3 Hz, 7.8 Hz, 1H), 2.79 (m, 2H), 1.53 (s, 9H), 1.36 (d, *J* = 6.9 Hz, 3H); ^{13}C NMR (50 MHz, $CDCl_3$) δ 208.3 (C), 166.9 (C), 159.7 (C), 158.5 (C), 130.6 (C), 129.4 (CH), 126.1 (CH), 125.0 (C), 124.1 (C), 123.7 (CH), 122.6 (CH), 102.3 (CH), 82.8 (C), 65.9 (CH_2), 42.1 (CH), 35.7 (CH_2), 28.0 ($3CH_3$), 16.7 (CH_3); HRMS (ESI^+) calcd. for $C_{20}H_{23}O_4$ [M+H] 327.1591, found 327.1590.

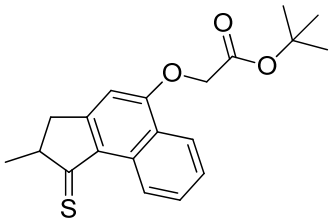

***tert*-butyl 2-((2-methyl-1-thioxo-2,3-dihydro-1*H*-cyclopenta[*a*]naphthalen-5-yl)oxy)-acetate 7**

To a solution of **6** (50 mg, 0.15 mmol) in THF (2 mL) was added Lawesson's reagent (74 mg, 0.18 mmol). The reaction mixture was stirred for 3.5 h at 50 °C. The solvent was removed *in vacuo* and the crude product was purified by column chromatography (SiO_2, toluene, R_f = 0.5) yielding **7** (40 mg, 78%) as a purple-red solid. Thioketone **7** could be stored at rt under inert atmosphere for at least three days without degradation. ^{1}H NMR (300 MHz, $CDCl_3$) δ 10.15 (d, *J* = 8.4 Hz, 1H), 8.40 (d, *J* = 8.1 Hz, 1H), 7.73 (t, *J* = 7.7 Hz, 1H), 7.56 (t, *J* = 7.5 Hz, 1H), 6.63 (s, 1H), 4.76 (s, 2H), 3.39 (dd, *J* = 6.4, 18.1 Hz, 1H), 3.10 (m, *J* = 7.0 Hz, 1H), 2.81 (d, *J* = 18.0 Hz, 1H), 1.53 (s, 9H), 1.47 (d, *J* = 7.3 Hz, 3H); ^{13}C NMR (75 MHz, $CDCl_3$) δ 245.6 (C), 166.9 (C), 161.5 (C), 160.1 (C), 134.3 (C), 131.6 (C), 131.0 (CH), 126.6 (CH), 125.5 (C), 124.3 (CH), 123.1 (CH), 102.1 (CH), 83.2 (C), 66.1 (CH_2), 55.1 (CH), 40.5 (CH_2), 28.3 ($3CH_3$), 22.0 (CH_3); HRMS (ESI^+) calcd. for $C_{20}H_{23}O_3S$ [M+H] 343.1362, found 343.1358.

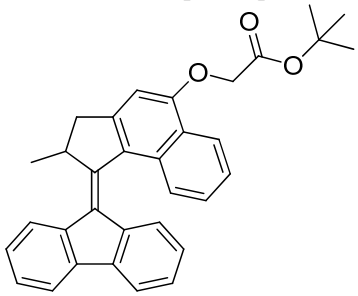

***tert*-butyl 2-((1-(9*H*-fluoren-9-ylidene)-2-methyl-2,3-dihydro-1*H*-cyclopenta[*a*]naph-thalen-5-yl)oxy)acetate 8**

A solution of **7** (108 mg, 0.316 mmol) and 9-diazofluorenone (100 mg, 0.521 mmol) in toluene (10 mL) was stirred at 50 ºC for 16 h. The solvent was removed *in vacuo* and the residue was purified by column chromatography (SiO_2, 1:1 heptane:toluene, R_f = 0.2) yielding a mixture of **8** and the corresponding episulfide. This mixture was dissolved in toluene (10 mL) and PPh_3 (250 mg, 0.95 mmol) was added and the solution was heated to reflux for 16 h. The volatiles were removed *in vacuo* and the residue was redissolved in Et_2O (10 mL). Methyl iodide (0.1 mL) was added and the mixture was stirred at rt for 3 h. A white precipitate was filtered off and the filtrate was concentrated. Column chromatography (SiO_2, 1:1 pentane:toluene) yielded **8** (98 mg, 65%) as a yellow solid. mp 153.5-154.3 °C; ^{1}H NMR (300 MHz, $CDCl_3$) δ 8.48 (d, *J* = 8.1 Hz, 1H), 7.99 (m, 1H), 7.87 (m, 1H), 7.77 (d, *J* = 7.5 Hz, 1H), 7.71 (d, *J* = 8.3 Hz, 1H), 7.48 (t, *J* = 7.2 Hz, 1H), 7.40-7.32 (m, 4H), 7.20 (t, *J* = 6.9 Hz, 1H), 6.83 (s, 1H), 6.80 (d, *J* = 7.1 Hz, 1H), 6.72 (d, *J* = 7.9 Hz, 1H), 4.84 (s, 2H), 4.35 (m, *J* = 6.3 Hz, 1H), 3.57 (dd, *J* = 5.6, 15.0 Hz, 1H), 2.72 (d, *J* = 15.1 Hz, 1H), 1.57 (s, 9H), 1.43 (d, *J* = 6.6 Hz, 3H); ^{13}C NMR (125 MHz, $CDCl_3$) δ 170.3 (C), 158.9 (C), 154.0 (C), 151.2 (C), 142.6 (C), 141.9 (C), 139.9 (C), 133.3 (C), 132.3 (C), 131.3 (C), 130.1 (CH), 130.0 (CH), 129.5 (CH), 129.2 (CH), 129.1 (CH), 128.5 (CH), 128.4 (CH), 127.7 (CH), 127.3 (C), 126.5 (CH), 125.7 (CH), 122.3 (CH), 121.6 (CH), 106.3 (CH), 85.3 (C), 68.9 (CH_2), 47.9 (CH), 45.2 (CH_2), 30.8

(3CH_3), 22.3 (CH_3); HRMS (ESI^+) calcd. for $C_{33}H_{30}O_3Na$ [M+Na] 497.2087, found 497.2097. Elemental analysis calcd. C: 83.51 H: 6.37 found C: 83.14 H: 6.27.

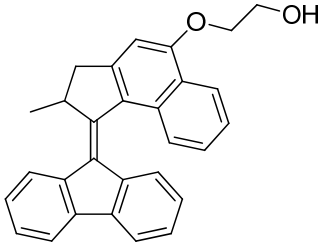

2-((1-(9*H*-fluoren-9-ylidene)-2-methyl-2,3-dihydro-1*H*-cyclopenta[*a*]naphthalen-5-yl)oxy)ethanol 9

To a solution of **8** (100 mg, 0.210 mmol) in THF (4 mL) at 0 °C was added $LiAlH_4$ (70 mg, 1.84 mmol). After stirring for 3 h at 0 °C the reaction was quenched by addition of excess $Na_2SO_4.10H_2O$. The mixture was allowed to warm to rt, filtered and concentrated *in vacuo*. The crude product was purified by column chromatography (SiO_2, 2:1 pentane:ethyl acetate, R_f = 0.2) yielding **9** (68 mg, 80%) as a yellow solid. ^{1}H NMR (300 MHz, DMSO) δ 8.39 (d, *J* = 8.4 Hz, 1H), 7.93 (m, 2H), 7.85 (d, *J* = 7.7 Hz, 1H), 7.52-7.30 (m, 5H), 7.19 (m, *J* = 7.1 Hz, 2H), 6.78 (t, *J* = 7.3 Hz, 1H), 6.58 (d, *J* = 8.1 Hz, 1H), 5.07 (t, *J* = 5.7 Hz, 1H), 4.33-4.18 (m, 3H), 3.91 (m, 2H), 3.34 (dd, *J* = 5.5, 15.6 Hz, 1H), 2.72 (d, *J* = 15.7 Hz, 1H), 1.28 (d, *J* = 6.2 Hz, 3H),; ^{13}C NMR (50 MHz, DMSO) δ 157.8 (C), 152.5 (C), 150.6 (C), 139.8 (C), 139.6 (C), 139.3 (C), 137.1 (C), 130.5 (C), 127.9 (CH), 127.8 (CH), 127.7 (C), 127.2 (2CH), 127.1 (2CH), 126.4 (CH), 125.6 (CH), 125.3 (CH), 124.7 (C), 124.2 (CH), 123.8 (CH), 120.6 (CH), 120.0 (CH), 104.7 (CH), 71.1 (CH_2), 60.3 (CH_2), 45.4 (CH), 42.7 (CH_2), 20.2 (CH_3); HRMS (ESI) calcd. for $C_{29}H_{25}O_2$ [M+H] 405.1849, found 405.1848.

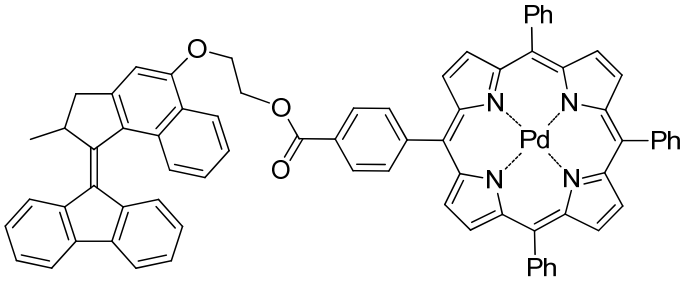

PdTPP-motor hybrid 13

A solution of **9** (41 mg, 0.101 mmol), **12** (77 mg, 0.1 mmol) 4-dimethylaminopyridine (DMAP) (15 mg, 0.12 mmol) and 1-ethyl-3-(3-dimethylaminopropyl) carbodiimide hydrochloride (EDC) (21 mg, 0.11 mmol) in CH_2Cl_2 (3 mL) at rt was stirred for 16 h in the dark. Another batch of EDC (5 mg, 0.026 mmol) was added and stirring was continued for 4 h. The volatiles were removed *in vacuo* and the residue was subjected to column chromatography (SiO_2, 1:1 pentane:$CHCl_3$) yielding **13** (103 mg, 88%) as a purple solid. ^{1}H NMR (500 MHz, $CDCl_3$) δ 8.87 (s, 6H), 8.80 (d, *J* = 4.8 Hz, 2H), 8.54 (d, *J* = 8.5 Hz, 1H), 8.50 (d, *J* = 8.0 Hz, 2H), 8.30 (d, *J* = 7.9 Hz, 2H), 8.19 (d, *J* = 6.6 Hz, 6H), 8.0 (d, *J* = 7.1 Hz, 1H), 7.88 (d, *J* = 7.3 Hz, 1H), 7.83-7.72 (m, 11H), 7.56 (t, *J* = 7.6 Hz, 1H), 7.47-7.37 (m, 2H), 7.22 (t, *J* = 7.4 Hz, 1H), 6.95 (s, 1H), 6.86 (t, *J* = 7.6 Hz, 1H), 6.78 (d, *J* = 6.8 Hz, 1H), 4.97 (s, 2H), 4.55 (s, 2H), 4.33 (m, 1H), 3.52 (dd, *J* = 15.0, 5.2 Hz, 1H), 2.72 (d, *J* = 15.2 Hz, 1H), 1.27 (d, *J* = 6.3 Hz, 3H); ^{13}C NMR (100 MHz, $CDCl_3$) δ 166.9 (C), 157.2 (C), 151.6 (C), 149.1 (C), 147.3 (C), 142.3 (2C), 142.2 (2C), 142.1 (3C), 142.0 (2C) 141.4 (2C), 140.3 (C), 140.2 (C), 139.6 (C), 137.6 (C), 134.6

(2CH), 134.4 (6CH), 131.8 (2CH), 131.6 (2CH), 131.5 (2CH), 131.1 (C), 130.9 (CH), 129.8 (C), 129.7 (C), 129.0 (C), 128.5 (2CH), 128.1 (3CH), 127.8 (CH), 127.7 (CH), 127.1 (7CH), 126.8 (2CH), 126.1 (2CH), 125.3 (CH), 125.2 (C), 124.1 (CH), 123.3 (CH), 122.5 (C), 122.4 (2C), 120.6 (C), 119.9 (CH), 119.1 (CH), 104.1 (CH), 104.0 (CH), 67.0 (CH_2), 63.7 (CH_2), 45.5 (CH), 42.9 (CH_2), 19.9 (CH_3); MS (EI) calcd. for $C_{74}H_{51}N_4O_3Pd$ [M+H] 1149.29, found 1149.17. HPLC Chiralpak AD column, 80:20 *n*-heptane:2-propanol, T = 50 °C, flow rate 1 mL/min, retention times 14 min, 18 min.

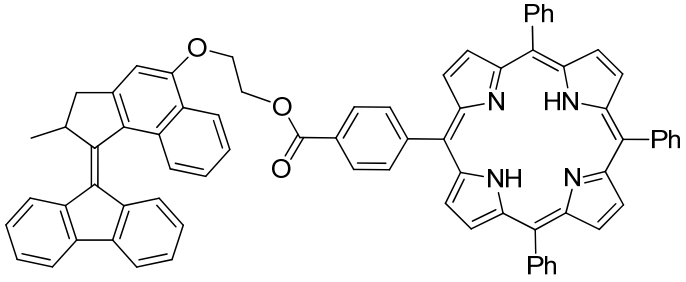

H_2TPP-motor hybrid 14

A solution of **9** (25 mg, 0.062 mmol), **11** (41 mg, 0.062 mmol) 4-dimethylaminopyridine (DMAP) (7.5 mg, 0.061 mmol) and 1-ethyl-3-(3-dimethylaminopropyl) carbodiimide hydrochloride (EDC) (14 mg, 0.073 mmol) in CH_2Cl_2 (3 mL) at rt was stirred for 2 d in the dark. The volatiles were removed *in vacuo* and the residue was loaded on a silica column. Unreacted starting material was eluted with 1:1 pentane:CH_2Cl_2, after which the porphyrin fraction was eluted with $CHCl_3$. The crude product was purified by recrystallization (CH_2Cl_2/MeOH, layer addition) yielding **14** (42 mg, 65%) as a purple solid. ^{1}H NMR (400 MHz, $CDCl_3$) δ 8.90 (s, 6H), 8.84 (d, J = 4.7 Hz, 2H), 8.60-8.52 (m, 3H), 8.37 (d, J = 8.0 Hz, 2H), 8.29-8.23 (m, 6H), 8.05-7.96 (m, 1H), 7.93-7.84 (m, 1H), 7.84-7.66 (m, 11H), 7.56 (t, J = 8.0 Hz, 1H), 7.46-7.33 (m, 3H), 7.21 (t, J = 7.2 Hz, 1H), 7.08 (s, 1H), 6.90-6.76 (m, 2H), 5.19-4.93 (m, 2H), 4.72 (d, J = 3.3 Hz, 2H), 4.43-4.28 (m, 1H), 3.60 (dd, J = 15.1, 5.6 Hz, 1H), 2.77 (d, J = 15.1 Hz, 1H), 1.45 (d, J = 6.6, 3H), -2.71 (s, 2H). ^{13}C NMR (50 MHz, $CDCl_3$) δ = 167.1 (C), 157.1 (C), 151.7 (C), 149.2 (2C), 147.7 (2C), 142.3 (4C), 140.1 (C), 140.0 (C), 139.5 (C), 137.5 (C), 134.9 (2CH), 134.8 (6CH), 130.9 (C), 129.5 (2C), 128.7 (C), 128.4 (3CH), 128.1 (4CH), 127.6 (3CH), 127.0 (8CH), 126.7 (2CH), 126.1 (CH), 126.0 (2CH), 125.3 (CH), 124.9 (C), 124.0 (CH), 123.2 (CH), 120.9 (C), 120.7 (2C), 119.9 (CH), 119.2 (CH), 118.7 (C), 103.8 (CH), 67.0 (CH_2), 63.8 (CH_2), 45.5 (CH), 42.8 (CH_2), 19.9 (CH_3). MS (EI) calcd. for $C_{74}H_{51}N_4O_3Pd$ [M+H] 1149.29, found 1149.17. HPLC Chiralpak AD column, 90:10 *n*-heptane:2-propanol, T = 50 °C, flow rate 1 mL/min, retention times 16 min, 21 min.

General procedure for irradiation experiments

UV/Vis absorption spectra were measured on Jasco V-630 spectrometer. Emission spectra were measured using a Jasco FP-6200 spectrofluorimeter. Room temperature phosphorescence spectra were obtained in 1,2-dichloroethane under Argon atmosphere with degassing by at least three freeze-pump-thaw cycles. Phosphorescence lifetimes were obtained using a home built system. Excitation was performed using the second harmonic (532 nm, 10 Hz, 25 mJ, 10 ns) of a Q-switched Nd:YAG laser (Innolas 400) with a Si-diode trigger sensor. The emission from the sample was focused into a Zolix Omni-λ 300 monochromator coupled with a Zolix PMTH-S1-CR131 side-on PMT. Emission decay traces were recorded with 50 Ohm termination on a Tetronix DPO 4032 digital phosphor Oscilloscope and transferred to a PC for data analysis using homebuilt software written in National Instruments LabVIEW 8.2.

Solutions of **1**, **2**, **13** and **14** were bubbled with Argon for at least two minutes before irradiation. For fluorescence and phosphorescence emission and lifetime measurements, the solutions were deoxygenated with at least three freeze-pump-thaw cycles. For irradiation with a fluorescent lamp, a 546±5 nm bandpass filter was used and the solutions were cooled to -40 °C using a cryostat. Depending on the concentration, irradiation times were up to 1 h at ~10^{-5} M and overnight for samples used for NMR spectroscopy (~10^{-3} M). Laser irradiation was employed at rt with care taken to perform measurements within 30 s of irradiation. In general, PSS was reached within 10 s of irradiation. To be certain photostationary states were reached, several spectra at set intervals were recorded. Thermal isomerization was performed by leaving the solutions in the dark at 20-40 °C for at least 20 min. The solution was then cooled again to the temperature at which irradiation was performed before further measurement.

Computational chemistry

Calculations of triplet excited state energy and CD spectra were performed using the Gaussian 09 program.[53] Geometry optimizations were performed at the B3LYP/6-31G(d,p) level using tight convergence criteria. Frequency analysis was performed on the optimized structures to ensure a true energy minimum was reached. CD spectra were calculated on B3LYP/6-31G++(d,p) and normalized to the highest band in the experimental spectrum.

References

[1] E. R. Kay, D. A. Leigh, F. Zerbetto, *Angew. Chem. Int. Ed.* **2007**, *46*, 72-191.
[2] A. Coskun, M. Banaszak, R. D. Astumian, J. F. Stoddart, B. A. Grzybowski, *Chem. Soc. Rev.* **2012**, *41*, 19-30.
[3] J. A. Faiz, V. Heitz, J. P. Sauvage, *Chem. Soc. Rev.* **2009**, *38*, 422-442.
[4] V. Balzani, A. Credi, M. Venturi, *Chem. Soc. Rev.* **2009**, *38*, 1542-1550.
[5] Molecular switches (Eds.: B. L. Feringa, W. R. Browne), Wiley-VCH, Weinheim, **2011.**
[6] H. M. Dhammika Bandara, S. C. Burdette, *Chem. Soc. Rev.* **2012**, *41*, 1809-1825.
[7] C. J. Barrett, J. Mamiya, K. G. Yager, T. Ikeda, *Soft Matter* **2007**, *3*, 1249-1261.
[8] K. Matsuda, M. Irie, *J. Photochem. Photobiol. C*, **2004**, *5*, 169-182.
[9] F. M. Raymo, M. Tomasulo, *Chem. Soc. Rev.* **2005**, *34*, 327-336.
[10] B. L. Feringa, *J. Org. Chem.* **2007**, *72*, 6635-6652.
[11] M. M. Pollard, M. Klok, D. Pijper, B. L. Feringa, *Adv. Funct. Mater.* **2007**, *17*, 718-729.
[12] A. A. Beharry, O. Sadovski, G. A. Woolley, *J. Am. Chem. Soc.* **2011**, *133*, 19684-19687.
[13] M. Pawlicki, H. A. Collins, R. G. Denning, H. L. Anderson, *Angew. Chem. Int. Ed.* **2009**, *48*, 3244-3266.
[14] R. H. Douglas, J. C. Partridge, K. S. Dulai, D. M. Hunt, C. W. Mullineaux, P. H. Hynninen, *Vision Res.* **1999**, *39*, 2817-2832.
[15] T. Okada, O. P. Ernst, K. Palczewski, K. P. Hofmann, *Trends Biochem. Sci.* **2001**, *26*, 318-324.
[16] S. K. Brayshaw, S. Schiffers, A. J. Stevenson, S. J. Teat, M. R. Warren, R. D. Bennett, I. V. Sazanovich, A. R. Buckley, J. A. Weinstein, P. R. Raithby, *Chem. Eur. J.* **2011**, *17*, 4385-4395.
[17] D. A. Leigh, J. K. Y. Wong, F. Dehez, F. Zerbetto, *Nature* **2003**, *424*, 174-179.
[18] V. Balzani, M. Clemente-Léon, A. Credi, B. Ferrer, M. Venturi, A. H. Flood, J. F. Stoddart, *Proc. Natl. Acad. Sci. U. S. A.* **2006**, *103*, 1178-1183.
[19] C. A. Hunter, L. D. Sarson, *Tetrahedron Lett.* **1996**, *37*, 699-702.
[20] J.-F. Morin, Y. Shirai, J. M. Tour, *Org. Lett.* **2006**, *8*, 1713-1716.
[21] H. Meier, *Angew. Chem. Int. Ed.* **1992**, *31*, 1399-1420.
[22] G. S. Hammond, J. Saltiel, A. A. Lamola, N. J. Turro, J. S. Bradshaw, D. O. Cowan, R. C. Counsell, V. Vogt, C. J. Dalton, *Am. Chem. Soc.* **1964**, *86*, 3197-3217.
[23] R. Benson, D. F. Williams, *J. Phys. Chem.* **1977**, *81*, 215-220.
[24] A. S. Lukas, M. R. Wasielewski in *Molecular Switches* (Ed.: B. L. Feringa), Wiley-VCH, Weinheim, **2001**, pp. 1-35.
[25] D. Gust, T. A. Moore, A. L. Moore, *Chem. Commun.* **2006**, 1169-1178.
[26] J. A. Mercer-Smith, D. G. Whitten, *J. Am. Chem. Soc.* **1978**, *100*, 2620-2625.

[27] M. Brink, O Wennerström, *J. Photochem. Photobiol., A* **2001**, *143*, 201-208.
[28] H. Möllerstedt, O. Wennerström, *J. Photochem. Photobiol., A* **2001**, *139*, 37-43.
[29] J. Vicario, A. Meetsma, B. L. Feringa, *Chem. Commun.* **2005**, 5910-5912.
[30] J. Vicario, M. Walko, A. Meetsma, B. L. Feringa, *J. Am. Chem. Soc.* **2006**, *128*, 5127-5135.
[31] J. Wang, A. Kulago, W. R. Browne, B. L. Feringa, *J. Am. Chem. Soc.* **2010**, *132*, 4191-4196.
[32] T. Arai, K. Tokumaru, *Chem. Rev.* **1993**, *93*, 23-39.
[33] N. J. Turro, *Modern Molecular Photochemistry*, University Science Books, Sausolito, **1991**, pp. 473-481.
[34] M. Klok, W. R. Browne, B. L. Feringa, *Phys. Chem. Chem. Phys.* **2009**, *11*, 9124-9131.
[35] D. Eastwood, M. J. Gouterman, *Mol. Spectrosc*. **1970**, *35*, 359-375.
[36] A. D. Becke, *J. Chem. Phys*. **1993**, *98*, 1372-1377.
[37] C. Lee, W. Yang, R. G. Parr, *Phys. Rev. B* **1988**, *37*, 785-789.
[38] R. Krishnan, J. S. Binkley, R. Seeger, J. A. Pople, *J. Chem. Phys.* **1980**, *72*, 650-654
[39] These calculations are known to have a significant margin in the determination of the energy of electronically excited states, see S. Grimme, F. Neese, *Chem. Phys.* **2007**, *127*, 154116.
[40] For a review on inter- and intermolecular energy transfer, see F. M. Raymo, M. Tomasulo, *Chem. Soc. Rev.* **2005**, *34*, 327-336.
[41] See for example: N. Aratani, D. Kim, A. Osuka, *Acc. Chem. Res.* **2009**, *42*, 1922-1934.
[42] M. M. Pollard, P. V. Wesenhagen, D. Pijper, B. L. Feringa, *Org. Biomol. Chem.* **2008**, 6, 1605-1612.
[43] G. Caroli, M. G. Kwit, B. L. Feringa, *Tetrahedron* **2008**, *64*, 5956-5962.
[44] J. P. C. Tomé, M. G. P. M. S. Neves, A. C. Tomé, J. A. S. Cavaleiro, A. F. Mendonça, I. N. Pegado, R. Duarte, M. L. Valdeira, *Bioorg. Med. Chem.* **2005**, *13*, 3878-3888.
[45] D. S. Sharada, A. Z. Muresan, K. Muthukumaran, J. S. Lindsey, *J. Org. Chem.* **2005**, *70*, 3500-3510.
[46] M. Gouterman, *J. Mol. Spectrosc.* **1961**, *6*, 138-163.
[47] J. R. Darwent, P. Douglas, A. Harriman, G. Porter, M.-C. Richoux, *Coord. Chem. Rev.* **1982**, *44*, 83-126.
[48] *Handbook of Photochemistry* (Eds.: M. Montalti, A. Credi, L. Prodi, M. T. Gandolfi), CRC Press, Boca Raton, **2006**, p. 609-610.
[49] J. Szychlinski, P. Bilski, K. Martuszewski, J. Blazejowski, *Analyst* **1989**, *114*, 739-741.
[50] J. Conyard, K. Addison, I. A. Heisler, A. Cnossen, W. R. Browne, B. L. Feringa, S. R. Meech, *Nature Chem.* **2012**, *4*, 547-551.
[51] J. E. Rogers, K. A. Nguyen, D. C. Hufnagle, D. G. Mclean, W. Su, K. M. Gossett, A. R. Burke, S. A. Vinogradov, R. Pachter, P. A. Fleitz, *J. Phys. Chem. A* **2003**, *107*, 11331-11339.
[52] *Handbook of Photochemistry* (Eds.: M. Montalti, A. Credi, L. Prodi, M. T. Gandolfi), CRC Press, Boca Raton, **2006**, p. 424.
[53] Gaussian 09, Revision B.1, M. J. Frisch, G. W. Trucks, H. B. Schlegel, G. E. Scuseria, M. A. Robb, J. R. Cheeseman, G. Scalmani, V. Barone, B. Mennucci, G. A. Petersson, H. Nakatsuji, M. Caricato, X. Li, H. P. Hratchian, A. F. Izmaylov, J. Bloino, G. Zheng, J. L. Sonnenberg, M. Hada, M. Ehara, K. Toyota, R. Fukuda, J. Hasegawa, M. Ishida, T. Nakajima, Y. Honda, O. Kitao, H. Nakai, T. Vreven, J. A. Montgomery, Jr., J. E. Peralta, F. Ogliaro, M. Bearpark, J. J. Heyd, E. Brothers, K. N. Kudin, V. N. Staroverov, R. Kobayashi, J. Normand, K. Raghavachari, A. Rendell, J. C. Burant, S. S. Iyengar, J. Tomasi, M. Cossi, N. Rega, J. M. Millam, M. Klene, J. E. Knox, J. B. Cross, V. Bakken, C. Adamo, J. Jaramillo, R. Gomperts, R. E. Stratmann, O. Yazyev, A. J. Austin, R. Cammi, C. Pomelli, J. W. Ochterski, R. L. Martin, K. Morokuma, V. G. Zakrzewski, G. A. Voth, P. Salvador, J. J. Dannenberg, S. Dapprich, A. D. Daniels, Ö. Farkas, J. B. Foresman, J. V. Ortiz, J. Cioslowski, D. J. Fox, Gaussian, Inc., Wallingford CT, **2009**.

Chapter 5: Scanning tunneling microscopy studies of molecular motors at the liquid/solid interface[I]

This chapter deals with the design, synthesis and STM studies of multimotor systems at the 1-phenyloctane/HOPG interface. Three different mulitmotor systems were synthesized and their self-assembly was studied using scanning tunneling microscopy. Irradiation of the molecules in solution resulted in photoisomerization, but on surface this could not be observed.

Introduction

Synthetic molecular motors have the potential to play an essential role in the development of nanoscale mechanical devices, as evident from the many fascinating natural systems that use nanometer-sized motors to drive crucial biological processes.[1,2] Many scientists, inspired by these natural systems, have attempted to mimic their functions with (semi)-synthetic molecular systems.[3,4] However, major challenges still exist including performing useful work, such as controlled, directional movement and the transport of cargo.

A key problem in nanotechnology research is Brownian motion, which can overwhelm controlled motion performed by molecular switches and motors. One strategy to reduce the influence of Brownian motion is to immobilize molecules on a solid surface. By introducing more order, it may be possible to take advantage of the collective motion to perform useful work.[5] There is already a large number of examples of light-activated switches covalently linked to surfaces,[6] and even electronic devices based on such systems have been made.[7] The molecular motors developed in our group have also been show to operate when attached to gold[8,9,10] or quartz.[11,12,13] The next step is to incorporate them as part of a nanoscale device or machine in order to take advantage of their unique unidirectional rotation. Some examples of nanomachines that might ultimately be able to achieve powered movement across surfaces have been reported recently,[14,15,16] all of which would make use of photochemical *E*-*Z* isomerization of either azobenzenes or overcrowded alkenes to drive them.

Scanning tunneling microscopy (STM) is the preferred technique for studying such a nanoscale machine on a surface, as it can be used to visualize the surface at submolecular resolution and even manipulate single-molecule devices.[17] However, this also introduces potential problems. Because STM needs to be carried out on a conducting substrate, excited states in photochemical conversions are easily quenched. The quenching can be diminished by increasing the distance between the photochromic molecule and the substrate. This strategy was successfully implemented in the photoisomerization of azobenzene on the Au(111) surface. By decorating the azobenzene with four *tert*-butyl groups, it no longer lays flat on a surface and *E*-*Z* isomerization could be induced by UV irradiation.[18,19] This was later expanded to other surfaces as well.[20,21,22]

An alternative approach is to use the STM tip to electrochemically induce isomerization.[23] In this way, isomerization of the motor units in a molecular nanocar on a Cu(111) surface was recently achieved.[24] By means of this isomerization, the molecule propels itself across the surface. Due to the design, the movement is directional, taking advantage of the unique properties of overcrowded alkene-based molecular motors.

[I] Part of the work presented in this chapter has been published: A. Cnossen, D. Pijper, T. Kudernac, M. M. Pollard, N. Katsonis, B. L. Feringa, *Chem. Eur. J.* **2009**, *15*, 2768-2772.

All these studies involving isomerization of azobenzenes and (overcrowded) alkenes on the surface were carried out under ultra-high vacuum (UHV) conditions and at cryogenic temperatures. Under these conditions, substrate-analyte interactions dominate, and the mobility of the analyte is minimized, allowing for the study of both monolayers and single molecules at maximum resolution. Still, a major challenge is to perform these experiments under ambient conditions, especially considering potential applications. This requires a careful balance between substrate-analyte, solvent-analyte and solvent-substrate interactions to prevent the molecules from either adhering too strongly to the surface or succumbing to Brownian motion. In this chapter, the design, synthesis and analysis of a number of systems intended for photoisomerization on surfaces under ambient conditions is described.

Results and discussion

Molecular design

Analyte-substrate interactions are crucial for STM. When using liquid/solid interface STM rather than UHV, analyte-analyte interactions become more important as well, because single molecules are generally too mobile to be observed. Intermolecular interactions allow for the formation of monolayers, which are easier to characterize using liquid/solid interface STM. The presence of a solvent means there is a dynamic equilibrium between physisorbed molecules and molecules in solution. This can be problematic, because if the interactions of the analyte with the substrate are not strong enough, it will simply remain in solution. On the other hand, the dynamic nature can be an advantage as self-assembly can be a powerful tool for obtaining complex, well-defined 2D structures.[25,26,27]

While overcrowded alkene-based molecular motors consist of large aromatic parts, the molecules are not flat and thus interactions with the substrate are limited. A single motor might not have enough interaction with the substrate to be imaged conveniently; therefore a large molecule comprising several molecular motors was designed.

1,3,5-ethynylbenzene was used as a central core. This allows for straight-forward coupling of halide-functionalized motors via a Sonogashira reaction. Furthermore, it has C3 symmetry, which may be favorable for self-assembly on the surface: there are in fact various examples of molecules with C3 symmetry aligning with HOPG.[28,29,30,31]

At first glance, attaching a fast motor seems preferable; the more isomerization steps take place in a certain timeframe, the more likely it is that an effect on the packing or a movement will be observed. On the other hand, if the isomerization of the motor takes place on a much shorter timescale than the measurements, it may not be possible to observe changes. This is further complicated by the fact that the isomerization pathways may change when the molecule is physisorbed on a surface.[32] For this reason, three different motors are employed with half-lives of 160 μs,[16] 190 s[33] and 829 h[34] in compounds **1**, **2** and **3**, respectively (Scheme 1).

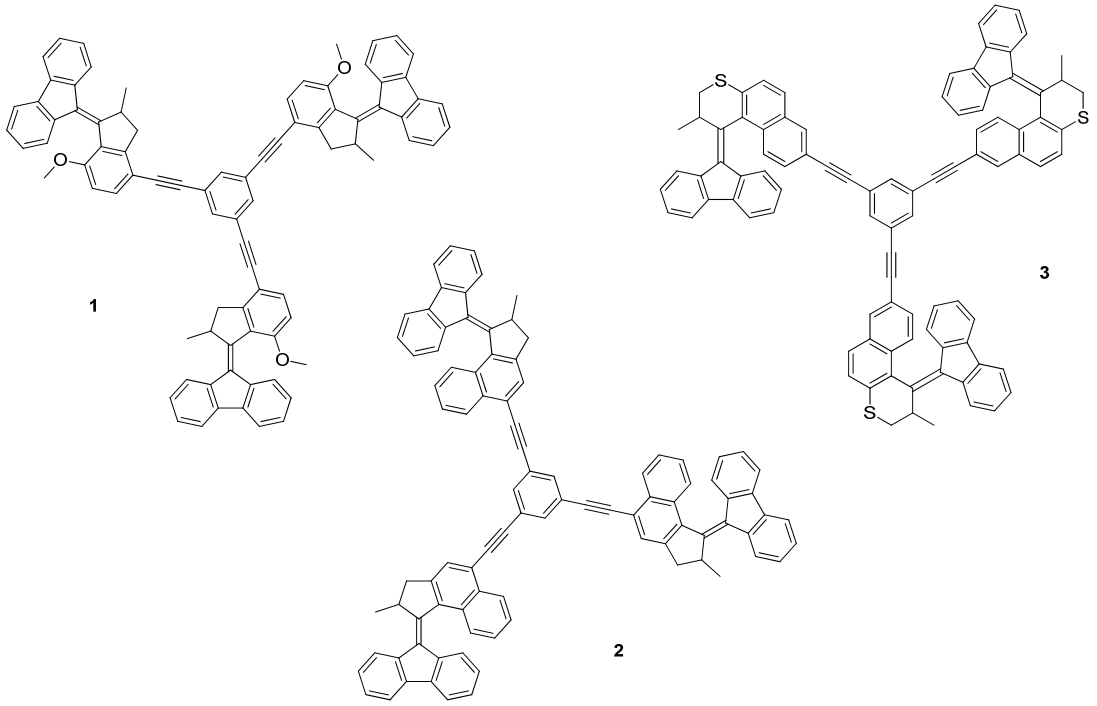

Scheme 1 Target compounds **1**-**3**.

Synthesis

Compound **1** was synthesized according to previously reported procedures.[16] In the final step, coupling of motor **4** with 1,3,5-triethynylbenzene yielded trimer **1** in 58% yield (Scheme 2).[35] The synthesis of compound **2** was also achieved by a triple Sonogashira coupling, in this case of motor **5** with 1,3,5-triethynylbenzene in 67% yield.

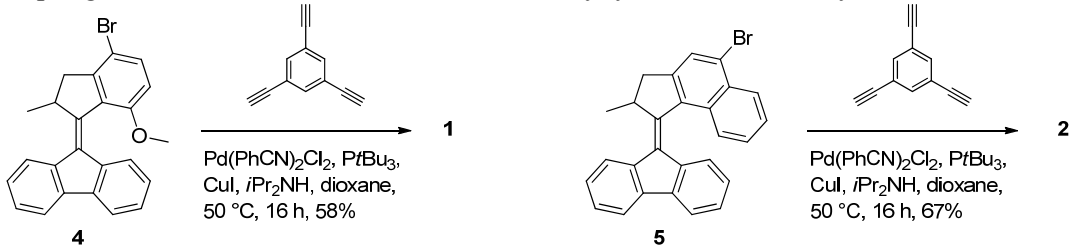

Scheme 2 Triple Sonogashira coupling in the synthesis of compounds **1** and **2**.

For the synthesis of **3**, ketone **6**[36] was first converted to hydrazone **7** using hydrazine hydrate in the presence of catalytic scandium triflate (Scheme 3). Oxidation to the corresponding diazo-compound **8** was carried out at -30 °C with phenyliodine diacetate as the oxidant, immediately followed by the addition of 9-thiofluorenone. The crude product was heated in the presence of triphenylphosphine to yield bromide-substituted motor **9** in 62% yield. Unfortunately, Sonogashira coupling between **9** and 1,3,5-triethynylbenzene under the previously employed conditions did not proceed. The bromide was substituted by the more reactive iodide in an aromatic Finkelstein reaction.[37] Coupling of iodide-substituted motor **10** and 1,3,5-triethynylbenzene was attempted following various protocols. Under copper-free conditions, no reaction took place in general, while in the presence of copper insoluble and/or polymeric products were obtained. The fact that this reaction was unsuccessful for **9** and **10**, but worked well for **4** and **5** is most likely due to steric hindrance. In the former two compounds, the halide is relatively accessible, while in the latter two, the close proximity of the fluorene presumably hinders the reaction.

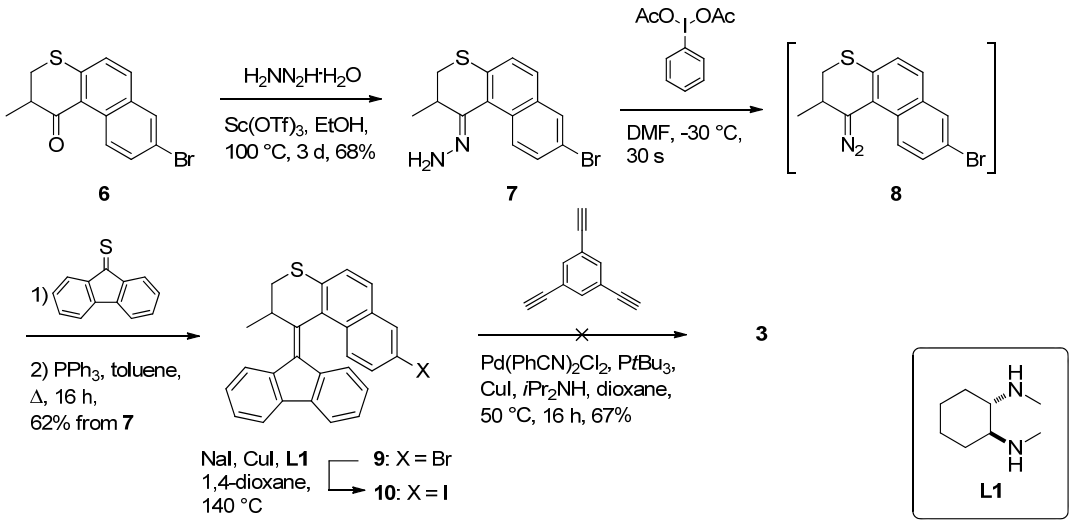

Scheme 3 Attempted synthesis of compound **3**.

The synthesis of larger systems based on motor **4** was also explored (Scheme 4). Mono-protection of 1,3,5-ethynylbenzene followed by Sonogashira coupling to **4** yields compound **12**. After removal of the silyl protecting group using TBAF, the free alkyne can be homocoupled in a Glaser-Hay reaction, yielding **13.**

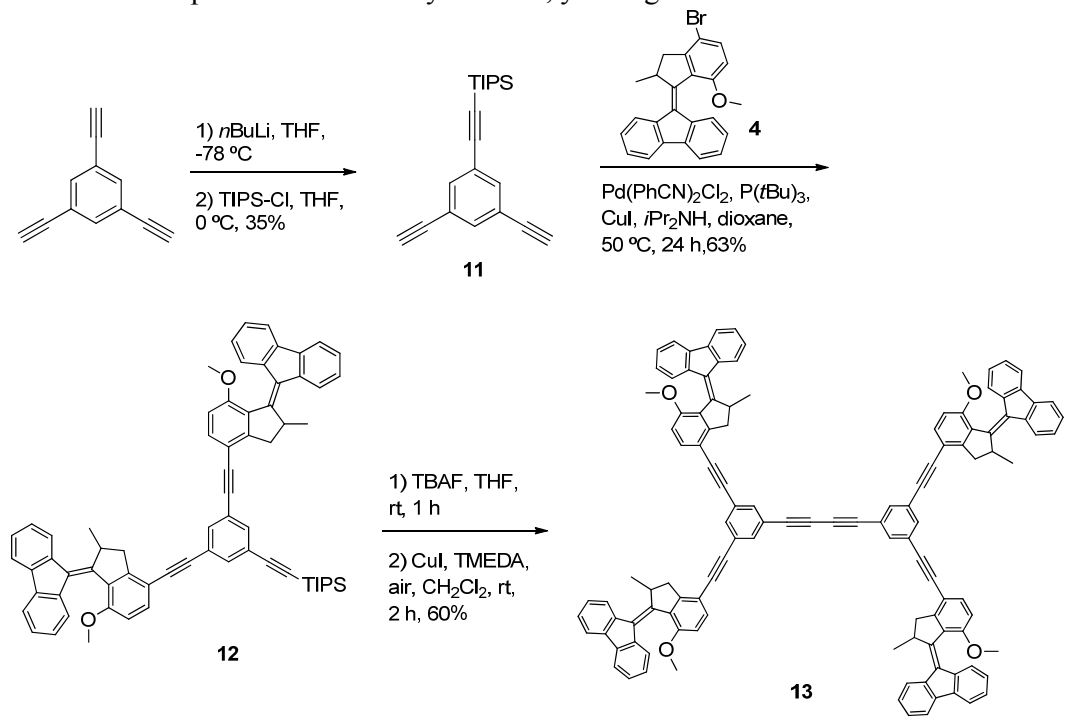

Scheme 4 Synthesis of compound **13**.

Taking this one step further, the synthesis of compound **14** containing 6 molecular motors was attempted by Sonogashira coupling of **12** and 1,3,5-triiodobenzene, however, this reaction was unsuccessful and resulted in the formation of a complex mixture of products (Scheme 5). Dendrimers based on the phenylacetylene motif of this size and larger have been reported in literature,[38] but in those cases no large aromatic groups were present. Other types of dendrimers have been equipped with more sterically demanding groups,

and photoswitching in dendrimers has been reported also.[39] Steric hindrance and solubility become an issue with higher generation dendrimers, unless more flexible scaffolds are used. However, increased flexibility makes it less likely that the molecules will form well-packed monolayers. In fact, even the phenylacetylene dendrimers likely adopt a more spherical shape in solution at higher generations, which makes them less suitable for STM studies; hence this line of research was not pursued any further.

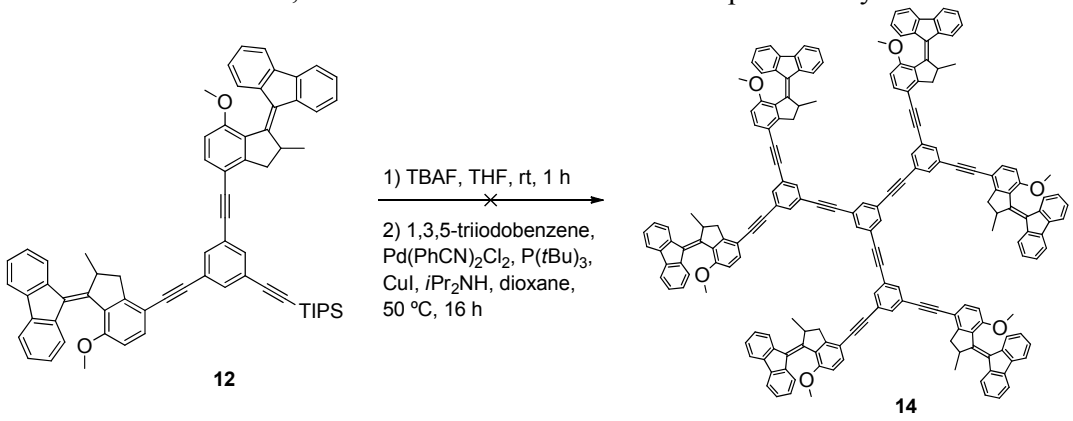

12 14

Scheme 5 Attempted synthesis of compound **14**.

Isomerization studies in solution

The isomerization of the motor units in compounds **2** and **13** was characterized with UV/vis absorption and CD spectroscopy, to ensure that the unidirectionality of the rotational process was retained when incorporated into larger assemblies (Scheme 6). In principle it is expected that the isomerization of a motor unit in the trimer is independent of the other motor units. Electronic interactions should be small due the *meta* substitution pattern on the core and steric interactions between the motor units are not expected because of the alkyne spacers.

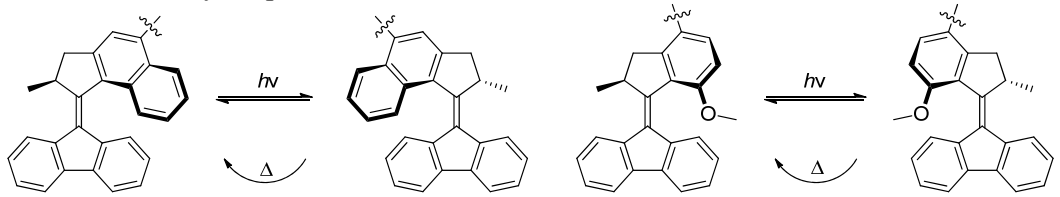

2a 2b 13a 13b

Scheme 6 Expected isomerization of the motor units in **2** and **13**

The UV/vis absorption spectrum of **2** is similar to that of parent motor **5**, but the absorption at the longest wavelength is red-shifted by about 50 nm (Figure 1). Upon UV irradiation (365±20 nm) this band shifts further to the red, indicative of the formation of the unstable form. Isosbestic points were maintained; presumably the isomerization of one motor unit does not influence the others because they are electronically decoupled. Upon heating to 40 °C for 20 min, the spectral changes were reverted.

Separation of the diastereoisomers of **2** was difficult to achieve by preparative chiral stationary HPLC, so instead the enantiomers of precursor **5** were separated, and the final step of the synthesis was repeated with enantiopure starting material. The CD spectrum of **2** is shown in Figure 1. Upon UV irradiation (365±20 nm), the major band around 425 nm begins to invert, which is consistent with the formation of the unstable form. Complete inversion is not observed, which indicates that photoisomerization is not complete, but a photostationary state is obtained that still has a considerable amount of the initial stable form. Again, the spectral changes were found to be reversible upon heating. The changes

in both the UV/vis absorption and the CD spectra are smaller than those found for the parent motor.[33]

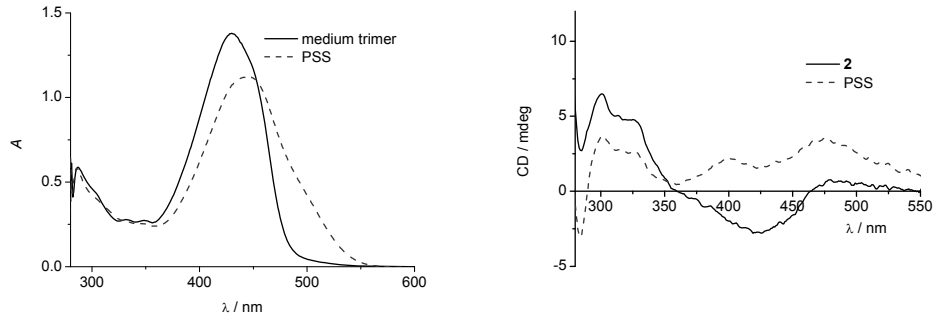

Figure 1 UV/vis absorption and CD spectra of **2** in CH_2Cl_2 (solid lines) and the mixture of **2** and its unstable forms at the PSS obtained after irradiation at 365 nm (dashed lines).

The photochemical quantum yield for *E-Z* isomerization was determined by irradiation of a solution of **2** in toluene at 365 nm. The conversion was followed at 500 nm, and by comparison to the rate of decomposition of ferrioxalate according to standard procedures[40] the photochemical quantum yield was calculated to be 0.004. This is significantly lower than that found for similar motors, see Chapter 3.

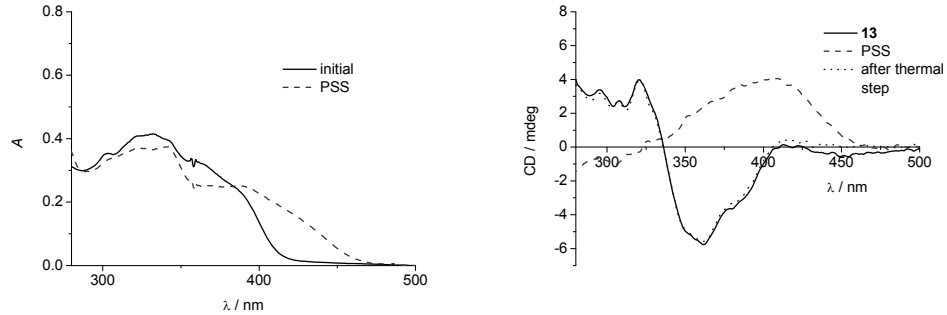

Figure 2 UV/vis absorption and CD spectrum of **13** in 1:1 CH_2Cl_2:DMF (solid lines) and the mixture of **13** and its unstable forms at the PSS obtained after irradiation at 365 nm (dashed lines) and the mixture after the thermal step (dotted line). CD data is smoothed with 3 point adjacent-average.

Similar UV/vis absorption and CD experiments were performed for tetramer **13**. However, since the rate of thermal helix inversion of the motor used in this system is significantly higher, the measurements needed to be carried out at 150 K to slow down the thermal isomerization. At this temperature, the solubility was problematic; eventually a 1:1 mixture of dichloromethane and dimethylformamide proved to be satisfactory. Upon UV irradiation (365 ±20 nm), a redshift was observed in the UV/vis absorption spectrum, which was attributed to the formation of the unstable form of the motor, having the opposite helicity. This was confirmed with CD spectroscopy, which shows an inversion of the major bands in the spectrum upon irradiation. When the temperature is increased to 200 K, the spectral changes in both the UV/vis absorption and the CD spectra were found to be reversibly. These data show that the unique rotational processes of the motor are conserved in the trimer and the tetramer.

Scanning tunneling microscopy studies

Two factors that play a major role in self-assembled monolayer formation are the nature of the substrate and the solvent. We chose to use HOPG as a substrate, as it is relatively cheap and easy to work with. The choice of solvent is important as there are many examples of the solvent influencing the packing on the surface.[41,42,43] However, the solubility of the large aromatic structures of **1**, **2** and **13** in long chain alkenes such as *n*-tetradecane is poor, and they are insoluble in aliphatic acids such as octanoic acid. This limits the solvent choice more or less to aromatic solvents. In the studies described in this chapter, 1-phenyloctane was used as a solvent.

Compound **1** was previously reported to form monolayers at the 1-phenyloctane/HOPG interface, both as a mixture of diastereoisomers and as a single diastereoisomer (Figure 3).[16,44] In principle, the three stereocenters would result in 8 diasteroisomers, however, due to symmetry there are only four different diastereoisomers in the racemic mixture in a 1:3:3:1 ratio (*SSS*, *SSR*, *SRR*, *RRR*). There are striking differences in packing between the racemic and diastereomerically pure forms. The expression of chirality in monolayers of organic molecules has been studied extensively.[45,46] The monolayers formed by diastereomerically pure **1** also express their chirality in the monolayer; this phenomenon was further investigated.

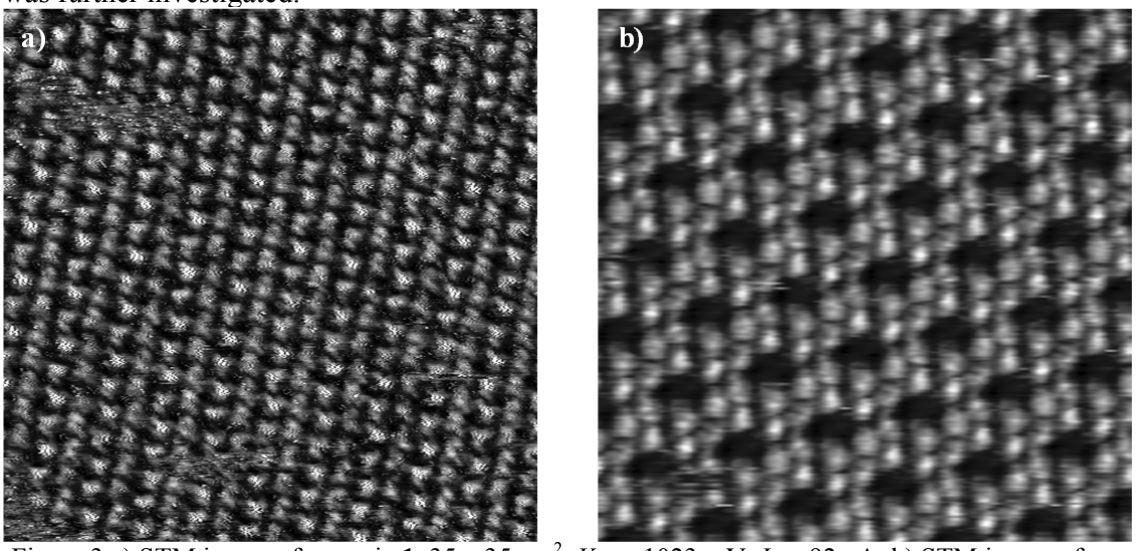

Figure 3 a) STM image of racemic **1**, 35 x 35 nm^2, V_T = -1023 mV, I_T = 92 pA. b) STM image of (*S*)-(*M*)-(*S*')-(*M*')-(*S*'')-(*M*'')-**1**, 18.2 x 18.2 nm^2, V_T = 739 mV, I_T = 21 pA.

Enantiopure **1** forms a honeycomb structure in which each hexagon is formed by six spots with a triangular shape (Figure 3b). Each spot with a triangular shape is composed of three bright spots. The dimensions of one bright spot (~8 Å) corresponds to the calculated dimensions of a single motor unit (~9 Å); therefore, it is concluded that a single triangle composed of three bright spots corresponds to one molecular motor trimer **1**. The central phenyl core is not visible and within a single molecule the three motor units have a different shape and contrast (Figure 4a). This might be a consequence of different conformations of motor parts within a trimer molecule or a consequence of their physisorption on different binding sites of HOPG. The unit cell contains two molecules of **1**; the unit cell parameters are a = 2.88 ± 0.1 nm, b = 2.97 ± 0.2 nm, α = 66.3 ± 4° (Figure 4b). Analysis of the orientation of the molecular pattern reveals that it forms an average angle of 15.6±5° with respect to the lattice of the underlying HOPG (*i.e.* the triangle of bright spots representing one molecule is not aligned perfectly with the graphite). Due to the variation of the contrast and shape of individual motor units this angle varies for the

triangles forming one hexagon, which induces a large standard deviation. The average angle is similar to the angle (18°) between the arms of 1,3,5-triethynylbenzene-based scaffold and the axis between the centre of the fluorenyl moiety and the central benzene ring (Figure 4c). Consequently, we can reasonably infer that the triethynylbenzene-based scaffold follows the symmetry and orientation of the underlying graphite.

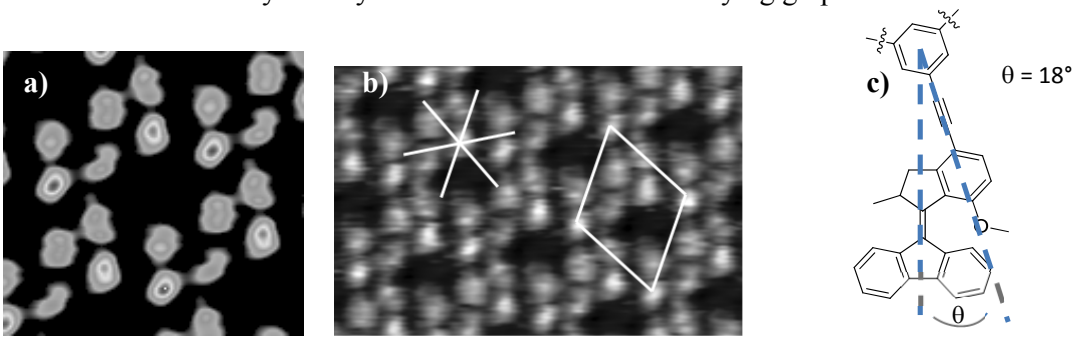

Figure 4 a) Symmetrized correlation-averaged image clearly showing different profile for each motor unit in a trimer. b) Expansion of Figure 3b in which the unit cell and the orientation of the underlying HOPG are indicated. c) Angle θ between the arms of the 1,3,5-triethynylbenzene-based scaffold and the axis between the center of the fluorenyl moiety and the central benzene ring.

Upon close inspection of the hexagonal pattern, it appears that the edge of a triangle representing a molecule is not pointing toward the centre of a hexagon, thus forming a chiral array characterized by a clockwise rotational symmetry (Figure 5a). While using enantiomerically pure (*S*)-(*M*)-(*S*')-(*M*')-(*S*'')-(*M*'')-**1**, only domains with clockwise orientation were observed, while (*S*)-(*M*)-(*S*')-(*M*')-(*R*'')-(*P*'')-**1** was not found to form stable monolayers.

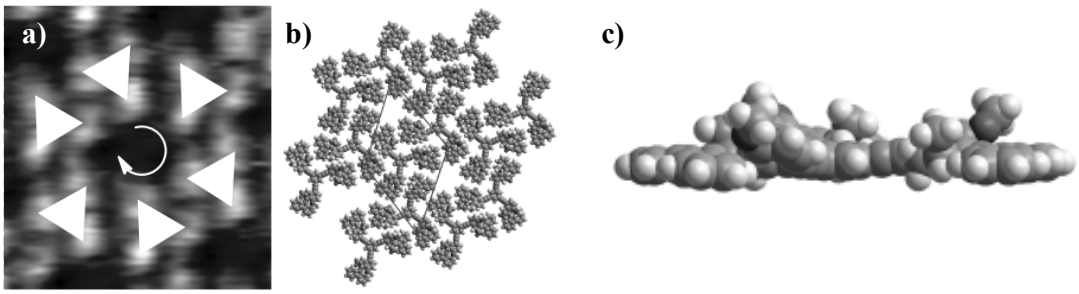

Figure 5 a) Expansion of Figure 3b in which white triangles indicate the orientation of trimers and the arrow indicates the rotational symmetry b) Tentative packing model of a geometry-optimized model of **1** in which the unit cell is indicated by the parallelogram. c) Side view of **1** after geometry optimization in the presence of an HOPG model surface with methyl and methoxy groups pointing out of the plane.

It is remarkable that large spots seem to be uncovered by **1** in the centre of the hexagon, represented by the dark areas in the middle of a hexagon. This is thermodynamically not favored because of the low surface coverage. Such empty voids are generally only observed in systems in which strong and highly directional intermolecular interactions are present.[47] In the case of **1**, only weak van der Waals interactions can be established between molecules. When a mixture of diastereoisomers of **1** is deposited on graphite, a self-assembled monolayer is also formed, but with a drastically different structure (Figure 3). Therefore, the formation of a "low" density packing containing empty voids is attributed to chiral self-recognition between the helically shaped motor units.[48,49] The apparent size of the voids is likely to be larger than the actual size (Figure 5a, Figure 5b).

Geometry optimization of **1** in the presence of an HOPG model surface (Figure 5c) yields a structure in which the methyl and methoxy groups all point upwards. The other side is relatively flat, allowing maximum interaction of the aromatic parts with the surface. Since the methyl groups are protruding from the surface, it is expected that the STM signal from the aromatic parts surrounding the empty voids is small compared to the contribution from the methyl groups.

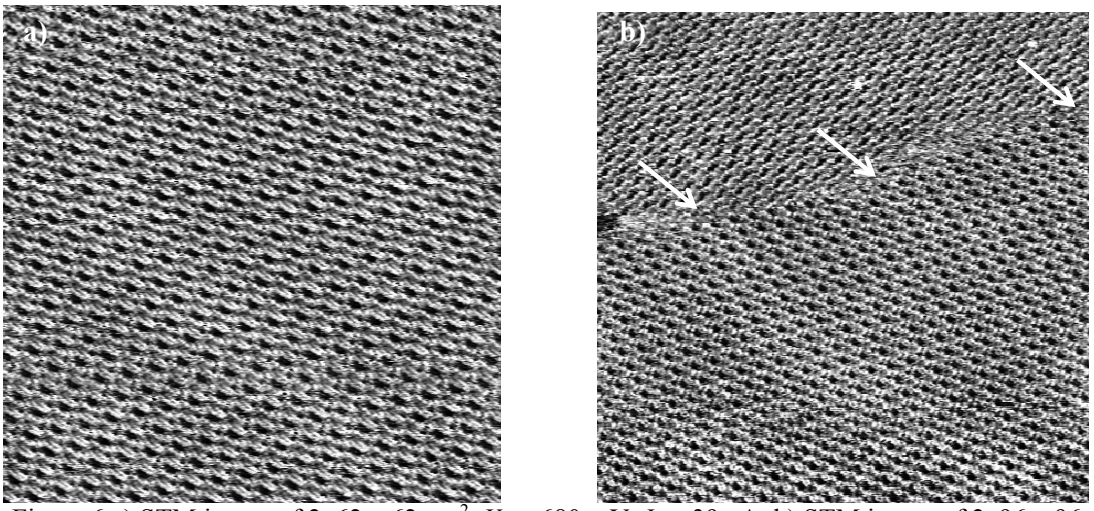

Figure 6 a) STM image of **2**, 62 x 62 nm^2, V_T = 680 mV, I_T = 39 pA. b) STM image of **2**, 96 x 96 nm^2, V_T = 680 mV, I_T = 33 pA. The white arrows indicate a domain boundary.

In contrast to **1**, racemic **2** was not found to form monolayers at the HOPG/1-phenyloctane. Enantiopure **2** did form stable monolayers; apparently the presence of the other diastereomers disturbs formation of monolayers. Compound **2** forms a hexagonal pattern at the HOPG/1-phenyloctane interface similar to **1** (Figure 6a). Domains of up 100 nm^2 were observed, often bordered by domains with a different orientation (Figure 6b). The difference in orientation was found to approximately 60° in all cases. The dimensions of one bright spot (~2.2 nm) correspond to one molecule of **2** (~2.4 nm). When the image is expanded, all bright spots have the approximately the same shape, indicating all molecules have the same conformation and are on similar binding sites of HOPG. The quality of the image is not sufficient for submolecular resolution, therefore it is impossible to accurately determine the orientation of the molecule. The unit cell and a tentative packing is illustrated in Figure 7; the unit cell parameters are a = 1.9 ± 0.2 nm, b = 1.9 ± 0.2 nm, α = 68 ± 4°.

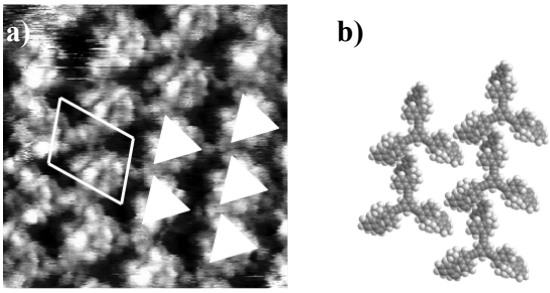

Figure 7 a) Expansion of an STM image of **2** which shows the unit cell (white parallelogram) and a tentative packing model (white triangles) b) Tentative packing model of geometry-optimized model of **2**.

Furthermore, small domains of several tens to hundreds of molecules were observed (Figure 8). These domains were less stable than the larger domains, but they were stable enough to be imaged. The domains all share the same packing defect, in which an entire row of molecules seems to be missing. These 'lines' of missing molecules appear in only three directions, with angles of approximately 60°. This led us to believe that they follow the symmetry of the underlying HOPG surface. In some cases, holes in the packing are observed, in which a single molecule is missing. Within one domain all molecules have the same shape and contrast, which indicates physisorption on the same binding site of HOPG for all molecules. There seem to be two types of domain with slightly different brightness; this might be caused by the molecules having two different orientations.

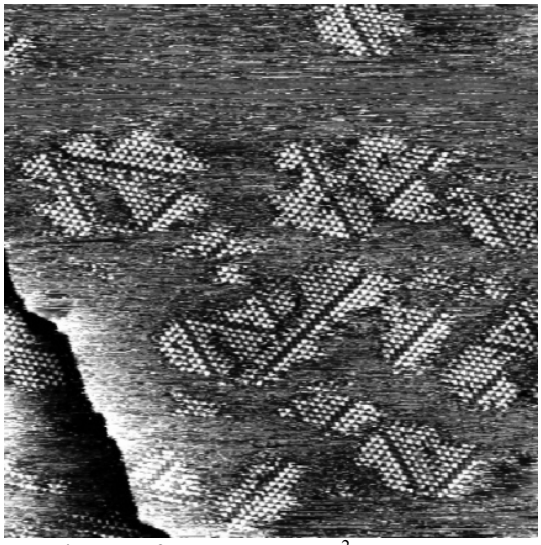

Figure 8 STM image of **2** 135 x 135 nm^2, V_T = 520 mV, I_T = 39 pA

Occasionally, small double layer domains were observed (Figure 9). The molecules in both layers have a different shape and contrast, which rules out tip artifacts. Strangely, the second layer only partially covers the first layer. If the first layer has stronger interactions to a second layer than HOPG, we would expect a complete double layer to be formed. If the second layer is only weakly stabilized, we would rather expect larger domains of **2** to form instead of stacked layers. The double layer domains had very limited stability to scanning, and generally disappear within 5 scans. Due to this instability, higher resolution images could not be obtained. Similar defects as were seen for single-layer small domains were also observed in the double layer domains (Figure 8, Figure 9b).

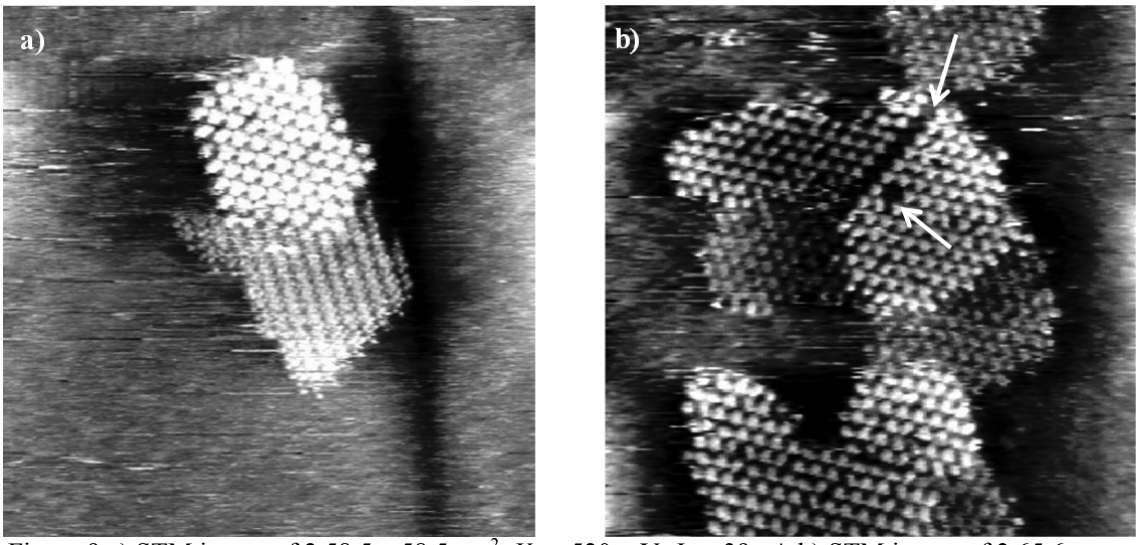

Figure 9 a) STM image of **2** 58.5 x 58.5 nm^2, V_T = 520 mV, I_T = 39 pA b) STM image of **2** 65.6 x 65.6 nm^2, V_T = 520 mV, I_T = 49 pA. The white arrows indicate a missing row and a single missing molecule.

Several different packings were observed for **2**. We hypothesized that the packing was concentration dependent: at lower concentration smaller domains are formed and more packing defects are introduced. To study this, STM images of **2** were recorded at concentrations ranging from 0.1 mg/mL to 1.5 mg/mL. From these experiments, a concentration dependence could not be derived: the domain size seemed to vary randomly. There was also no correlation between the observed packing and the time allowed for the molecules to assemble on the surface. The larger domains were found to be the most stable; if after imaging the surface was rinsed with clean solvent, the large domains persisted. The smaller domains disappeared on a timescale of minutes.

For compound **13** stable monolayers could not be observed by STM. This was somewhat surprising, as it is similar to **1**, contains the same groups and is even larger, which should lead to more interaction with the surface. The most plausible explanation is that **13** lacks the C3 symmetry that both **1** and **2** possess. The C3 symmetry allows these molecules to better fit the underlying graphite by following the corrugation of the surface. In the case of **13**, this may not be possible, which would lead to less favorable interactions with the surface.

Irradiation experiments on surface

The monolayers of both **1** and **2** on HOPG were subjected to UV irradiation (365 nm) to see if isomerization on surface could be visualized. In solution, irradiation at this wavelength initiates photoisomerization to form the unstable form, which has a different conformation. Therefore, it would likely display a different packing or disturb the existing monolayer. Unfortunately, changes upon irradiation of monolayers of either **1** or **2** were not observed. On occasion, monolayers break up or disappear, but this happens without irradiation as well, and irradiation did not seem to increase the frequency of monolayer disassembly.

Several explanations for the absence of an effect were considered. First, it is possible that photoisomerization does take place, but it is not observed by STM. Either the difference between the stable and unstable forms does not have a significant influence on the packing, or after isomerization the molecules have decreased interaction with the surface, and go into solution to be replaced by a molecule still in the stable form. In this case, liquid/solid interface STM is not a useful technique to analyze the isomerization process.

Second, photoisomerization might not take place on the surface, possibly due to quenching. As mentioned before, quenching is a problem due to the need for a conducting surface in STM. A possible solution for quenching is increasing the distance between the motor and the conductive surface. This might be achieved by using adlayers. The use of pentacontane ($C_{50}H_{102}$) has been reported in the literature as a means of modifying surface properties, and it is possible to form monolayers of organic material on top of the pentacontane monolayers.[50] More recently, it was also used in the visualization of single molecules, and proposed as a track for molecular motor-based surface walkers.[51]
A monolayer of pentacontane on graphite was created by depositing a solution in tetradecane or 1-phenyloctane on freshly cleaved HOPG. After confirming the monolayer was present using STM, the excess of pentacontane solution was rinsed off, and subsequently a solution of **1**, **2** or **13** was added. However, single molecules or monolayers on top of the pentacontane layer were not observed in any case. Evidently, these molecules do not have enough favorable interactions with the modified surface. Perhaps the presence of long alkyl chains is required in this case, which would likely increase the affinity for the surface. The use of pentacontane as an 'isolating' layer is still a useful concept, albeit requiring design modification.

Conclusion

Three arrays of molecular motors of different speeds were synthesized with the aim of studying their ability to form monolayers at the HOPG/1-phenyloctane interface. Using UV/vis absorption and CD spectroscopy it was shown that the photochemical and thermal isomerization processes of the motor units in the array were retained. For compound **2** the photochemical quantum yield for photoisomerization was determined to be 0.0041, which is low compared to similar motors.
Compounds **1** and **2** were found to form stable monolayers at the HOPG/1-phenyloctane interface when used in enantiopure form, whereas compound **13** did not. This is ascribed to the fact that the C3 symmetry of **1** and **2** facilitates interactions with HOPG. The monolayers formed by **1** show a hexagonal pattern, with large open voids. The origin of these voids is helical self-recognition of the motor units; their size is also somewhat overestimated because the STM signal of the aromatic parts of the motor is overwhelmed by that of the methyl groups which point upwards. For compound **2**, many different surface packings were observed, ranging from large domains to domains of several tens of molecules to double layers. No concentration or time dependence was found, however, the larger domains were found to be the most stable.
The monolayers of **1** and **2** were subjected to UV irradiation to induce photoisomerization. Influence of irradiation on the surface packing was not observed in any case. The use of pentacontane as an isolating layer was also explored, but the molecules did not self-assemble on the modified surface.
If photoisomerization on surface proves to be unfeasible, thermal isomerization should also be considered. An array of slow motors could be irradiated to the PSS prior to deposition on the surface. Over time, thermal relaxation will take place, which could also be promoted by mild heating. This should cause the same changes as photoisomerization, albeit in the opposite direction, and is not limited by quenching of the excited state by the surface.

Acknowledgements

Tibor Kudernac is gratefully acknowledged for his contributions to the STM experiments. The synthesis of compound **6** was performed by Jort Robertus.

Experimental section

Synthesis

For general comments, see Chapter 2. Trimer **1**[44] and 9-(5-bromo-2-methyl-2,3-dihydro-1*H*-cyclopenta[*a*]naphthalen-1-ylidene)-9*H*-fluorene **5**[52] were synthesized according to previously reported procedures.

Trimer 2

In a flame-dried flask under a N_2 atmosphere was placed CuI (1.0 mg, 5.2 μmol), $Pd(PhCN)_2Cl_2$ (2.8 mg, 7.3 μmol), P(*t*-Bu)$_3$ (3.6 μL, 3.0 mg, 14.8 μmol), diisopropylamine (50 μL, 0.36 mmol), **5** (60 mg, 0.14 mmol), 1,3,5-triethynylbenzene (5.3 mg, 0.035 mmol) and dioxane (0.3 mL). The solution was stirred overnight at 50 °C and then diluted with EtOAc. The organic layer was washed with water, 2 N aqueous HCl and brine, and dried on Na_2SO_4. The solvent was removed *in vacuo* and the crude product was purified by column chromatography (pentane:CH_2Cl_2, gradient 3:1 to 1:1) to yield **2** as a orange solid (28 mg, 67 %). ^{1}H NMR (300 MHz, $CDCl_3$) δ 8.63 (d, *J* = 8.3 Hz, 2H), 8.01 (s, 6H), 7.95 (s, 3H), 7.88 (t, *J* = 7.3 Hz, 6H), 7.77 (d, *J* = 7.4 Hz, 3H), 7.66 (t, *J* = 7.5 Hz, 3H), 7.41 (t, *J* = 6.6 Hz, 9H), 7.23 (d, *J* = 7.4 Hz, 3H), 6.83 (t, *J* = 7.5 Hz, 3H), 6.75 (d, *J* = 7.8 Hz, 3H), 4.38 (m, 3H), 3.62 (dd, *J* = 15.0, 5.3 Hz, 3H), 2.81 (d, *J* = 15.1 Hz, 1H), 1.44 (d, *J* = 6.5 Hz, 3H); ^{13}C NMR (75 MHz, $CDCl_3$) δ 151.2 (3C), 150.3 (3C), 146.5 (3C), 104.5 (3C), 140.0 (3C), 139.9 (3C), 138.2 (3C), 137.2 (3C), 134.6 (3CH), 132.8 (3C), 129.9 (3C), 128.8 (3CH), 128.2 (3CH), 127.49 (3CH), 127.44 (3CH), 127.40 (3CH), 127.3 (3CH), 126.7 (3CH), 126.3 (3CH), 126.1 (3CH), 124.7 (3C), 124.4 (3CH), 122.7 (3C), 120.0 (3CH), 119.3 (3CH), 94.5 (3C), 90.0 (3C), 45.5 (3CH), 41.9 ($3CH_2$), 19.5 ($3CH_3$); HRMS (APCI) calcd for $C_{93}H_{60}$ 1177.4723, found 1177.4779.

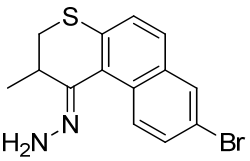

(8-bromo-2-methyl-2,3-dihydro-1*H*-benzo[*f*]thiochromen-1-ylidene)hydrazine 7

To a mixture of **6** (500 mg, 1.6 mmol) and hydrazine monohydrate (5 mL) in EtOH (20 mL) was added $Sc(OTf)_3$ (20 mg, 0.04 mmol). The mixture was heated to 100 °C for 3 d and subsequently concentrated to ~5 mL. CH_2Cl_2 (200 mL) and H_2O (150 mL) were added and the layers were separated. The water layer was extracted with CH_2Cl_2 and the combined organic layers were dried over Na_2SO_4 and concentrated. The residue was purified by column chromatography (gradient 1:1 pentane:CH_2Cl_2 to CH_2Cl_2) to yield **7** (353 mg, 68%) as a slightly yellow solid. ^{1}H NMR (300 MHz, $CDCl_3$) δ 8.32 (d, *J* = 9.2 Hz, 1H), 7.90 (d, *J* = 2.1 Hz, 1H), 7.52 (m, 2H), 7.34 (d, *J* = 8.6 Hz, 1H), 5.60 (bs, 2H), 3.46 (m, 1H), 3.16 (dd, *J* = 12.8, 5.9 Hz, 1H), 2.68 (dd, *J* = 12.8, 9.5 Hz, 1H), 1.27 (d, *J* = 6.8 Hz, 3H); ^{13}C NMR (75 MHz, $CDCl_3$) δ 151.2 (C), 149.1 (C), 136.5 (C), 134.4 (C), 131.1 (C), 130.9 (C), 130.1 (2CH), 128.4 (CH), 127.5 (CH), 126.9 (CH), 119.5 (C), 36.5 (CH_2), 33.8 (CH), 15.0 (CH_3).

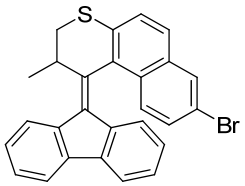

8-bromo-1-(9*H*-fluoren-9-ylidene)-2-methyl-2,3-dihydro-1*H*-benzo[*f*]thiochromene 9
To a solution of 9-fluorenone (400 mg, 2.21 mmol) in toluene (10 mL) was added Lawesson's reagent (1.2 g, 3.0 mmol). The mixture was heated at reflux for approximately 3 h, until TLC analysis started to show degradation. The mixture was concentrated and the residue was purified by quick column chromatography (toluene) to yield the crude thioketone. A solution of **7** (145 mg, 0.45 mmol) in DMF (4 mL) was cooled to -30 °C and iodobenzene diacetate (152 mg, 0.47 mmol) was added. The mixture was stirred for 30 s before addition of a solution of the crude thioketone in CH_2Cl_2 (5 mL). The mixture was allowed to warm to rt and stirred overnight. The volatiles were removed *in vacuo* and the residue was dissolved in toluene (15 mL). PPh_3 (150 mg, 0.57 mmol) was added and the solution was heated to reflux overnight. The solution was concentrated and the residue was purified by column chromatography (6:1 pentane:CH_2Cl_2, R_f = 0.5) to yield **9** (125 mg, 62%) as a yellow solid. ^{1}H NMR (300 MHz, $CDCl_3$) δ 8.09 (m, 1H), 8.01 (d, *J* = 2.0 Hz, 1H), 7.81 (m, 1H), 7.75 (d, *J* = 8.8 Hz, 2H), 7.62 (dd, *J* = 7.9, 5.0 Hz, 2H), 7.44 (m, 2H), 7.28 (dd, *J* = 9.2, 2.1 Hz, 1H), 7.09 (t, *J* = 7.5 Hz, 1H), 6.61 (dd, *J* = 11.3, 4.1 Hz, 1H), 5.75 (d, *J* = 8.0 Hz, 1H), 4.80 (m, 1H), 3.38 (dd, *J* = 12.3, 7.2 Hz, 1H), 2.64 (dd, *J* = 12.3, 7.2 Hz, 1H), 1.37 (d, *J* = 6.8 Hz, 3H); ^{13}C NMR (75 MHz, $CDCl_3$) δ 141.6 (2C), 140.1 (C), 137.9 (C), 137.7 (C), 137.6 (C), 134.8 (C), 134.4 (C), 133.5 (C), 132.1 (C), 130.8 (CH), 130.4 (CH), 128.6 (CH), 128.3 (CH), 127.7 (CH), 127.6 (CH), 127.4 (CH), 127.1 (CH), 126.7 (CH), 125.4 (CH), 125.2 (CH), 120.1 (CH), 119.8 (C), 119.3 (CH), 38.8 (CH), 37.4 (CH_2), 18.8 (CH_3); HRMS (APCI) calcd for $C_{27}H_{20}BrS$ [M-H] 453.0307, found 453.0302.

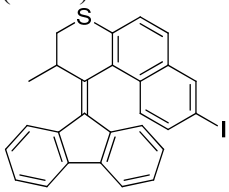

1-(9*H*-fluoren-9-ylidene)-8-iodo-2-methyl-2,3-dihydro-1*H*-benzo[*f*]thiochromene 10
To a solution of **9** (50 mg, 0.11 mmol) in dioxane (3 mL) was added NaI (150 mg, 1.0 mmol), CuI (20 mg, 0.11 mmol), and *trans*-*N*,*N*'-dimethyl-1,2-cyclohexanediamine (70 μL, 0.44 mmol). The flask was purged with Ar, sealed and heated to 140 °C overnight. After cooling, the volatiles were removed *in vacuo* and the residue was purified by column chromatography (6:1 pentane:CH_2Cl_2, R_f = 0.5) to yield **10** (52 mg, 94%) as a yellow solid. ^{1}H NMR indicated the presence of 10% of **9**, but **10** was used without further purification. ^{1}H NMR (400 MHz, $CDCl_3$) δ 8.23 (s, 1H), 8.08 (d, *J* = 7.4 Hz, 1H), 7.80 (d, *J* = 6.6 Hz, 1H), 7.71 (d, *J* = 8.6 Hz, 1H), 7.60 (m, 3H), 7.43 (m, 3H), 7.09 (t, *J* = 7.4 Hz, 1H), 6.61 (t, *J* = 7.7 Hz, 1H), 5.75 (d, *J* = 7.9 Hz, 1H), 4.79 (m, 1H), 3.37 (dd, *J* = 12.3, 7.2 Hz, 1H), 2.64 (dd, *J* = 12.2, 7.1 Hz, 1H), 1.36 (d, *J* = 6.7 Hz, 3H); ^{13}C NMR (75 MHz, $CDCl_3$) δ 141.6 (C), 141.6 (C), 140.1 (C), 137.9 (C), 137.8 (C), 137.7 (C), 137.1 (CH), 136.0 (CH), 134.8 (C), 134.3 (C), 133.9 (C), 132.4 (C), 128.4 (CH), 128.3 (CH), 127.6 (CH), 127.4 (CH), 127.4 (CH), 127.1 (CH), 126.5 (CH), 125.4 (CH), 125.2 (CH), 120.1 (CH), 119.2 (CH), 91.4 (C), 38.7 (CH), 37.3 (CH_2), 18.8 (CH_3).

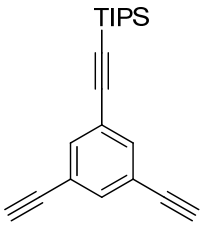

((3,5-diethynylphenyl)ethynyl)triisopropylsilane 11
Synthesized according to a modified literature procedure.[53] In a flame-dried flask under a N_2 atmosphere, [triethynylbenzene] (106 mg, 0.71 mmol) was dissolved in THF (100 mL). The solution was cooled to -78 °C and *n*-BuLi (0.44 mL of a 1.6 M solution in hexanes, 0.70 mmol) was added dropwise. Stirring was continued for 1 h before adding triisopropylsilyl chloride (0.15 mL, 0.71 mmol). The solution was stirred at 0 °C for 30 min and then concentrated. The residue was divided between H_2O (100 mL) and Et_2O (100 mL). The organic layer was dried on Na_2SO_4 and concentrated. The crude product was purified by column chromatography (heptane) to give **11** (81 mg, 37%), as well as the double protected product (81 mg, 25%) and unreacted starting material (17 mg, 16%). ^{1}H NMR (100 MHz, $CDCl_3$) δ 7.56 (s, 2H), 7.53 (s, 1H), 3.09 (s, 2H), 1.12 (s, 21H); ^{13}C NMR (400 MHz, $CDCl_3$) δ 135.8 (2CH), 135.3 (C), 124.5 (CH), 123.0 (2CH), 105.0 (2C), 92.9 (C), 82.0 (C), 78.7 (2C), 18.9 ($6CH_3$), 11.5 (3CH). Double protected: ^{1}H NMR (300 MHz, $CDCl_3$) δ 7.52 (bs, 3H), 3.08 (s, 1H), 1.13 (s, 42H).

Compound 12
In a flame-dried flask under Ar atmosphere was placed CuI (1.0 mg, 5.2 μmol), $Pd(PhCN)_2Cl_2$ (3.8 mg, 9.9 μmol), P(*t*-Bu)$_3$ (4.8 μL, 4.0 mg, 19.8 μmol), diisopropylamine (0.14 mL, 1 mmol), **4** (250 mg, 0.62 mmol), [monoTIPStriethynylbenzene] (81 mg, 0.26 mmol) and dioxane (0.5 mL). The tube was sealed and heated at 60 °C overnight. Another portion of $Pd(PhCN)_2Cl_2$ (3.8 mg, 9.9 μmol) was added and stirring at 60 °C was continued for another 16 h. The reaction mixture was taken up in EtOAc and washed with 0.2 N aqueous HCl and brine. The organic layer was concentrated and the residue was purified by column chromatography (2:1 pentane:$CHCl_3$) yielding **12** (144 mg, 58%) as a yellow solid. ^{1}H NMR (400 MHz, $CDCl_3$) δ 7.90 (d, *J* = 7.9 Hz, 2H), 7.80 (m, 2H), 7.74 (d, *J* = 7.5 Hz, 2H), 7.68 (s, 1H), 7.62 (s, 2H), 7.57 (d, *J* = 8.5 Hz, 2H), 7.35 (m, 4H), 7.28 (m, 4H), 7.16 (m, 2H), 6.89 (d, *J* = 8.5 Hz, 2H), 4.22 (m, 2H), 3.77 (s, 6H), 3.43 (dd, *J* = 15.6, 5.7 Hz, 2H), 2.93 (d, *J* = 15.5 Hz, 2H), 1.40 (d, *J* = 6.5 Hz, 6H), 1.18 (s, 21H); ^{13}C NMR (75 MHz, $CDCl_3$) δ 157.4 (2C), 152.4 (2C), 147.4 (2C), 139.8 (2C), 139.7 (2C), 139.6 (2C), 138.2 (2C), 134.4 (CH), 134.3 (2CH), 131.3 (C), 129.3 (2C), 127.3 (2CH), 127.2 (2CH), 127.1 (2CH), 126.1 (2CH), 125.5 (2CH), 124.5 (4C), 124.4 (2CH), 119.9 (2CH), 119.0 (2CH), 112.9 (2C), 110.0 (2CH), 105.7 (C), 92.5 (C), 90.2 (2C), 88.8 (2C), 55.1 ($2CH_3$) 44.0 (2CH), 41.2 ($2CH_2$), 19.4 ($2CH_3$), 19.0 ($6CH_3$), 11.6 (3CH); HRMS (APCI) calcd for $C_{69}H_{63}O_2Si$: 951.4592, found 951.4598.

Compound 13
To a solution of **12** (70 mg, 0.074 mmol) in THF was added tetrabutylammonium fluoride (1 mL of a 1 M solution in THF, 1 mmol). The mixture was stirred at rt for 1 h before quenching by addition of excess $CaCl_2$. The solids were separated by filtration and the solution was concentrated to give the crude deprotected acetylene: ^{1}H NMR (400 MHz, $CDCl_3$) δ 7.88 (d, *J* = 7.4 Hz, 2H), 7.79 (d, *J* = 4.5 Hz, 2H), 7.73 (d, *J* = 7.7 Hz, 2H), 7.72 (s, 1H), 7.67 (s, 2H), 7.57 (d, *J* = 8.5 Hz, 2H), 7.34 (m, 4H), 7.26 (m, 4H), 7.16 (m, 2H),

6.89 (d, J = 8.6 Hz, 2H), 4.21 (m, 2H), 3.77 (s, 6H), 3.42 (dd, J = 15.7, 5.7 Hz, 2H), 2.91 (d, J = 15.6 Hz, 2H), 2.36 (s, 1H), 1.40 (d, J = 6.5 Hz, 6H). The residue was dissolved in CH_2Cl_2 (10 mL) in a 250 mL round-bottom flask. The solution was stirred vigorously under air for 30 min, then CuI (420 mg, 2.2 mmol) and TMEDA (0.35 mL, 2.3 mmol) were added. Stirring was continued for 2 h, then the reaction mixture was diluted with CH_2Cl_2 (50 mL) and washed with H_2O (100 mL). The organic layer was concentrated and the residue was purified by column chromatography (1:1 pentane:CH_2Cl_2) yielding **13** (35 mg, 60%) as an orange solid. ^{1}H NMR (400 MHz, $CDCl_3$) δ 7.88 (m, 4H), 7.79 (m, 4H), 7.73 (d, J = 7.6 Hz, 4H), 7.72 (s, 2H), 7.67 (d, J = 1.4 Hz, 4H), 7.56 (d, J = 8.5 Hz, 4H), 7.35 (m, 8H), 7.30 (m, 4H), 7.25 (d, J = 7.7 Hz, 4H), 7.14 (t, J = 7.6 Hz, 4H), 6.89 (d, J = 8.6 Hz, 4H), 4.21 (m, J_{app} = 6.7 Hz, 4H), 3.77 (s, 12H), 3.42 (dd, J = 15.5, 5.9 Hz, 4H), 2.91 (d, J = 15.6 Hz, 4H), 1.40 (d, J = 6.7 Hz, 12H)); ^{13}C NMR (125 MHz, $CDCl_3$) δ 157.5 (4C), 152.4 (4C), 147.2 (4C), 144.6 (2C), 140.4 (4C), 139.7 (8C), 138.1 (4C), 134.8 (4CH), 134.2 (4CH), 131.2 (4C), 127.1 (12CH), 126.0 (4CH), 125.4 (4CH), 124.8 (4C), 124.4 (4CH), 122.6 (4C), 120.5 (2CH), 119.8 (4CH), 118.9 (4CH), 112.7 (4C), 110.0 (4CH), 89.8 (4C), 89.2 (4C), 80.8 (2C), 74.9 (2C), 55.1 ($4CH_3$), 44.0 (4CH), 41.2 ($4CH_2$), 19.3 ($4CH_3$);

STM experiments

All STM experiments were performed at room temperature, using a PicoSPM machine (Molecular Imaging, Scientec). Pt/Ir STM tips were prepared mechanically from Pt/Ir wire (80:20, diameter 0.25 mm, Goodfellow). Prior to STM imaging, the compound was dissolved in 1-phenyloctane (Aldrich) at a concentration of ~0.1 mM by sonication (5 min) and heating at ~60 ºC (10 min). A drop of the warm solution was applied to a freshly cleaved surface of highly oriented pyrolytic graphite (HOPG, Goodfellow) and the STM tip immersed into the solution for imaging. The parameters of the unit cells were measured after drift effects were corrected with the Scanning Probe Image Processor (SPIP) software (Image Metrology ApS) or WSxM.[54] For irradiation experiments, a high-pressure mercury lamp was used, equipped with a 365±5 nm bandpass filter and a fiber-optic cable to lead the light onto the sample.

References

[1] *Molecular Motors* (Ed.: M.Schliwa), Wiley-VCH, Weinheim, **2003**.
[2] M. G. L. van den Heuvel, C. Dekker, *Science* **2007**, *317*, 333-336.
[3] E. R. Kay, D. A. Leigh, F. Zerbetto, *Angew. Chem. Int. Ed.* **2007**, *46*, 72-191.
[4] W. R. Browne, B. L. Feringa, *Nature Nanotechnol.* **2006**, *1*, 25-35.
[5] A. Coskun, M. Banaszak, R. D Astumian, J. F. Stoddart, B. A. Grzybowski, *Chem. Soc. Rev.* **2012**, *41*, 19-30.
[6] N. Katsonis, M. Lubomska, M. M. Pollard, B. L. Feringa, P. Rudolf, *Prog. Surf. Sci.* **2007**, *82*, 407-434.
[7] A. J. Kronemeijer, H. B. Akkerman, T. Kudernac, B. J. van Wees, B. L. Feringa, P. W. M. Blom, B. de Boer, *Adv. Mater.* **2008**, *20*, 1467-1473.
[8] R. A. van Delden, M. K. J. ter Wiel, M. M. Pollard, J. Vicario, N. Koumura, B. L. Feringa, *Nature* **2005**, *437*, 1337-1340.
[9] M. M. Pollard, M. K. J. ter Wiel, R. A. van Delden, J. Vicario, N. Koumura, C. R. van den Brom, A. Meetsma, B. L. Feringa, *Chem. Eur. J.* **2008**, *14*, 11610-11622.
[10] G. T. Carroll, M. M. Pollard, R. A. van Delden, B. L. Feringa, *Chem. Sci.* **2010**, *1*, 97-101.
[11] M. M. Pollard, M. Lubomska, P. Rudolf, B. L. Feringa, *Angew. Chem. Int. Ed.* **2007**, *46*, 1278-1280.
[12] G. London, G. T. Carroll, T. Fernández Landaluce, M. M. Pollard, P. Rudolf, B. L. Feringa, *Chem. Commun.* **2009**, 1712-1714.
[13] G. T. Carroll, G. London, T. Fernández Landaluce, P. Rudolf, B. L. Feringa, *ACS Nano* **2011**, *5*, 622-630.
[14] J.-F. Morin, Y. Shirai, J. M. Tour, *Org. Lett.* **2006**, *8*, 1713-1716.
[15] T. Sasaki, J. M. Tour, *Org. Lett.* **2008**, *10*, 897-900.
[16] A. Cnossen, *Master's Thesis*, University of Groningen, **2008**.

[17] L. Grill, K.-H. Rieder, F. Moresco, G. Rapenne, S. Stojkovic, X. Bouju, C. Joachim, *Nature Nanotechnology* **2007**, *2*, 95-98.
[18] M. J. Comstock, N. Levy, A. Kirakosian, J. Cho, F. Lauterwasser, J. H. Harvey, D. A. Strubbe, J. M. J. Fréchet, D. Trauner, S. G. Louie, M. F. Crommie, *Phys. Rev. Lett.* **2007**, *99*, 038301.
[19] M. Bazarnik, J. Henzl, R. Czajka, K. Morgenstern, *Chem. Commun.* **2011**, *47*, 7754-7766.
[20] S. Hagen, P. Kate, F. Leyssner. D. Nandi, M. Wolf, P. Tegeder, *J. Chem. Phys.* **2008**, *129*, 164102.
[21] N. Henningsen, R. Rurali, K. J. Franke, I. Fernádez-Torrente, J. I. Pascual, *Appl. Phys. A: Mater. Sci. Process.* **2008**, *93*, 241-246.
[22] D. Bléger, A. Ciesielski, P. Samorì, S. Hecht, *Chem. Eur. J.* **2010**, *16*,14256-14260.
[23] M. Alemani, M. V. Peters, S. Hecht, K.-H. Rieder, F. Moresco, L. Grill, *J. Am. Chem. Soc.* **2006**, *128*, 14446-14447.
[24] T. Kudernac, N. Ruangsupapichat, M. Parschau, B. Macia, N. Katsonis, S. R. Harutyunyan, K.-H. Ernst, B. L. Feringa, *Nature* **2011**, *479*, 208-211.
[25] J. Liu, T. Chen, X. Deng, D. Wang, J. Pei, L.-J. Wan, *J. Am. Chem. Soc.* **2011**, *133*, 21010-21015.
[26] S. Lei, M. Surin, K. Tahara, J. Adisoejoso, R. Lazzaroni, Y. Tobe, S. De Feyter, *Nano Lett.* **2008**, *8*, 2541-2546.
[27] K. S. Mali, J. Adisoejoso, E. Ghijsens, I. De Cat, S. De Feyter, *Acc. Chem. Res.* **2012**, *45*, 1309-1320.
[28] X. Zhang, T. Chen, Q. Chen, L. Wang, L.-J. Wan, *Phys. Chem. Chem. Phys.* **2009**, *11*, 7708-7712.
[29] M. Lackinger, S. Griessl, W. M. Heckl, M. Hietschold, G. W. Flynn, *Langmuir* **2005**, *21*, 4984-4988.
[30] X. Feng, J. Wu, M. Ai, W. Pisula, L. Zhi, J. P. Rabe, K. Müllen, *Angew. Chem Int. Ed.* **2007**, *46*, 3033-3036.
[31] S.-S. Jester, E. Sigmund, L. M. Röck, S. Höger, *Angew. Chem. Int. Ed.* **2012**, DOI: 10.1002/anie.201204006
[32] D. Riedel, M. Cranney, M. Martin, R. Guillory, G. Dujardin, M. Dubois, P. Sonnet, *J. Am. Chem. Soc.* **2009**, *131*, 5414-5423.
[33] J. Vicario, A. Meetsma, B. L. Feringa, *Chem. Commun.* **2005**, 5910-5912.
[34] M. Klok, M. Walko, E. M. Geertsema, N. Runagsupapichat, J. C. M. Kistemaker, A. Meetsma, Ben. L. Feringa, *Chem. Eur. J.* **2008**, *14*, 11183-11193.
[35] T. Hundertmark, A. F. Littke, S. L. Buchwald, G. C. Fu, *Org. Lett.* **2000**, *2*, 1729-1731.
[36] Commerically available 6-bromo-2-naphthol was converted to the corresponding thiol via a Newman-Kwart rearrangement sequence. The ketone was synthesized analogously to literature procedure: N. Koumura, E. M. Geertsema, M. B. van Gelder, A. Meetsma, B. L. Feringa, *J. Am. Chem. Soc.* **2002**, *124*, 5037-5051.
[37] A. Klapars, S. L. Buchwald, *J. Am. Chem. Soc.* **2002**, *124*, 14844-14845.
[38] Z. Xu, M. Kahr, K. L. Walker, C. L. Wilkins, J. S. Moore, *J. Am. Chem. Soc.* **1994**, *116*, 4537-4550.
[39] R. Deloncle, A.-M. Caminade, *J. Photochem. Photobiol. C* **2010**, *11*, 25-45.
[40] *Handbook of Photochemistry* (Eds.: M. Montalti, A. Credi, L. Prodi, M. T. Gandolfi), CRC Press, Boca Raton, **2006**, pp. 602-604.
[41] W. Mamdouh, H. Uji-i, J. S. Ladislaw, A. E. Dulcey, V. Percec, F. C. De Schryver, S. De Feyter, *J. Am. Chem. Soc.* **2006**, *128*, 317-325.
[42] K. S. Mali, K. Lava, K. Binnemans, S. De Feyter, *Chem. Eur. J.* **2010**, *16*, 14447-14458.
[43] N. Katsonis, H. Xu, R. M. Haak, T. Kudernac, Z. Tomović, S. George, M. Van der Auweraer, A. P. H. J. Schenning, E. W. Meijer, B. L. Feringa, S. De Deyter, *Angew. Chem. Int. Ed.* **2008**, *47*, 4997-5001.
[44] A. Cnossen, D. Pijper, T. Kudernac, M. M. Pollard, N. Katsonis, B. L. Feringa, *Chem. Eur. J.* **2009**, *15*, 2768-2772.
[45] J. A. A. W. Elemans, I. De Cat, H. Xu, S. De Deyter, *Chem. Soc. Rev.* **2009**, *38*, 722-736.
[46] J. A. A. W. Elemans, S. Lei, S. De Feyter, *Angew. Chem. Int. Ed.* **2009**, *48*, 7298-7332.
[47] T. Kudernac, S. Lei, J. A. A. W. Elemans, S. De Feyter, *Chem. Soc. Rev.* **2009**, *38*, 402-421.
[48] R. Fasel, M. Parschau, K.-H. Ernst, *Nature* **2006**, *439*, 449-452.
[49] N. Katsonis, A. Minoia, T. Kudernac, T. Mutai, H. Xu, H. Uji-i, R. Lazzaroni, S. De Feyter, B. L. Feringa, *J. Am. Chem. Soc.* **2008**, *130*, 386-387.
[50] L. Piot, A. Marchenko, J. Wu, K. Müllen, D. Fichou, *J. Am. Chem. Soc.* **2005**, *127*, 16245-16250.
[51] J. Visser, *Ph. D. Thesis*, University of Groningen, **2012**.
[52] N. Ruangsupapichat, *Ph. D. Thesis*, University of Groningen, **2012**.
[53] S. Huang, J. M. Tour, *J. Org. Chem.* **1999**, *64*, 8898-8906.
[54] I. Horcas, R. Fernández, J. M. Gómez-Rodríguez, J. Colchero, J. Gómez-Herrero, A. M. Baro, *Rev. Sci. Instrum.* **2007**, *78*, 013705.

Chapter 6: Incorporation of light-driven molecular motors into polymers

In this chapter the incorporation of molecular motors into polymers is described. Incorpation of motors into a polyisocyanate was unsuccessful due to the high reactivity of the functionalized isocyanate monomer. A ring-opening metathesis approach was more successful: short, well-defined polymers were obtained with a molecular motor on each monomeric unit. The motor function was retained in the polymer and isomerization of the motor was found to affect the conformation of the polymer.

Introduction

As discussed in previous chapters, Brownian motion is a major challenge in the application of synthetic molecular motors.[1] Controlled motion at the molecular scale[2] is overwhelmed readily by random thermal motion. A possible approach to solve this problem is to bring ensembles of molecular motors together and use their combined motion to perform useful work, similar to how cooperative action of muscle proteins controls mechanical motion in our muscles. This concept was demonstrated by Gaub and coworkers, who measured the force generated upon *E-Z* isomerization of azobenzenes incorporated into a polymer chain.[3] The incorporation of various molecular switches in polymers has led to the development of a wide variety of photoresponsive systems.[4,5] Azobenzenes are used primarily and the resulting polymers are candidates for future data storage materials.[6] Furthermore, several light-driven actuators have been reported that can convert switching on the molecular level to motion on the micrometer scale using polymeric materials.[7] In these photoactuators, the azobenzene switch can be either added as a dopant to a polymer or covalently attached. Upon photoisomerization, the azobenzene changes shape, which causes stress in the material. When thin films are irradiated from one side, more isomerization takes place near the surface, as the light intensity is attenuated deeper in the film. This causes contraction on one side of the film, resulting in a bending motion.

In this chapter, a proof-of-principle study of overcrowded alkene-based molecular motors incorporated into macromolecules and how this affects their behavior is presented.[8,9] Overcrowded alkenes are expected to be suitable photochromic switches for photoresponsive systems. They undergo a large geometrical change upon isomerization, as with azobenzenes, and their thermal stability is highly tunable.[10] In this chapter, two approaches to incorporate molecular motors in polymers are presented. In the first part, the synthesis of an isocyanate-functionalized motor is described, with the aim of studying the interaction between the rotation of the motor and the conformation of the polymer. In the second part, a system based on ring-opening metathesis polymerization is described, in which the conformation can be influenced by irradiation and changing the temperature, as was demonstrated using temperature-dependent CD and DOSY measurements. Polymers of which the properties such as solubility can be controlled with external stimuli have potential applications as sensor materials.[11]

Polyisocyanates

Polyisocyanates are a polymer class in which the backbone consists of repeating amide bonds. Due to steric interactions between the substituents on the amide nitrogen, the backbone tends to adopt a helical structure.[12,13] The polymer exists as a dynamic mixture

of left- and right-handed helical chains with infrequent helix reversals. This equilibrium can be influenced by the presence of chiral groups.[14] When photochromic switches are incorporated into these systems, the chirality can be controlled with light. This has been shown with azobenzenes[15,16,17] and more recently with overcrowded alkene-based molecular motors.[18,19,20]

We are interested in further studying the interplay between the dynamic helical structure of the polyisocyanate chain and the controllable helicity of the molecular motor. This can be expressed in a change in the chirality of the polymer chains upon irradiation due to isomerization of the molecular motor, but the chirality of the polymer could also influence the behavior of the molecular motor. In a previous report it was shown that a single molecular motor can influence the helicity of a polyisocyanate chain.[18] However, when multiple motors are present, likely of opposing helicity, the system becomes more complicated. It could cause a helix reversal in the polymer backbone, which forces an energy penalty. On the other hand, the polymer backbone may only force those motors to isomerize, which do not fit the (locally) dominant helicity. Consider for example two motors in the unstable form, one of each enantiomer, are present in a polymer chain with a certain helicity. The chiral environment might promote thermal helix inversion of the motor with the mismatched helicity, while retarding it for the motor of which the chirality matches that of the polymer. Furthermore it is of interest to determine whether there is a crowding effect when many motors are forced into proximity. This kind of effect was demonstrated previously in mono- and multilayers of molecular motors, in which increased surface coverage caused a decrease in the rate of rotation.[21] A similar effect was reported for rotaxanes, which were incorporated into dendrimers,[22] and azobenzene molecular switches in polymer sidechains in a film below the polymer glass transition temperature.[23] In the latter case, retardation of the thermal isomerization of the *Z*-isomer of the azobenzene is explained by a combination of steric and dipolar effects.

Molecular design

In earlier systems, which use azobenzene molecular switches to influence the conformation of polyisocyanates, a two-carbon spacer was used,[15] possibly because having the polymerizable group directly attached to the azobenzene will give too much steric hindrance for the polymerization to proceed. However, a long linker may prevent the interactions that we would like to study with the present system. The design of our monomer is based on compound **1** (Scheme 1).

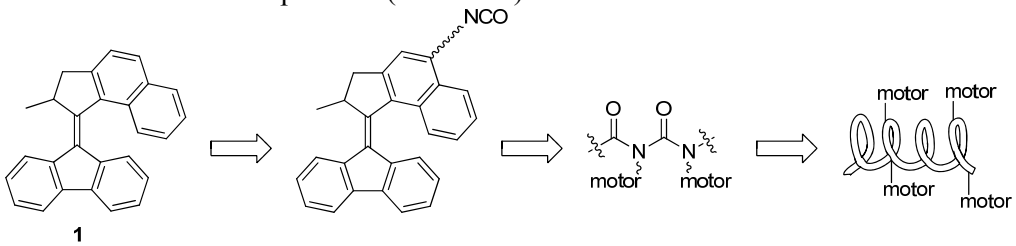

Scheme 1 Functionalizing molecular motor **1** with an isocyanate and subsequent polymerization yields a highly functionalized helical polymer.

This molecular motor is well-studied in the literature and operates over a convenient temperature range over which the rate of thermal isomerization can be controlled without going to extreme conditions.[24,25] As was already demonstrated in the previous chapters, this molecular motor can conveniently be functionalized at the 4'-position without affecting the rate of thermal isomerization.[26] A short ethyloxy spacer between the polymerizable group and the molecular motor is employed, because steric hindrance might retard polymerization otherwise.

Synthesis

The direct conversion of an alcohol to an isocyanate can be performed using the isocyanate anion as a nucleophile in combination with activation of the alcohol. Both the use of cyanuric chloride (2,4,6-trichloro-1,3,5-triazine) [27] and triphenylphosphine/DDQ[28] has been reported, with tetrabutylammonium isocyanate as a nucleophile. Alcohol-functionalized motor **2**, which was synthesized in seven steps as described previously in Chapter 4, was chosen as substrate (Scheme 2). Unfortunately, neither set of conditions gave the desired product using this substrate, but resulted in the formation of complex mixtures as determined by TLC and ^{1}H NMR spectroscopy.

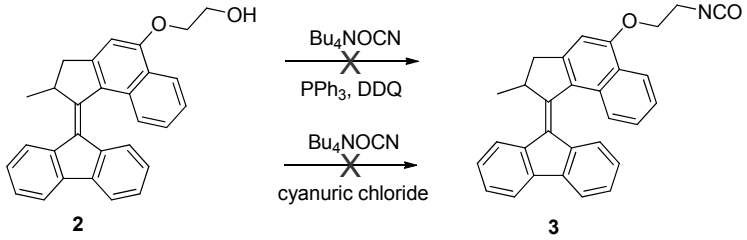

Scheme 2 Attempted substitution of the alcohol functionality in motor **2** with an isocyanate group.

As an alternative route, the alcohol in **2** can be converted to a better leaving group. Mesylation of the alcohol moiety in THF proceeded to give **4** in 94% yield. Conversion of the alcohol to a bromide via the Appel reaction gave compound **5** in good yield (Scheme 3).

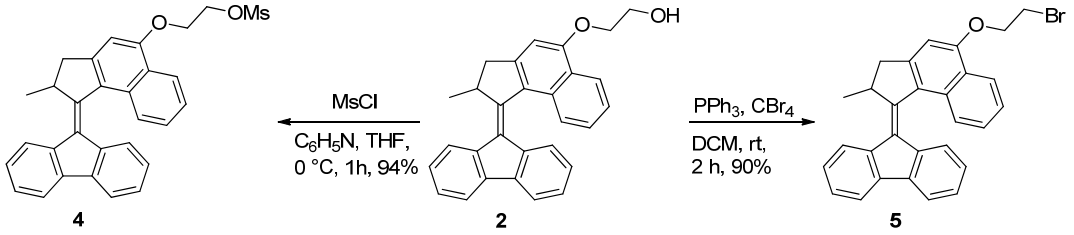

Scheme 3 Synthesis of mesylated motor **4** and brominated motor **5**.

Both **4** and **5** were used as a substrate for nucleophilic substitution with isocyanate. A range of conditions were tested: the use of either NBu_4OCN or KOCN as an isocyanate source, DMF or acetonitrile as solvents and the addition of NBu_4I to catalyze the reaction. The desired product could not be isolated in any case, even though the starting material was converted. Isocyanates are reactive functional groups which are prone to nucleophilic attack and polymerization, nevertheless the apparent degree of instability was surprising. It is possible that it is inherent to the specific structure of compound **3**. The ether functionality increases the reactivity of the isocyanate due to neighboring group participation (Scheme 4). Attack of the ether oxygen on the isocyanate generates a five-membered ring intermediate, which is susceptible to nucleophilic attack or further reaction via a different pathway. This could explain the evident instability of desired monomer **3**.

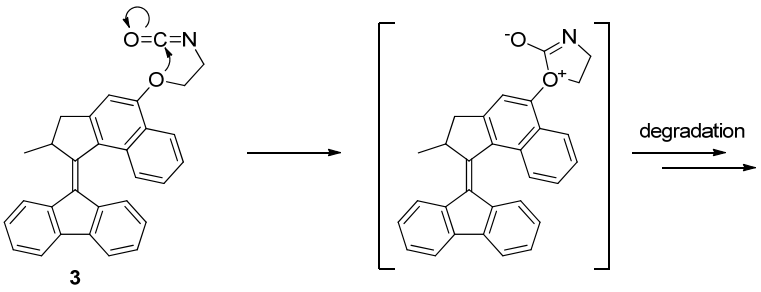

Scheme 4 Degradation of **3** potentially proceeds via neighboring group participation of the ether oxygen.

To circumvent this effect, a new target was designed in which a longer spacer was used. Intramolecular attack in this case would yield a seven-membered ring, which is thermodynamically unfavorable. Furthermore, we chose to install the isocyanate functionality via a Curtius rearrangement rather than via nucleophilic substitution, so that there are no potentially nucleophilic leaving groups which could initiate polymerization or degradation.

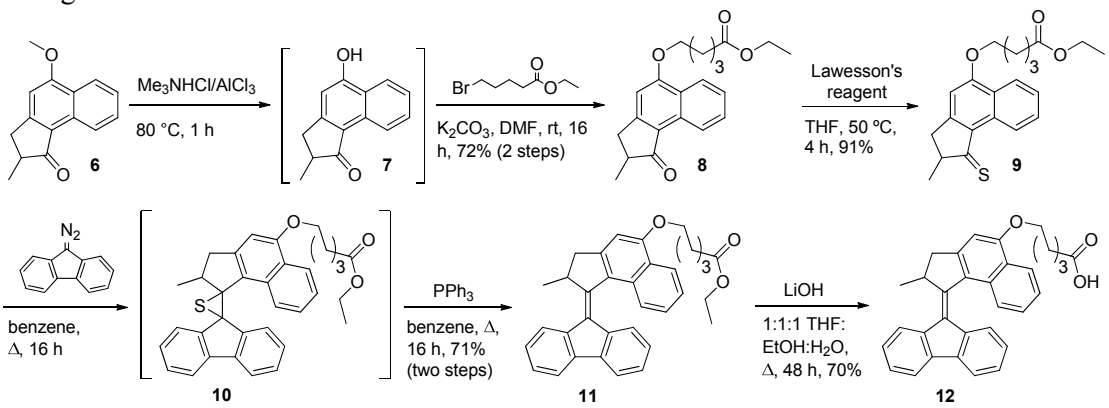

Scheme 5 Synthesis of carboxylic acid-functionalized motor **12**.

Starting from ketone **6**, which is a known compound,[26] the methoxy group was deprotected in the presence of a trimethylamine hydrochloride-aluminium trichloride ionic liquid (Scheme 5). After aqueous workup, the crude product **7** was immediately alkylated using ethyl 5-bromovalerate to yield ketone **8**. The ketone moiety was converted to a thioketone using Lawesson's reagent in a remarkably high yield. Subsequently, thioketone **9** was reacted with 9-diazofluorenone to give the intermediate episulfide **10**, which was not isolated but instead desulfurized directly with triphenylphosphine to yield motor **11** in a relatively high yield (71%) over two steps. Hydrolysis of the ester functional group was achieved by treatment with lithium hydroxide in a THF-ethanol-water mixture to yield carboxylic acid-functionalized motor **12**.

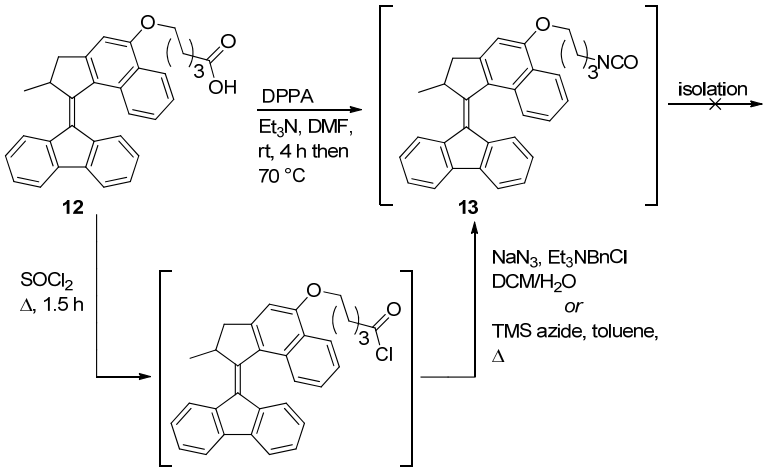

Scheme 6 Attempted synthesis of isocyanate-functionalized motor **13**.

Several methods are available for the conversion of a carboxylic acid to an isocyanate. Initially, we chose to use diphenylphosphoryl azide (DPPA) as an azide transfer reagent (Scheme 6). Reaction of compound **12** with DPPA in toluene yields an acyl azide intermediate, which is converted to the isocyanate *in situ* by heating. The formation of an isocyanate functional group was confirmed by FT-IR spectroscopy, however, isolation of **13** proved unsuccessful. In an alternative method, compound **12** was converted to the corresponding acyl chloride, which was reacted with either NaN_3 or $TMSN_3$ to give the acyl azide. After heating, the appearance of an absorption at 2265 cm^{-1} in the FT-IR spectrum of the reaction mixture was observed, which is assigned to the isocyanate. Unfortunately, purification and isolation of the product from the reaction mixture did not succeed. Aqueous workup followed by extraction led to the isolation of the corresponding amine, as determined by FT-IR spectroscopy. Column chromatography failed because the column material (either silica or alumina) reacted with the product, resulting in the formation of a purple band that could not be removed from the column. The desired product was not obtained as determined by ^1H NMR spectroscopy. Kugelrohr distillation was unsuccessful, possibly because the boiling point of the product is too high, even under reduced pressure.

Outlook

The synthesis of a functional monomer proved more difficult than expected. Another option to obtain the functionalized polymer is by post-polymerization modification;[29] this approach was explored briefly. An ester-functionalized polyisocyanate was synthesized according to a literature procedure.[30] Ester exchange with alcohol **2** could then provide a motor-functionalized polymer. However, under acidic conditions compound **2** was not stable, while polyisocyanates tend to degrade under basic conditions. Chloride and iodide substituted isocyanates are also known.[30] S_N2 type displacement with a nucleophile-substituted motor could lead to desired polymer. The nucleophile can not be strongly basic and typically needs to be present in large excess. Furthermore, any post-polymerization modification has the disadvantage that it is difficult to achieve a high degree of functionalization while still having the substituents in proximity to the polymer backbone.

Ring-opening metathesis polymerization

Ring-opening metathesis polymerization (ROMP) has received considerable attention recently, especially in the field of functional materials.[31,32] ROMP is a chain-growth polymerization which converts cyclic olefins to polymers with a low polydispersity index (generally <1.30) (Scheme 7). The reaction is typically catalyzed with ruthenium or molybdenum catalysts, which have good functional group tolerance, although acids, alcohols and aldehydes can be problematic.[32]

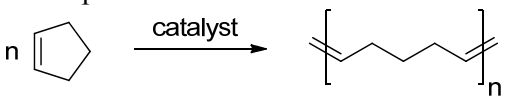

Scheme 7 Example of a ring-opening metathesis polymerization.

One of the advantages of ROMP in the field of material science is that it allows for the installation of functionality in a well-defined and controlled manner. Polymer chain length is controlled and also the shape can be directed if ring-expansion metathesis polymerization is used.[33] The precise integration of functionality by modular assembly of parts with different properties can lead to unique materials.[34] We want to apply this to our overcrowded alkene-based molecular motors. By incorporating light-driven molecular motors in this way photocontrol over a variety of materials properties may be possible.

Molecular design

ROMP generally makes use of monomers with a considerable degree of ring strain. This provides an enthalpic driving force to counter the entropic penalty for polymerization. We chose a norbornene-based monomer fused with a succinimide, which has been reported in the synthesis of polymers with various sidechains on the imide nitrogen.[33,35,36] The molecular motor is attached via a phenylacetylene spacer. Even though there is more than one reactive group in the molecule, metathesis should only take place on the norbornene double bond. The central double bond of the molecular motor should be too hindered to allow the catalyst to bind. Also, even though metathesis catalysts can react with alkynes, ruthenium-based catalysts are known to be more reactive towards alkenes.[37] The acetylene can be conveniently coupled to a bromide-functionalized molecular motor via Sonogashira coupling.

Synthesis

A convergent synthesis route was devised to prepare a monomer containing a ring-strained alkene and a molecular motor. First, a functionalized norbornene was synthesized (Scheme 8). The synthesis began with 4-iodoaniline **13**, which was reacted with TIPS-acetylene in a Sonogashira coupling to yield compound **14**. To synthesize the polymerizable group, freshly distilled cyclopentadiene was reacted with maleic anhydride (**15**) at room temperature to give Diels-Alder adduct **16**. Imide formation between compounds **14** and **16** was performed by heating in acetic anhydride yielding functionalized norbornene **17** in 77%.

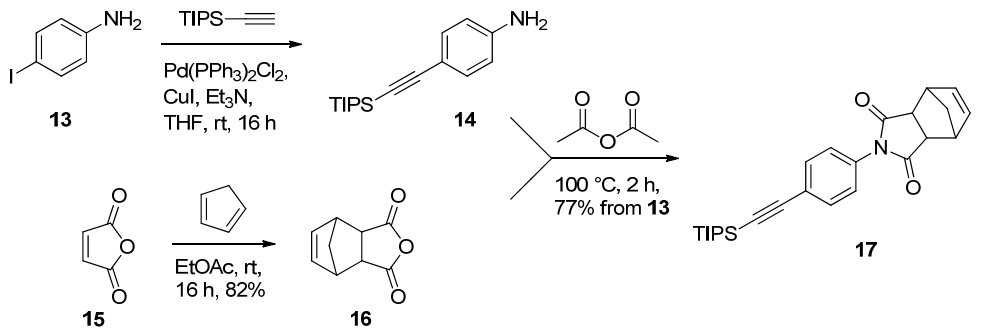

Scheme 8 Synthesis of functionalized norbornene **17**.

The TIPS group in compound **17** was removed using tetrabutylammonium fluoride to generate free alkyne **18**. Directly after quenching with $CaCl_2$ and filtration, compound **18** was reacted in another Sonogashira coupling with bromide-functionalized motor **19**.

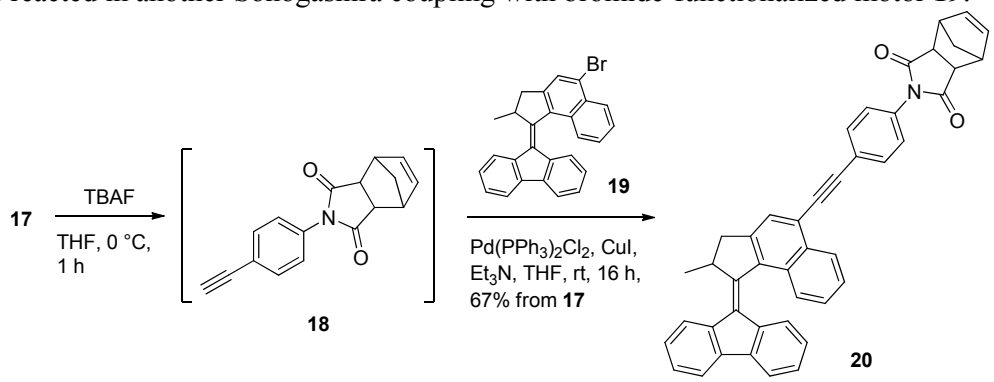

Scheme 9 Synthesis of monomer **20**.

Methyl substituted monomer **21** was synthesized as a model compound for optimizing polymerization conditions.[38] Polymerization was carried out using Grubbs first generation catalyst **22**. It was crucial to perform the polymerization reaction under oxygen-free conditions. Model compound **21** was polymerized with 5 mol% of catalyst in CH_2Cl_2 at room temperature (Table 1). After precipitation from methanol product **23** was obtained in excellent yield. The same conditions were applied in the polymerization of **20**, however, after one hour the conversion was low and the product was obtained in <10% yield. Increasing the temperature to 40 °C and the catalyst loading to 10 mol% increased the yield to 21%. The yield could be further improved by increasing the reaction time and adding the catalyst in portions, showing that deactivation of the catalyst was a problem. However, adding the catalyst portionwise would increase the polydispersity of the resulting polymer greatly, losing one of the advantages of ROMP. By changing the solvent to *ortho*-dichlorobenzene (ODCB) the yield was further improved, presumably because the catalyst is better stabilized in aromatic solvents, and because the temperature can be increased further. Under these conditions, both the model polymer and polymer **24** could be obtained in good yield.

Table 1 Optimization of conditions for ring-opening metathesis polymerization of compounds **20** and **21**.

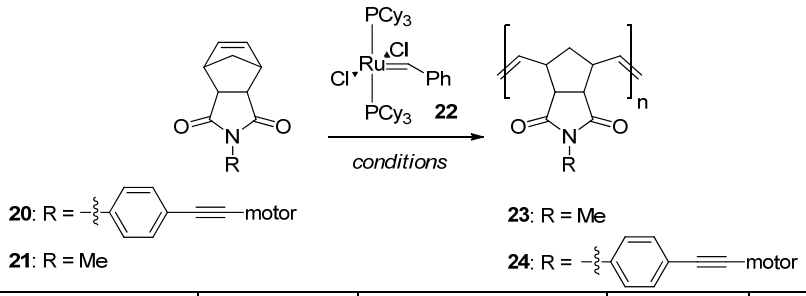

Substrate	Catalyst loading	Solvent	Temperature (ºC)	Time (h)	Yield (%)[a]
21	5%	CH_2Cl_2	20	1	99%
20	5%	CH_2Cl_2	20	1	<10%
20	10%	CH_2Cl_2	40	2	21%
20	4 x 5%[b]	CH_2Cl_2	40	4 d	60%
21	10%	ODCB	60	1	99%
20	10%	ODCB	60	4	96%

[a] Crude yield after precipitation. [b] Portions of catalyst were added every 24 h.

TLC analysis of polymer **24** in CH_2Cl_2 showed the presence of several small fast-moving spots, which were presumed to be degradation products of monomer or dimers. These were removed by repeated precipitation from CH_2Cl_2/MeOH. In the ^{1}H NMR spectrum the formation of a polymer is inferred from the broadening of the peaks. Furthermore, the signal of the hydrogen atoms on the double bond shifts from 6.3 ppm in the norbornene to 5.8 ppm in the polymer. The tacticity of polynorbornenes can be determined from ^{13}C NMR; the carbon atoms from the main chain double bond around 130 ppm shift to higher field in an isotactic polymer compared to a syndiotactic polymer.[39,40] In the present case, numerous peaks were observed for carbons of the double bond, indicating a complex and atactic microstructure of the polymer. The molar mass and polydispersity of polymer **24** was determined by gel permeation chromatography (GPC) in THF using universal calibration. The number average molar mass M_n was found to be 6.37 x 10^3 g/mol, while the weight average molar mass was determined to be 6.94 x 10^3 g/mol with a polydispersity of 1.09 using universal calibration. This indicates a well-defined polymer with on average a little over ten monomer units per chain. Similar results were obtained for two different batches. The low polydispersity is typical for a polymer obtained from a living polymerization.

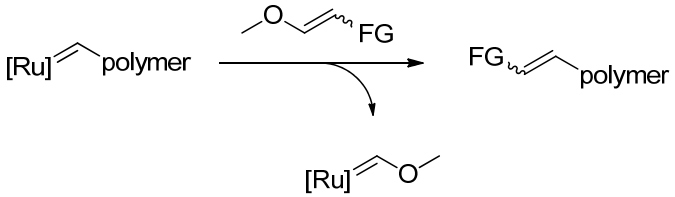

Scheme 10 Vinyl ether termination of metathesis polymerization.

Because ROMP is a living polymerization, there is the possibility of further reaction after the polymerization has finished. This can be polymerization with a different monomer to construct block copolymers or endcapping to introduce a specific group or functionality. Various methods for end-capping are available, but vinyl ether termination is the most

general approach to introduce a functional group.[41] This introduces an electronically deactivated carbene on the ruthenium center that does not re-initiate metathesis reactions (Scheme 10). Some initial studies were made to introduce a fluorinated group on polymer **24**, but this was unsuccessful.

Photochemical and thermal isomerization

The photochemical and thermal isomerization (Scheme 11) of the molecular motors in monomer **20** and polymer **24** were evaluated using UV/vis absorption and CD spectroscopy. Compound **20** and **24** show similar UV/vis absorption spectra to that of compound **1**, although in both the absorption at longest wavelength shows a red-shift of about 30 nm (Figure 1).[24] This band is also slightly broader for the polymer than for the monomer.

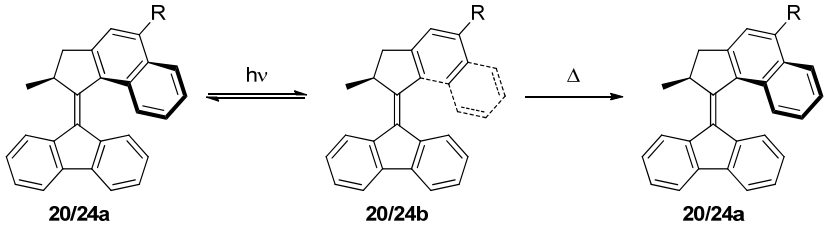

Scheme 11 Photochemical and thermal isomerization of the molecular motor units in monomer **20** and polymer **24**.

Upon irradiation (365±20 nm) of a solution of compound **20** in $CHCl_3$ at -40 °C, the band around 410 nm shifts to longer wavelength. This is attributed to the formation of the thermally unstable isomer **20b**. The same is observed for polymer **24**. Although irradiation of a solution of **20** or **24** open to the air resulted in some degradation, with argon or nitrogen purging photoisomerization proceeded cleanly and isosbestic points were maintained. The spectral changes were fully reversed upon heating to 40 °C for 30 min for both compounds.

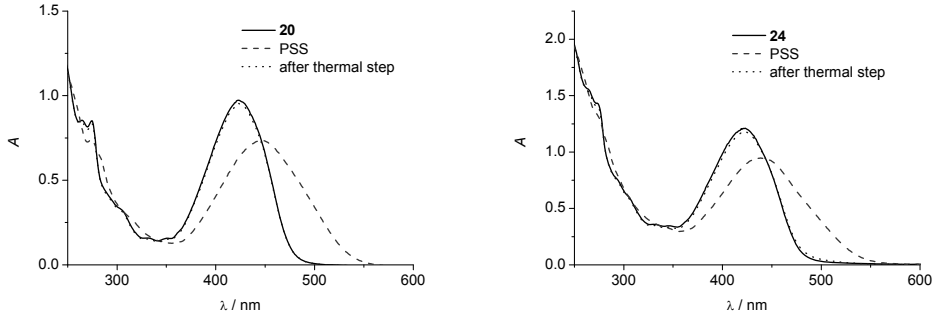

Figure 1 UV/vis absorption spectra of **20** and **24** in chloroform before irradiation (full line), after UV irradiation (365±20 nm) to the PSS (dashed line) and after thermal relaxation (dotted line).

Although we were unable to separate **20** by chiral stationary phase HPLC, enantiopure material was obtained by separation of the precursor **19** and repeating the final steps of the synthesis (Scheme 9). Characterization data of the optically active polymer was identical to that of racemic **20**. The CD spectra of monomer **20** and polymer **24** in chloroform are practically identical (Figure 2). By comparison with the spectrum calculated on the B3LYP/6-31G(d,p) level of theory the absolute stereochemistry was assigned to be *R*. Upon irradiation (365±20 nm) at -40 °C, inversion of the major bands in the spectrum is observed, which indicates that the thermally unstable form **20**/**24b**, which has opposite helicity, is obtained. Upon heating to 40 °C, the spectral changes reversed

fully. From both UV/vis absorption and CD spectroscopy it is clear that the rotary function of the molecular motors is fully retained in the polymer. From the ^{1}H NMR spectrum, the ratio of **20a** to **20b** was determined to be 66:34, similar to that obtained for **1**. For **24**, accurate integration was precluded by the broadening, which causes overlap of the peaks of interest, however, from the changes in both the UV/vis absorption and CD spectra a similar ratio as for **20** can be estimated.

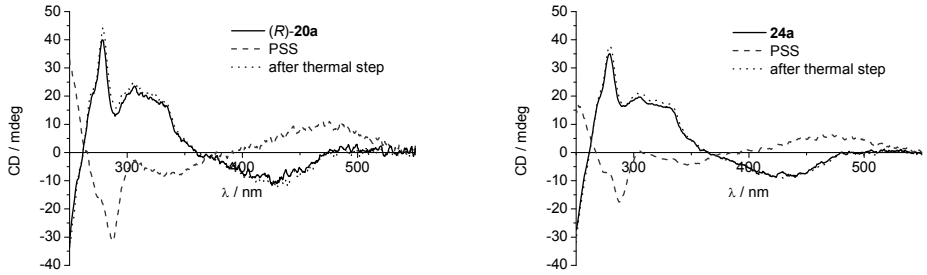

Figure 2 CD spectra of (*R*)-**20** and polymer **24** in chloroform before irradiation (full line), after UV irradiation (365±20 nm) to the PSS (dashed line) and after thermal relaxation (dotted line).

Cooling down of a solution of **24** in chloroform reveals a temperature dependence of the CD spectrum.[42] This may be indicative of a change in structure upon cooling; similar behavior has been observed in, for example, phenylacetylene-based foldamers[43] and helical supramolecular assemblies.[44] The changes are relatively small, but a clear trend can be observed. The effect is also dependent on the solvent:[45] in chloroform and ether the intensity increases when the temperature is lowered (Figure 3). In toluene, the trend is reversed and the intensity decreases when the temperature is lowered below 0 °C. In the unstable form the temperature seems to have less of an effect, but there is insufficient data to draw a clear conclusion. The CD signal of the PSS mixture was only measured at three temperatures, because the unstable form starts to convert to the stable form when the temperature is above -20 °C, and at lower temperatures the low solubility precludes the acquisition of further data over a broader temperature range.

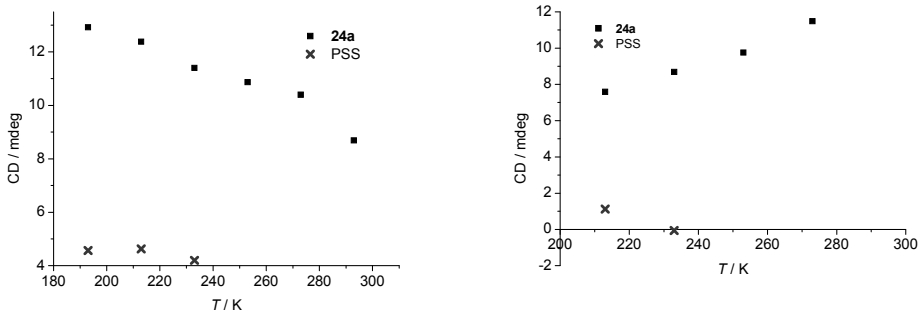

Figure 3 a) Temperature dependence of the CD signal (334 nm) of **24** in ether before (squares) and after (crosses) irradiation at 365±20 nm. b) Temperature dependence of the CD signal (334 nm) of **24** in toluene before (squares) and after (crosses) irradiation at 365±20 nm.

To further investigate whether there is a change in the conformation of the polymer upon cooling, the diffusion constant for polymer **24** was measured. If the polymer indeed folds up or adopts a more extended conformation, this will result in a change in its diffusion constant. Diffusion-ordered NMR spectroscopy (DOSY) can be used to determine diffusion constants in macromolecular system, which can provide information on the structure at a molecular level such as, for example, chain length and aggregation[46] or

threading of rotaxanes.[47] The diffusion constant of **24** was determined by DOSY in chloroform at room temperature and -40 °C (Table 2). As a control experiment, the diffusion constant of monomer **20** was also determined.

Table 2 Diffusion constants of **20** and **24** in $CDCl_3$ at different temperatures.

Compound	T (K)	D (x10^{-6} cm^2 s^{-1})
20	293	4.2±0.2
20	233	0.8±0.03
24	293	2.8±0.3
24	233	5.7±0.3
PSS mixture of **24a** and **24b**	233	5.0±0.2

The diffusion coefficient decreases with temperature, but is also dependent on solvent viscosity, which is in turn dependent on the temperature. For monomer **20** a decrease in diffusion coefficient is seen upon lowering the temperature. In contrast, for polymer **24** the diffusion constant increases with decreasing temperature. This is consistent with the earlier hypothesis that the conformation of the polymer is temperature dependent. If the temperature is lowered, chloroform becomes a poorer solvent and the polymer adopts a more collapsed conformation. This decreases the effective radius and increased the diffusion constant. The solubility of polymers is known to be sensitive to a number of variables, including structure and conformation.[48] Polymers that are responsive to external stimuli such as pH, temperature and UV irradiation have also been reported.[49,50]
The effect of UV irradiation on the diffusion coefficient of **24** was also investigated. When a solution of **24** was irradiated to PSS, the diffusion coefficient is slightly decreased. *E*-*Z* isomerization of the motor units on the polymer apparently also affects the conformation of the polymer. The effect is smaller than the effect of temperature, but it is significant even though the motor is present as a mixture of stable and unstable form. If the PSS could be enriched in **24b**, the effect would likely be more pronounced.

Conclusion

In the first part of this chapter, the synthesis of an isocyanate-functionalized molecular motor was attempted. An initial approach failed, likely due to the intrinsically high reactivity of the isocyanate functionality. A second approach was described, in which the molecular motor could be functionalized with an isocyanate. In this case, purification was problematic. In the end, the desired polymer could not be obtained. However, during the synthesis a number of molecular motors substituted with a variety of functional groups was successfully synthesized which may prove useful for other applications.
In the second part of the chapter, the synthesis of a highly functionalized ring-opening metathesis polymer was described. Molecular motor **20** could be polymerized using a ruthenium based metathesis catalyst to give well defined polymers with a narrow polydispersity index. The photochemical and thermal isomerization processes of the molecular motor were fully retained in the polymer. The conformation of the polymer could be influenced by changing the temperature or by UV-irradiation as was confirmed using CD spectroscopy and DOSY measurements.
These results could lead to the incorporation of molecular motors in functional polymeric structures. Ring-opening metathesis polymerization is a particularly effective way towards such systems, because it allows for the introduction of various functional groups via endcapping and synthesis of block copolymers and telechelic polymers.[51,52] Furthermore, photochromic polymers have potential applications in data storage.

Although the current system has low thermal stability, other overcrowded alkenes with better thermal stability might be used. Because these can function as molecular switches with four different states, as opposed to only two for azobenzenes, this could dramatically increase the density of memory storage.

Acknowledgements

Gel permeation chromatography was performed by Joop Vorenkamp, who is acknowledged for his contributions. Pieter van der Meulen is acknowledged for his assistance with DOSY NMR measurements.

Experimental section

For general comments, see Chapter 2. The synthesis of 2-((1-(*9*H-fluoren-9-ylidene)-2-methyl-2,3-dihydro-1*H*-cyclopenta[*a*]naphthalen-5-yl)oxy)ethanol **2** was described in Chapter 4. 5-Methoxy-2-methyl-2,3-dihydro-1*H*-cyclopenta[*a*]naphthalen-1-one **6**,[26] 4-((triisopropylsilyl)ethynyl)aniline **14**,[53,54] 3a,4,7,7a-tetrahydro-4,7-methanoisobenzofuran-1,3-dione **16**[55] and 9-(5-bromo-2-methyl-2,3-dihydro-1*H*-cyclopenta[*a*]naphthalen-1-ylidene)-9*H*-fluorene **19**[56] were synthesized according to previously reported procedures.

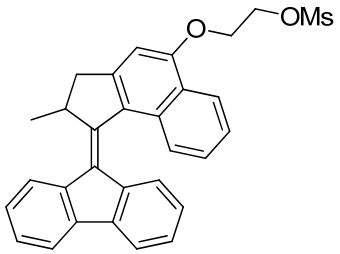

2-((1-(9*H*-fluoren-9-ylidene)-2-methyl-2,3-dihydro-1*H*-cyclopenta[*a*]naphthalen-5-yl)oxy)ethyl methanesulfonate 4

To a solution of compound **2** (54 mg, 0.13 mmol) in THF (2 mL) at 0 °C was added pyridine (0.5 mL) and methanesulfonyl chloride (~50 μL, excess). The mixture was allowed to warm to rt over 1 h and concentrated. The residue was passed through a short silica column (CH_2Cl_2) to yield **4** (61 mg, 94%). ^{1}H NMR (400 MHz, $CDCl_3$) δ 8.38 (d, *J* = 8.4 Hz, 1H), 7.99 (m, 1H), 7.87 (m, 1H), 7.79 (d, *J* = 7.5 Hz, 1H), 7.74 (d, *J* = 8.3 Hz, 1H), 7.49 (m, 1H), 7.41 (m, 2H), 7.36 (m, 1H), 7.22 (t, *J* = 7.4 Hz, 1H), 6.91 (s, 1H), 6.83 (t, *J* = 7.7 Hz, 1H), 6.73 (d, *J* = 7.9 Hz, 1H), 4.75 (m, 2H), 4.48 (m, 2H), 4.32 (m, 1H), 3.51 (dd, *J* = 15.1, 5.6 Hz, 1H), 3.13 (s, 3H), 2.70 (d, *J* = 15.1 Hz, 1H), 1.40 (d, *J* = 6.7 Hz, 3H); ^{13}C NMR (50 MHz, $CDCl_3$) δ 156.3 (C), 151.5 (C), 149.0 (C), 140.1 (C), 140.0 (C), 139.5 (C), 137.4 (C), 130.8 (C), 129.8 (C), 128.9 (C), 127.7 (CH), 127.6 (CH), 127.1 (CH), 126.8 (CH), 126.8 (CH), 126.1 (CH), 125.9 (CH), 125.3 (CH), 124.6 (C), 124.1 (CH), 122.8 (CH), 119.9 (CH), 119.2 (CH), 103.8 (CH), 67.8 (CH_2), 66.5 (CH_2), 45.4 (CH), 42.7 (CH_2), 38.2 (CH_3), 19.8 (CH_3). HRMS (ESI) calcd. for $C_{30}H_{27}O_4S$ [M+H] 483.1625, found 483.1591.

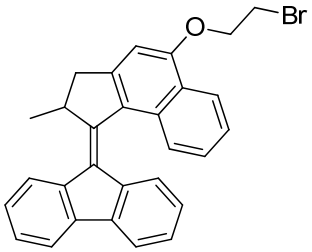

9-(5-(2-bromoethoxy)-2-methyl-2,3-dihydro-1*H*-cyclopenta[*a*]naphthalen-1-ylidene)-9*H*-fluorene 5

To solution of triphenylphosphine (196 mg, 0.75 mmol) and tetrabromomethane (124 mg, 0.38 mmol) in dry CH_2Cl_2 (4 mL) was added **2** (100 mg, 0.25 mmol). The reaction mixture was stirred at rt for 1.5 h and subsequently concentrated *in vacuo*. The residue was purified by column chromatography (1:1 pentane:ethyl acetate, R_f = 0.9) to give **5** (103 mg, 90%) as a yellow solid. ^{1}H NMR (300 MHz, $CDCl_3$) δ 8.42 (d, *J* = 8.2 Hz, 1H), 7.99 (m, 1H), 7.87 (m, 1H), 7.78 (d, *J* = 7.5 Hz, 1H), 7.73 (d, *J* = 8.3 Hz, 1H), 7.49 (t, *J* = 7.2 Hz, 1H), 7.38 (m, 3H), 7.22 (t, *J* = 7.4 Hz , 1H), 6.92 (s, 1H), 6.83 (t, *J* = 7.7 Hz, 1H), 6.74 (d, *J* = 7.9 Hz, 1H), 4.56 (t, *J* = 5.9 Hz, 2H), 4.33 (m, 1H), 3.85 (t, *J* = 6.0 Hz, 2H), 3.54 (dd, *J* = 15.1, 5.6 Hz, 1H), 2.71 (d, *J* = 15.1 Hz, 1H), 1.40 (d, *J* = 6.7 Hz, 3H); ^{13}C NMR (75 MHz, $CDCl_3$) δ 156.5 (C), 151.5 (C), 149.0 (C), 140.1 (C), 140.0 (C), 139.5 (C), 137.4 (C), 130.9 (C), 129.6 (C), 128.8 (C), 127.61 (CH), 127.56 (CH), 127.0 (CH), 126.7 (CH), 126.6 (CH), 126.1 (CH), 125.9 (CH), 125.2 (CH), 124.8 (C), 124.0 (CH), 123.0 (CH), 119.9 (CH), 119.1 (CH), 103.8 (CH), 68.4 (CH_2), 45.4 (CH), 42.7 (CH_2), 29.3 (CH_2), 19.81 (CH_3).

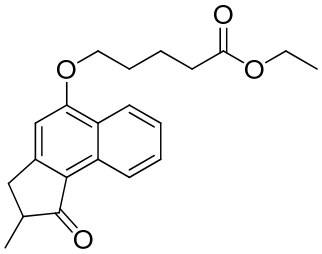

ethyl 5-((2-methyl-1-oxo-2,3-dihydro-1H-cyclopenta[a]naphthalen-5-yl)oxy)pentanoate 8

To a suspension of $AlCl_3$ (35.2 g, 0.26 mol) in CH_2Cl_2 (150 mL) at 0 °C was added trimethylamine hydrochloride (12.6 g, 0.13 mol) in five portions. After stirring for 20 min, **6** (3.0 g, 13.2 mmol) was added and stirring was continued for 10 min. The solvent was removed *in vacuo* and the resulting paste was stirred at 80 °C for 1 h. The reaction mixture was diluted with CH_2Cl_2 and poured into ice water (300 mL). The mixture was extracted with ethyl acetate (3x100 mL). The organic layers were combined and concentrated to yield crude **7**. This was dissolved in DMF (120 mL) and ethyl 5-bromovalerate (2.37 mL, 15 mmol) and K_2CO_3 (2.1 g, 15 mmol) were added. The reaction mixture was stirred at rt for 16 h. The volatiles were removed and the residue was taken up in H_2O (300 mL) and ethyl acetate (300 mL). After acidification with 2 N aqueous HCl, the organic layer was separated, dried on Na_2SO_4 and concentrated. The residue was purified by column chromatography (5:2 pentane:ethyl acetate, R_f = 0.5) to yield **8** (3.22 g, 72%) as a pale yellow solid. mp 72.7 °C; ^{1}H NMR (400 MHz, $CDCl_3$) δ 9.02 (d, *J* = 8.2 Hz, 1H), 8.12 (d, *J* = 8.3 Hz, 1H), 7.54 (t, *J* = 7.6 Hz, 1H), 7.40 (t, *J* = 7.6 Hz, 1H), 6.50 (s, 1H), 4.05 (dt, *J* = 12.5, 6.3 Hz, 4H), 3.16 (dd, *J* = 17.2, 7.0 Hz, 1H),

2.58 (m, 2H), 2.36 (t, J = 6.5 Hz, 2H), 2.12-1.63 (m, 4H), 1.24 (d, J = 7.0 Hz, 3H) 1.18 (t, J = 7.0 Hz, 3H); ^{13}C NMR (101 MHz, $CDCl_3$) δ 208.9 (C), 173.4 (C), 160.8 (C), 159.4 (C), 130.7 (C), 129.2 (CH), 125.9 (CH), 125.2 (C), 123.8 (CH), 123.2 (C), 122.5 (CH), 102.2 (CH), 68.3 (CH_2), 60. (CH_2), 42.3 (CH), 35.9 (CH_2), 34.0 (CH_2), 28.6 (CH_2), 21.9 (CH_2), 17.0 (CH_3), 14.4 (CH_3); HRMS (ESI) calcd. for $C_{21}H_{25}O_4$ [M+H] 341.1747, found 341.1742.

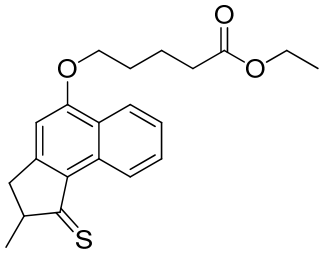

ethyl 5-((2-methyl-1-thioxo-2,3-dihydro-1H-cyclopenta[a]naphthalen-5-yl)oxy)pentanoate 9

To a solution of **8** (3.16 g, 9.28 mmol) in THF (100 mL) was added Lawesson's reagent (4.55 g, 11.2 mmol). The mixture was stirred at 50 ºC for 4 h. The volatiles were removed *in vacuo* and the residue was purified by column chromatography (15:1 toluene:ethyl acetate, R_f = 0.5) yielding **9** (3.04 g, 8.53 mmol, 92%) as a red solid. ^{1}H NMR (400 MHz, $CDCl_3$) δ 10.18 (d, J = 8.5 Hz, 1H), 8.31 (d, J = 8.3 Hz, 1H), 7.73 (t, J = 7.7 Hz, 1H), 7.54 (t, J = 7.6 Hz, 1H), 6.78 (s, 1H), 4.18 (m, 4H), 3.44 (dd, J = 18.1, 6.4 Hz, 1H), 3.11 (m, 1H), 2.85 (d, J = 18.0 Hz, 1H), 2.46 (t, J = 7.0 Hz, 2H), 2.00 (m, 4H), 1.50 (d, J = 7.2 Hz, 3H), 1.27 (t, J = 7.1 Hz, 3H); ^{13}C NMR (75 MHz, $CDCl_3$) δ 244.2 (C), 172.9 (C), 162.0 (C), 160.9 (C), 133.1 (C), 131.0 (C), 130.1 (CH), 125.8 (CH), 125.0 (C), 123.8 (CH), 122.4 (CH), 101.5 (CH), 68.1 (CH_2), 60.1 (CH_2), 54.5 (CH), 40.0 (CH_2), 33.6 (CH_2), 28.1 (CH_2), 21.6 (CH_3), 21.4 (CH_2), 14.0 (CH_3); HRMS (ESI) calcd. for $C_{21}H_{25}O_3S$ [M+H] 357.1519, found 357.1511.

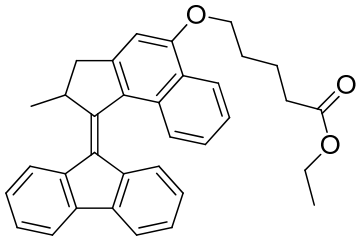

ethyl 5-((1-(9H-fluoren-9-ylidene)-2-methyl-2,3-dihydro-1H-cyclopenta[a]naphthalen-5-yl)oxy)pentanoate 11

To a solution of **9** (3.00 g, 8.42 mmol) in benzene (100 mL) was added 9-diazofluorene (3.00 g, 15.6 mmol). The solution was heated to reflux for 16 h, then triphenylphosphine (2.23 g, 8.5 mmol) was added and heating was continued for another 16 h. The solution was allowed to cool to rt and MeI (1 mL) was added. After stirring for 3 h the mixture was filtered and concentrated *in vacuo*. The residue was purified by column chromatography (gradient 2:1 pentane:toluene to 100% toluene). The product was recrystallized from ethanol yielding **11** (2.92 g, 5.98 mmol, 71%) as a yellow solid. mp 140.7 °C; ^{1}H NMR (300 MHz, $CDCl_3$) δ 8.39 (d, J = 8.3 Hz, 1H), 8.05-7.95 (m, 1H), 7.85 (m, 1H), 7.73 (m, 2H), 7.40 (m, 4H), 7.21 (t, J = 7.3 Hz, 1H), 6.94 (s, 1H), 6.83 (t, J = 7.5 Hz, 1H), 6.75 (d, J = 7.8 Hz, 1H), 4.45-4.05 (m, 5H), 3.55 (dd, J = 15.1, 5.6 Hz, 1H), 2.72

(d, J = 15.1 Hz, 1H), 2.50 (t, J = 6.9 Hz, 2H), 2.03 (m, 4H), 1.41 (d, J = 6.6 Hz, 3H), 1.29 (t, J = 7.1 Hz, 3H); ^{13}C NMR (75 MHz, $CDCl_3$) δ 173.7 (C), 157.6 (C), 152.1 (C), 149.6 (C), 140.2 (C), 140.0 (C), 139.5 (C), 137.6 (C), 130.9 (C), 128.8 (C), 128.4 (C), 127.7 (CH), 127.4 (CH), 127.1 (CH), 126.7 (CH), 126.6 (CH), 126.1 (CH), 126.0 (CH), 125.0 (CH), 124.9 (C), 124.0 (CH), 123.1 (CH), 119.9 (CH), 119.2 (CH), 103.5 (CH), 68.1 (CH_2), 60.7 (CH_2), 45.4 (CH), 42.8 (CH_2), 34.3 (CH_2), 29.0 (CH_2), 22.2 (CH_2), 20.0 (CH_3), 14.6 (CH_3); HRMS (ESI) calcd. for $C_{34}H_{33}O_3$ [M+H] 489.2424, found 489.2422.

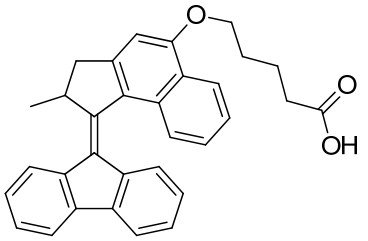

5-((1-(9H-fluoren-9-ylidene)-2-methyl-2,3-dihydro-1H-cyclopenta[a]naphthalen-5-yl)oxy)pentanoic acid 12

To a mixture of H_2O (5 mL), THF (5 mL) and ethanol (5 mL) was added **11** (77 mg, 0.16 mmol) and LiOH (60 mg, 2.5 mmol). The suspension was heated at reflux for 48 h, during which all solids dissolved. After cooling to rt the pH was adjusted to 3-4 with 2 M aqueous HCl. Water (50 mL) was added and the mixture extracted with ethyl acetate (50 mL). The organic layer was washed with water (50 mL) and brine (50 mL) and concentrated *in vacuo*. The residue was purified by column chromatography (16:4:1 pentane:ethyl acetate:formic acid, R_f = 0.3) yielding **12** (51 mg, 0.11 mmol, 70%) as a yellow solid. mp 200.7 °C; ^{1}H NMR (300 MHz, $CDCl_3$) δ 8.37 (d, J = 8.4 Hz, 1H), 7.98 (m, 1H), 7.88 (m, 1H), 7.77 (d, J = 7.6 Hz, 1H), 7.71 (d, J = 8.4 Hz, 1H), 7.45 (dd, J = 14.0, 6.1 Hz, 1H), 7.33 (m, 3H), 7.20 (t, J = 7.8 Hz, 1H), 6.93 (s, 1H), 6.82 (t, J = 7.6 Hz, 1H), 6.73 (d, J = 8.0 Hz, 1H), 4.30 (m, 3H), 3.55 (dd, J = 15.0, 5.6 Hz, 1H), 2.71 (d, J = 15.1 Hz, 1H), 2.57 (t, J = 6.8 Hz, 2H), 2.10 (m, 4H), 1.40 (d, J = 6.7 Hz, 3H); ^{13}C NMR (75 MHz, $CDCl_3$) δ 180.0 (C), 157.4 (C), 151.9 (C), 149.4 (C), 140.2 (C), 140.0 (C), 139.4 (C), 137.5 (C), 130.8 (C), 128.8 (C), 128.4 (C), 127.6 (CH), 127.4 (CH), 127.0 (CH), 126.59 (CH), 126.55 (CH), 126.1 (CH), 125.9 (CH), 125.0 (CH), 124.9 (C), 124.0 (CH), 123.0 (CH), 119.9 (CH), 119.1 (CH), 103.4 (CH), 68.0 (CH_2), 45.4 (CH), 42.8 (CH_2), 34.0 (CH_2), 28.9 (CH_2), 21.9 (CH_2), 19.9 (CH_3); HRMS (ESI) calcd. for $C_{32}H_{29}O_3$ [M+H] 461.2111, found 461.2096.

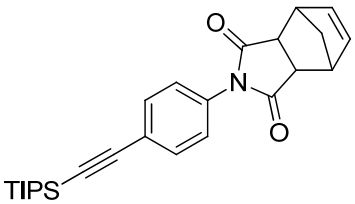

2-(4-((triisopropylsilyl)ethynyl)phenyl)-3a,4,7,7a-tetrahydro-1*H*-4,7-methanoisoindole-1,3(2*H*)-dione 17

Compound **14** was placed in a round-bottomed flask and acetic anhydride (20 mL), acetic acid (2 mL) and **16** (824 mg, 5.0 mmol) were added. The mixture was heated to reflux for 16 h, and then the volatiles were removed *in vacuo*. The residue was taken up in ethyl acetate (100 mL) and washed with saturated aqueous $NaHCO_3$ (100 mL) and H_2O (100 mL). The organic layer was dried on Na_2SO_4 and concentrated. The residue was purified

by column chromatography (1:1 pentane:ethyl acetate) to give **17** (1.5 g, 77% over two steps) as a brown oil which solidified on standing. ^{1}H NMR (300 MHz, $CDCl_3$) δ 7.56 (d, *J* = 8.3 Hz, 2H), 7.08 (d, *J* = 8.3 Hz, 2H), 6.29 (bs, 2H), 3.55 (m, 2H), 3.48 (m, 2H), 1.76 (d, *J* = 9.0 Hz, 1H), 1.55 (d, *J* = 9.0 Hz, 1H), 1.12 (s, 21H); ^{13}C NMR (75 MHz, $CDCl_3$) δ 173.3 (2C), 139.7 (C), 134.0 (2CH), 129.3 (2CH), 125.0 (C), 119.7 (2CH), 106.3 (C), 93.2 (C), 53.3 (CH_2), 47.6 (2CH), 46.7 (2CH), 19.2 (6CH_3), 11.8 (3CH); HRMS (APCI) calcd for $C_{26}H_{34}NO_2Si$ [M+H] 420.2353.

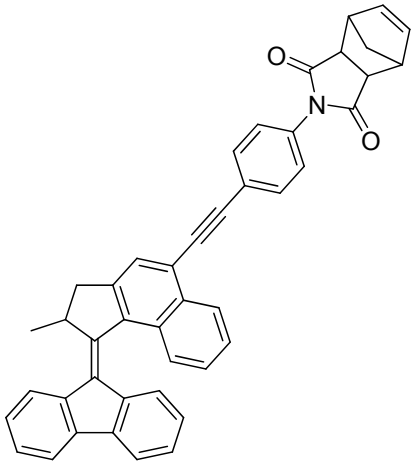

2-(4-((1-(9*H*-fluoren-9-ylidene)-2-methyl-2,3-dihydro-1*H*-cyclopenta[*a*]naphthalen-5-yl)ethynyl)phenyl)-3a,4,7,7a-tetrahydro-1*H*-4,7-methanoisoindole-1,3(2*H*)-dione 20

To a solution of **17** (619 mg, 1.48 mmol) in THF (15 mL) at 0 °C was added tetrabutylammonium fluoride (1.6 mL of a 1M solution in THF, 1.6 mmol). The solution was stirred at rt for 1 h, and then an excess of $CaCl_2$ was added. Stirring was continued for 10 min before the solids were separated by filtration. The solution was concentrated to give crude **18**. This was placed in a two-necked flask, **19** (425 mg, 1.0 mmol), $Pd(PPh_3)_2Cl_2$ (71 mg, 0.10 mmol), CuI (19 mg, 0.10 mmol), *i*Pr_2NH (1 mL) and THF (10 mL) were added and the mixture was thoroughly degassed and saturated with N_2. The mixture was heated at 50 °C overnight. The volatiles were removed *in vacuo* and the residue was dissolved in EtOAc and washed with 1 M aqueous HCl, H_2O and brine. The organic layer was concentrated and the residue was purified by column chromatography (3:1 pentane:ethyl acetate) to give **20** (399 mg, 67%) as an orange solid. mp >250 °C; ^{1}H NMR (300 MHz, $CDCl_3$) δ 8.54 (d, *J* = 8.3 Hz, 1H), 7.99 (m, 1H), 7.86 (m, 3H), 7.75 (m, 3H), 7.59 (t, *J* = 7.2 Hz, 1H), 7.40 (m, 3H), 7.24 (m, 3H), 6.81 (t, *J* = 7.5 Hz, 1H), 6.73 (d, *J* = 7.9 Hz, 1H), 6.30 (s, 2H), 4.35 (m, 1H), 3.58 (m, 3H), 3.46 (m, 2H), 2.77 (d, *J* = 15.0 Hz, 1H), 1.81 (d, *J* = 8.9 Hz, 1H), 1.62 (d, *J* = 9.0 Hz, 1H), 1.41 (d, *J* = 6.7 Hz, 3H); ^{13}C NMR (75 MHz, $CDCl_3$) δ 176.8 (C), 150.5 (C), 146.6 (C), 140.5 (C), 140.00 (C), 139.96 (C), 137.9 (C), 137.9 (C), 134.9 (CH), 132.8 (C), 132.5 (CH), 132.2 (C), 131.8 (C), 129.9 (C), 128.7 (CH), 128.2 (CH), 127.5 (CH), 127.40 (CH), 127.36 (CH), 127.2 (CH), 127.0 (CH), 126.6 (CH), 126.4 (CH), 126.2 (CH), 124.5 (CH), 123.8 (C), 123.0 (C), 120.1 (CH), 119.4 (CH), 95.5 (C), 89.5 (C), 52.5 (CH_2), 46.1 (CH), 45.9 (CH), 45.6 (C), 41.9 (CH_2), 19.6 (CH_3); HRMS (ESI) calcd. for $C_{44}H_{31}NO_2Na$ [M+Na] 628.2247, found 628.2232.

General procedure for polymerization

Catalyst loading, solvent, temperature, reaction time and yield for the polymerizations are summarized in Table 1. To an Ar-purged solution of the monomer (50 mg) in the indicated solvent (concentration = 0.1 M) was added benzylidene-bis(tricyclohexylphosphine)dichlororuthenium (first generation Grubbs catalyst). The solution was heated for the indicated time and then vinyl acetate (excess) was added. The solution was allowed to cool to rt and added dropwise to a tenfold excess of methanol. The product was isolated by filtration as a yellow to gray powder. Further purification was performed by dissolving in a minimal amount of CH_2Cl_2 and precipitating from methanol. Polymer **24**: ^{1}H NMR (300 MHz, $CDCl_3$) δ 8.54 (1H), 8.00-7.60 (8H), 7.60-7.00 (6H), 6.77 (2H), 5.80 (2H), 4.24 (1H), 3.60-3.20 (2H), 3.03 (1H), 2.74 (1H), 2.10-1.50 (2H), 1.50-0.90 (3H).

Irradiation experiments

UV/Vis absorption spectra were measured on a Jasco V-630 or a Hewlett-Packard 8453 spectrometer. CD spectra were measured on a Jasco J-815 CD spectrometer. Irradiation experiments of **20** and **24** were performed under nitrogen atmosphere in spectroscopic grade solvent. For irradiation a spectroline ENB-280C/FE lamp (λ_{max} = 365 nm) was used. To be certain photostationary states were reached, several spectra at set intervals were recorded. Thermal isomerization was performed by leaving the solutions in the dark at 20-40 °C for at least 20 min. The solution was then cooled again to the temperature at which irradiation was performed before further measurement.

References

[1] A. Coskun, M. Banaszak, R. D. Astumian, J. F. Stoddart, B. A. Grzybowski, *Chem. Soc. Rev.* **2012**, *41*, 19-30.

[2] P. Lussis, T. Svaldo-Lanero, A. Bertocco, C.A. Fustin, D. A. Leigh, A.-S. Duwez, *Nature Nanotechnol.* **2011**, *6*, 553-557.

[3] T. Hugel, N. B. Holland, A. Cattani, L. Moroder, M. Seitz, H. E. Gaub, *Science* **2002**, *296*, 1103-1106.

[4] Z. Sekkat, W. Knoll in *Molecular Switches* (Eds.: B. L. Feringa, W. R. Browne), Wiley-VCH, Weinheim, **2011**, pp. 423-516.

[5] F. Ercole, T. P. Davis, R. A. Evans, *Polym. Chem.* **2010**, *1*, 37-54.

[6] C. R. Medonça, D. T. Balogh, L. De Boni, D. S. dos Santos Jr., V. Zucolotto, O. N. Oliveira Jr. in *Molecular Switches* (Eds.: B. L. Feringa, W. R. Browne), Wiley-VCH, Weinheim, **2011**, pp. 399-422.

[7] T. Ikeda, J. Mamiya, Y. Yu, *Angew. Chem. Int. Ed.* **2007**, *46*, 506-528.

[8] D. Pijper, *Ph. D. Thesis*, University of Groningen, **2008**.

[9] A. Kulago, *Ph. D. Thesis*, University of Groningen, **2011**.

[10] M. M. Pollard, M. Klok, D. Pijper, B. L. Feringa, *Adv. Funct. Mater.* **2007**, *17*, 718-729.

[11] C. Pietsch, U. S. Schubert, R. Hoogenboom, *Chem. Commun.* **2011**, *47*, 8750-8765.

[12] M. M. Green, N. C. Peterson, T. Sato, A. Teramoto, R. Cook, S. Lifson, *Science* **1995**, *268*, 1860-1866.

[13] M. M. Green, J.-W. Park, T. Sato, A Teramoto, S. Lifson, R. L. B. Selinger, J. V. Selinger, *Angew. Chem. Int. Ed.* **1999**, *38*, 3138-3154.

[14] D. Pijper, B. L. Feringa, *Soft Matter* **2008**, *4*, 1349-1372.

[15] M. Müller, R. Zentel, *Macromolecules* **1994**, *27*, 4404-4406.

[16] G. Maxein, R. Zentel, *Macromolecules* **1995**, *28*, 8438-8440.

[17] M. Müller, R. Zentel, *Macromolecules* **1996**, *29*, 1609-1617.

[18] D. Pijper, B. L. Feringa, *Angew. Chem. Int. Ed.* **2007**, *46*, 3693-3696.

[19] D. Pijper, M. G. M. Jongejan, A. Meetsma, B. L. Feringa, *J. Am. Chem. Soc.* **2008**, *130*, 4541-4552.

[20] G. T. Carroll, M. G. M. Jongejan, D. Pijper, B. L. Feringa, *Chem. Sci.* **2010**, *1*, 469-472.

[21] G. T. Carroll, G. London, T. Fernández Landaluce, P. Rudolf, B. L. Feringa, *ACS Nano*, **2011**, *5*, 622-630.

[22] D. A. Tramontozzi, N. D. Suhan, S. Holger Eichhorn, S. J. Loeb, *Chem. Eur. J.* **2010**, *16*, 4466-4476.

[23] C. Barrett, A. Natansohn, P. Rochon, *Macromolecules* **1994**, *27*, 4781-4786.

[24] J. Vicario, A. Meetsma, B. L Feringa, *Chem. Commun.* **2005**, 5910-5912.

[25] J. Vicario, M. Walko, A. Meetsma, B. L. Feringa, *J. Am. Chem. Soc.* **2006**, *128*, 5127-5135.
[26] M. M. Pollard, P. V. Wesenhagen, D. Pijper, B. L. Feringa, *Org. Biomol. Chem.* **2008**, *6*, 1605-1612.
[27] B. Akhlaghinia, S. Samiei*, Turk. J. Chem.* **2007**, *31*, 35-43.
[28] B. Akhlaghinia, *Synthesis* **2005**, *12*, 1955-1958.
[29] G. Koeckelberghs, M. Van Beylen, C. Samyn, *Mat. Sci. Eng., C* **2001**, *18*, 15-20.
[30] K. Schlögl, *Monatsh. Chem.* **1958**, *89*, 61-73.
[31] S. Sutthasupa, M. Shiotsuki, F. Sanda, *Polym. J. (Tokyo)* **2010**, *42*, 905-915.
[32] C. W. Bielawski, R. H. Grubbs, *Prog. Polym. Sci* **2007**, *32*, 1-29.
[33] A. J. Boydston, T. W. Holcombe, D. A. Unruh, J. M. J. Fréchet, R. H Grubbs, *J. Am. Chem. Soc.* **2009**, *131*, 5388-5389.
[34] K. Takamizu, K. Nomura, *J. Am. Chem. Soc.* **2012**, *134*, 7892-7895.
[35] K. Vehlow, D. Wang, M. R. Buchmeiser, S. Blechert, *Angew. Chem. Int. Ed.* **2008**, *47*, 2615-2618.
[36] S. Hilf, F. Wurm, A. F. M. Kilbinger, *J. Polym. Sci. A* **2009**, *47*, 6932-6940.
[37] K. W. Kim, T. Ok, K. Lee, H.-S. Lee, K. T. Chang, H. Ihee, J.-H. Sohn, *J. Am. Chem. Soc.* **2010**, *132*, 12027-12033.
[38] D. Birney, T. K. Lim, J. H. P. Koh, B. R. Pool, J. M. White, *J. Am. Chem. Soc.* **2002**, *124*, 5091-5099.
[39] J. G. Hamilton, *Polymer*, **1998**, *39*, 1669-1689.
[40] L. Delaude, A. Demonceau, A. F. Noels, *Macromolecules* **2003**, *36*, 1446-1456.
[41] S. Hilf, A. F. M. Kilbinger, *Nature Chem.* **2009**, *1*, 537-546.
[42] Although we did not perform this experiment with the monomer, this behavior was never observed for this type of molecular motor.
[43] K. Morino, K. Maeda, Y. Okamoto, E. Yashima, T. Sato, *Chem. Eur. J.* **2002**, *8*, 5112-5120.
[44] A. Gopal, M. Hifsudheen, S. Furumi, M. Takeuchi, A. Ajayaghosh, *Angew. Chem. Int. Ed.* **2012**, *51*, 10505-10509.
[45] A. Khan, C. Kaiser, S. Hecht, *Angew. Chem. Int. Ed.* **2006**, *45*, 1878-1881.
[46] T. F. A. De Greef, M. J. Kade, K. E. Feldman, E. J. Kramer, C. J. Hawker, E. W. Meijer, *J. Polym. Sci., Part A: Polym. Chem.* **2011**, *49*, 4253-4260.
[47] T. Zhao, H. W. Backham, H. W. Gibson, *Macromolecules* **2003**, *36*, 4833-4837.
[48] B. A. Miller-Chou, J. L. Koenig, *Prog. Polym. Sci.* **2003**, *28*, 1223-1270.
[49] J. J. Young, G. R baker, G. R Newkome, *Macromolecules* **1994**, *27*, 3464-3471.
[50] F. D. Jochum, L. zur Borg, P. J. Roth, P. Theato, *Macromolecules* **2009**, *42*, 7854-7862.
[51] J. B. Matson, R. H. Grubbs, *Macromolecules* **2010**, *43*, 213-221.
[52] R. M. Thomas, R. H. Grubbs, *Macromolecules* **2010**, *3705-3709.*
[53] S. Anderson, *Chem. Eur. J.* **2001**, *7*, 4706-4714.
[54] S. Grunder, D. Muñoz Torres, C. Marquardt, A. Błaszczyk, R. Krupke, M. Mayor, *Eur. J. Org. Chem.* **2011**, 478-496.
[55] A. bin Sadikun, D. I. Davies, R. F. Kenyon, *J. Chem. Soc., Perkin Trans. 1* **1981**, 2299-2305.
[56] N. Ruangsupapichat, *Ph. D. Thesis*, University of Groningen, **2012**.

Summary

Nanotechnology takes place on a scale of 10^{-9} (= 0.000000001) m. In molecular nanotechnology individual molecules or parts of moleculens are used as building blocks to obtain certain material properties or functions. Fascinating examples of this are found in the development of nanoscale analogues of tools and machines, based on molecules, which are a billion times smaller than their normal macroscopic counterparts. This has led to the construction of switches, a lift, scissors, cars and many more.
The molecular motors in this thesis are also an example. At the molecular scale, rotation is nothing special: in almost all molecules continual rotation takes place in random direction. The molecular motors are a special case because rotation can be induced around a bond which normally does not allow rotation, and because there is control over the direction of the rotation. Potential applications of this controlled rotation in nanotechnology can be envisioned, like for example the transport of molecules in a directed manner.
The research described in this thesis deals with molecular motors based on the sterically overcrowded alkenes as first developed in the research group of prof. Feringa in 1999. In the introductory chapter of the thesis an overview is given of the literature of this field of research. The developments since the first example of these motors are presented, as well as the current challenges. In this thesis the so-called second generation molecular motors are used. These molecules comprise two large aromatic parts connected by a double bond; this double bond acts as the axis of the rotation. Due to the size of the aromatic groups on the double bond the molecule is not flat, but rather adopts helical shape (conformation).

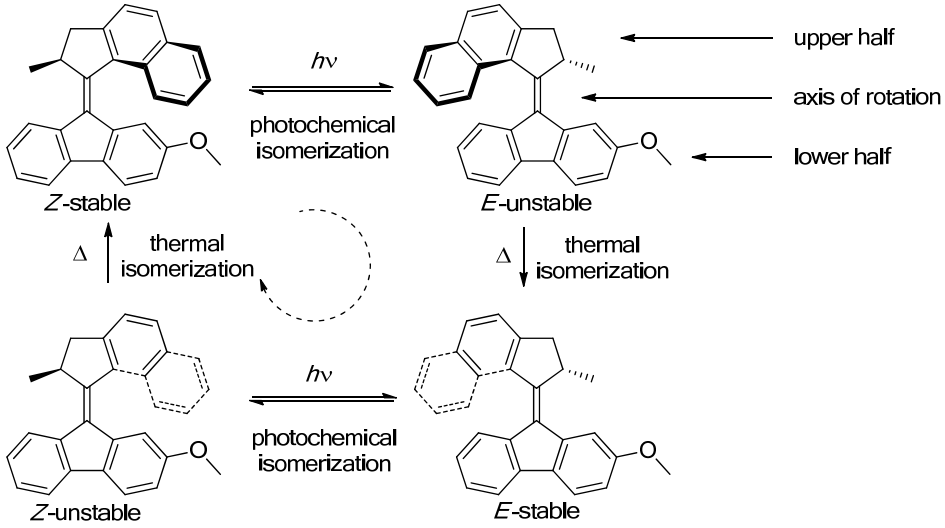

Scheme 1 The four isomerization steps in the rotation of a molecular motor. Bolded parts of the molecule are pointing forward (out of the paper) while dashed parts of the molecule are pointing backward (into the paper).

As mentioned, the central double is the axis of the rotation. The rotation around this bond can be divided into four steps (Scheme 1). Starting from the structure on the top-left, first a photochemical isomerization takes place, induced by UV light, in which the upper half of the motor rotates nearly 180 degrees relative to the lower half. This puts the molecule in a thermodynamically unfavorable conformation: part of the upper half in pushed too close to the lower half. If the molecule has enough thermal energy, it will undergo a thermal isomerization in which the upper half rotates further relative to the lower half. Now the upper half has completed exactly one half of a rotation relative to the lower half.

A second photoisomerization, which again generates an unstable conformation, followed by a second thermal isomerization completes a full rotation. If UV light and heat are supplied at the same time, continuous rotation takes place, but the isomerization steps can also be performed one by one. In this way the rotation process can be followed by UV/vis absorption and circular dichroism (CD) spectroscopy. Using these techniques use the absorption of (polarized) light can be determined, which changes each time the molecule isomerizes. From the measurements the conformation of the molecule can be derived, which can be used to determine whether rotation takes place.
The goal of the research in this thesis is to study in which way the rotation of molecular motors could be applied in nanotechnology. Because the direction of rotation can be controlled, they could conceivably be used to transport molecules on the nanoscale, for example. Extensive knowledge of the motion in the molecule during the rotation and which factors influence this are required for this. In the first chapters of this thesis the different isomerization steps in the rotation process are studied using various spectroscopic techniques. In the later chapters molecular motors are incorporated into multicomponent system to investigate how this influences the rotation process.
In chapter two of this thesis the conformational changes of molecular motors during thermal isomerization is studied. A combination of quantum-mechanical calculations and UV/vis absorption and CD spectroscopy was employed. A series of four molecular motors with different bridging groups in the lower half was studied: S, O, $C(CH_3)_2$ and $Si(CH_3)_2$ (**1**-**4**, Scheme 2). Using density functional theory (DFT) calculations two different pathways for the thermal relaxation of the unstable form were found. The intermediates in the relaxation are similar for **1**-**4**, with small deviations for **4**. The barrier of the rate determining step of the thermal isomerization was calculated: this was determined to be dependent on the flexibility of the lower half, which is influenced by the bridging group X. The calculated energy barrier were in good accordance with the experimentally determined barriers for **1**, **3** and **4**, but deviated for **2**. The relaxation in **2** is probably not a helix inversion, as it is for the others, but an *E*-*Z* isomerization. This would mean that the rotation of **2** is no longer unidirectional, but further studies are needed to ascertain this.

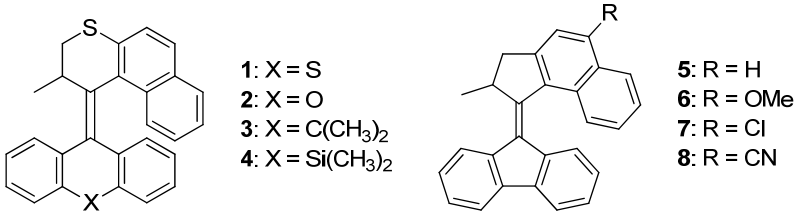

Scheme 2 Molecular motors **1**-**8**.

In chapter three efforts to gain more insight into the conformational changes during photoisomerization are presented. A series of four molecular motors with different electron withdrawing and electron donating substituents was studied (**5**-**8**, Scheme 2). In a previous study it was already concluded that these substituents have no effect on thermal isomerization, but they do influence the photochemical isomerization. Here we explain this using DFT calculations, which show no influence of the substituents on the conformation of the molecule. The quantum yield of the photosiomerization was determined for the four motors in the series: this was found to be highest for molecules with electron withdrawing substituents and lower for molecules with electron donating substituents. The photoisomerization was followed using time-resolved fluorescence up-conversion spectroscopy with a time resolution of ca. 100 fs (= 10^{-13} s). The entire process takes several picoseconds (= 10^{-12} s) depending on the substituent: with electron

withdrawing substituents the process was faster than with electron donating substituents. Furthermore, two vibrational modes were identified which were excited along with the electronic excitation. These vibrations are likely connected to the conformational changes during the photochemical isomerization. To determine which parts of the molecule are involved, IR and Raman spectroscopy can be employed. In this work, this was first used on the molecules in the ground state; from the results no direct conclusion can be draw about process in the excited state. However, this study can be used as the groundwork for time-resolved vibrational spectroscopy, which can used to study the conformational changes in the excited state.

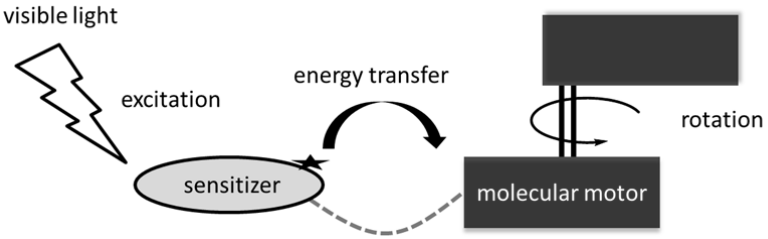

Scheme 3 A molecular motor driven by visible light.

The research in chapter four focuses on the development of a molecular motor which can be driven by visible light instead of UV light. This was accomplished by using palladium tetraphenylporphyrin as a sensitizer. The porphyrin acts like an antenna, which absorbs visible light and transfers the energy to the molecular motor (Scheme 3). The energy transfer can be performed both in inter- and intramolecular fashion. The porphyrin absorbs the visible light (532 or 546 nm) and subsequently reaches a triplet excited state. Next, the energy transfer to the motor takes place and the motor reaches a triplet excited state. In this excited state, *E-Z* isomerization can take place, which is follow by a thermal helix inversion as in the case of UV light excitation. The rotation is still unidirectional, as was shown using UV/vis absorption, CD and ^{1}H NMR spectroscopy. If a different sensitizer would be used, light of longer wavelength might be used, which could allow for the use of molecular motors in combination with biological systems, which tend to be incompatible with UV irradiation.

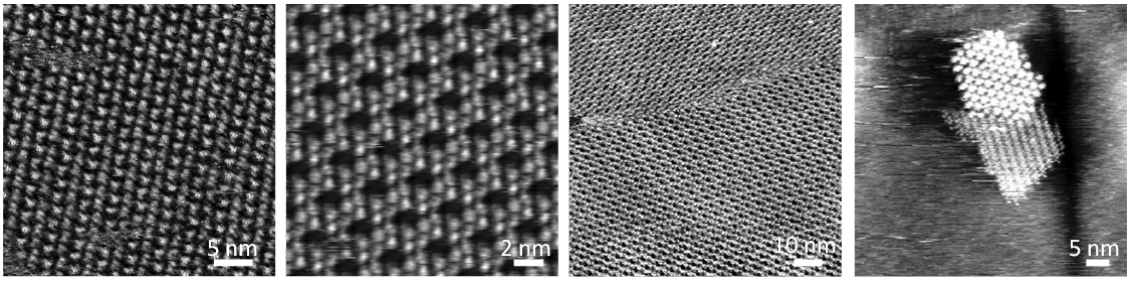

Figure 1 Examples of STM images of the molecules found in chapter five.

In chapter five multimotor systems for self-assembly on graphite are described. By making ordered monolayers of molecular motors, their collective motion could potentially be used to perform useful work. Three different systems with motors of different speed were synthesized. In all cases, the motor function was retained in the mulitmotor systems in solution which was proven using UV/vis absorption and CD spectroscopy. Subsequently, the self-assembly of the molecules at the 1-phenyloctane/graphite interface was studied using scanning tunneling microscopy (STM), which allows for the imaging of monolayers with molecular resolution. The symmetry of the multimotor systems was found to be important: only the molecules with C3

symmetry, similar to that of the graphite, were found to form stable, ordered monolayers. Domains of several tens to several hundreds of molecules with different kinds of packings were observed (Figure 1). The interactions between the aromatic parts of the motors and the surface and between helically shaped motor units were found to play an important role in the self-assembly. The monolayers were also subjected to UV irradiation to investigate whether rotation of the motor is retained while on the surface. However, no changes were observed upon irradiation, most likely due to rapid quenching of the excited state by the surface.

The research in chapter six focuses on the development of macromolecular system incorporating molecular motors in order to study the interaction between the rotation of the motor and the polymer chain. In the first part of the chapter, efforts to incorporate molecular motors into polyisocyanates are presented. Polyisocyanates adopt a helical structure, which can be influenced by the motor; however, the motor might also be influenced by the polymeric environment. Unfortunately, the high reactivity of isocyanate-functionalized motors precluded their purification, and the synthesis was abandoned. In the second part of the chapter polymers based on the ring opening of norbornene are used. The norbornenes were substituted with a molecular motor and subsequently polymerized by ring-opening metathesis polymerization (ROMP). UV/vis and CD spectroscopy demonstrated that the rotation of the motor in the polymer was retained in solution. The conformation of the polymer in solution was shown to be temperature dependent by CD spectroscopy and DOSY (diffusion-ordered spectroscopy) NMR measurements. At lower temperature, the polymer adopts a more collapsed conformation, which increases the diffusion coefficient. Moreover, the conformation of the polymer is dependent on the conformation of the motor, which means that the polymer conformation can also be influenced by UV light.
Overall, the research presented in this thesis contributes to our knowledge of molecular motors based on sterically overcrowded alkenes. Using DFT calculations and various spectroscopic techniques, we gained more insight in the conformational changes of the molecular motors during the rotation process, which is crucial for future application of these molecules. Furthermore, a number of multimotor systems were designed and synthesized. The collective motion of a large number of molecular motors could be a way to perform useful work on the nanoscale.

Samenvatting

Nanotechnologie speelt zich af op een schaal van 10^{-9} (= 0.000000001) m. In de moleculaire nanotechnologie worden individuele moleculen of delen daarvan gebruikt als bouwstenen om tot materialen met bepaalde eigenschappen of functies te komen. Aansprekende voorbeelden zijn de ontwikkeling van nano-versies van werktuigen en machines, gebaseerd op moleculen, die rond een miljard keer kleiner zijn dan hun normale, macroscopische versies. Zo zijn er voorbeelden van schakelaars, een lift, een schaar, een auto en nog veel meer.
De moleculaire rotatiemotoren beschreven in dit proefschrift zijn hier ook een voorbeeld van. Op zich is rotatie op moleculaire schaal niets speciaals: in bijna alle moleculen vindt continu rotatie plaats in willekeurige richtingen. Het bijzondere aan deze motoren is dat de rotatie kan worden gestimuleerd om een binding waar dit niet spontaan plaatsvindt, en dat de rotatie één kant op gaat. Deze gecontroleerde draaibeweging kan mogelijk worden toegepast in de nanotechnologie, bijvoorbeeld om andere moleculen gericht te verplaatsen.
Het onderzoek in dit proefschrift betreft moleculaire motoren gebaseerd op sterisch gehinderde alkenen, die voor het eerst werden gemaakt in de onderzoeksgroep van prof. Feringa in 1999. In het introductiehoofdstuk van dit proefschrift wordt een overzicht gegeven van de literatuur op het gebied van deze moleculen. Hierin wordt uiteengezet wat we weten over moleculaire motoren en waar de uitdagingen liggen. De motoren die in dit onderzoek werden gebruikt behoren tot de zogenoemde tweede generatie. Deze moleculen bestaan uit twee aromatische delen die zijn verbonden via een dubbele binding, die ook de as van de rotatie is. Omdat de aromatische groepen aan de dubbele binding groot zijn, kan het molecuul niet vlak zijn, maar buigen de aromatische groepen weg van elkaar. Het resultaat is dat het molecuul een helixvorm (helische conformatie) heeft.

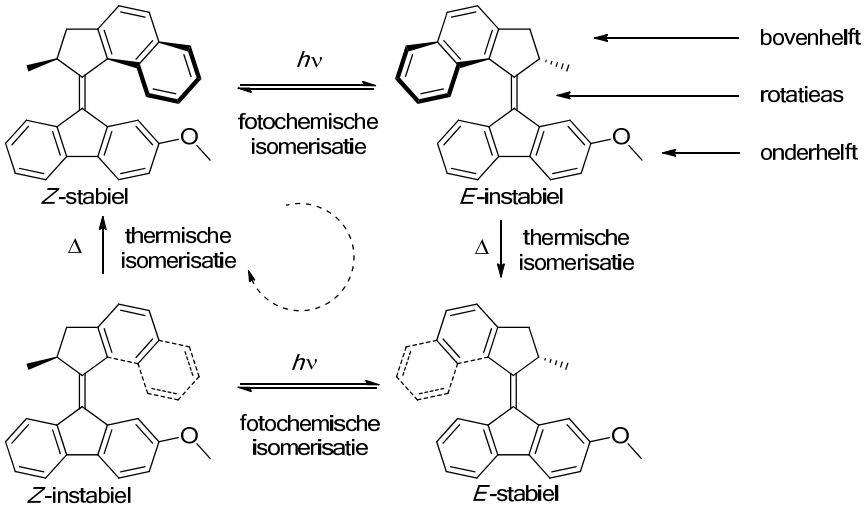

Schema 1 De vier isomerisatiestappen in de rotatie van een moleculaire motor. Diktgedrukte delen van het molecuul staan naar voren (‘uit het papier’) en gestippelde delen naar achteren (‘achter het papier’).

Zoals gezegd is de centrale dubbele binding de as van de rotatie. De rotatie om deze binding kan worden opgedeeld in vier stappen (Schema 1). Beginnend bij de structuur linksboven vindt er eerst een fotochemische isomerisatie plaats onder invloed van UV-licht, waarbij de bovenhelft bijna 180 graden draait ten opzichte van de onderhelft. Het

molecuul eindigt in een conformatie die thermodynamisch niet gunstig is: de onderhelft en de bovenhelft worden als het ware te dicht naar elkaar toe gedrukt. Als er genoeg warmte aanwezig is, kan het molecuul een conformatieverandering ondergaan, waarbij de bovenhelft verder langs de onderhelft draait. Het molecuul heeft nu precies een halve rotatie voltooid en zit in een thermodynamisch stabiele conformatie. Nu kan het echter een tweede fotochemische isomerisatie ondergaan, waarbij weer een instabiele conformatie ontstaat, en na een tweede thermische isomerisatie is één volledige rotatie voltooid. Als er tegelijk UV-licht en warmte wordt toegevoerd, is er sprake van continue rotatie, maar de stappen kunnen ook één voor één worden uitgevoerd. Op die manier kan het hele proces gevolgd worden; hiervoor wordt gebruik gemaakt van UV/vis absorptiespectroscopie en circulair dichroisme (CD) spectroscopie. Met deze technieken wordt gekeken naar de verschillen in de absorptie van (gepolariseerd) licht, die steeds verandert als het molecuul een isomerisatie ondergaat. Zo kan worden bepaald in welke conformatie het molecuul zich op elk moment bevindt, en of er rotatie plaatsvindt.
Het doel van het onderzoek in dit proefschrift is te bestuderen hoe de rotatie van moleculaire motoren zou kunnen worden toegepast in de nanotechnologie. Omdat er controle is over de draairichting van deze moleculen, zouden ze misschien kunnen worden ingezet om bijvoorbeeld voorwerpen te transporteren op de nanoschaal. Om dit te realiseren is het nodig om een goed inzicht te hebben hoe de draaibeweging precies tot stand komt en welke factoren de draaiing beïnvloeden. In de eerste hoofdstukken van dit proefschrift worden de verschillende isomerisatiestappen tijdens de rotatie bestudeerd met verschillende spectroscopische technieken. In de latere hoofdstukken worden moleculaire motoren ingebouwd in multicomponente systemen en wordt er gekeken welk effect dit heeft op de rotatie.
In hoofdstuk twee werden de conformatieveranderingen van moleculaire motoren tijdens de thermische isomerisatie bestudeerd. Hierbij werd gebruik gemaakt van zowel quantum-mechanische berekeningen als UV/vis absorptie en CD spectroscopie. Een serie van vier verschillende motoren werd bestudeerd, die alle een verschillende verbindende groep in de onderhelft hebben: S, O, $C(CH_3)_2$ en $Si(CH_3)_2$ (**1**-**4**, Schema 2). Met behulp van DFT-berekeningen (Engels: density functional theory, 'dichtheidsfunctionaaltheorie') zijn twee paden gevonden voor de relaxatie van de instabiele vorm van deze motoren. Moleculen **1**-**4** hebben intermediairen met vergelijkbare conformaties, maar molecuul **4** wijkt iets af. De barrière voor de relaxatie werd ook bepaald uit de berekeningen; deze lijkt afhankelijk te zijn van de buigzaamheid in de stator, die voornamelijk wordt bepaald door de verbindende groep X. De hoogte van de berekende barrières vertoonde goede overeenkomst met de experimenteel bepaalde barrières, behalve voor molecuul **2**. Waarschijnlijk is de relaxatie in dit geval niet een helixinversie maar een *E*-*Z* isomerisatie. Dit zou betekenen dat de rotatie van **2** onder invloed van warmte en licht beide kanten op gaat, maar dit moet verder onderzocht worden voordat een definitieve conclusie getrokken kan worden.

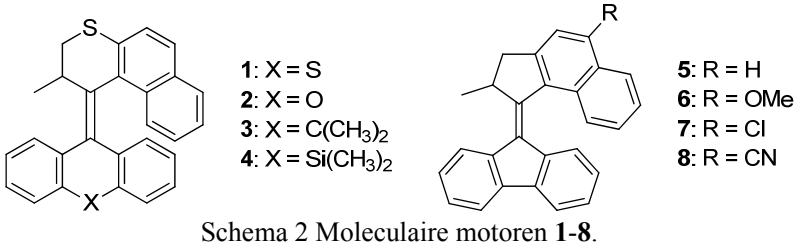

Schema 2 Moleculaire motoren **1**-**8**.

In hoofdstuk drie wordt beschreven hoe werd geprobeerd om meer inzicht te krijgen in de conformatieveranderingen tijdens de fotochemische isomerisatie. Een serie moleculaire

motoren met elektronenzuigende en –stuwende substituenten werd bestudeerd (**5-8**, Schema 2). Hiervan was eerder al gebleken dat er geen invloed van de substituenten was op de thermische isomerisatie, maar wel op de fotochemische isomerisatie. Dit werd in dit onderzoek verklaard met behulp van DFT-berekeningen; er werd geen significante invloed van de substituenten op de conformatie van het molecuul gevonden. De kwantumopbrengst van de fotochemische isomerisatie werd bepaald voor de serie motoren. De moleculen met een elektronenzuigende groep bleken een hogere kwantumopbrengst te hebben dan die met een elektronenstuwende groep. Met behulp van tijdsopgeloste fluorescentie op-conversiespectroscopie werd de fotochemische isomerisatie gevolgd met een resolutie van ca. 100 femtoseconde (= 10^{-13} s). Het hele proces duurt enkele picoseconden (= 10^{-12} s) afhankelijk van de substituent: voor elektronenzuigende substituenten was het sneller dan voor elektronenstuwende substituenten. Bovendien werden er twee vibraties gevonden die tegelijk met de elektronische excitatie werden aangeslagen. Deze vibraties zijn waarschijnlijk verbonden met de veranderingen in conformatie tijdens de fotochemische isomerisatie. Om exact vast te stellen welke delen van het molecuul hierbij betrokken zijn kan gebruik worden gemaakt van vibratiespectroscopie: IR absorptie en Raman spectroscopie. Dit werd eerst toegepast op de moleculen in de grondtoestand; hieruit kunnen nog geen directe conclusies worden getrokken over wat er gebeurt in de aangeslagen toestand. Wel kan deze studie worden gebruikt als uitgangspunt voor tijdsopgeloste vibratiespectroscopie, waarmee de conformatieveranderingen in de aangeslagen toestand kunnen worden bestudeerd.

Het onderzoek in hoofdstuk vier richtte zich op de ontwikkeling van een manier om moleculaire motoren aan te drijven met zichtbaar licht in plaats van met UV licht. Hiervoor werd gebruik gemaakt van palladium tetrafenylporfyrine als sensitizer. Het porfyrine kan gezien worden als een antenne, die zichtbaar licht opvangt en de energie daarvan overdraagt aan de moleculaire motor (Schema 3). De energieoverdracht kan intermoleculair plaatsvinden, maar is efficiënter in een intramoleculair systeem. Het porfyrine absorbeert het zichtbare licht (532 of 546 nm) en komt in een triplet-aangeslagen toestand. Vervolgens wordt de energie overgedragen naar de motor, waardoor deze in een triplet-aangeslagen toestand komt. Hierin kan *E*-*Z* isomerisatie plaatsvinden, wat wordt gevolgd door thermische helixinversie zoals in het geval van excitatie met UV licht. Met behulp van UV/vis absorptie, CD en ^{1}H-NMR spectroscopie werd aangetoond dat de rotatie van de motor nog steeds unidirectioneel is. Door gebruikt te maken van een andere sensitizer kan mogelijk licht met nog langere golflengte gebruikt worden. Dit zou betekenen dat moleculaire motoren gebruikt kunnen worden in biologische systemen, die niet compatibel zijn met UV licht.

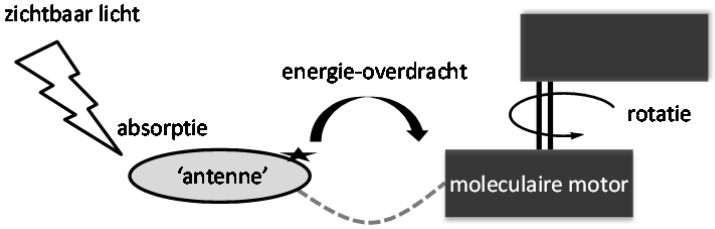

Schema 3 Moleculaire motor aangedreven met zichtbaar licht.

In hoofdstuk vijf worden multimotorsystemen voor zelfassemblage op grafiet beschreven. Door geordende monolagen te maken kan er mogelijk gebruik worden gemaakt van de collectieve beweging van een groot aantal motoren om werk te verrichten. Drie verschillende systemen met motoren met verschillende snelheden werden gesynthetiseerd. De werking van de motoren in de multimotorsystemen in oplossing werd

vastgesteld met UV/vis absorptie en CD spectroscopie. Vervolgens werd de zelfassemblage op het grensvlak van grafiet en 1-fenyloctaan onderzocht met STM (Engels: scanning tunneling microscopy, 'rastertunnel-microscopie'), waarmee in principe een resolutie tot op moleculair niveau kan worden behaald. Hierbij bleek de symmetrie van de multimotorsystemen van belang te zijn: alleen de systemen met C3 symmetrie, die lijkt op de symmetrie van het grafiet, vormden georganiseerde monolagen. Domeinen van enkele tientallen tot enkele honderden moleculen met verschillende pakking werden waargenomen (Figuur 1). Interacties van de vlakke aromatische groepen van de moleculen met het oppervlak en interacties tussen de helische gedeelten van de moleculen onderling spelen een belangrijke rol bij de zelfassemblage. De monolagen werden ook blootgesteld aan UV licht om te onderzoeken of de rotatie van de motor nog werkt op het oppervlak. Er werden echter geen veranderingen waargenomen, waarschijnlijk omdat de aangeslagen toestand wordt gedeactiveerd door energieoverdracht naar het oppervlak.

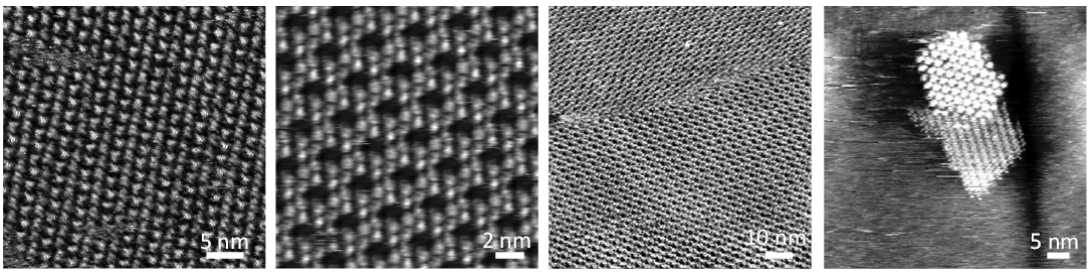

Figuur 1 Voorbeelden van STM plaatjes van de moleculen in hoofdstuk vijf.

Hoofdstuk zes richtte zich op de ontwikkeling van macromoleculaire systemen met moleculaire motoren om te bestuderen hoe de rotatie van de motor het polymeer beïnvloedt en andersom. In het onderzoek beschreven in het eerste deel van het hoofdstuk werd geprobeerd om moleculaire motoren te incorporeren in poly-isocyanaten, met als doel de interactie tussen het helische polymeer en de rotatie van de motoren te bestuderen. De synthese van deze polymeren was echter niet succesvol omdat het monomeer te reactief was. In het tweede deel van het hoofdstuk wordt gebruik gemaakt van ringopeningspolymeren van norborneen. De norbornenen werden gesubstitueerd met een moleculaire motor en vervolgens gepolymeriseerd door middel van een ringopening metathese polymerisatie (ROMP). Met UV/vis en CD spectroscopie werd vastgesteld dat de fotochemische en thermische isomerisatieprocessen van de motor nog steeds plaatsvinden in het polymeer. De conformatie van het polymeer in oplossing is temperatuursafhankelijk. Dit werd vastgesteld met behulp van CD en DOSY (Engels: diffusion-ordered spectroscopy, 'diffusie-geordende spectroscopie') NMR-metingen. Bij lage temperatuur neemt het polymeer waarschijnlijk een meer ineengekrompen conformatie aan, waardoor de diffusiecoëfficiënt toeneemt. Bovendien is dit nog afhankelijk van de conformatie van de motor, zodat de conformatie van het polymeer ook met UV-licht kan worden beïnvloed.

Al met al draagt het werk in dit proefschrift bij aan onze kennis over moleculaire motoren gebaseerd op sterisch gehinderde alkenen. Met behulp van DFT-berekeningen en verscheidene spectroscopische technieken werd meer inzicht verkregen in de conformatieveranderingen van de moleculaire motoren tijdens de rotatie, wat essentieel is met het oog op toekomstige toepassingen. Verder werden er een aantal multimotorsystemen ontwikkeld en gesynthetiseerd. De collectieve rotatie van een groot aantal moleculaire motoren zou een manier kunnen zijn om deze systemen werk te laten verrichten.

Acknowledgments

Over the last years I've found Groningen a great place for doing my Ph. D. studies. There are so many different people with different backgrounds and expertise that there is always something new to learn. In my mind Ben, you are the *pater familias* overseeing this all, and I'm grateful that you gave me the opportunity and the freedom to learn about everything from synthesis to calculations and from time-resolved spectroscopy to STM. I am grateful to Wesley for help and useful discussions throughout my research and especially for the massive help with the writing. In this regard I also owe thanks to the member of the reading committee, Prof. Brouwer, Prof. Herrmann and Prof. Meech for their critical reading of my manuscript.

Discussion and exchange of ideas are crucial for good science. I've appreciated the time spent drawing crazy ideas on the blackboard over coffee breaks, discussing mechanism and synthesis routes in the problem sessions and talking chemistry behind the fumehood with my labmates. In my research I've been privileged to work together with many people on numerous projects; I want thank everyone for their help, input and critical eye. I thank especially Jamie Conyard and Steve Meech for the fruitful collaboration and for hosting me in Norwich to take a look in the kitchen of ultrafast spectroscopy.

Of course besides work there has to be time to relax. To all my friends I would like to say thank you for all the good times I've had playing football, skiing, dungeon crawling, pub quizzing, dancing, having (or listening to) unorthodox conversations over lunch and more. I know I will miss you all far more than you realize.